EPRI

Development of Advanced Concepts for Nuclear Processes in Deuterated Metals

WARNING:
Please read the Export Control Agreement on the back cover.

Technical Report

Development of Advanced Concepts for Nuclear Processes in Deuterated Metals

The excess heat generated in electrochemical cells with palladium cathodes and heavy water electrolyte appears to be far too large to result from chemical or metallurgical transformation. The evidence implies that the heat source is a nuclear reaction of some as yet undetermined nature.

INTEREST CATEGORY

Advanced nuclear systems

KEYWORDS

Electrochemical power generation
Palladium
Heavy water
Deuterium
Cold fusion
Heat source independent

BACKGROUND Since first announced in 1989 by Fleischmann, Pons, and Hawkins, "cold fusion" has been the subject of widespread interest and intense controversy. Palladium (Pd) cathodes electrochemically charged with deuterium (D) to unusually high D/Pd ratios exhibit episodes of heat in excess of measured electrical inputs. Although nuclear reaction products commensurate with the excess heat have not yet been observed, small but definite evidence of nuclear reactions have been detected at levels some 40 orders of magnitude greater than predicted by conventional nuclear theory.

OBJECTIVES To measure, optimize, and control the excess heat produced in highly deuterated palladium cathodes; to measure any signatures of possible nuclear reactions associated with the production of excess heat.

APPROACH The project team designed electrochemical cells that allowed precision calorimetry to be conducted while measuring all input heat from electrochemical and calibration resistor currents. The team operated 25 separate cell/calorimeters for periods of several days to several weeks each. Separately, the team operated 80 open cells to test various procedures for obtaining high cathode D/Pd ratios, a key condition for obtaining excess heat.

RESULTS Three conditions were found characteristic of all cells yielding episodes of excess heat: (1) a D/Pd ratio >0.9, (2) initial appearance times of 8 to 23 days, and (3) cathodic current densities above 0.1 A/cm^2. Excess powers ranging between a few percent to ~350% were observed, measured to an accuracy of ~0.5%. These excess powers integrated to a total of ~0.1 to 1.1 MJ for a ~2.5 g (1/40 mole) palladium cathode. Thus, the excess heats ranged between 4 to 44 MJ/mole of palladium, which was well above the largest known heats of chemical transformation in this or any other metal. The largest heat of chemical transformation in palladium is to the bromide at 0.9 MJ/mole. If the integrated excess powers are diluted by the electrochemically generated heat during the long initiation periods, net positive heat balances of 2 to 4% are obtained.

EPRI PERSPECTIVE This work confirms the claims of Fleischmann, Pons, and Hawkins of the production of excess heat in deuterium-loaded palladium cathodes at levels too large for chemical transformation. However, the phenomena were

obtained in only about half the cells. From the conditions of loading, initiation time, and current density on the successful observations of excess heat, it is understood why the phenomena are so difficult to attain. The conditions in the successful cells were not entirely under experimental control because the closed cells slowly leach silica and other materials from the anode and its supports as well as from the cell walls. This leached material can deposit on the cathode surface and interfere with the loading process. Also, the palladium purity depended on whatever was available from the manufacturer. Subsequent research has shown a pronounced batch effect on successful loading from different shipments of palladium from the same as well as from different suppliers. It is suspected that metallurgical conditions as well as impurity content may be the source of this batch effect.

The primary objective of further work on this subject will be to demonstrate which nuclear reactions, if any, are generating the excess heat. The only way to do this is to observe in at least roughly quantitative fashion the nuclear reaction products or "ashes." At this time, it is thought that the most likely ashes will be helium of mass 4 observable in the vapor phase of closed cells. The reaction producing helium needs to be known in order to maximize this excess heat phenomena for practical uses in the nuclear power industry.

PROJECT

RP3170-01

Project Managers: Thomas O. Passell; Joseph Santucci

Nuclear Power Group

Contractors: SRI International; Lockheed Missiles and Space Company, Inc.

For further information on EPRI research programs, call EPRI Technical Information Specialists (415) 855-2411.

Development of Advanced Concepts for Nuclear Processes in Deuterated Metals

TR-104195
Research Project 3170-01

Final Report, August 1994

Prepared by
SRI INTERNATIONAL
333 Ravenswood Avenue
Menlo Park, California 94025-3493

LOCKHEED MISSILES AND SPACE COMPANY, INC.
3251 Hanover Street
Palo Alto, California 94304

Principal Investigators
M. C. H. McKubre
S. Crouch-Baker
F. L. Tanzella
S. I. Smedley
M. Williams
S. Wing
M. Maly-Schreiber
R. C. Rocha-Filho
P. C. Searson
J. G. Pronko
D. A. Kohler

Prepared for
Electric Power Research Institute
3412 Hillview Avenue
Palo Alto, California 94304

EPRI Project Managers
T. Passell
J. Santucci

Deuterated Metals
Nuclear Power Group

DISCLAIMER OF WARRANTIES AND LIMITATION OF LIABILITIES

ORGANIZATION(S) THAT PREPARED THIS REPORT:

SRI INTERNATIONAL
LOCKHEED MISSILES AND SPACE COMPANY, INC.

ORDERING INFORMATION

Requests for copies of this report should be directed to the EPRI Distribution Center, 207 Coggins Drive, P.O. Box 23205, Pleasant Hill, CA 94523, (510) 934-4212. There is no charge for reports requested by EPRI member utilities.

ABSTRACT

An experimental program sponsored by the Electric Power Research Institute (EPRI) was undertaken at SRI International to explore the central idea proposed by Fleischmann et al. that heat, and possibly nuclear products, could be created in palladium lattices under electrolytic conditions. Three types of experiments were performed to determine the factors that control the extent of deuterium (D) loading in the Pd lattice and to search for unusual calorimetric and nuclear effects.

The overall conclusions of the loading studies are that, by careful control of the electrode pretreatment, the electrolyte composition, and the current density, Pd can be loaded to an atomic ratio D/Pd ≈ 1 and this loading may be sustained for periods of weeks.

Accurate, closed cell, state-of-the-art, mass flow calorimeters were designed, constructed, and calibrated. Extended calorimetric studies have confirmed the presence of a heat source that may be observed when certain criteria are met.

Rigorous attempts have been made to anticipate, exclude and define quantitative upper limits on artifacts and systematic error sources that may give the appearance of excess power. None of the artifactual sources considered can account for the excess power and heat observed. It is therefore concluded, tentatively, that the source of excess energy is an unexpected, and as yet unexplained, property of the D/Pd system. Further, the excess energy observed exceeds that of known chemical processes by two or more orders of magnitude.

Limited nuclear detection capability was included within this first project phase. Low-level detection was not attempted. These observations nevertheless indicate that any nuclear reaction quantitatively associated with the observed power and energy excess can only yield low-energy or stable products. Tritium, neutrons, or gamma rays are not quantitatively correlated with the excess power production observed.

ACKNOWLEDGMENT

The work described in this report was performed over a number of years and with the support and guidance of a number of individuals. In particular the authors would like to recognize the technical contributions of Jason Chao, Bindi Chexal, Thomas Passell, Joseph Santucci, and Robert Weaver, and the special support and guidance of John Taylor, all of EPRI.

An intellectual debt is acknowledged also to our advisors and mentors. Martin Fleischmann, Peter Hagelstein, Giuliano Preparata and Kevin Wolf.

Finally, those of us who have worked on this document would like to acknowledge our debt to the missing author, Andrew Riley, without whom this work would have been less.

CONTENTS

ILLUSTRATIONS

TABLES

1

INTRODUCTION

An experimental program sponsored by the Electric Power Research Institute (EPRI) was undertaken at SRI International to explore the central idea proposed by Fleischmann et al.[1] that heat, and possibly nuclear products, could be created in palladium lattices under electrolytic conditions. Three types of experiments were performed to determine the factors that control the extent of deuterium (D) loading in the Pd lattice and to search for unusual calorimetric and nuclear effects. We summarize here selected examples of power and energy output observed calorimetrically to be in excess of known sources of input power and energy.

Following the results reported by Fleischmann et al.[1] considerable effort has been expended to test the hypothesis that the electrochemical loading of deuterium into palladium leads to the production of more energy than is predicted to arise from known chemical or electrochemical phenomena. From all the calorimetric results reported to date, it is evident that the ultimate acceptance or rejection of the original hypothesis will not be determined by calorimetry alone but only in addition to the confirmed observation of other products of the energy-producing process, which will ultimately lead to the development of supportable new theories. However, because of the potential importance of the energy-related aspects of the phenomenon, calorimetric studies provide the most appropriate basis from which to undertake a comprehensive investigative program.

Some of the discrepancies in the results of the various calorimetric studies undertaken thus far may be traced to the different experimental approaches adopted; not all of these may be expected to be equally accurate or reliable. More important, perhaps, in accounting for the variety of reported calorimetric results, is the wide range of possible conditions that may be employed (or encountered) in a given experiment, some of which will be difficult to control or reproduce. This consideration, in particular, may hinder attempts to replicate the original experiments of Fleischmann et al. Nonetheless, the calorimetric results reported to

date make it evident that the experimental hypothesis referred to above cannot be supported *as stated;* additional criteria must be satisfied.

The central postulate guiding the experimental program was that anomalous effects previously unobserved or currently unexplained in the deuterium-palladium system occur at a very high atomic ratio of D/Pd. Emphasis was placed on studying phenomena that provide a fundamental understanding of the mechanism by which D gains access to the Pd lattice and how very high atomic ratios (near, at, or perhaps beyond unity) can be achieved and maintained.

With appropriate control of the interfacial conditions, we have shown it possible to load both H and D into Pd to molar ratios of approximately unity. Electrode preconditioning apparently plays a significant role in the ability to attain and maintain high loading under electrochemical conditions and in the appearance of unaccounted-for heat in deuterium-loaded systems. Helium implantation provides a suitable means of surface activation to facilitate loading; the presence of such implanted helium is not obviously implicated in the generation of excess power.

At the outset of the experimental program described here, it was postulated that anomalous effects previously unobserved—and presently unexplained—in the deuterium-palladium system will occur at deuterium loadings (D/Pd atomic ratios) approaching or exceeding unity. Thus a central feature of the experiments described here is the (electrochemical) control and continual *in situ* measurement of the deuterium (and hydrogen) loading during the entire calorimetric experiment.

Further, it was decided that the most accurate and sensitive thermal measurements would be obtained using a sealed (thermodynamically closed) electrochemical cell—with knowledge at all times of the composition of the reacting system—in combination with a flow calorimeter. The experimental approach adopted here thus differs significantly from that originally described by Fleischmann et al. [2] and from the majority of subsequent calorimetric studies.

To characterize the electrochemical kinetic and thermodynamic processes that control the absorption of D into Pd, we measured the interfacial impedance and the Pd cathode voltage with respect to a reference electrode. Measurements of the Pd solid phase resistivity were used to monitor on-line the degree of loading atomic

ratios, specifically D/Pd, H/Pd, and H/D. The resistance ratio/atomic ratio functionality was calibrated primarily by reference to the works of Baranowski[2-4] and Smith[5,6] but also by volumetric observation of the displacement of gas during loading in a closed system at constant pressure and temperature and by anodic coulometry.

The overall conclusions of the loading studies are that, by careful control of the electrode pretreatment, the electrolyte composition, and the current density, Pd can be loaded to atomic ratio D/Pd ≈ 1 and this loading sustained for periods of weeks.

Calorimetric experiments were performed in palladium rods highly loaded with D and/or H and electrolyzed at substantial current densities (typically 300-600 mA cm^{-2}, but up to 6400 mA cm^{-2}) for considerable periods (typically 1000-2000 hours).

Our calorimeters were designed with the philosophy that, in precise calorimetry and in the search for unusual reaction products, it is desirable to have a closed system and a knowledge at all times of the composition of the reacting system. All experiments were performed with closed and sealed electrochemical cells operating from 40 to 10,000 psi above atmospheric pressure. Axial resistance measurements were made to monitor the D/Pd or H/Pd ratio.

Approximately 30 experiments have been performed with flow calorimeters operating at constant power input. The calorimeters were designed and constructed with the following features:

- A conceptually simple system based on the first law of thermodynamics.
- Maintenance of complete control of operating parameters (including cell temperature).
- A large working range of power input and output (0.1-100 W).
- On-line monitoring of all important variables.
- Multiple redundancy of measurement of critical variables such as temperature.
- High accuracy (the greater of 50 mW or 0.5%) and precision (10 mW or 0.1%)
- Known sources of potential error to yield conservative estimates of output power.
- Steady state operation, leading to simple analysis.

Two systems of flow calorimeters were designed in accordance with the principles outlined above. One system accommodated up to four large electrochemical cells (working volume up to 500 cm^3 and power input ≥ 100 W). The other accommodated three "small" cells (working volume 50 cm^3 and power input up to ~ 30 W).

All experiments were performed with thermodynamically closed electrochemical cells at D_2 partial pressures between ambient and ~10,000 psi. In high pressure cells, the charging current was sustained by the anodic reaction $1/2\ D_2 + OD^- \rightarrow D_2O + e^-$ (in base). At higher anodic current densities or low D_2 partial pressures, O_2 was evolved at the anode. A large area catalyst was provided in the head space of the cells to recombine evolved O_2 and D_2 so that the net reaction in all cells after the Pd rod is loaded is $D_2O \rightarrow D_2O$, for which the thermoneutral voltage is zero.

Constant current or slowly ramped conditions were used in all cases so as to minimize the potential for unmeasured contributions to the input power. Commonly, experiments were performed electrically in series to test the effects of different variables, e.g., D_2O compared to H_2O.

The power input to the calorimeter by the electrochemical current was considered to be the product of that current and the voltage *at the isothermal boundary*. Under experimental conditions, this input power changed owing to voltage or resistance variations in the cell, or at times when the current was ramped. This change had two undesirable consequences. A change in input power changed the cell temperature so that the electrochemical conditions were no longer under control. A change in the temperature also moved the calorimeter from its steady state as the calorimeter contents took up or released heat. To minimize these effects, we used a compensation heater to correct for changes in electrochemical power so that the sum of the heater and electrochemical power input to the calorimeter was held constant. A computer-controlled power supply was used to drive the compensation heater element operated in galvanostatic mode to avoid possible unmeasured root-mean-square (rms) heat input. This heater was also used for calorimeter calibration, in which the input power was measured as the product of the heater current and voltage at the isothermal boundary.

For the thermodynamically closed and intentionally isothermal systems described here, output power was observed to be as much as 300% in excess of the electrochemical input power or 24% above the known total input power. When excess power was present, it was more typically in the range 5%-10%, in a calorimeter that was accurate to better than ±0.5%. The largest excess energy observed corresponded to 1.08 MG, or 45.1 MJ/mol, or ~450 eV/atom normalized to the Pd lattice or to the deuterium in the palladium at a loading of ~1.

The experiments exhibit internal repeatability when the three criteria above are achieved. Apparent excess power was observed under these conditions when the current density reached a critical value, and excess power was not observed when the current density was reduced below the critical value. Furthermore, the threshold current density appeared to decrease with time, up to the point that, because of interfacial or external effects, high values of loading could no longer be attained or maintained, and no excess power was observed on ramping the current.

Some degree of experimental reproducibility between cells was also observed. Five experiments were performed in an attempt to replicate a prototype experiment, with only minor variations in electrode and electrolyte treatment. All the heavy water experiments produced excess heat, reproducing in general form the observation of excess heat in the prototype experiment. However, excess power in these four experiments was *not* produced in exactly the same amounts, or at exactly the same times, in response to the same stimuli. Neither could we reproduce exactly the electrochemical conditions of cathodic overvoltage, the loading (resistance ratio), and the interfacial impedance. Clearly, there are issues of interfacial contamination that arise in experiments with sustained high current electrolysis and await resolution in future research.

Except for times when the calorimeter was caused to depart significantly from its steady state condition and during periodic fluctuations introduced by nonconstant recombiner operation, "negative excess" was never observed. Where significant quantities of H_2O were used in the electrolyte, P_u was always zero. Also, no excess was observed before a critical "initiation time," even in cells that later yielded values of $P_u > 0$.

As demonstrated in twin series experiments (P13 and P14, P15 and P16), excess power was observed asynchronously in series cells. That is, cells subjected to the same current from the same source and monitored in a multiplexed manner to the same electronics were observed to yield $P_u = 0$ in one cell but $P_u > 0$ in the other. It is very difficult to attribute such an observation to an artifact of the common instrumentation.

The association of apparent excess power with a set of necessary conditions for the D/Pd system implies a degree of reproducibility. These conditions are not easy to attain, a fact that may explain the irreproducibility of the phenomenon of excess heat. Examined separately, the three criteria may be taken as normal conditions of reacting systems (chemical or nuclear). The criterion of loading indicates a thermodynamic driving force, a measure of the activity or chemical potential of a possible reactant species. The need to maintain loading for considerable periods of time before the onset of excess heat suggests a mass transport constraint, possibly involving nucleation and growth of an active region within the volume of the bulk Pd lattice. The final requirement of a large interfacial current density suggests a kinetic criterion. Because of the intimate coupling between electron flux and the creation of adsorbed D, and a very facile equilibrium between adsorbed and absorbed D, current density can be viewed as the means by which absorbed D are given the energy to undergo reaction.

As a final note, we are unable to account for the observed excess heat by any artifact known to us and are forced to conclude that the source of the excess power is a property of the D/Pd system. Further, we cannot account for the measured excess power and energy by any chemical or mechanical process with which we are familiar.

1.1 References

1. M. Fleischmann, S. Pons and M. Hawkins, "Electrochemically Induced Nuclear Fusion of Deuterium", J. Electroanal. Chem., **261** (1989) p. 301 and errata, **203** (1989), p. 87.
2. B. Baranowski and R. Wisniewski, Phys. Stat. Sol. 35, 593 (1969).
3. B. Baranowski, S. M. Filipek, M. Szustakowski, J. Farny and W. Woryna, J. Less-Common Metals, **158**, 347 (1990).
4. A. W. Szafranski and B. Baranowski, Phys. Stat. Sol. (a) **9**, 435 (1972).

5. G. Bambakidis, R. J. Smith and D. A. Otterson, Phys. Rev. **177**, 1044 (1969).
6. R. J. Smith and D. A. Otterson, J. Phys. Chem. Solids **31**, 187 (1970).
7. B. Baranowski and R. Wisniewski. Phys. Stat. Sol., **35**, 593 (1969).
8. A. W. Szafranski and B. Baranowski. Phys. Stat. Sol. (a), **9**, 435 (1972).

2

DEGREE-OF-LOADING STUDIES

2.1 Introduction

Of central importance to the study of anomalous power generation in deuterated palladium systems are the means by which the deuterium is *introduced* into the palladium, and the means by which it is *retained* within the palladium (for the extended periods of time necessary for comprehensive calorimetric studies). In this study, a series of electrochemical experiments were carried out (so-called degree-of-loading experiments) to determine the important factors in accomplishing both the introduction and retention of deuterium (and hydrogen) in palladium cathodes. The understanding and insight thus gained were utilized in the various calorimetric experiments reported in Section 3.

The section on experimental method is a slight modification of the text of the manuscript "Aspects of the electrochemical loading of hydrogen and its isotopes into palladium," published in Proceedings of the *Symposium on Hydrogen Storage Materials, Batteries, and Electrochemistry*, Eds. D. A. Corrigan and S. Srinivasan, Electrochemical Soc. Inc., 1992, p. 269. It deals with the important experimental methods employed in the degree-of-loading experiments as well as with pertinent physical properties of the cathode compositions of interest.

2.2 Experimental Methods

The section on degree-of-loading experiments summarizes all the degree-of-loading experiments undertaken during this program and presents a detailed description of those of significance.

At room temperature, palladium reacts with each of the isotopes of hydrogen to form two binary phases, designated α- and β-, both of which are considered to contain the light element in the octahedral interstices of the face centered cubic (f.c.c) palladium[1,2]. At 303 K, the phase limits in the cases of hydrogen and deuterium are $\alpha_H\ 0 \le x \le 0.009$; $\beta_H\ x \ge 0.608$; $\alpha_D\ 0 \le x \le 0.01$; $\beta_D\ x \ge 0.60$, where x denotes the loading, *i*.e. the H(D)/Pd atomic ratio. Although the properties of the α-phase have been

extensively documented,[1,2] somewhat less characterization has been reported for the β-phase, especially at loadings significantly larger than those corresponding to 1 atm of gas pressure (e.g. at 303 K, for loadings larger than 0.70 in the case of hydrogen and 0.67 for deuterium[3]). Some aspects of the preparation and characterization of the highly loaded β-phases of the H-Pd and D-Pd systems are briefly reviewed below. Included in this review is a brief discussion of some of the methods employed for the measurement of high hydrogen loadings.

Although electrochemical methods have been employed to load hydrogen into palladium (see below), it is not widely recognized that such methods may also be used to prepare highly loaded β-phase compositions in the H-Pd and D-Pd systems. This work includes some experimental demonstrations of the attainment and *in situ* measurement of high loadings in these systems by electrochemical means.

2.2.1 Conventional Methods for Characterization of the β-Phase Measurement of High Hydrogen Loadings Phase

Although a variety of techniques have been employed to measure loadings in the H-Pd and D-Pd systems, not all of these are suitable for the measurement of high loadings in the β-phase. Some that have been used for in this purpose are described briefly below.

Mass Spectrometry. A direct but *ex situ* method entails vacuum desorption of the absorbed hydrogen at elevated temperature, followed by quantitative mass spectrometric analysis.[4-6] Owing to the tendency of highly loaded palladium to lose some hydrogen relatively quickly once the confining gas pressure is removed, any ex situ method will necessarily give a conservative estimate of the loading. However, this method, among others, is useful in that it serves to calibrate indirect but *in situ* loading measurement methods.

Resistance Ratio. Since the work of Fischer,[7] it is recognized that the electrical resistance of a sample of palladium exposed to hydrogen (or deuterium) varies systematically with hydrogen content.[1] At room temperature, the resistance ratio (defined as R/R° where R is the resistance at a particular loading and R_0 is the resistance of pure palladium), increases from unity as the loading increases from

zero, reaching a maximum at a loading of approximately 0.7, irrespective of the hydrogen isotope employed. Thereafter, the resistance ratio decreases relatively quickly with increasing loading. The resistance ratio/loading variations for hydrogen and deuterium are shown in Figure 2-1. These composite curves are designed to best represent the results obtained from a variety of loading studies.[5,6,8-14] Although the detailed form of the variations shown in Figure 2-1 has been the subject of extensive discussion (see, for example, (Refs. 15 and 16), these curves are treated here as a convenient empirical tool by which the loading may be estimated. *In situ* measurement of the electrical resistance of a β-phase sample is particularly useful for studying electrochemical loading, since it enables relatively subtle loading effects associated with changes in current density and overvoltage, for example, to be monitored.

Volumetric methods. A volumetric method has been employed for direct measurement of the composition in situ during the electrochemical loading of palladium cathodes.[17] In this technique, an otherwise sealed electrochemical cell is connected to a manometer. Initially, the head space above the cell is filled with hydrogen (or deuterium) and contains a hydrogen-oxygen recombination catalyst. During electrolysis, the oxygen evolved at the anode is converted to water; hence, at constant pressure, a decrease in volume is observed owing to hydrogen uptake by the cathode. With this technique, the loading may be measured to an accuracy of a few per cent.

2.2.2 Preparation of the β-Phase

Two methods are commonly employed for preparation of highly loaded β-phase: gas-phase loading and electrochemical loading. The former has been more extensively studied, most notably by Baranowski and co-workers (for a review, see Ref. 18).

With high-pressure apparatuses, the properties of the β-phase have been characterized up to approximately 20,000 atm of gas pressure, which corresponds to loadings in excess of unity, as described further below. In gas-loading experiments, the pressure, P, is conveniently employed as the independent variable. When the chemical properties of the β-phase are of interest, it is more useful to express results

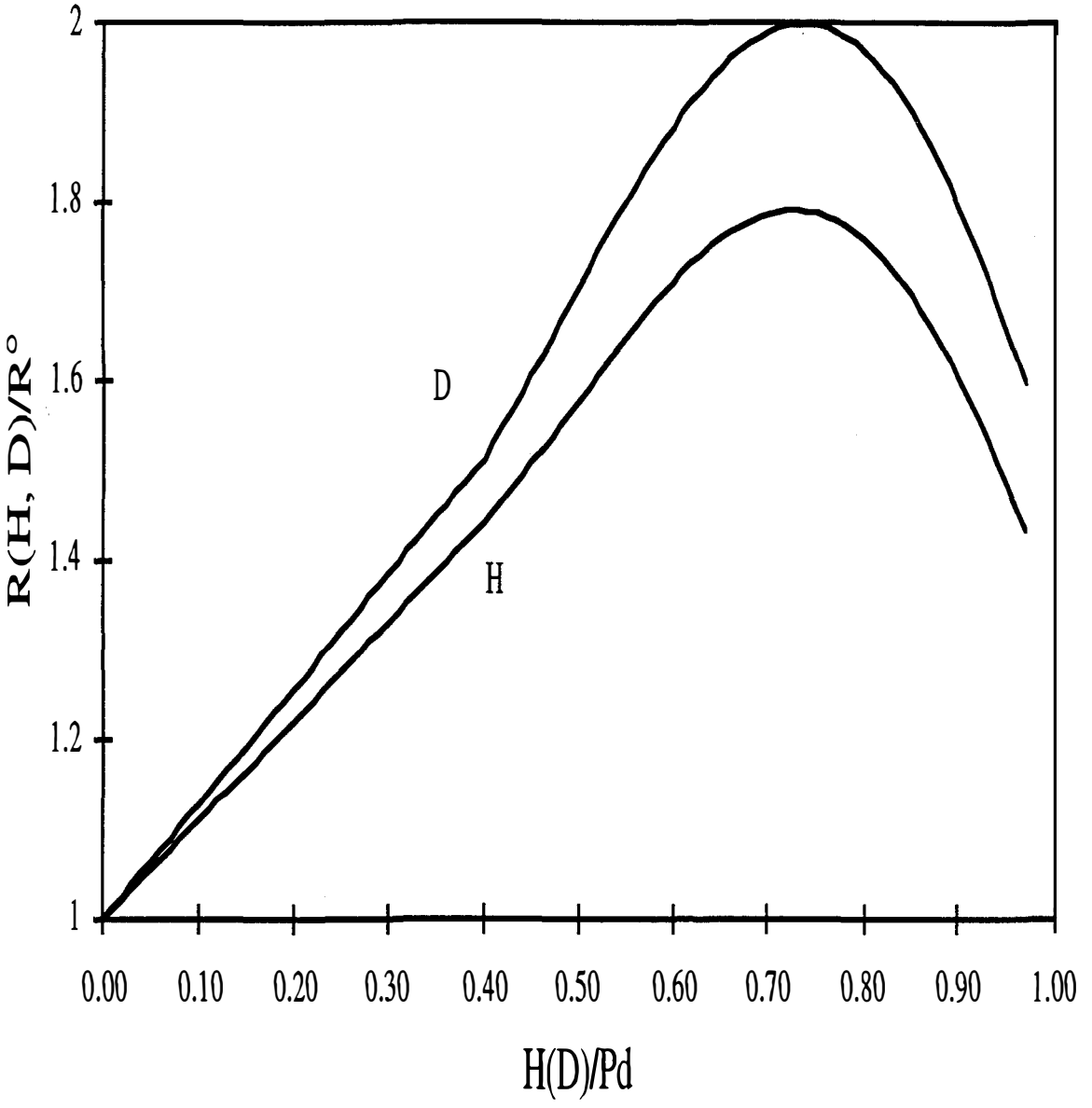

Figure 2-1
Resistance/loading variations in the H-Pd and D-Pd systems at 298 K.

in terms of the gas fugacity, f, as the independent variable. For a pure gas, the fugacity and the pressure are related by[19]

$$\ln \frac{f}{P} = \int_0^P \left\{ \frac{V_m}{RT} - \frac{1}{P} \right\} dP \qquad (2\text{-}1)$$

where $\frac{f}{P} \rightarrow 1$ as $P \rightarrow 0$ and V_m is the pressure-dependent molar volume. Up to a pressure of approximately 20,000 atm, V_m has been determined for both hydrogen and deuterium (see, for example, Refs. 20 and 21). The resulting fugacity/pressure relationship at 298 K for either gas is shown in Figure 2.-2 (the results for hydrogen and deuterium are closely similar when the scales in Figure 2-2 are used. Further, for convenience in calculation, it is of interest that the fugacity/pressure variation in Figure 2-2 is closely approximated by

$$\phi = \Pi \varepsilon \xi \pi \left\{ \frac{\alpha \supseteq \Pi}{P \supseteq T} \right\} \qquad (2\text{-}2)$$

where P is given in atmospheres, R = 8.314 JK^{-1} mol^{-1}, T = 298 K, a = 1.3) in the appropriate units).

It is not readily apparent from the early literature that electrochemical loading of palladium cathodes can produce highly loaded β-phase. For example, loadings of 0.7 in the case of hydrogen[11] and 0.67 for deuterium[13] were reported. Later studies, however, showed that still higher loadings could be achieved at modest current densities. Thus, for deuterium, a loading of approximately 0.9 was obtained at 273 K with an acidic electrolyte.[5] Further, in the hydrogen case, a loading of approximately 0.95 has been achieved under similar conditions.[6]

2.2.3 *Physical Properties of the β-Phase*

Primarily as a result of gas-loading measurements, the following physical prperties, among others, of the β-phase may be described.

Loading/Pressure Variation. Experimental data[12,14,22] for the variation of loading with pressure for the β-phase of the H-Pd system at 298 K are shown in Figure 2-3. These data indicate that a hydrogen pressure in excess of 10,000 atm. is necessary to achieve an approximate loading of unity at this temperature. Note that, at a pressure of 10,000 atm, the corresponding hydrogen fugacity is approximately

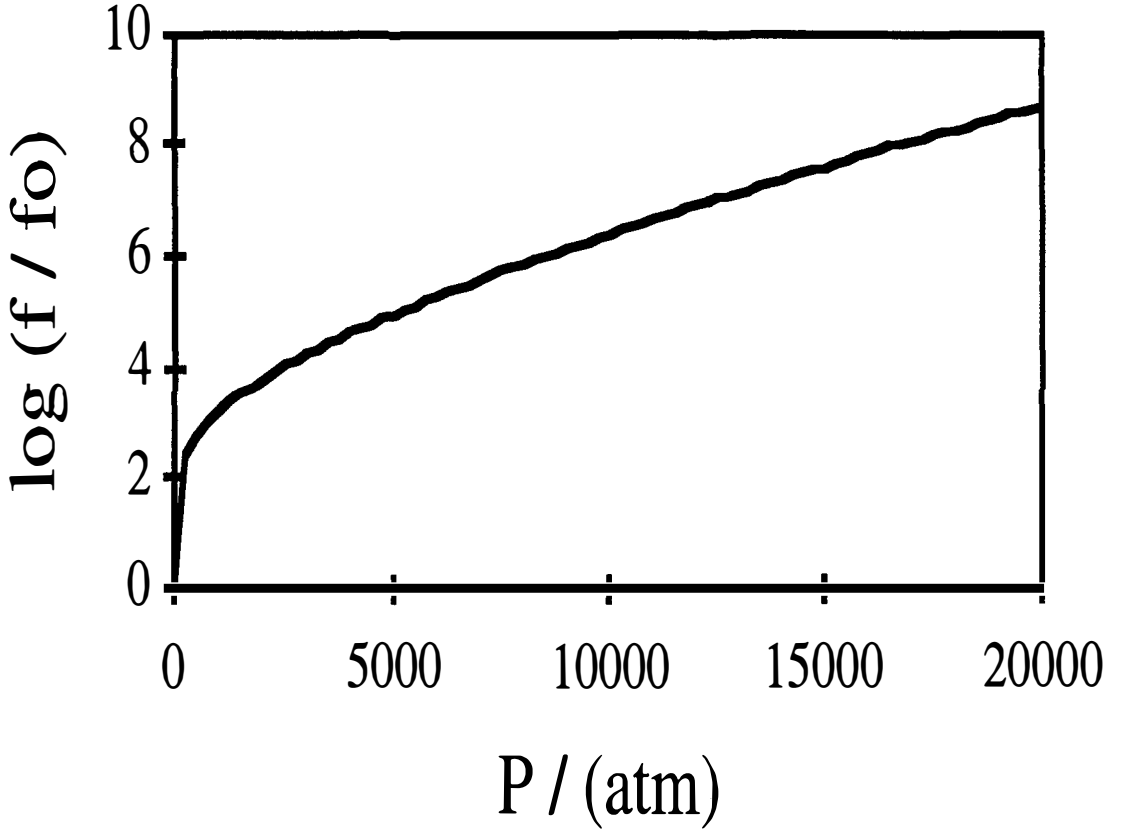

Figure 2-2
Fugacity/Pressure Variation for Hydrogen at 298 K.

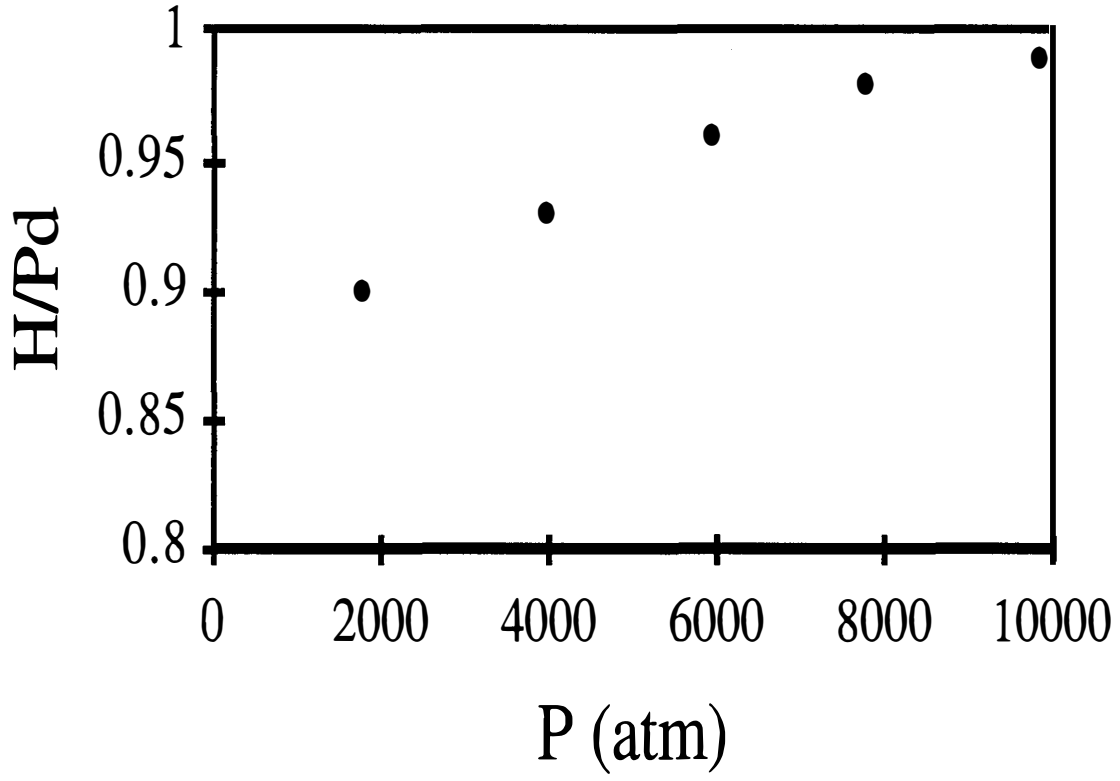

Figure 2-3
Loading/pressure variation in the H-Pd system at 298 K.[14,22].

2.5×10^6 atm. For loadings in excess of 0.9, the corresponding data for deuterium do not appear to have been measured directly. However, an approximation to the loading/pressure variation for deuterium may be obtained using the results of Wicke and Nernst,[3] as described by Baranowski et al.[14] It is apparent that, for the same gas pressure, the deuterium loading is approximately 0.025 less than the corresponding hydrogen loading in the range $0.9 \leq x < 1.0$.

Resistance Ratio/Fugacity Variation. The variations of the resistance ratio of the highly loaded b-phase (with both hydrogen and deuterium) with fugacity at 298 K have been determined experimentally[12,14,15,23] and are shown in Figure 2-4. At very high fugacities, corresponding to loadings approximately equal to and in excess of unity, a distinct change in the slopes of the resistance/fugacity curves is apparent. This change of slope has been interpreted in terms of the occupation of tetrahedral sites at very high loadings.[14,15] Firm crystallographic evidence, which has not yet been obtained, is required to substantiate this interpretation. In this context, the preparation and preliminary characterization of a tetragonal hydride phase of nominal composition $PdH_{1.33}$ has been reporte.[24,25] This phase, formed either by bombarding palladium films with hydrogen ions or by heating palladium films in hydrogen and cooling rapidly, is stated to contain the hydrogen within the approximately tetrahedral interstices of a body centered tetragonal palladium lattice.

Chemical Diffusion Coefficient. The time-dependent relaxation behavior of the resistance ratio of a β-phase sample exposed to an incremental change in loading may be employed to evaluate the composition dependence of the chemical diffusion coefficient of hydrogen (or deuterium).[26,27] At 298 K, the chemical diffusion coefficients of both hydrogen and deuterium in the β-phase are roughly equal; both decrease smoothly from approximately 10^{-6} cm^2 s^{-1} at $x = 0.8$ to less than 10^{-7} cm^2 s^{-1} as the loading approaches unity.

Hydrogen Overvoltage. In the case of electrochemical loading of palladium, it is of interest to determine how the loading is related to the thermodynamic part of the cathode overvoltage. In the case of the hydrogen evolution reaction, various relationships between the overvoltage, equivalent pressure, and the details of the hydrogen evolution kinetics have been discussed.[28] Referred to the standard hydrogen electrode, the purely thermodynamic part of the hydrogen overvoltage,

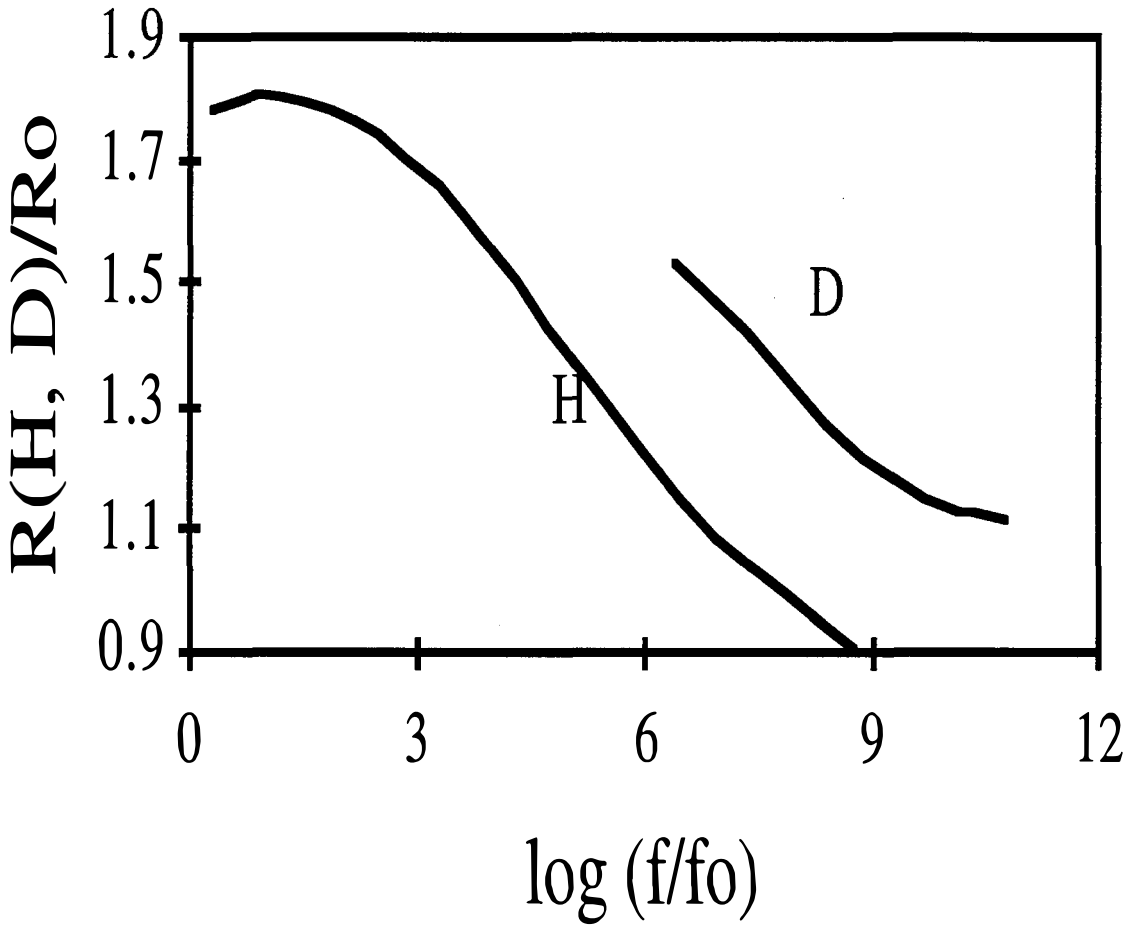

Figure 2-4
Resistance/fugacity variations in the H-Pd and D-Pd systems at 298 K.[12,14,15,23]

η_{th}, is related to the gas fugacity on the cathode surface (and, hence, the loading) by

$$\eta\tau_{\eta} = -\frac{RT}{2F} \ln f \qquad (2\text{-}3)$$

Thus, at 298 K, a fugacity of 10^7 atm is equivalent to a thermodynamic overvoltage of approximately - 200 mV.

2.2.4 Experimental Aspects Of Electrochemical Loading

To study the electrochemical loading of palladium, two (similar) designs of electrochemical cell were employed, one of which is shown in Figure 2-5. In this design, a quartz tube approximately 1 inch in diameter and 4 inches long was employed as the cell container. The top of the tube, of somewhat larger diameter, was used to contain the recombination catalyst. A cylindrical cage was constructed of quartz rods, held together with PTFE discs, and located within the cell container. A platinum wire (0.5 mm diameter, 1 m long) wound on the outside of this cage served as the anode. The cylindrical palladium cathode was mounted vertically in the center of the cage. To monitor pressure changes inside the cell and thus determine the reliability of the recombination catalyst over long periods, the cell, which was otherwise sealed, was connected via a gas vent to a bubbler. In a second cell configuration, designed for use at moderately elevated pressures if necessary, a sealable cell container was constructed of nickel. The dimensions of the nickel cell body, as well as the internal cell configuration, were similar to those of the quartz cell body described above. A thin PTFE liner was inserted within the cell body to prevent corrosion of the cell by the alkaline electrolyte. During loading measurements, the cells were mounted within a water bath held at approximately 30°C.

Cylindrical palladium cathodes 3 mm in. diameter and 3 - 5 cm long were made from wire supplied by Engelhard. (The as-supplied wire diameter was slightly larger than 3 mm; the excess material was removed mechanically). Typically, the cathodes were annealed *in vacuo* at 800°C for 3 hours and cooled in 1 atm of argon. The cathodes were then etched in aqua regia (deuterated if necessary) and rinsed with (light or heavy) water to remove any oxide surface films.

In situ loading measurements were made via determination of the axial resistance of the palladium cathode with a Tecrad DMO-350 (3-1/2 digit) digital micro-ohmmeter.

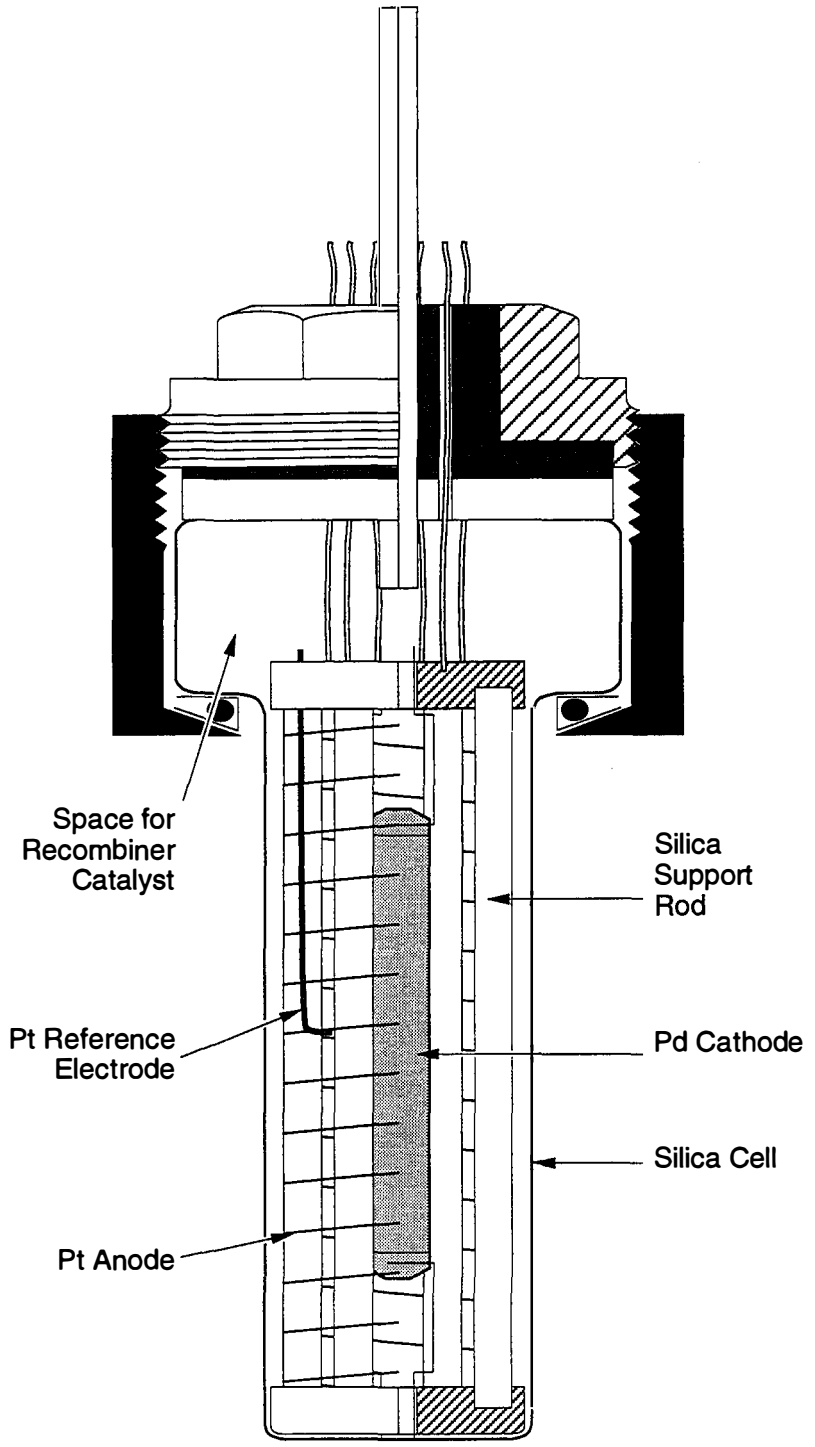

Figure 2-5
Electrochemical Cell Used for Loading Measurements

This instrument is capable of measuring resistance values in the range 10^{-8} to 0.2 Ω. Each cathode was furnished with four notches (each 1 mm wide and 1 mm deep), two at each end of the rod (1 mm apart). Platinum leads were wound and spot-welded within each notch. One pair of leads, located effectively at the ends of the cathode, served to deliver a 10-A square-wave pulse of approximately 20 ms duration; the resulting voltage was detected using the second pair of leads (located within the first pair, with respect to the rod axis). Resistance measurements were made at 5-minute intervals during loading. For the cathode geometry employed here, the unloaded palladium resistance was approximately 410 mΩ for a 3-cm rod.

2.2.5 *Results and Discussion*

The variations of cathode resistance with time for three loading experiments are shown in Figures 2-6 through 2-8. The conditions for each experiment are described in the figure captions. These three examples are only a small fraction of the loading experimentation that has been carried out; however, they are representative of the results that may be obtained if attention is paid to certain aspects of the loading process.

In all three experiments, the formation of highly loaded β-phase occurs in a few tens of hours at the current densities employed here. The results in Figures 2-6 through 2-8 indicate that, for both hydrogen and deuterium, the maximum value of the resistance ratio is lowered under dynamic conditions, relative to the value expected under equilibrium conditions, (Figure 2-1). This is due to the presence of H (or D) concentration gradients within the cathodes during the loading process; this effect is effectively absent once a steady-state loading has been achieved. By reference to Figure 2-1, it is apparent that steady-state loadings of at least 0.9 have been achieved in the three experiments reported here.

From the data shown in Figures 2-6 through 2-8, it is apparent that a current density of approximately 100 mA cm^{-2} is required to achieve loadings of 0.9 or more in the cell configuration employed here. Previous studies[5] have reported achieving similarly high loadings for deuterium in fine palladium wires by using a current density of approximately 12 mA cm^{-2}. In this previous study, a porous membrane was used to minimize the possibly deleterious effects of diffusion of oxygen from the anode to the palladium cathode. The observation that similar loadings may be achieved at different current densities is not surprising. As discussed above, the

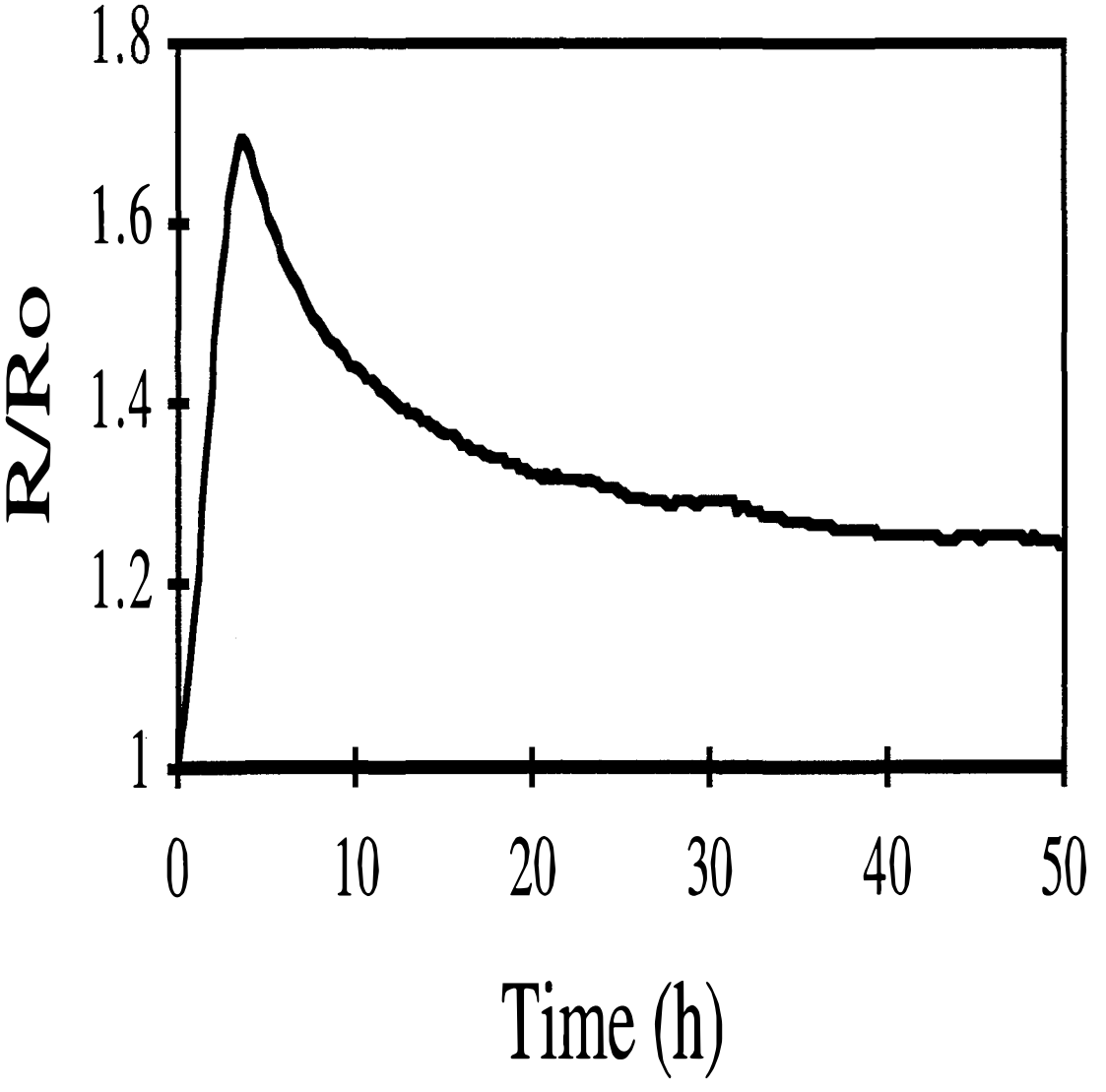

Figure 2-6
Resistance/time variation for a palladium cathode under the following conditions: Electrolyte = 1 M LiOH; current density = 100 mA cm^{-2}.

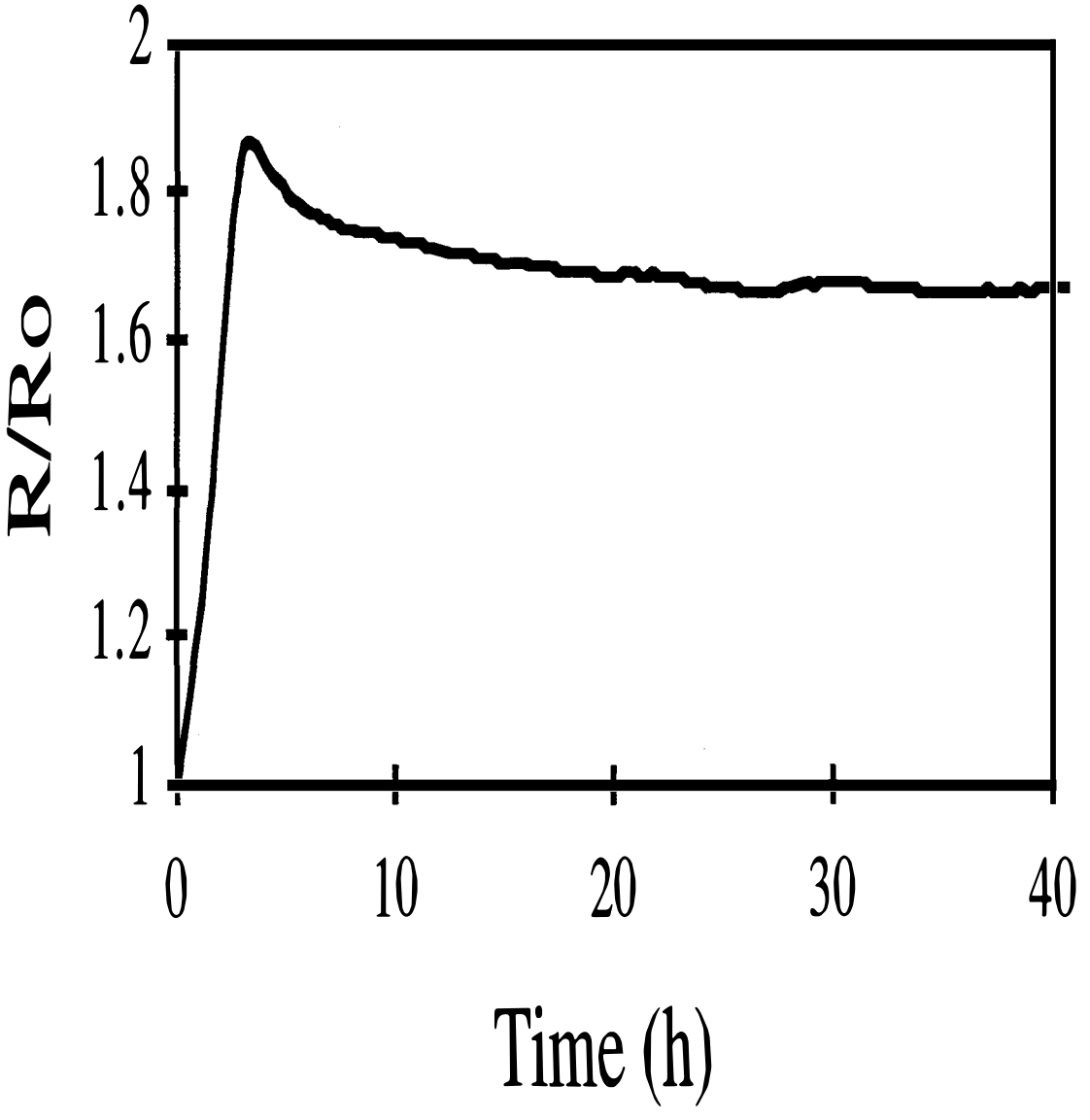

Figure 2-7
Resistance/time variation for a palladium cathode under the following conditions: Electrolyte = 1 M LiOD + $(NH_2)_2CS$; current density = 100 mA cm^{-2}

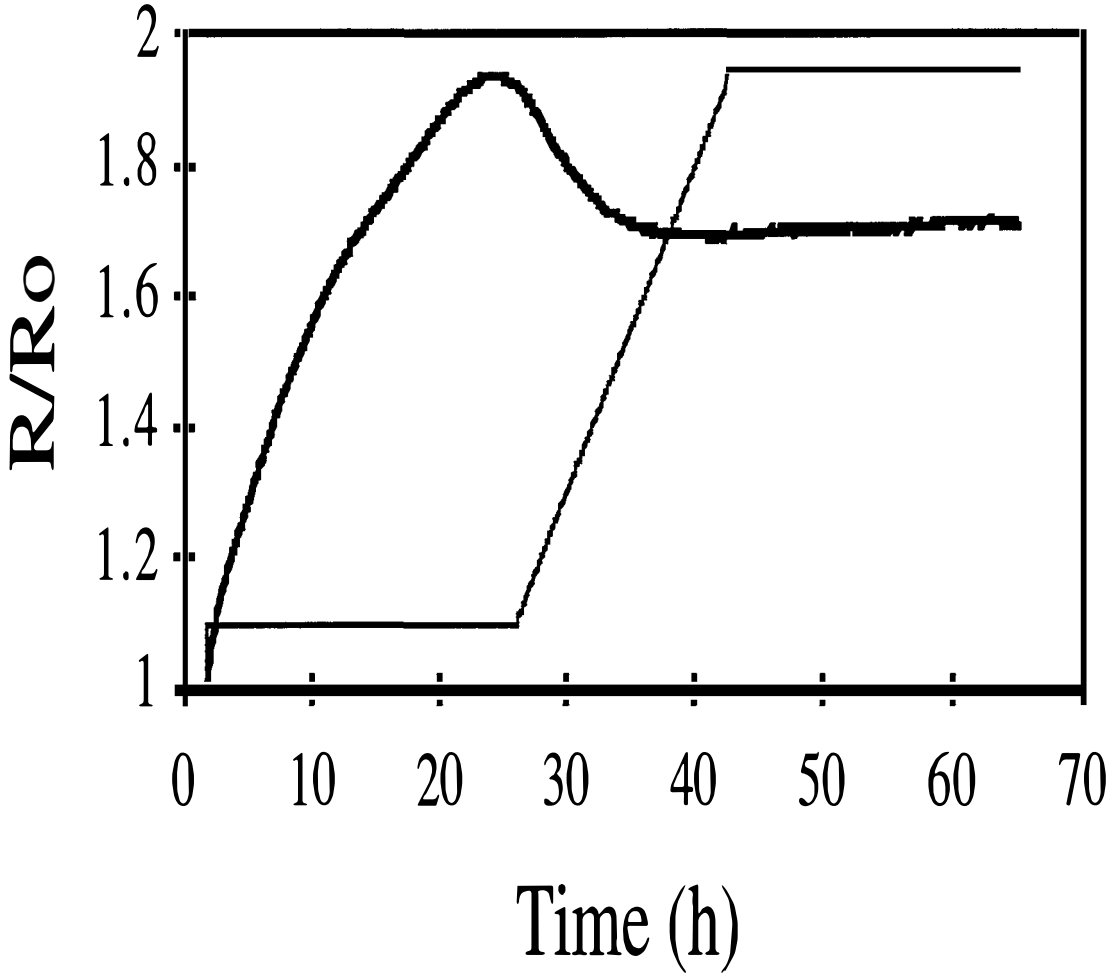

Figure 2-8
Resistance/time variation for a palladium cathode under the following conditions: Electrolyte = 1 M LiOD; current density = 33 mA cm^{-2}, ramped to 333 mA cm^{-2}. The current ramp profile is shown as a solid line.

steady-state loading is determined essentially by the thermodynamic part of the cathode overvoltage and is not, in the first instance, determined directly by the current density. Thus, for cells with differing geometries and, more importantly, *differing states of the cathode surface*, at the same current density, the cathode overvoltages (and hence the loadings) may differ. For a given electrode, however, the cathode overvoltage and the current density are, of course, related. Hence, to achieve uniform loading, it is important that the current density be uniform over the entire electrode.

To attain and *sustain* high loadings, it is essential to guarantee that the cathode surface is maintained in a suitable condition, and thus minimize those effects, both mechanical and electrochemical, that tend to promote deloading. Two effects are particularly important in this regard:

(i) It is unlikely that the current density will be uniform within a surface crack or fissure, and such features will act as sites for deloading. Cracks may form during the loading process as the α/β miscibility gap is traversed. The tendency for crack formation may be minimized by loading relatively slowly in the initial stages; it has been observed that cathodes which load quickly up to the resistance maximum rarely load further. An alternative procedure is to pre-load the palladium from the gas phase (to a loading of approximately 0.7) at an elevated temperature such that the miscibility gap is not encountered, and then cool slowly to room temperature.

(ii) Certain chemical species, when deposited on the cathode surface, will tend to lower the cathode overvoltage by catalyzing the recombination of adsorbed hydrogen atoms. Platinum may be particularly deleterious in this regard. Clearly, the presence of such species should be minimized. Another group of additives, the so-called recombination poisons, may be advantageous in the early stages of loading. However, they are typically relatively complex chemical species that are susceptible to decomposition within the electrochemical cell. Thus, their effects are typically short-lived.

This list is not intended to be exhaustive. The *reproducible* attainment and maintenance of high loadings may be realized only when a suitable cathode surface state has been achieved. Undoubtedly, several factors are important in determining the optimum surface condition, not all of which are presently understood.

2.2.6 Conclusions

(i) Highly loaded compositions within the β-phase of the H-Pd and D-Pd systems may be prepared by both gas-phase and electrochemical means. Several physical properties of the β-phase have been studied up to loadings of unity and possibly beyond.

(ii) On-line resistance measurements provide a particularly convenient method for monitoring the loading in a palladium cathode.

(iii) Loadings of 0.9 or more can be achieved electrochemically.

2.3 Degree-Of-Loading Experiments

Table 2-1 presents an overview of all the degree-of-loading experiments undertaken during this program. This section discusses the resistance/time data for experiments P20 - P29 and summarizes theoretical calculations of resistance/time data for various loading conditions.

2.3.1 *Results From Electrodes P20 Through P29*

The resistance ratio (R/R°) as a function of time for electrodes P20 through P29 is shown in Figures 2-9 through 2-18. All R/R° curves exhibit a characteristic shape with an initial increasing region leading to a maximum value followed by a decrease to a final value that usually varied somewhat with time.

Figure 2-19 shows the short-time loading curves (up to 30 hours) for electrodes P25 [1 M LiOD + $(NH_2)_2CS$], P26 (1 M LiOD + Na_2S), and P28 (1 M LiOD). These three electrodes exhibited relatively fast increases in R/R°, with a maximum value after about 3 hours of charging. Figure 2-20 shows the short-time curves for electrodes P23 (0.5 M D_2SO_4 + As_2O_3), P24 (1 M LiOD + As_2O_3), and P27 (1 M LiOD + As_2S_2). These three electrodes were run in electrolytes containing arsenic salts and exhibited much slower rates of loading, with no maximum value during the first 30 hours. The lowest rate of loading is seen for the electrode in acidic solution (P23), in comparison to the two electrodes in alkaline electrolytes (P24 and P27). Figure 2-21 shows the short-time behavior for electrodes P20 (0.5 M D_2SO_4) and P22 (0.5 M D_2SO_4 + NaI). These two electrodes exhibited relatively fast increases in R/R° but did not exhibit a maximum value during the first 30 hours. Finally, Figure 2-22 shows R/R° for the electrodes in H_2O: P21 (0.5 M H_2SO_4) and P29 (1 M LiOH).

TABLE 2-1

DEGREE OF LOADING EXPERIMENTS

Cath.	Start date	Finish date	Duration (h)	D/H	Electrolyte	Additive	Comments	Max I / A	Min R/Ro
P1	2/23/90	3/13/90	432	H	0.1 M LiOH	None	System test		
P2	3/26/90	4/9/90	336	D	0.1 M LiOD	None	External cat.	0.8	1.75
P3	3/26/90	4/9/90	336	D	1 M LiOD	None	External cat.	0.8	
P4	3/26/90	4/9/90	336	D	0.5 M Li2SO4	None	External cat.	0.8	1.9
P5	3/26/90	4/9/90	336	D	0.05M Li2SO4 +0.05M D2SO4	None	External cat.	0.8	
P6	3/26/90	4/9/90	336	D	0.5M Li2SO4 +0.5M D2SO4	None	External cat.	0.8	1.8
P7	4/16/90	5/3/90	408	D	0.5 M Li2SO4	None	Internal cat.	0.75	1.73
P8	4/16/90	5/3/90	408	D	0.5 M Li2SO4	None	External cat.	0.75	
P9	4/16/90	5/3/90	408	H	0.5 M Li2SO4	None	Internal cat.	0.75	1.55
P10	4/16/90	5/3/90	408	H	0.5 M Li2SO4	None	External cat.	0.75	
P11	4/16/90	5/3/90	408	D	1 M LiOD	None	Internal cat.	0.75	
P12	5/11/90	5/31/90	480	D	1 M LiOD	None	Internal cat.	1	
P13	5/11/90	5/31/90	480	D	1 M LiOD	As2O3	Internal cat.	1	
P14	5/11/90	5/31/90	480	D	0.5 M Li2SO4	None	Internal cat.	1	
P15	5/11/90	5/31/90	480	D	0.5 M Li2SO4	As2O3	Internal cat.	1	
P16	5/23/90	5/31/90	192	D	0.5 M Li2SO4	None	Internal cat.	1	
P17	5/23/90	5/31/90	192	D	0.5 M Li2SO4	As2O3	Internal cat.	1	
P18	5/23/90	5/31/90	192	D	0.5 M Li2SO4	(NH2)2CS	Internal cat.	1	
P19	5/23/90	5/31/90	192	D	0.5 M Li2SO4	Na2S	Internal cat.	1	

TABLE 2-1 (cont.)

DEGREE OF LOADING EXPERIMENTS

P20	6/6/90	6/14/90	192	D	0.5 M D2SO4	None	No cat.	0.4	1.9
P21	6/6/90	6/14/90	192	H	0.5 M H2SO4	None	No cat.	0.4	1.65
P22	6/6/90	6/14/90	192	D	0.5 M D2SO4	NaI	No cat.	0.4	1.88
P23	6/6/90	6/14/90	192	D	0.5 M D2SO4	As2O3	No cat.	0.4	2
P24	6/6/90	6/14/90	192	D	1 M LiOD	As2O3	No cat.	0.4	1.8
P25	6/6/90	6/14/90	192	D	1 M LiOD	(NH2)2CS	No cat.	0.4	1.7
P26	6/6/90	6/14/90	192	D	1 M LiOD	Na2S	No cat.	0.4	1.78
P27	6/6/90	6/14/90	192	D	1 M LiOD	As2S3	No cat.	0.4	1.8
P28	6/6/90	6/14/90	192	D	1 M LiOD	None	No cat.	0.4	1.83
P29	6/6/90	6/14/90	192	H	1 M LiOH	None	No cat.	0.4	1.25
P30	9/13/90	9/26/90	312	D	0.1 M D2SO4	in CD3OD	CO2 /		
P31	9/13/90	9/26/90	312	D	0.1 M LiOD	in CD3OD	isopropanol		
P32	9/13/90	9/26/90	312	H	0.1 M H2SO4	in CH3OH	bath, -77 oC		
P33	9/13/90	9/26/90	312	H	0.1 M LiOH	in CH3OH			
P34	11/5/90	11/26/90	504	D	1 M D2SO4	in CD3OD	Liq. N2 /		
P35	11/5/90	11/26/90	504	D	0.75M D2SO4+ 0.25M Li2SO4	in CD3OD	xylene, -55oC		
P36	11/5/90	11/26/90	504	H	1 M H2SO4	in CH3OH			
P37	11/5/90	11/26/90	504	H	0.75M H2SO4+ 0.25M Li2SO4	in CH3OH			
P38	11/28/90	1/8/91	984	D	1 M LiOD	None		0.9	1.7
P39	11/28/90	1/8/91	984	D	1 M LiOD	200 ppm Al		0.9	1.7
P40	11/28/90	1/8/91	984	D	1 M LiOD	None	He3 implant	0.9	1.85
P41	11/28/90	1/8/91	984	D	1 M LiOD	200 ppm Al	He3 implant	0.9	1.7
P42	1/17/91	3/5/91	1128	D	1 M LiOD	None		0.95	
P43	1/17/91	3/5/91	1128	D	1 M LiOD	None		0.95	1.43
P44	1/17/91	3/5/91	1128	D	1 M LiOD	None		0.95	1.6
P45	1/17/91	3/5/91	1128	D	1 M LiOD	200 ppm Al		0.95	1.65

TABLE 2-1 (cont.)

DEGREE OF LOADING EXPERIMENTS

P46	1/17/91	3/5/91	1128 D	1 M LiOD	200 ppm Al		0.95	1.7
P47	1/17/91	3/5/91	1128 D	1 M LiOD	200 ppm Zn		0.95	1.85
P48	1/17/91	3/5/91	1128 D	1 M LiOD	200 ppm Hg		0.95	
P49	1/17/91	3/5/91	1128 D	1 M LiOD	200 ppm SiO2		0.95	1.5
P52	3/14/91	4/3/91	480 D	1 M LiOD	None	New etch soln	1	1.45
P53	3/14/91	4/3/91	480 D	1 M LiOD	None	Used etch soln	1	1.65
P54	3/14/91	4/3/91	480 D	1 M LiOD	200 ppm LiCl	Reused etch	1	1.42
P55	3/14/91	4/3/91	480 D	1 M LiOD	None	No etch	1	1.7
P56	3/14/91	4/3/91	480 D	1 M LiOD	200 ppm Bi	No etch	1	1.7
B1	5/8/91	7/10/91	1512 D	1 M LiOD	None	B alloy (1%)	0.95	
B2	5/8/91	7/10/91	1512 D	1 M LiOD	None	B alloy (.5%)	0.95	
P59	5/8/91	7/10/91	1512 D	1 M LiOD	200ppm Al +15mg/25ml H3BO3		0.95	
P60	5/8/91	7/10/91	1512 D	1 M LiOD	200ppm Al +15mg/25ml H3BO3		0.95	
P61	5/8/91	7/10/91	1512 D	1 M LiOD	15mg/25ml H3BO3		0.95	
P70	7/12/91	8/8/91	648 D	1 M LiOD	15mg/25ml H3BO3		0.95	
P71	7/12/91	8/8/91	648 D	1 M LiOD	150mg/25ml H3BO3		0.95	
P72	7/12/91	8/8/91	648 D	1 M LiOD	1.5g/25ml H3BO3		0.95	
P73	7/12/91	8/8/91	648 D	1 M LiOD	15mg/25ml H3BO3		0.95	
P74	7/12/91	8/8/91	648 D	1 M LiOD	150mg/25ml H3BO3		0.95	
P75	7/12/91	8/8/91	648 D	1 M LiOD	1.5g/25ml H3BO3		0.95	
P80	8/19/91	8/30/91	264 D	1 M LiOD	200 ppm Al		0.95	1.6
P81	8/19/91	8/30/91	264 D	1 M LiOD	15mg/25ml H3BO3		0.95	
P82	8/19/91	8/30/91	264 D	1 M LiOD	15mg/25ml H3BO3		0.95	
P83	8/19/91	8/30/91	264 D	0.3 M LiCl	None		0.95	1.68
P84	8/19/91	8/30/91	264 D	0.3 M LiCl	200 ppm Al		0.95	1.65
P85	8/19/91	8/30/91	264 D	1 M LiOD	Be		0.95	

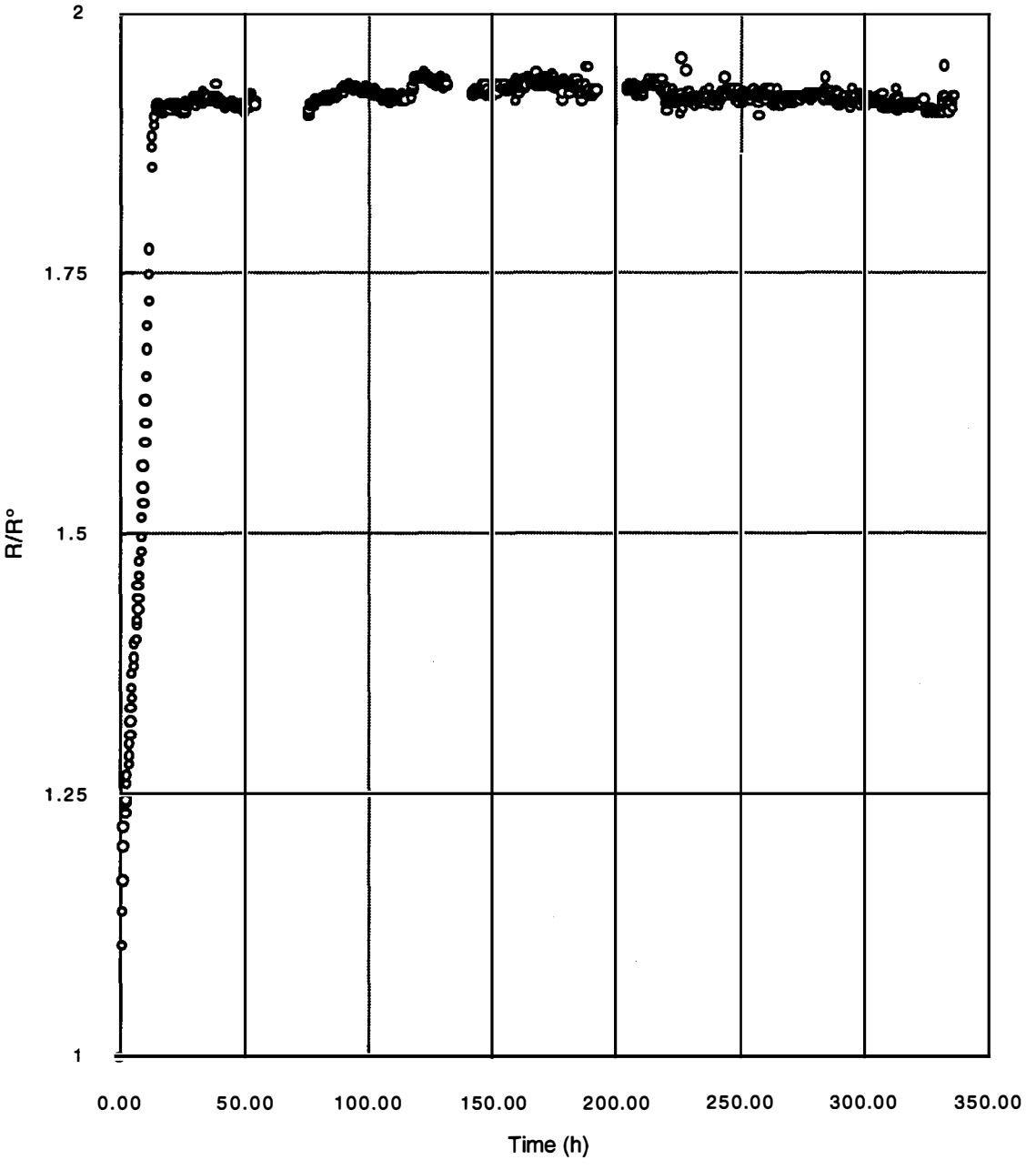

Figure 2-9
Resistance/Time Data for Electrode P20 (0.5 M D_2SO_4)

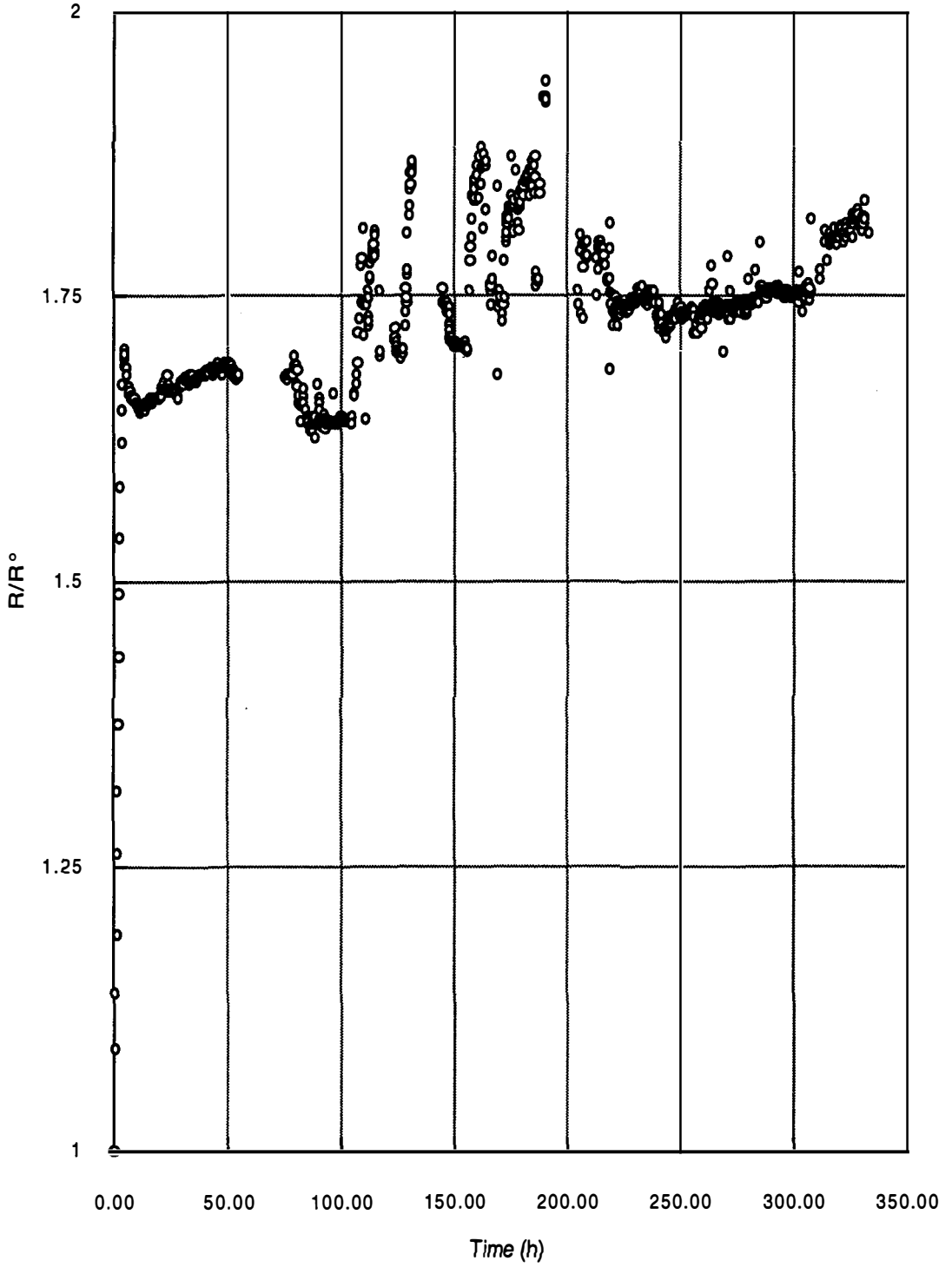

Figure 2-10
Resistance/Time Data for Electrode P21 (0.5 M H_2SO_4)

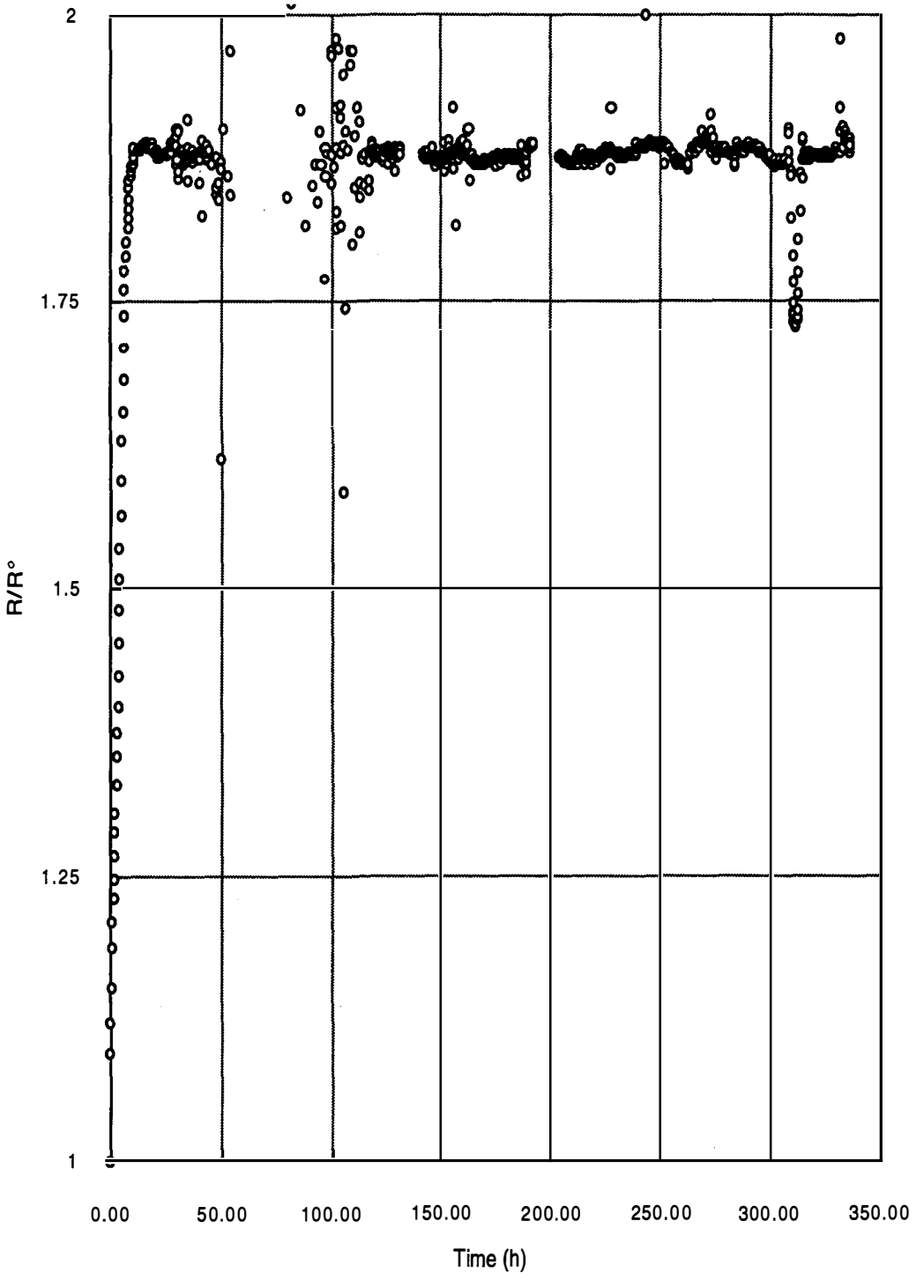

Figure 2-11
Resistance/Time Data for Electrode P22 (0.5 M D_2SO_4) + 0.005 M NaI)

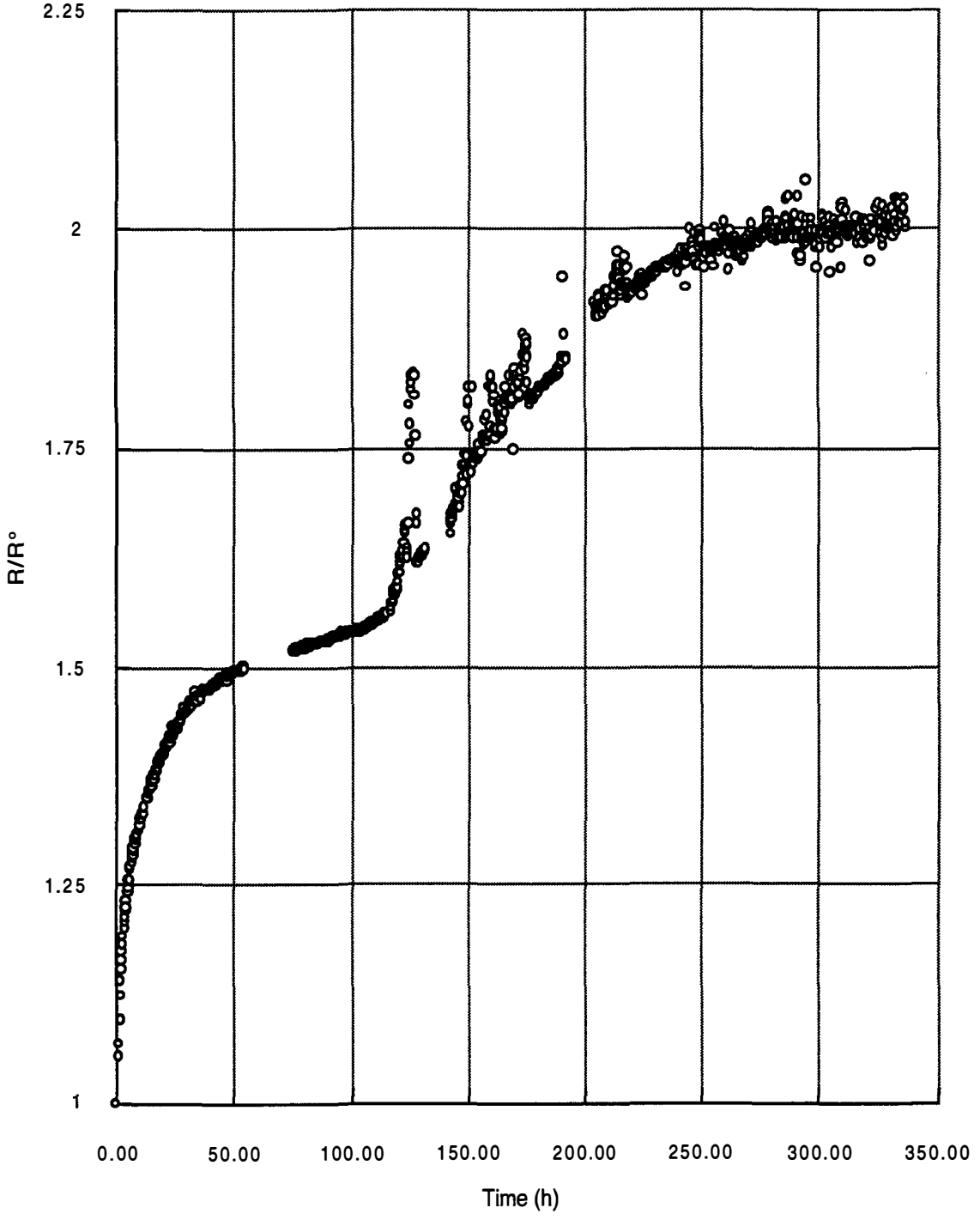

Figure 2-12
Resistance/Time Data for Electrode P23 (0.5 M D_2SO_4 + As_2O_3)

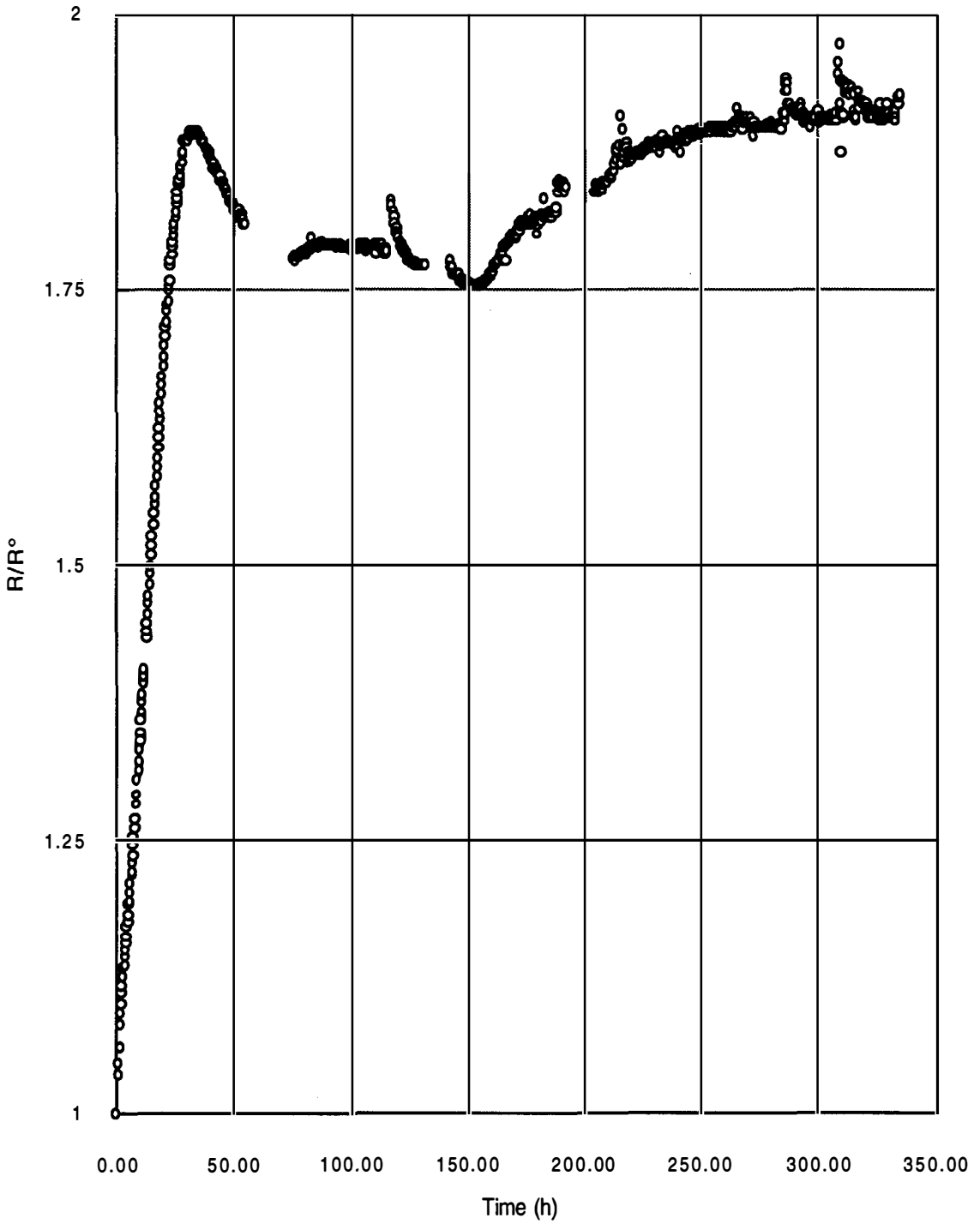

Figure 2-13
Resistance/Time Data for Electrode P24 (1 M LiOD + As_2O_3)

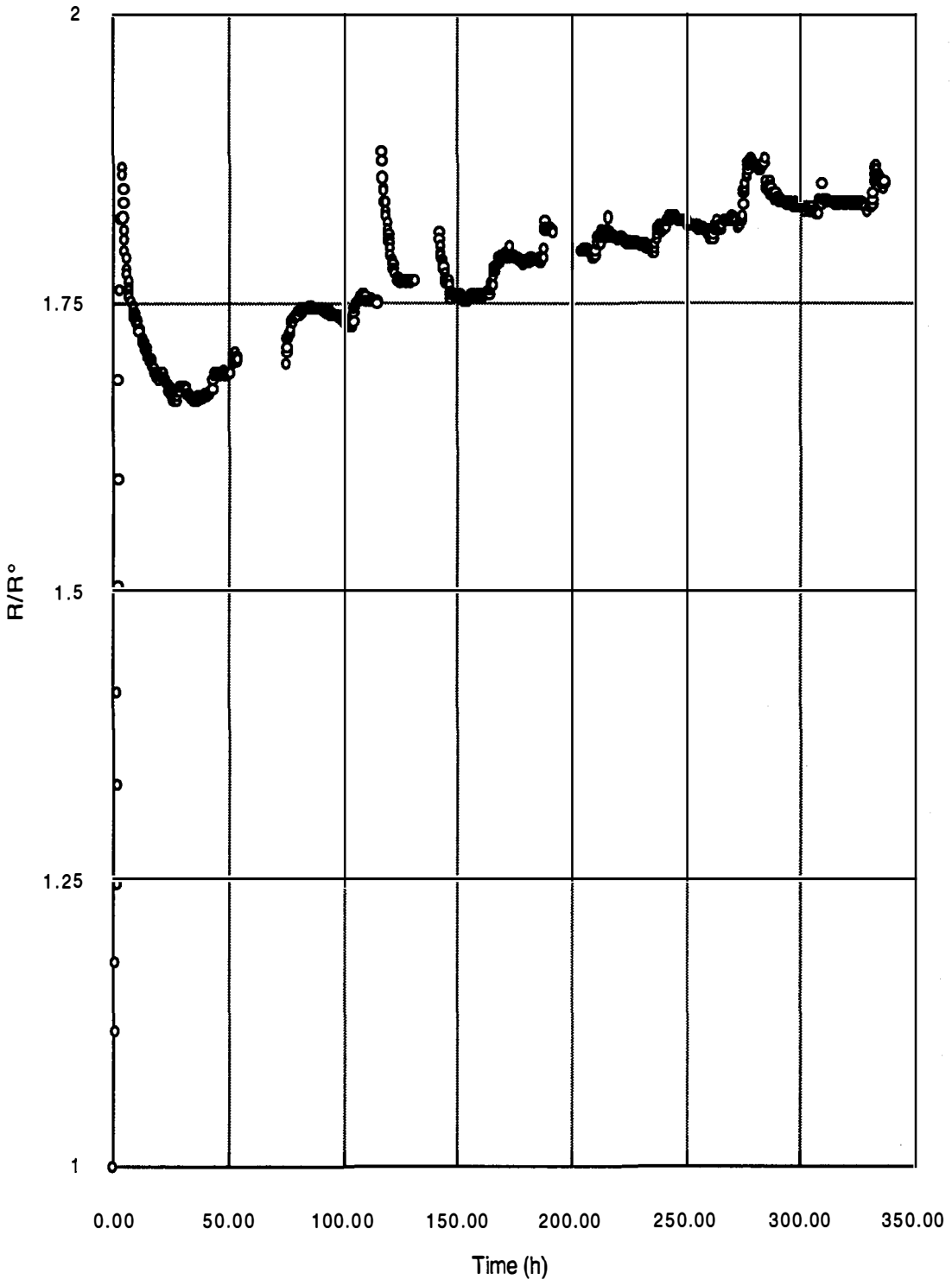

Figure 2-14
Resistance/Time Data for Electrode P25 [1 M LiOD + $(NH_2)_2CS$]

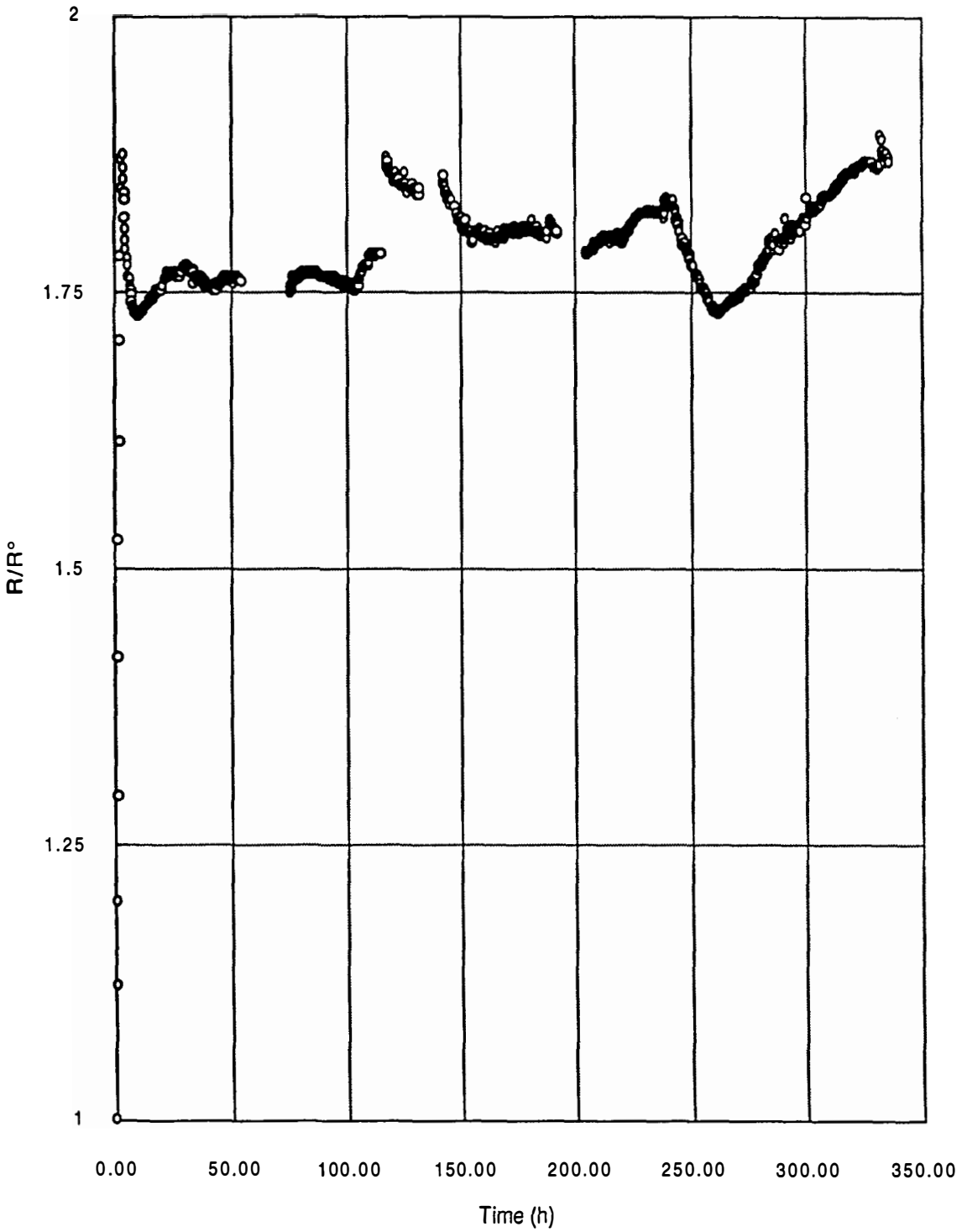

Figure 2-15
Resistance/Time Data for Electrode P26 (1 M LiOD + Na_2S)

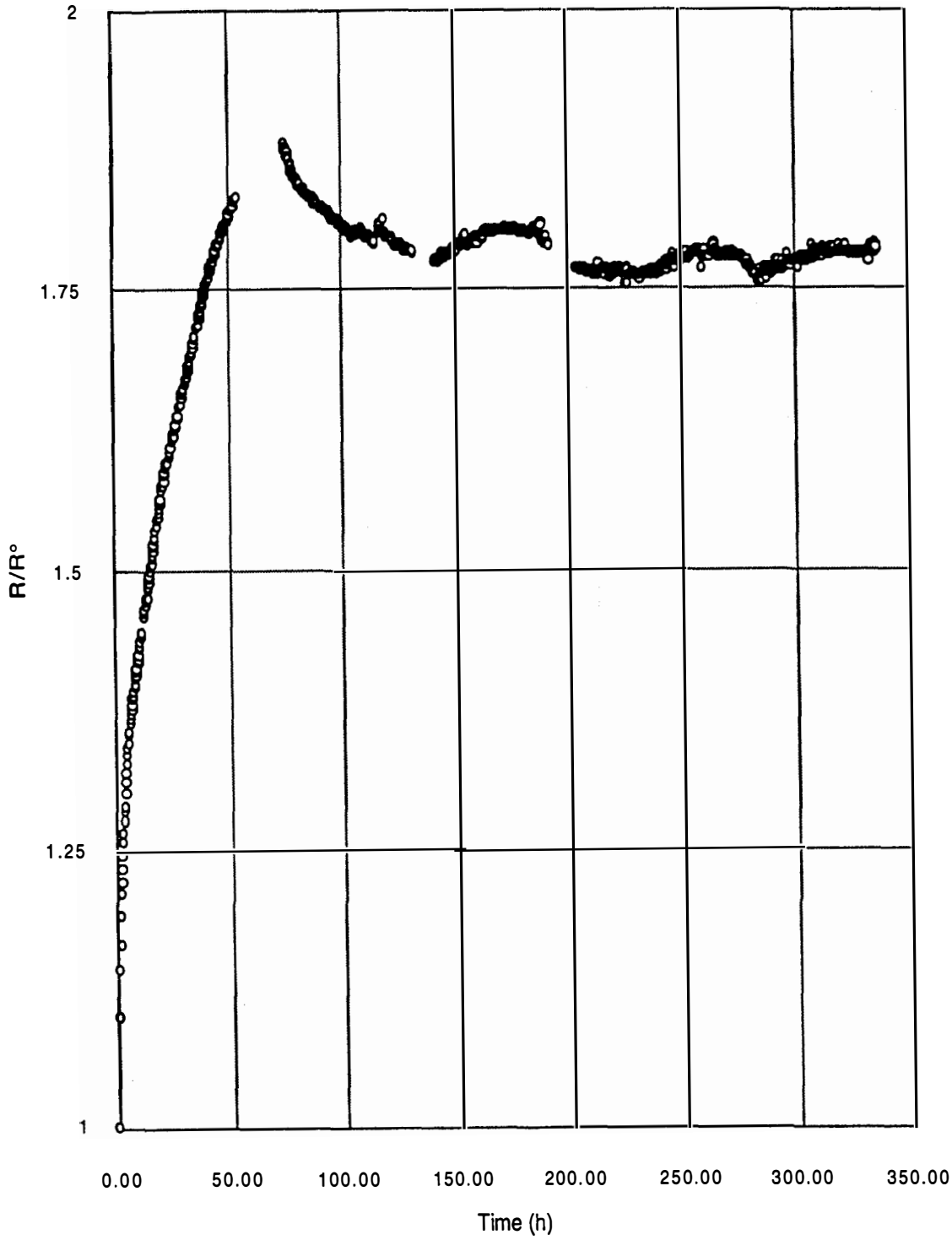

Figure 2-16
Resistance/Time Data for Electrode P27 (1 M LiOD + As_2S_2)

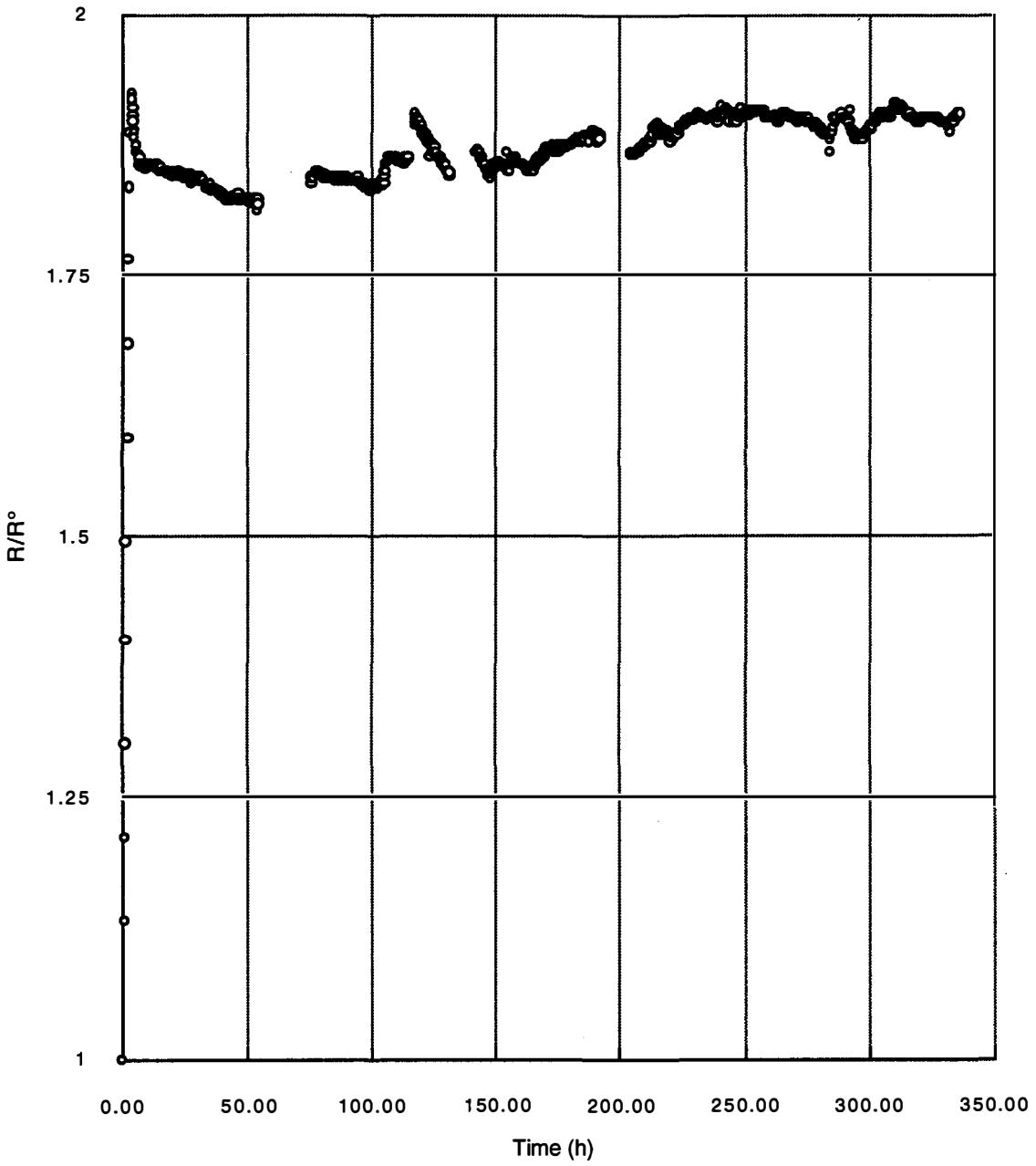

Figure 2-17
Resistance/Time Data for Electrode P28 (1M LiOD)

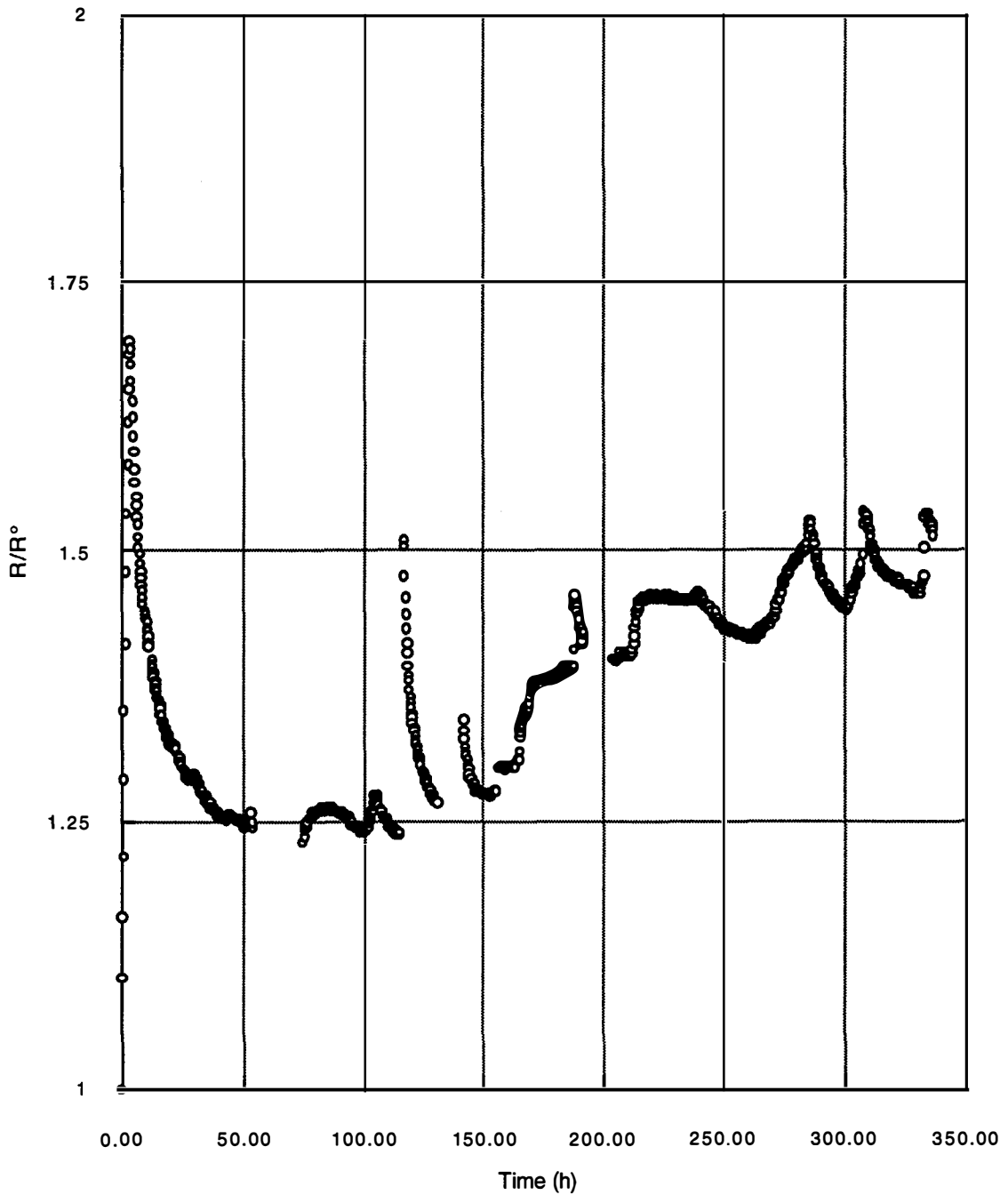

Figure 2-18
Resistance/Time Data for Electrode P29 (1 M LiOH)

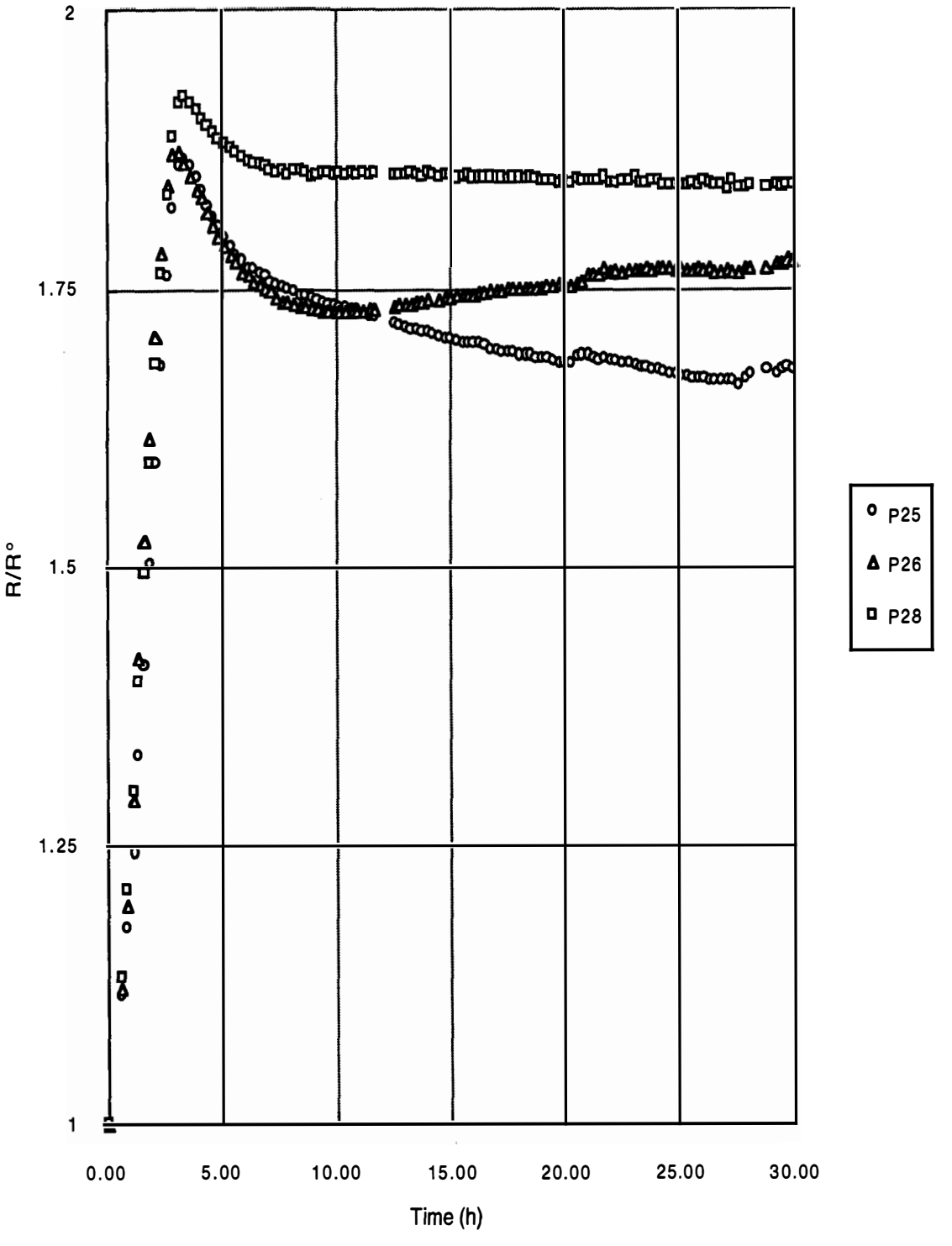

Figure 2-19
Resistance Ratio for Electrodes P25, P26 and P28

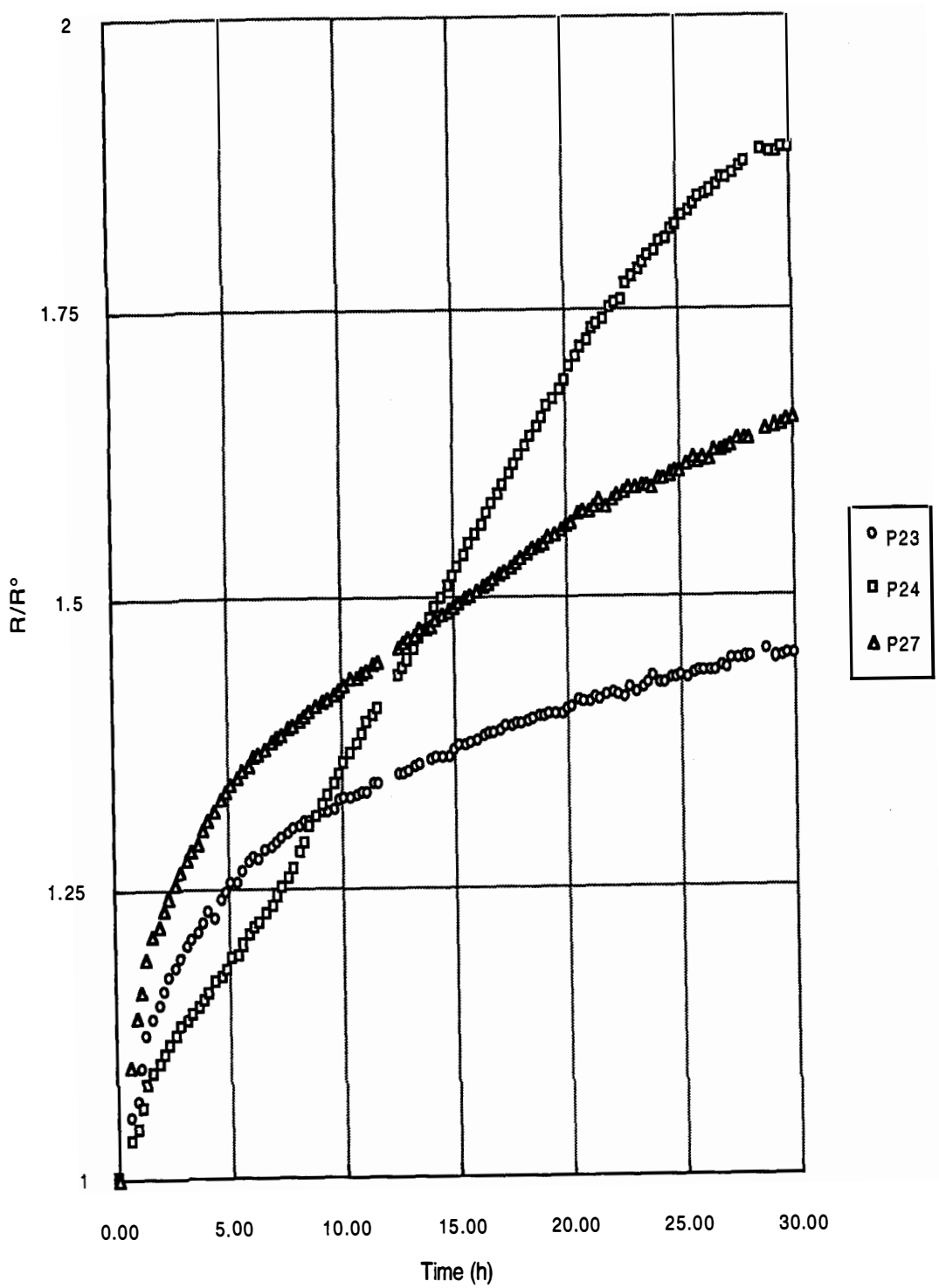

Figure 2-20
Resistance Ratio for Electrodes P23, P24, and P27

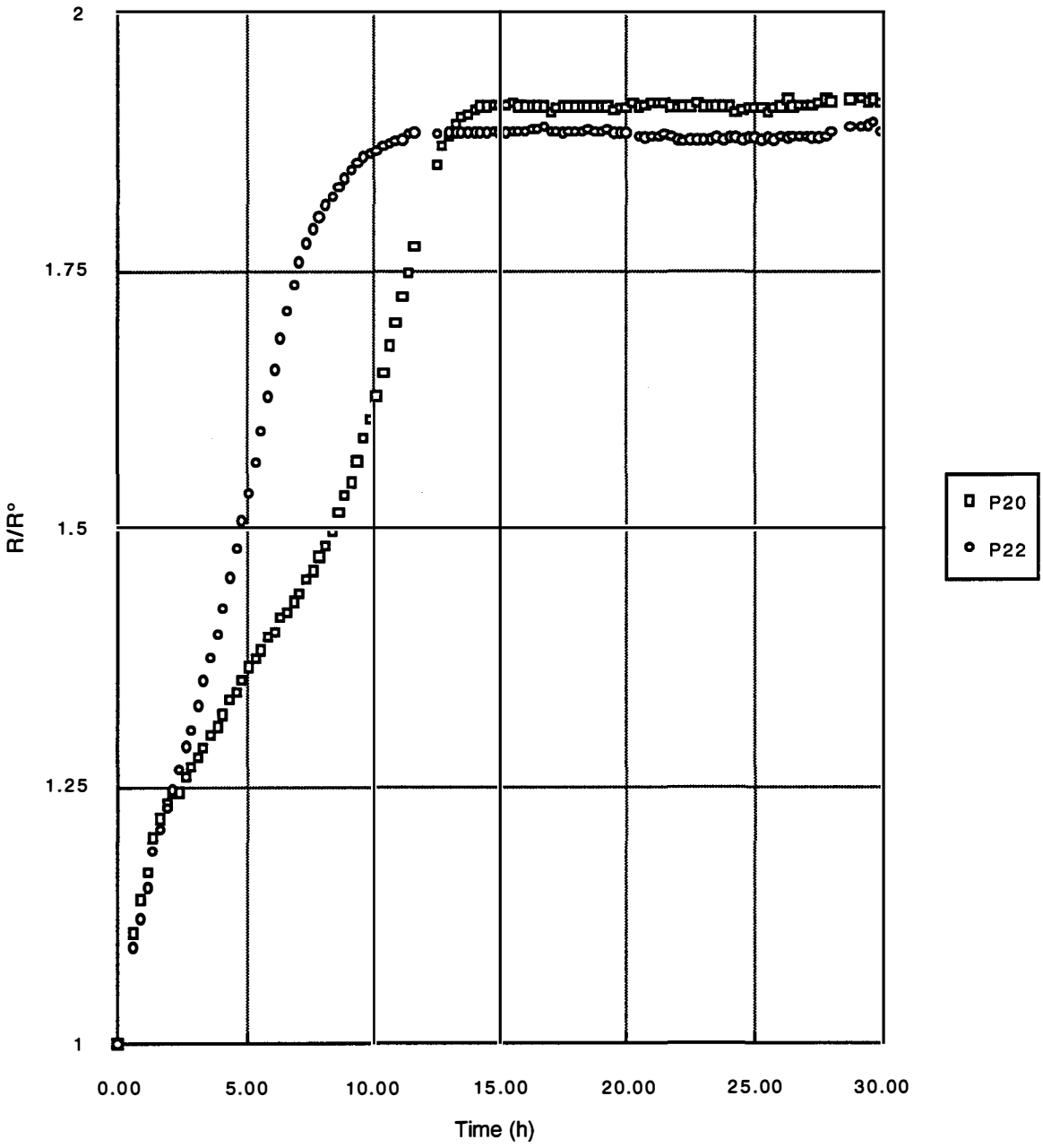

Figure 2-21
Resistance Ratio for Electrodes P20 and P22

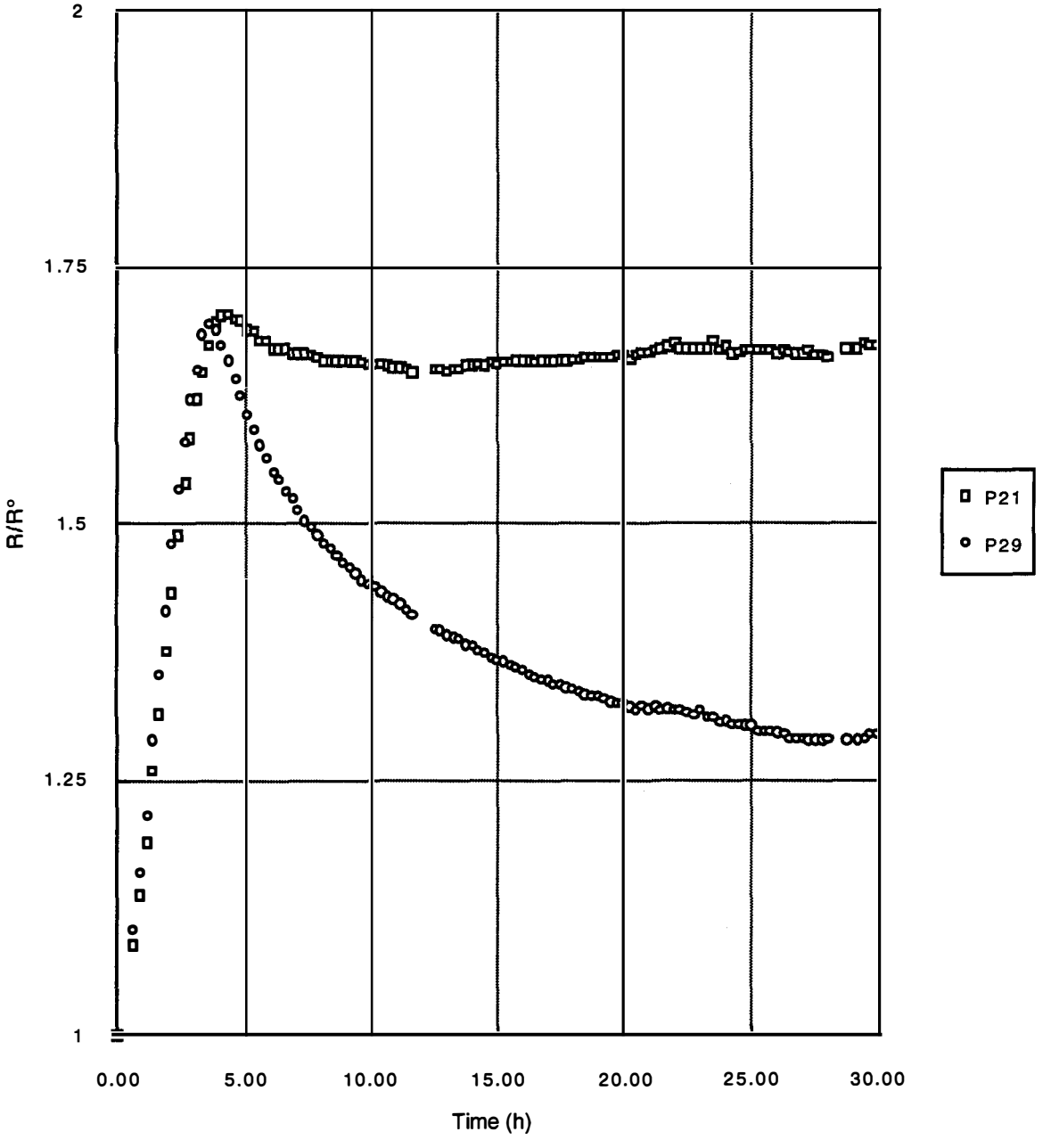

Figure 2-22
Resistance Ratio for Electrodes P21 and P29

A feature of many of the curves was a slight change in the resistance ratio over the final 200 hours of the tests. A gradual increase in R/R° with time can be interpreted as a decrease in the entry surface concentration, whereas a gradual decrease in R/R° can be assumed to be due to an increase in the entry surface concentration.

From these resistance loading curves, the following generalizations can be made:

Heavy Water:

- The fastest loading is achieved in alkaline conditions: electrodes P25 [LiOD + $(NH_2)_2CS$], P26 (LiOD + Na_2S), and P28 (LiOD). These three electrodes reached a peal R/R° value of about 1.9 after about 3 hours (Figure 2-19). Since the subsequent plateau value for the LiOD alone (P28) is slightly higher than those for the electrodes with additives, it appears that the additives also result in a slightly higher final loading.
- The electrolytes containing arsenic salts—P23 (D_2SO_4 + As_2O_3), P24 (LiOD + As_2O_3), and P27 (LiOD + As_2S_2)—all exhibited slow rates of loading; none of these three electrodes had attained a maximum value in the first 30 hours (Figure 2-20). The effect of arsenic salts is apparently similar in either acidic (P23) or alkaline (P24, P27) conditions, although in the acidic electrolyte the peak value of the resistance ratio was reached after more than 200 hours (Figure 2-12), compared to 30 hours and 70 hours, respectively, for the two electrodes in alkaline conditions. Note that although the rate of loading is considerably slower for these three electrodes, the final plateau value is similar to those for the other electrodes in heavy water.
- Electrodes P20 (D_2SO_4) and P22 (D_2SO_4 + NaI) represent intermediate cases between the alkaline electrolyte and the electrolytes containing arsenic salts. Both resistance ratio curves for these two electrodes reach a maximum value between 10 and 20 hours (Figure 2-21), and both electrodes exhibit a two-stage curve similar to those for the arsenic salt electrolytes.
- The maximum R/R° value of about 1.9 for all of the heavy water experiments suggests a final loading level corresponding to a D/Pd ratio between 0.8 and 0.9.

Light Water:

- The two light water experiments both exhibited a peak R/R° value of 1.7 after about 4 hours; however, the subsequent values at 300 hours were 1.8 and 1.5 for P21 (H_2SO_4) and P29 (LiOH), respectively. The value for the alkaline electrolyte corresponds to an H/Pd ratio between 0.9 and 1.0. Indeed, the lowest value of R/R° after the maximum was about 1.3, corresponding to an even higher loading; this can be compared to a maximum loading between 0.7 and 0.8 for the electrode in the acidic electrolyte.

2.3.2 *Theoretical Calculations*

To relate the resistance ratio (R/R°) data to loading of deuterium (or hydrogen) in palladium, it is necessary to have some idea of the concentration profiles in the sample. To achieve a semiquantitative understanding of the resistance ratio plots, theoretical R/R° versus time plots were calculated for different loading conditions.

The theoretical curves were generated in the following manner. Concentration profiles as a function of time were calculated for three entry surface conditions: constant flux, constant concentration, and an exponentially increasing concentration. The concentration profile at each time increment was divided into a number of segments from the surface to the center of the palladium rod. Fifth-order polynomial approximations of the resistance ratio versus composition curves were then used to compute the resistance ratio of each segment for either hydrogen or deuterium loading. Finally, the average value of the resistance ratio was calculated from the average of all the segments.

For the H/Pd system, the resistance ratio is related to the loading x by

$$R/R° = 0.97227 + 2.2091x - 9.2431x^3 - 30.958x^4 + 11.083x^5 \qquad (2\text{-}4)$$

where x = H/Pd.

For the D/Pd curve, the corresponding polynomial expression is

$$R/R^{\circ} = 0.97869 + 3.001x - 15.09x^2 + 44.155x^3 - 49.119x^4 + 17.577x^5 \qquad (2\text{-}5)$$

where x = D/Pd.

The concentration profiles for the three different loading conditions were calculated from standard analytical solutions that are described in more detail below. For all calculations, the values for the radius of the palladium rod (0.15 cm) and the charging current density (0.106 mA cm^{-2}) were identical to the values in the experimental work. The diffusion coefficient was assumed to be 3.4 x 10^{-7} cm^2 s^{-1} in both the α and β-phases.

Constant Flux at the Entry Surface. The concentration profile as a function of distance for the boundary condition of constant flux at the entry surface was calculated from Eq. 2-6 below. The value of the input flux was assumed to be equal to the charging current density multiplied by the absorption efficiency, and calculations were performed for efficiencies in the range 0.05 to 0.3 (i.e., 5-30%).

$$C(x) = -\frac{fr}{D}\left(\frac{2Dt}{r^2} + \frac{x^2}{2r^2} - \frac{1}{4} - 2\,\Sigma \exp\left(\frac{D\alpha_n^2 t}{r^2}\right)\frac{J_0\left[\frac{x\alpha_n}{r}\right]}{\alpha^2 J_0[\alpha\,]}\right) \qquad (2\text{-}6)$$

where

C = concentration at distance x from center (mol cm^{-3})

x = distance from center of cylinder (cm)

f = flux at surface (mol cm^{-2} s^{-1}); f = 0.106 x efficiency/96485

r = radius of rod (0.15 cm)

D = diffusion coefficient (3.4 x 10^{-7} cm^2 s^{-1})

t = time (s)

α_n = positive roots of Bessel function J_0 [α_n] = 0
(3.8317, 7.0156, 10.1735, 13.3237, 16.4706, 19.6159)

J_0[] = Bessel function of order zero

Figure 2-23 shows concentration profiles for a palladium rod at a charging current density of 0.106 A cm^{-2} and with an absorption efficiency of 0.1 assumed. The absorption efficiency represents the fraction of the applied current density (0.106 A cm^{-2}) that results in hydrogen, or deuterium, absorbed into the palladium lattice. The fluxes of hydrogen, or deuterium, at 0.106 A cm^{-2} and efficiencies between 0.05 and 0.3 are given in Table 2-2.

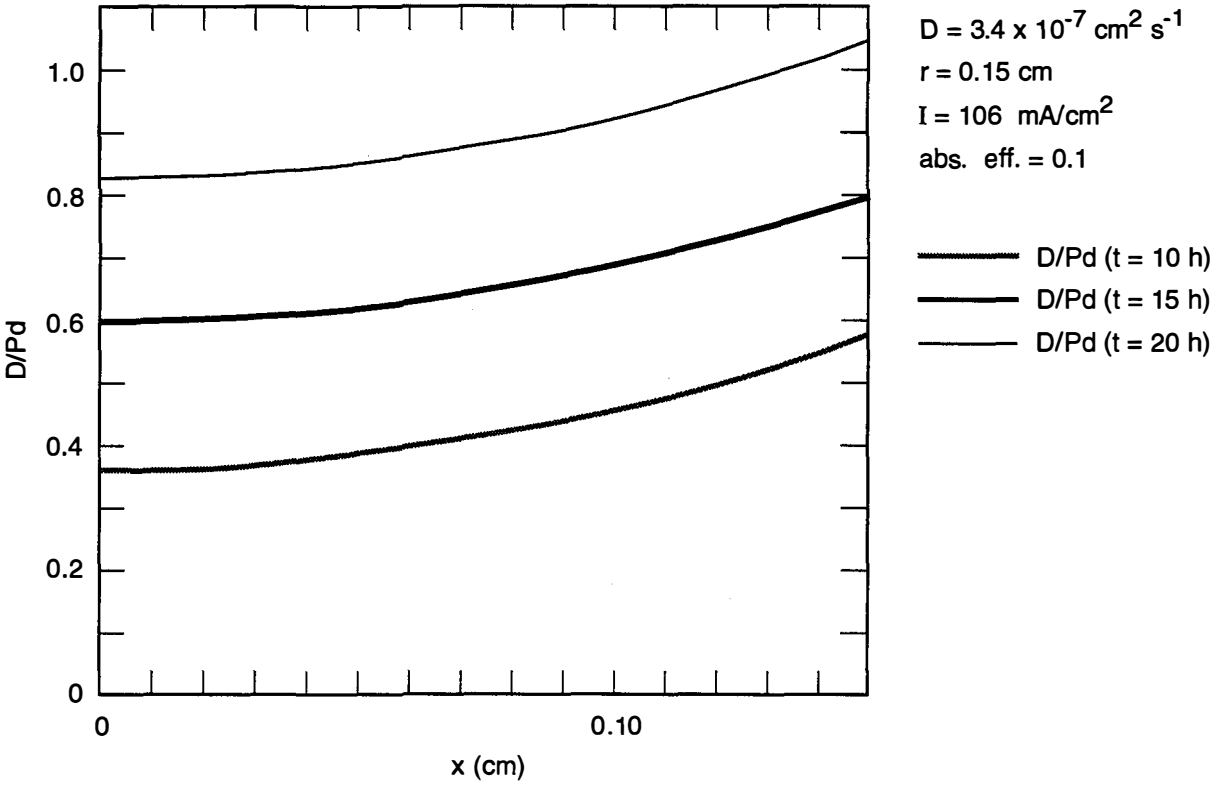

Figure 2-23
Concentration profiles for a Pd rod at a charging current density of 0.106 A cm^{-2} and with an absorption efficiency of 0.1 assumed.

Table 2-2

FLUX OF HYDROGEN, OR DEUTERIUM, AT A CHARGING CURRENT DENSITY OF 0.106 A CM^{-2} AS A FUNCTION OF ABSORPTION EFFICIENCY

Absorption Efficiency	Flux (mol cm^{-2} s^{-1})
0.05	0.55×10^{-7}
0.1	1.1×10^{-7}
0.2	2.2×10^{-7}
0.3	3.3×10^{-7}

In Figure 2-23, x = 0 corresponds to the center line of the rod and x = 0.15 corresponds to the entry surface. Under conditions of constant flux, once the hydrogen or deuterium has penetrated to the center of the rod, the concentration profiles are identical in shape as a function of time but are shifted to higher concentrations. Although the constant flux condition is most appropriate for charging at constant current, it has the inherent disadvantage of predicting infinite surface concentration at infinite time, which is clearly unreasonable.

Figures 2-24 and 2-25 show plots of R/R° versus time as a function of absorption efficiency for hydrogen and deuterium, respectively. Certain features are common to both figures. First, with increasing flux (increasing absorption efficiency), curves reach a peak value of R/R° at shorter times. In addition, the maximum value of R/R° systematically decreases with increasing flux because the fact that the concentration profile exhibits a greater degree of curvature at higher fluxes. These curves provide a theoretical basis for interpreting the attenuation of the maximum value of R/R° and exhibit shapes similar to those seen from the experimental work.

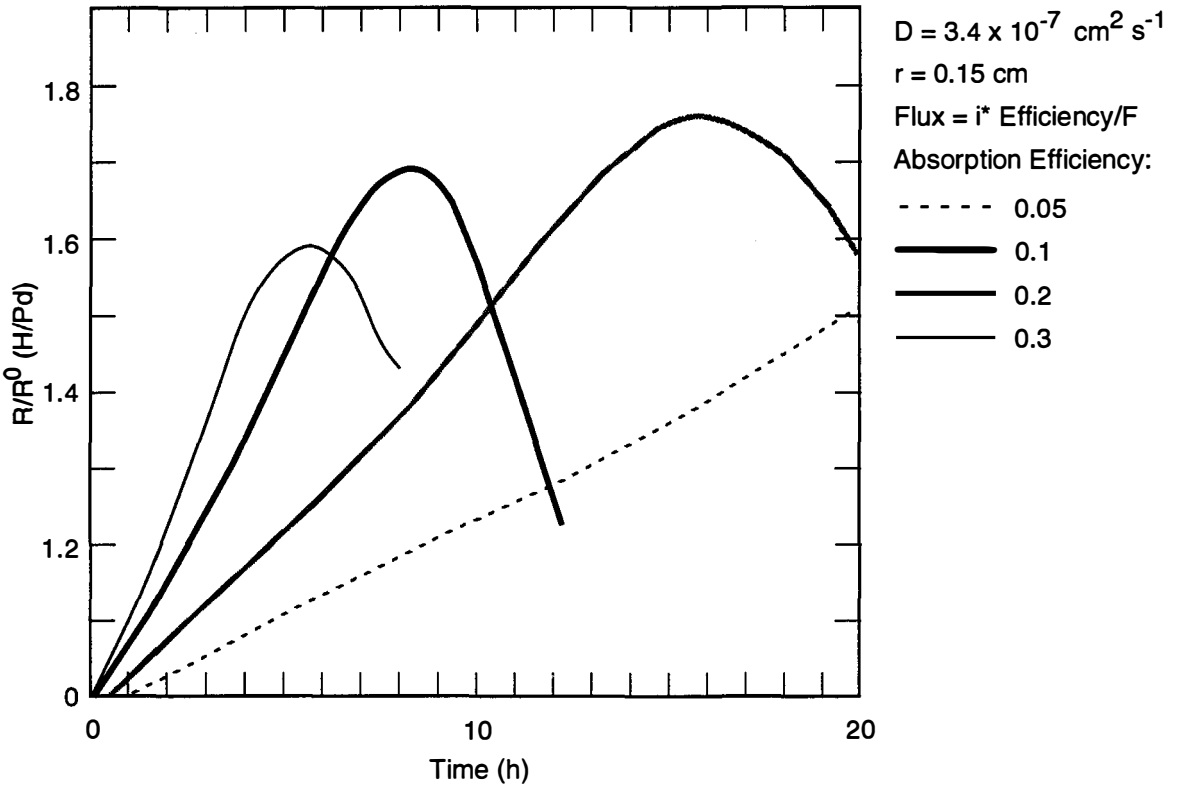

Figure 2-24
Plots of R/R° versus time as a function of absorption efficiency for hydrogen.

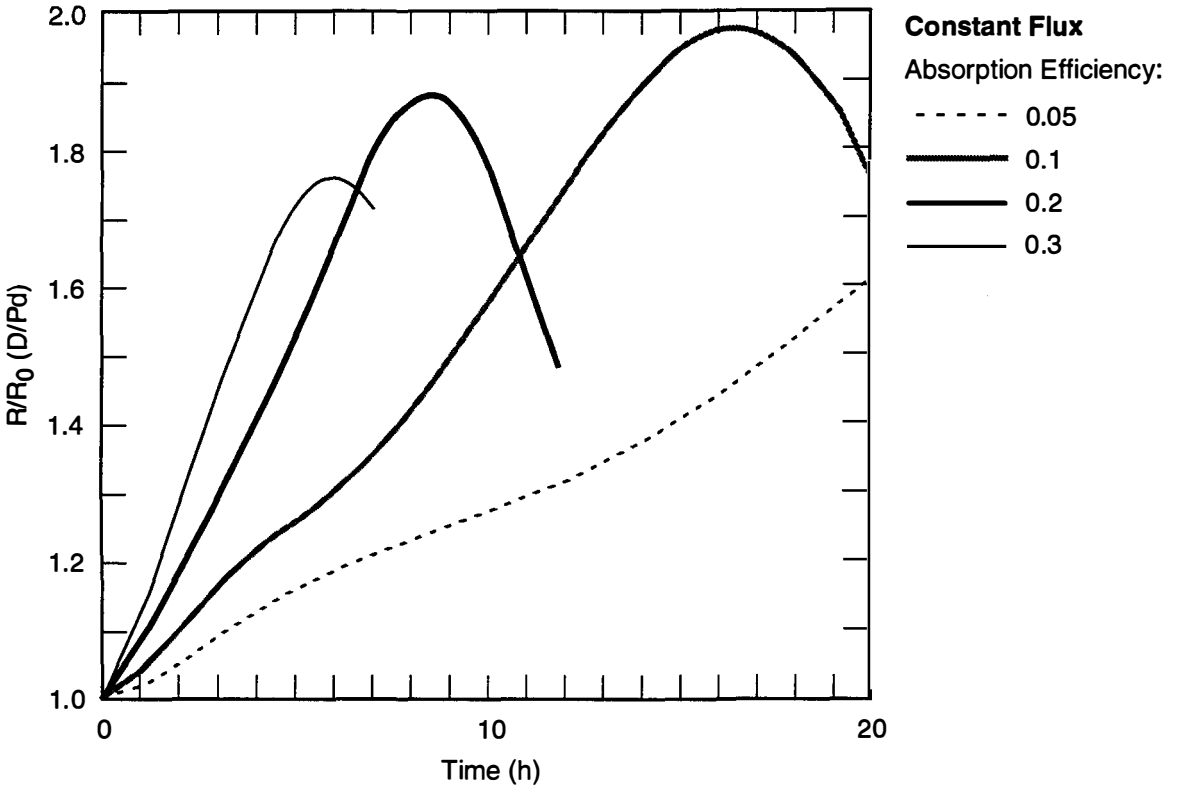

Figure 2-25
Plots of R/R° versus time as a function of absorption efficiency for deuterium.

The limitation to the constant flux analysis, as described above, is that the R/R° curves do not reach the expected steady state.

Constant Concentration at the Entry Surface. The concentration profiles under the boundary condition of a constant surface concentration were calculated from Eq. 2-7:

$$C_o = -\frac{fr}{D}\left(\frac{2Dt}{r^2} + \frac{x^2}{2r^2} - \frac{1}{4} - 2\,\Sigma \exp\left(\frac{D\alpha_n^2\, t}{r^2}\right) \frac{J_1\left[\frac{x\alpha_n}{r}\right]}{\alpha^2 J_1[\alpha\,]}\right) \qquad (2\text{-}7)$$

where

C_o = entry surface concentration

α_n = positive roots of Bessel function $J_1[a_n]=0$
(2.4048, 5.5201, 8.6537, 11.7915, 14.9309, 18.0711, 21.2116)

$J_1[\,]$ = first order Bessel function

The constant entry surface concentration condition is not expected to accurately represent loading under conditions of constant current; however, it has the advantage of a maximum value of the entry surface concentration, in contrast to the constant flux condition described above.

Figure 2-26 shows concentration profiles as a function of time for a palladium rod with an entry surface concentration ratio of 0.8. These curves would be the same for both hydrogen and deuterium, and they show the concentration profiles increasing to a flat distribution within the rod after about 30 hours. Figure 2-27 shows the corresponding fluxes as a function of time calculated from the incremental increase in the total volume of absorbed hydrogen (or deuterium). It is apparent from this

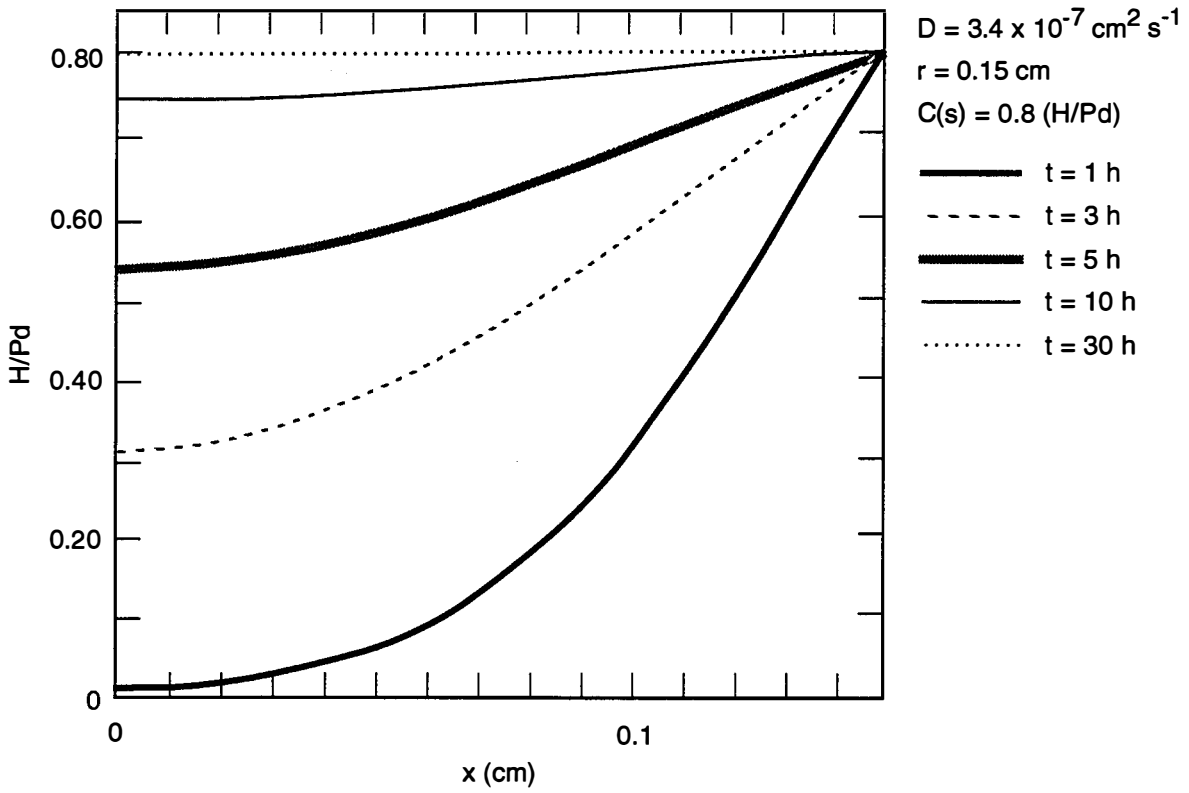

Figure 2-26
Concentration profiles as a function of time for a Pd rod with C(s) = 0.8.

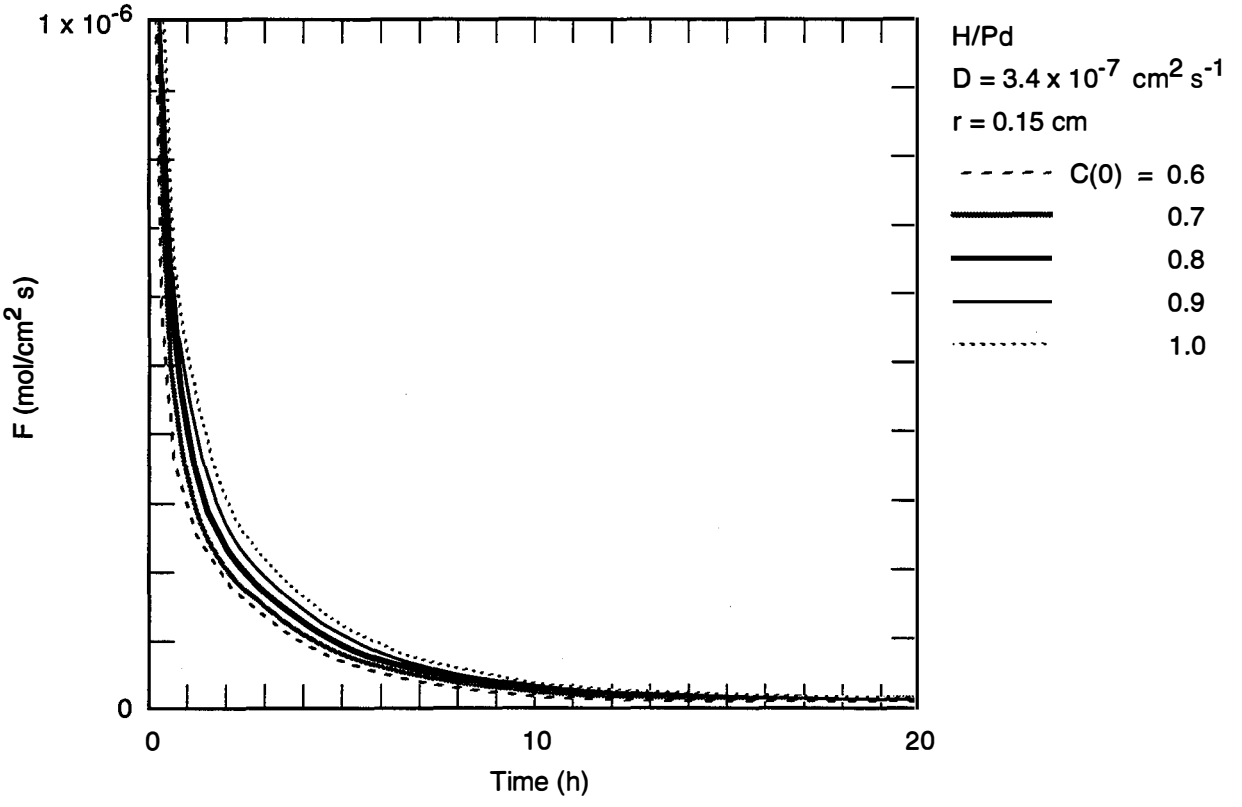

Figure 2-27
F profiles as a function of time for a Pd rod of radius 0.15 cm and diffusion coefficient 3.7 x 10^{-7} cm^2 s^{-1}.

figure that the flux is initially very high and decreases to small values after about 20 hours with little dependence on the entry surface concentration.

Figure 2-28 shows a plot of R/R° versus time for hydrogen loading as a function of entry surface concentration. The curves for entry surface concentrations in excess of 0.8 show the characteristic R/R° peak seen in the experimental data and a steady-state value at longer times. However, the short-time behavior of these curves is clearly different from that of the experimental curves, which are closely approximated by the constant flux condition.

Variable Concentration at Entry Surface. To approximate the constant flux condition at short times and have a maximum concentration at longer times, calculations were performed assuming an exponential increase in the entry surface concentration to a maximum value.

$$C(x) = C_o\left(1 - \frac{J_0[\sqrt{\beta}x^2/D]}{J_0[\sqrt{\beta}r^2/D]} - \exp(\beta t) + \frac{2\beta}{D}\Sigma\frac{\exp(-D\alpha_n^2 t/r^2)J_0[\alpha_n x/r]}{\alpha_n J_1[\alpha_n]\left(\frac{\alpha_n^2}{r^2} - \frac{\beta}{D}\right)}\right) \qquad (2\text{-}8)$$

and

$$\text{surface concentration, } C_s = C_0\,[1 - \exp(-\beta t)] \qquad (2\text{-}9)$$

where

b = constant
a_n = positive roots of Bessel function $J_1\,[a_n] = 0$
(2.4048, 5.5201, 8.6537, 11.7915, 14.9309, 18.0711, 21.2116)

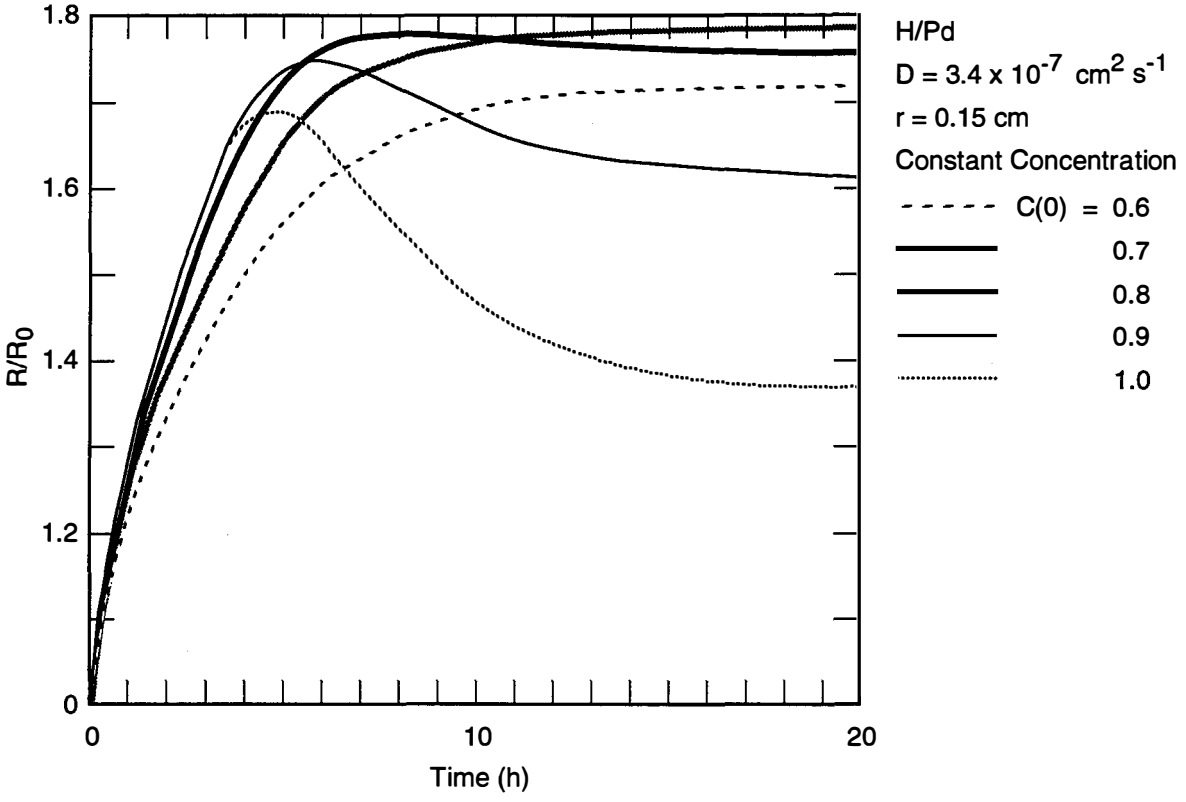

Figure 2-28
R/R° versus time for hydrogen loading as a function of entry surface concentration.

In this series of calculations, the entry surface concentration varies as a function of time according to Eq. 2-9. Figure 2-29 shows the entry surface concentration (C_s) as a function of time for different values of the constant β. For large values of β, the surface concentration increases rapidly to a maximum value. At intermediate times (between 3 and 10 hours) the concentration profiles are similar in shape to those for the constant flux case, whereas the profiles become relatively flat as the maximum entry surface concentration is attained. Figure 2-31 shows concentration profiles for the same parameters as shown in Figure 2-30 except β=0.5. In this latter case, the fast rise of the entry surface concentration gives rise to the steeper profiles. Figure 2-32 shows the corresponding entry fluxes as a function of β. The fluxes shown in Figure 2-32 can be compared to the fluxes listed in Table 2-2 for the constant flux case. It can be seen that for larger values of β, the flux is relatively constant during the first few hours of charging.

Figure 2-33 shows R/R° plotted against time as a function of β for C_0 (H/Pd)=0.9. These curves show good qualitative agreement with the shapes of the experimental curves for light water. Similarly, Figure 2-34 shows the corresponding curves for C_0 (D/Pd)=0.9, which exhibit characteristic shapes similar to those of the experimental curves for heavy water.

2.3.3 *Conclusions*

The results from the experimental work show that, at the same charging current density, all electrodes eventually attain a similar loading level. Faster loading rates are generally achieved in alkaline electrolytes. Slower rates of loading occur in acidic electrolytes and in the presence of arsenic salts.

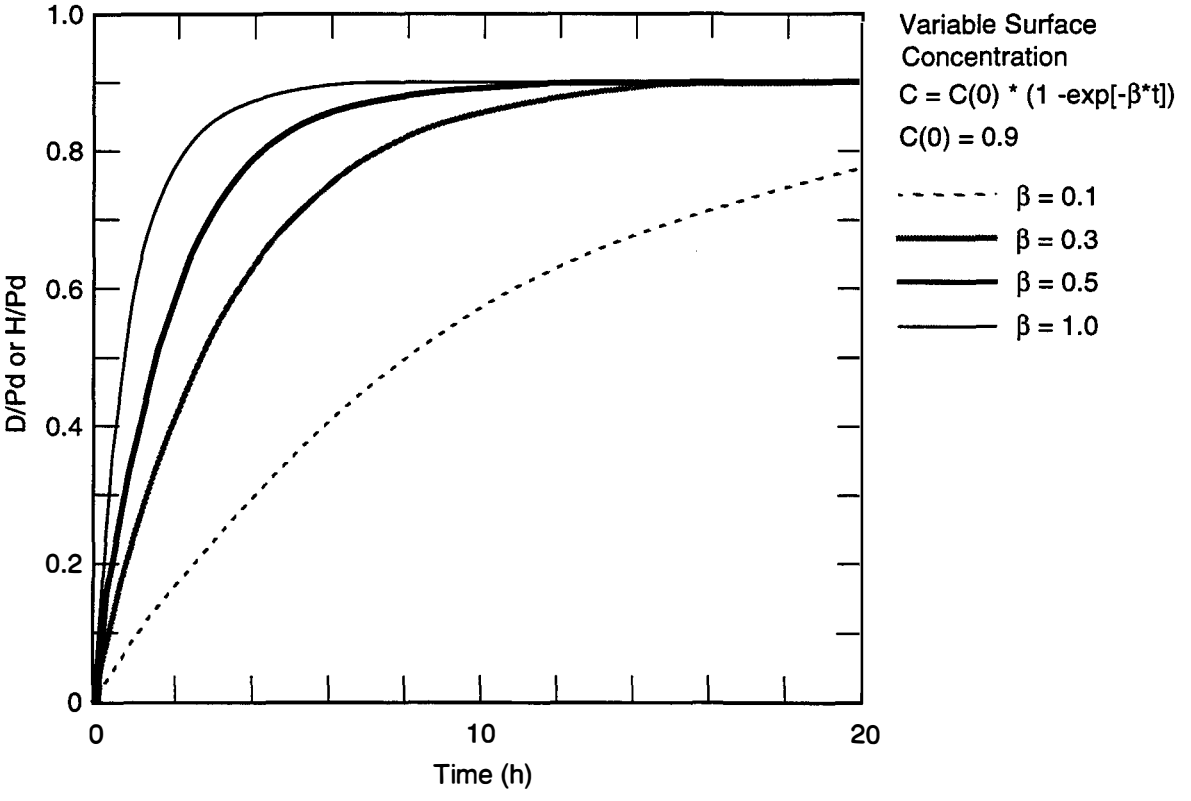

Figure 2-29
Entry surface concentration (Cs) as a function of time for different values of β.

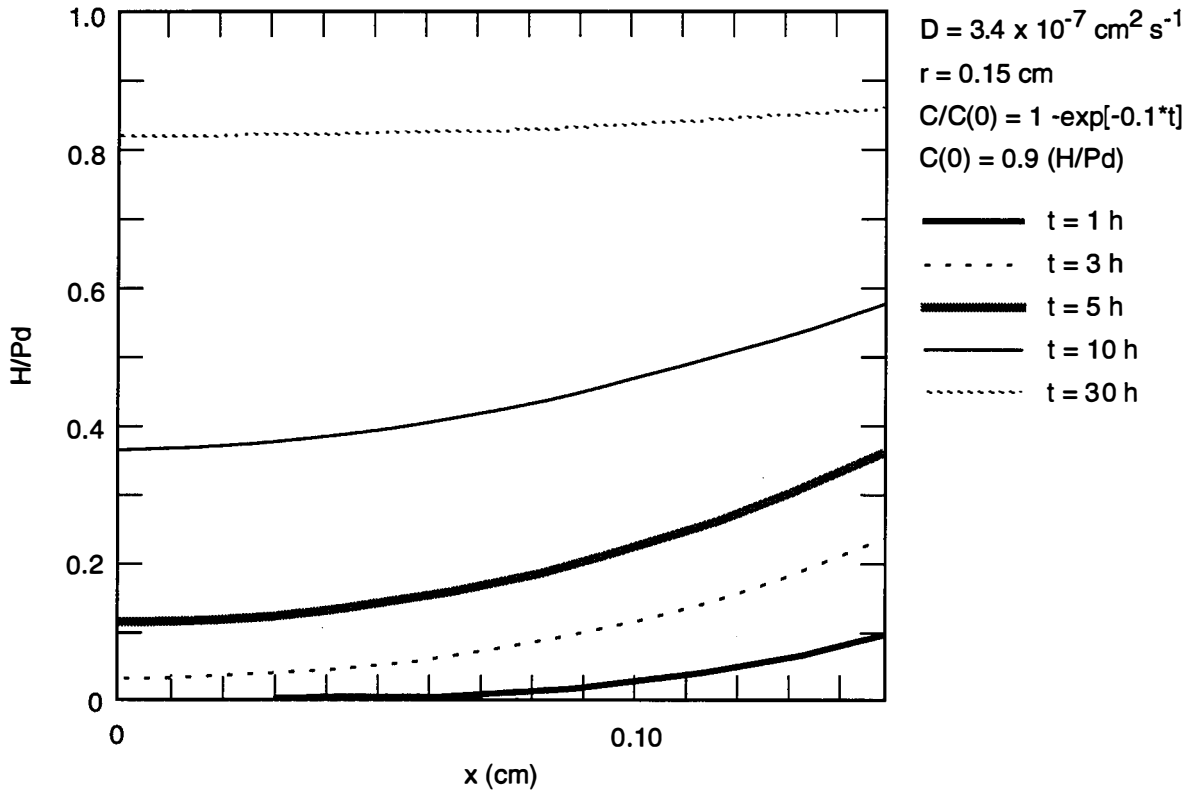

Figure 2-30
Variation of hydrogen loading with distance for variable surface concentration.

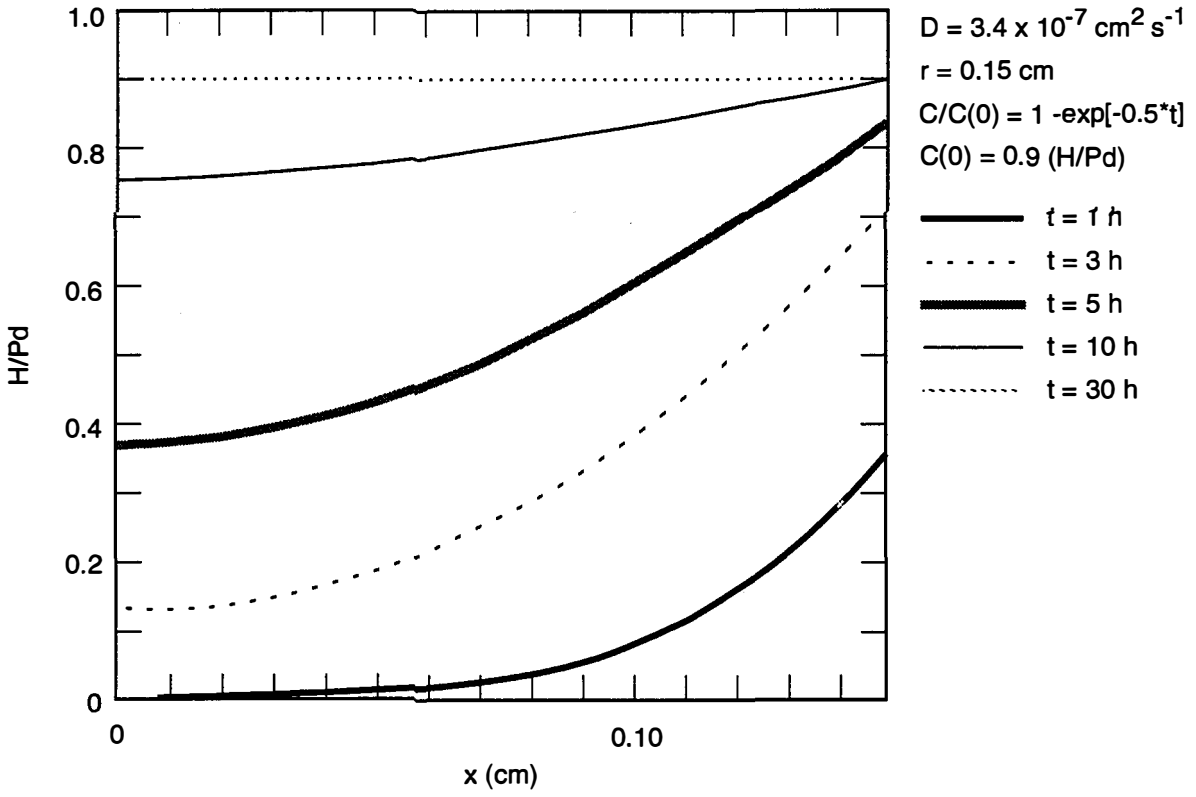

Figure 2-31
Variation of hydrogen loading with distance for variable surface concentration.

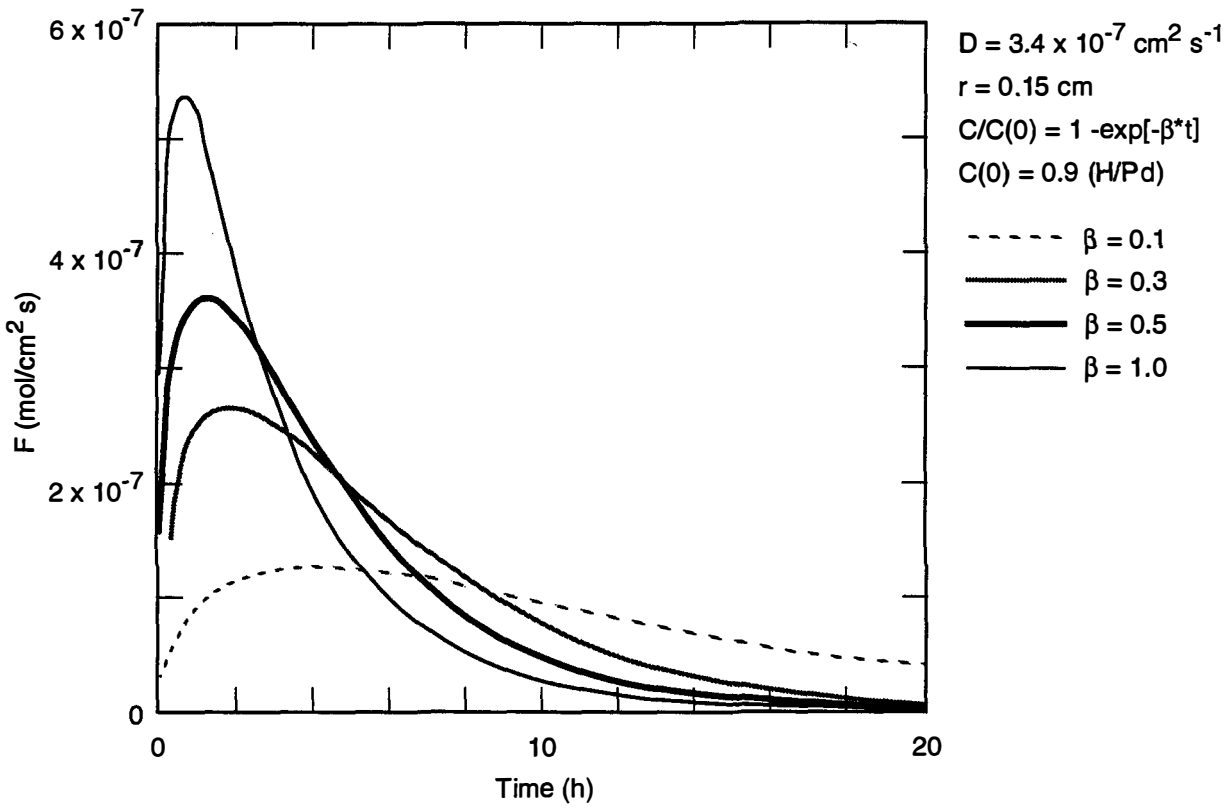

Figure 2-32
Variation of surface entry flux with time.

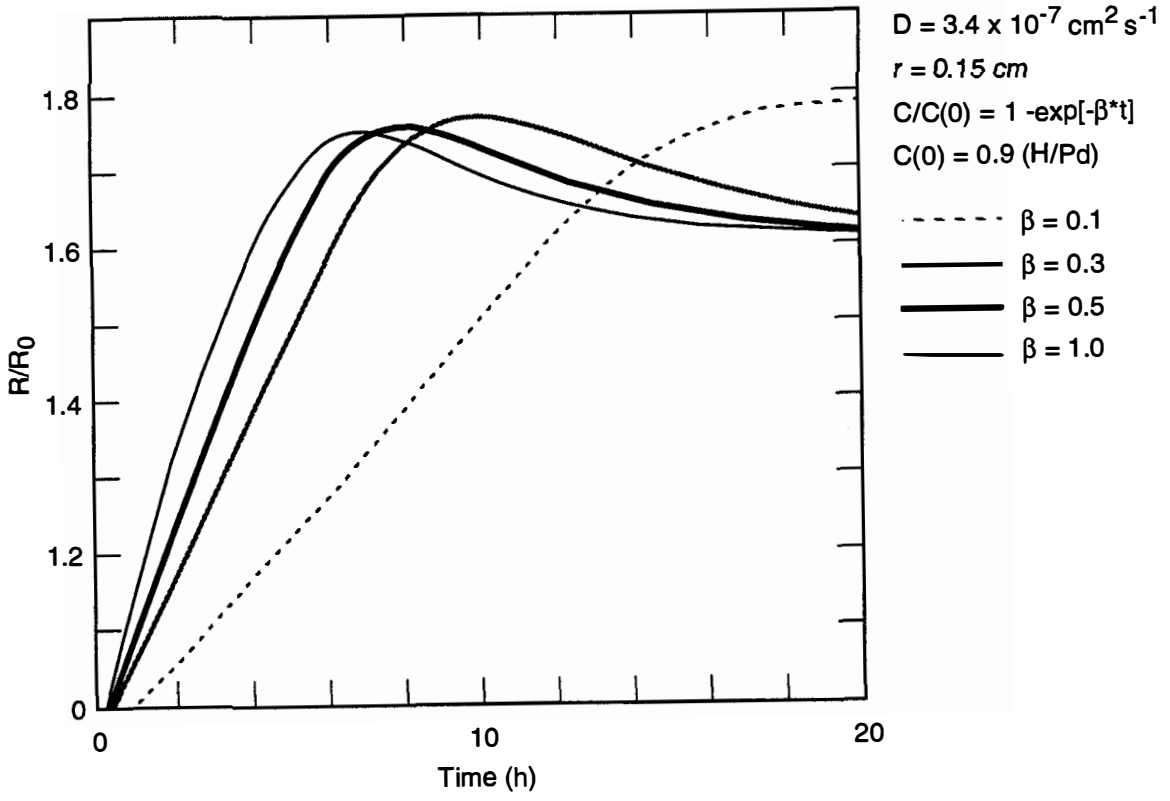

Figure 2-33
Variation of resistance ratio with time.

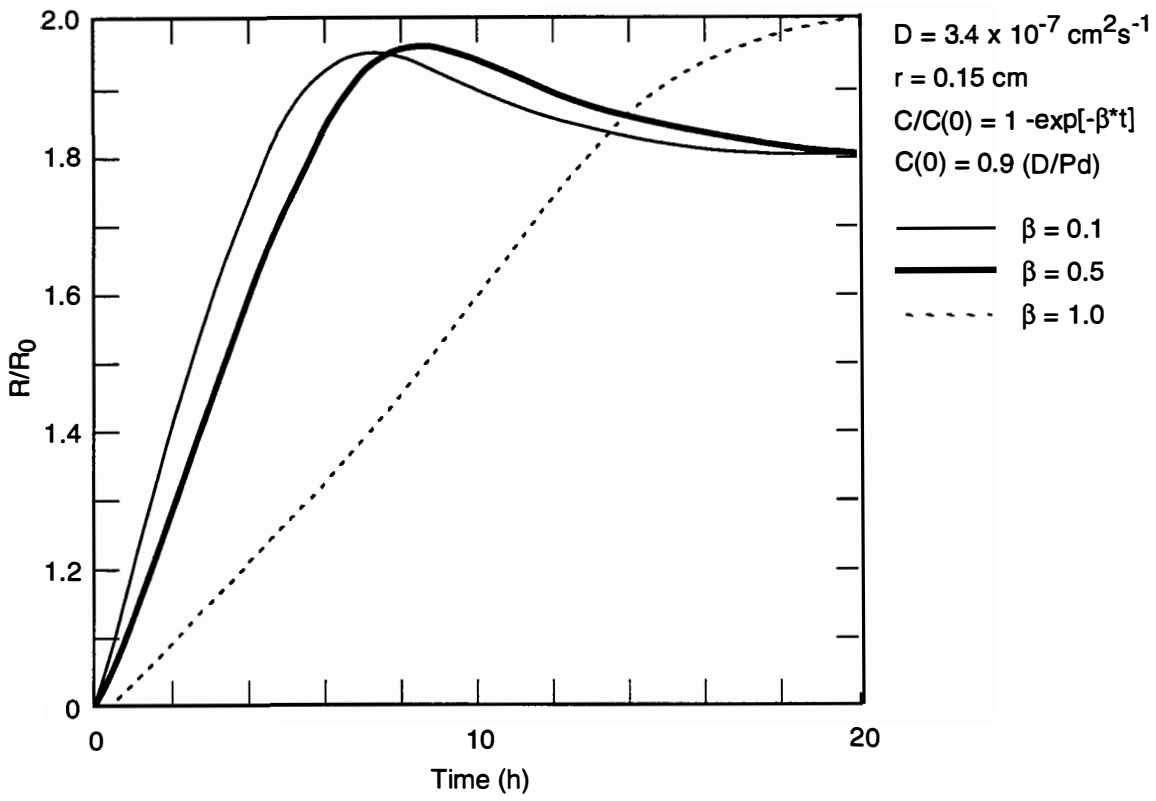

Figure 2-34
Variation of resistance ratio with time.

The theoretical calculations show that the resistance ratio versus time curves can be interpreted in terms of an exponentially increasing entry surface concentration rising to a steady-state value. The theoretical curves exhibit the features of the experimental curves, including an initial two stage region increasing to a maximum value, followed by a decrease to a constant value at long times. In addition, the theoretical curves show an attenuation in the maximum value due to the nonuniformity of the concentration profiles, as seen in the experimental curves.

2.3.4 References

1. F. A. Lewis. *The Palladium Hydrogen System.* San Diego: Academic Press, 1967.
2. E. Wicke and H. Brodowsky. In *Hydrogen in Metals II*, Eds. G. Alefeld and J. Völkl. Berlin: Springer-Verlag, 1978, p. 73.
3. E. Wicke and G. H. Nernst. Ber. Bunsenges. Phys. Chem. **68**, 224 (1964).
4. B. Baranowski, S. Majchrzak, and T. B. Flanagan. J. Phys. F **1**, 258 (1971).
5. G. Bambakidis, R. J. Smith, and D. A. Otterson. Phys. Rev. **177**, 1044 (1969).
6. R. J. Smith and D. A. Otterson. J. Phys. Chem. Solids **31**, 187 (1970).
7. F. Fischer. Ann. Phys. **20**, 503 (1906).
8. T. B. Flanagan and F. A. Lewis. J. Chem. Phys. **29**, 1417 (1958).
9. T. B. Flanagan and F. A. Lewis. Trans. Faraday Soc. **55**, 1400 (1959).
10. T. B. Flanagan and F. A. Lewis. Z. Phys. Chem. N. F. **27**, 104 (1961).
11. J. C. Barton, F. A. Lewis, and I. Woodward. Trans. Faraday Soc. **59**, 1201 (1963).
12. B. Baranowski and R. Wisniewski. Phys. Stat. Sol. **35**, 593 (1969).
13. T. B. Flanagan. J. Phys. Chem. **65**, 280 (1961).
14. B. Baranowski, S. M. Filipek, M. Szustakowski, J. Farny, and W. Woryna. J. Less-Common Metals, **158**, 347 (1990).
15. A. W. Szafranski and B. Baranowski. Phys. Stat. Sol. (a) **9**, 435 (1972).
16. A. W. Szafranski. Phys. Stat. Sol. (a) **19**, 459 (1973).
17. A. M. Riley, J. D. Seader, and D. W. Pershing. J. Electrochem. Soc., **139**, 1342 (1992).
18. B. Baranowski. In *Hydrogen in Metals II*, Eds. G. Alefeld and J. Völkl. Berlin: Springer-Verlag, 1978, p. 157.
19. K. Denbigh. *The Principles of Chemical Equilibrium.* Cambridge, UK: Cambridge University Press, 1971.
20. R. L. Mills, D. H. Liebenberg, J. C. Bronson, and L. C. Schmidt. J. Chem. Phys. **66**, 3076 (1977).
21. R. L. Mills, D. H. Liebenberg, and J. C. Bronson. J. Chem. Phys. **68**, 2663 (1978).

22. M. Tkacz and B. Baranowski. Roczn. Chemii **50**, 2159 (1976).
23. B. Baranowski and R. Wisniewski. J. Phys. Chem. Solids **29**, 1275 (1968).
24. S. A. Semiletov, R. V. Baranova, Yu. P. Khodyrev, and R. M. Imarnov. Sov. Phys. Crystallogr. **25**, 665 (1980).
25. R. V. Baranova, Yu. P. Khodyrev, R. M. Imamov, and S. A. Semiletov. Sov. Phys. Crystallogr. **25**, 736 (1980).
26. M. Kuballa and B. Baranowski. Ber. Bunsenges. Phys. Chem. **78**, 335 (1974).
27. S. Majorowski and B. Baranowski. J. Phys. Chem. Solids **43**, 1119 (1982).
28. J. O'M. Bockris and P. K. Subramanyan. Electrochim. Acta **16**, 2169 (1971).
29. M. McKubre. Unpublished data.
30. J. Crank. *The Mathematics of Diffusion.* UK: Oxford, Clarendon Press, (1975).

3

CALORIMETRIC STUDIES

3.1 Introduction

Table 3-1 describes the conditions employed and the results obtained in the significant calorimetric experiments carried out in this program. Certain experiments are described in this Section, as outlined below. A comprehensive compilation of the data obtained in one particular experiment, denoted P19, is included in a separate section, Section 3A. Another separate section, Section 3B, reports the details of the one well-characterized observation of temperature excess for the Pd-coated reference cell.

3.1.1 *Outline*

3.1 Introduction

3.2 Experiments P1 and P2
Section 3.2 has been published as a manuscript entitled "Calorimetry and Electrochemistry in the D/Pd System" in *Proceedings of the First Annual Conference on Cold Fusion*, National Cold Fusion Institute, Salt Lake City, UT, 1990, p. 20.

3.3 Experiments P12 through P16
This contents of Section 3.3 were originally published as a manuscript entitled "Isothermal Flow Calorimetric Investigations of the D/Pd System" in *The Science of Cold Fusion*,, Eds. T. Bressani, E. Del Giudice, and G. Preparata, Conference Proceedings Vol. 33, Italian Physical Society, Bologna, 1992, p. 419. The account included here is an updated version based on a presentation given at the Eighth Australasian Electrochemistry Conference, Auckland, New Zealand (February 1992).

3.4. Description of experiment C1.
Section 3.4 is based on a presentation given at the Third International Conference on Cold Fusion, Nagoya, Japan, 1992.

3.1.2 *Overview of Significant Calorimetric Experiments*

Table 3-1 summarizes the cell configurations, operating conditions, and excess power/energy results for the significant calorimetric experiments undertaken during the period covered by this report.

3.2 Experiments P1 and P2

Following the announcement in 1989 by Fleischmann, Pons, and Hawkins[1] of anomalous effects in the D/Pd system, we performed a series of experiments designed to examine anomalous excess enthalpy associated with this system and to discover some of the experimental variables that might be important to the effects. We designed our experiments with two important principles in mind: the need for precise calorimetric measurements in a closed system and the need for knowledge at all times of the composition of the reacting system. These principles were based on the understanding that calorimetry in an open system is subject to more error than in a closed one; this is especially important when one is seeking small excess enthalpies relative to the total power input into the system. The second principle is based on the belief that anomalous phenomena associated with the D/Pd system probably are related in some way to the D/Pd ratio, and that a high ratio, which is equivalent to a high D fugacity in the metal, is an important factor in determining the onset of the phenomena. To facilitate high loading, we have operated our calorimetric electrochemical charging cells at an elevated pressure of D_2 gas and at low temperatures. Deuterium solubility in Pd is a function of the applied electromotive force (emf), the D_2 gas pressure, and the temperature. The effect of temperature on solubility is very significant; the solubility at 5°C is 7-fold that at 50°C, so lowering the temperature (and thereby increasing the deuterium solubility) is equivalent to increasing the gas pressure. A high pressure of D_2 also has the important effect of depolarizing the anode reaction and hence reducing problems associated with O_2 production.

A further feature of all our experiments was to have comprehensive monitoring of all the experimental parameters, e.g., cell current and voltage, reference voltage, Pd cathode resistance, electrochemical impedance, gas pressure, and all temperatures pertinent to the experiment.

TABLE 3-1

CELL CONFIGURATION

				Electrolyte				Maximum				Duration		Maximum Power			Total Energy			Excess
	length	dia.	A	Type	Conc	Add.	Bath T	Pressure	Current	Loading		Expt.	Init.	Input	Excess		Input	Excess		Observations
#	(cm)	(cm)	(cm^2)		(M)		(°C)	(psi)	(A/ cm^2)	R/R°	D/Pd	(hours)	(hours)	(W)	(W)	%	(MJ)	(MJ)	%	#
7mm diameter (differential calorimeter)																				
P1a	5	0.7	11.0	LiOD	1.0	none	7	650	682	1.20	1.058	696	369	3.35	1.75	52.2%	3.4	0.07	2.11%	5
P1b	5	0.7	11.0	LiOD	1.0	none	7	650	682	?	?	696	299	3	0.2	6.7%	3.0	0.01	0.47%	2
4mm diameter Johnson Matthey																				
P2	4.5	0.3	4.2	LiOD	1.0	none	4	1000	495	1.65	0.937	1393	504.33	3.8	2	52.6%	50.2	1.07	2.14%	4
3mm diameter Engelhardt Pd																				
P3	4.5	0.3	4.2	LiOD	1.0	none	25	1000	354	1.70	0.920	1250					18.0			0
P4	5	0.3	4.7	LiOD	0.1	none	30	100	509	1.80	0.885	1165					16.8			0
P5	5	0.3	4.7	Li2SO4	0.5	none	16	100	849	1.70	0.920	287					4.1			0
P6	5	0.3	4.7	Li2SO4	0.5	As2O3	30	100	573	1.70	0.920	649					9.3			0
P7	4.5	0.3	4.2	LiOD	1.0	none	8	1000	259	?	?	145					2.1			0
P8	3	0.3	2.8	LiOD	0.1	none	35	100	637	1.65	0.920	186					2.7			0
P9	3	0.3	2.8	LiOD	1.0	none	35	50	531	1.65	0.920	597					21.5			0
P10	4.5	0.3	4.2	LiOD	1.0	none	35	900	47	?	0.937	18					0.3			0
P11	4.5	0.3	4.2	LiOD	1.0	none	35	1050	1179	1.65	0.937	85					1.2			0
Al additions commenced																				
P12	3	0.3	2.8	LiOD	1.0	4He,Al	30	50	884	1.55	0.937	1631	316	10	0.97	9.7%	58.7	0.80	1.36%	4
P13	3	0.3	2.8	LiOH	1.0	Al	30	50	884	1.1*	0.966	815		15	0	0.0%	11.7	0.00	0.00%	0
P14	3	0.3	2.8	LiOD	1.0	3He,Al	30	50	884	1.60	0.951	692	184	10.5	0.5	4.8%	10.0	0.20	1.96%	2
P15	3	0.3	2.8	LiOD	1.0	Al*	30	40	884	1.58	0.957	1104	684	10	2.4	24.0%	39.7	0.55	1.38%	3
P16	3	0.3	2.8	LiOD	1.0	3He,Al*	30	40	884	1.70	0.920	1104	948	10	0.4	4.0%	39.7	0.10	0.24%	4
P17	3	0.3	2.8	LiOD	1.0	Si	30	40	389	1.29	1.036	1202	1040	10	0.2	2.0%	13.0	0.10	0.75%	2
P18	3	0.3	2.8	LiOD	1.0	Al	35	40	884	Failed early due to electrical contact					Calorimetry started 677 h					
P19	3	0.3	2.8	LiOD	1.0	**B**	35	40	672	1.45	0.993	1287	261	0.25	0.85	340%	23.2	0.41	1.79%	4*
P20	3	0.3	2.8	LiOD	1.0	Al	35	40	707	1.55	0.966	954	650	12	0.28	2.3%	17.2	0.16	0.96%	3
P21	3	0.3	2.8	LiOD	1.0	**B**	30	40	707	1.60	0.951	764	390	10.5	0.6	5.7%	13.8	0.04	0.28%	2
P22	3	0.3	2.8	LiOD	1.0	**B**	30	40	707	1.30	1.032	1480	378	0.27	0.08	29.6%	21.3	0.27	1.29%	3**
1mm diameter & 100μm foil (Johnson Matthey)																				
C1	30	0.1	9.4	LiOD	1.0	Al	30	50	764	1.65	0.937	866	390	45	1.35	3.0%	49.1	1.12	2.28%	1
C2	25	μm	60.0	LiOD	1.0	Al	30	50	120	1.60	0.951	356	190	35	3	8.6%	14.4	0.56	3.88%	1

* Last event spontaneous, persisted through stripping cycle

** First event spontaneous, persisted through stripping cycle, last event terminated by H2O addition

3.2.1 *Resistance Measurements*

None of the "cold fusion" electrolysis experiments described to date contain any means of determining the D/Pd content *in situ.* Yet this ratio may be a crucial difference between those experiments that have produced a Fleischmann-Pons effect and those that have not. The resistance of Pd metal is a function of its hydrogen content[2] and is, in principle, the easiest way of determining the state of the Pd electrode as the experiment proceeds. Unfortunately, the relationship between the resistance and the D/Pd ratio is known only up to 0.65, but until further calibration experiments are performed, these data can be used at least as an indicator that the ratio is ≥0.65. Also, comparisons can be made with the H/Pd system, which is calibrated in resistance change up to H/Pd = 1.1.[3]

Figure 3-1 shows the known data for the resistance ratio, R/R°, as a function of hydrogen loading (from the data of Baranowski and Wisniewski[3]) and deuterium loading (from the data of Barton, Lewis, and Woodward[4]). The solid line shows an extrapolation of the D/Pd resistance data, based on the assumption that the resistance behaviors of the H and D systems are similar and that resistance maxima occur at the same degree of loading. The inferences that we make about degrees of loading higher than 0.65 for D/Pd are based on this assumption and were obtained by fitting the measured resistance ratio data to the fifth-order polynomial given in Figure 3-1. It is clear that the assumption of similar resistance behavior for H and D in Pd, differing only in the magnitude of the effect and the length of the extrapolation, results in significant quantitative uncertainty at high loading levels. We nevertheless expect the loading levels inferred from resistance measurements to be useful qualitatively.

Several factors may influence the measured resistance. Of these, temperature, the occurrence of cracking, and inhomogeneity of loading in the metal phase produce the most significant effects. As shown in Figure 3-2, the temperature coefficient of resistance for the H/Pd system varies over a considerable range, from the pure metal to H/Pd $\simeq$ 0.7; however, we have no data on the behavior in this regard of D/Pd up to 0.7, or of any hydrogen isotope at higher loadings. Our own results suggest that the behavior shown in Figure 3-2 is closely obeyed in the deuterium system but that the temperature coefficient remains more or less constant at ~ 2×10^{-3} K^{-1} at higher loadings. This functional form is assumed in correcting our resistance data for temperature effects.

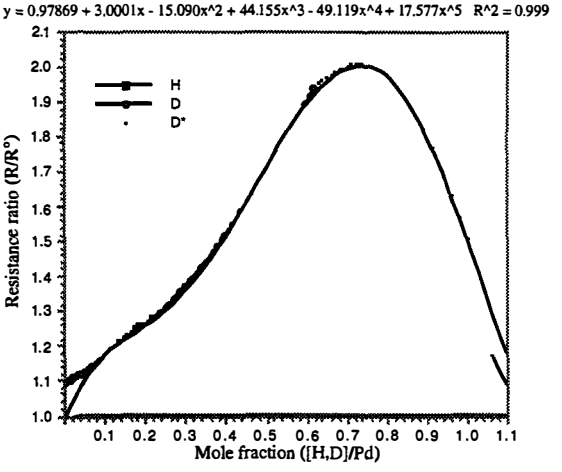

Figure 3-1 R/R° versus loading; data from Refs. 4 (for H) and 5 (for D).

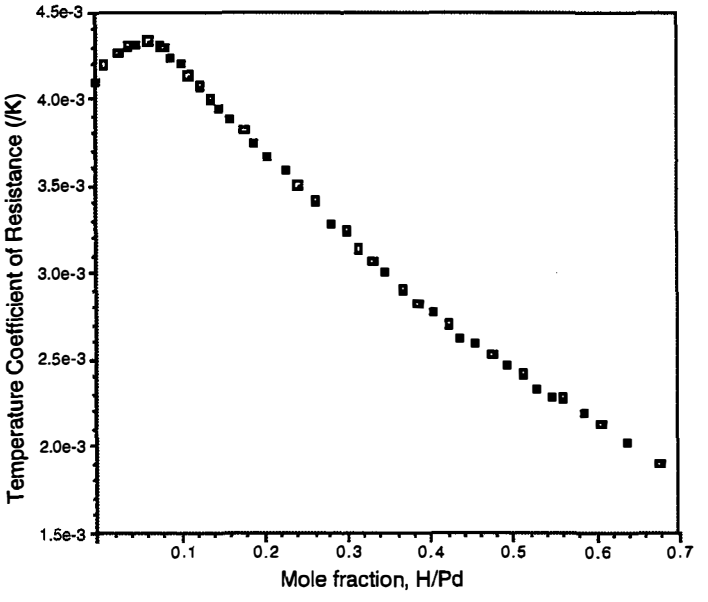

Figure 3-2. Temperature coefficient of resistance of palladium as a function of hydrogen loading After Ref. 4.

When the profile of composition in the metal phase is significantly nonuniform, owing to high absorptions or desorption fluxes, the average resistance may not reflect the average loading. This problem arises particularly during anodic deloading, when the surface achieves the low resistance of the α-phase. At low

absorption fluxes, the concentration profiles are sufficiently flat that this problem seldom complicates the interpretation of resistance data.

Resistance inhomogeneities due to cracking or phase nucleation also may yield measured resistances that do not reflect the average composition of the D/Pd system. The extent of cracking can be minimized by loading the electrode unidirectionally, or by pre-loading at temperatures higher than ~350°C, to avoid the α to β-phase transformation.

3.2.2 *Differential Calorimetry*

Concept. Because the applied current, electrochemical "cold fusion" cells produce Joule heat, and any extraneous heat-producing reactions must be detected in addition to this heat. A convenient way of detecting chemical or nuclear reaction enthalpy is by comparing the temperature or heat flux from identical cells where one cell is restricted to producing Joule heat only.
Heat is produced in an electrochemical cell with D_2O electrolyte and Pd cathode as a result of several phenomena: absorption of D in Pd, overvoltages on the cathode and anode, and I^2R heating in the electrolyte. The first of these factors becomes less significant once the D/Pd ratio has reached a steady state. Ideally, the other two factors should be the same in the experimental cell and the reference cell, the latter being the cell where the heat production is limited to Joule heating only. In this program, Joule heating differences in the two cells were minimized by using electrode surfaces and cells of identical size and shape, as well as identical electrolytes. Any bulk phase reactions arising from the palladium were minimized in the reference cell by using a palladized Cu electrode. This approach to the construction of the reference cell is based upon the tenet that fusion reactions occur, if at all, in the bulk phase and not on the surface of the electrode. If surface reactions are heat producing, then they are likely to occur in the Cu/Pd cathode before comparable reactions occur in the bulk Pd rod, since the thin Pd layer on the Cu rod would become saturated with deuterium before the Pd rod.

An alternative approach is to use H_2O in the reference cell. However, because H_2O electrolytes have different overpotentials and different electrical and thermal conductivities than their D_2O equivalents, the Joule heating will be different. In addition, the heat of adsorption of D in Pd is significantly different from that of H in

Pd. For these reasons, light water provides a poor blank for the experiments described below.

The electrolysis of water in our cells was minimized by keeping the applied cell voltage below that required for oxygen evolution. From the known thermodynamic and kinetic values, we calculated the minimum cell voltage required for the evolution of oxygen from light water as 1.27 V, and even at 1.8 V the electrolysis current would not be above 1 mA.

Experimental Approach. Figure 3-3 illustrates a cell design that incorporates the features referred to above and except for the Pd electrode, is the same for both the experimental and reference cells.

The body of the cell was constructed from copper, which was chosen for its high thermal conductivity, low solubility and diffusivity of hydrogen isotopes, and ability to accommodate a pressure of at least 50 atm. All interior surfaces were platinum (5 μm) coated on nickel (25 μm). Both these metals are resistant to corrosion in LiOD under the conditions applicable to this experiment. Temperature was measured with a four-terminal resistance temperature device (RTD) embedded in each cathode.

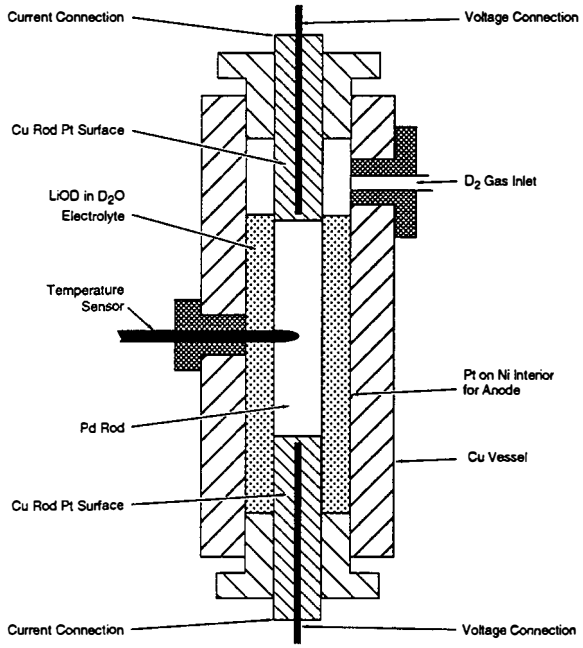

Note that the reference cell is identical except for the Pd electrode, which is pallidized Cu.

Figure 3-3 Cell for Differential Calorimeter

For the experimental cell, the cathode was made from twice vacuum melted Pd, which was machined, then annealed in a vacuum at 800°C for 3 hours, then backfilled at temperature with D_2. Palladized copper was used for the reference cell cathode. The electrolyte was prepared by the addition of 99.9% Li metal (Ventron Alfa Products) to 99.9% D_2O (Aldrich Chemicals).

The cells were placed, as shown in Figure 3-4, in an insulated bath cooled to ~7°C. Pressure was applied to the cells from a D_2 gas cylinder. Each cell could be pressurized independently or removed from the gas system; a relief valve was also included to prevent overpressurization of the system in the event of a large exothermic reaction.
An Apple Macintosh microcomputer with a Keithley data acquisition system was used to monitor (once a minute) the temperature of the Pd and Cu cathodes, the bath temperature, both cell voltages, and the current. The interfacial impedances were measured every 10 minutes during the final 400 hours of the experiment.

The cells were filled with electrolyte, and the cathodes were then charged galvanostatically in series at 10 mA cm^{-2} for five days. On the establishment of steady-state temperatures and voltages, the Pd electrode resistance was measured and the current increased by an amount just sufficient to keep the applied cell voltage below 1.5 V, to prevent oxygen evolution. The above sequence was repeated periodically.

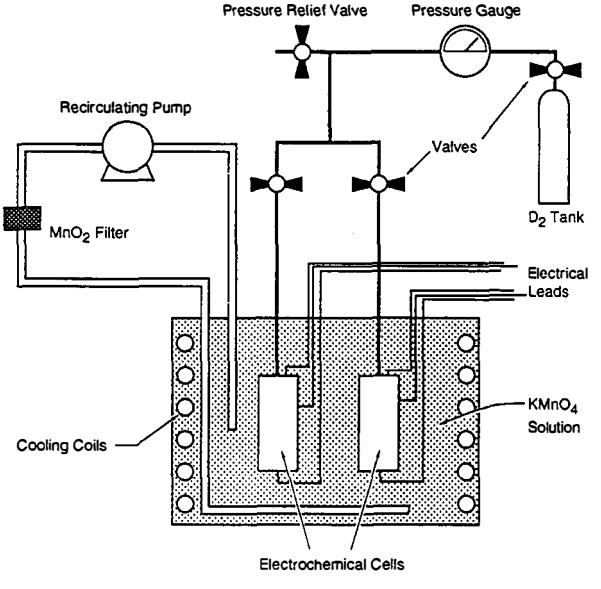

Figure 3-4 Schematic Diagram of Differential Calorimeter

At intervals during the charging process, the resistance of the bulk palladium electrode was measured using a four-terminal AC measurement of the longitudinal impedance to determine the deuterium loading level. Measurements also were made of the two-terminal cell impedance, to determine what fraction of the DC cell voltage was associated with IR drop in the electrolyte and what was due to the deuterium redox overpotential.

Calorimetry. If I is the current and V the cell voltage, then in the steady state the input power is the sum of the product IV and any extraneous sources of heat, Q_u. If the calorimeter heat capacity and cooling constant are C_p and K, respectively, then for an elapsed time t,

$$IV + Q_u/t = (C_p + K)\,\Delta T \tag{3-1}$$

where $\Delta T = T_{cell} - T_{bath}$.

This relationship can be further expressed as

$$IV = C_p\,\Delta T - Q_u/t \tag{3-2}$$

The calorimeter was calibrated by varying the input electrochemical power to the two cells in series. With $Q_u = 0$, we expect a linear relationship between the input Joule power to each cell, IV, and the observed temperature difference between cell and bath:

$$IV = a\Delta T + b \tag{3-3}$$

The cells were calibrated according to Eq. 3-3 using both stepped and ramped currents, to establish a steady-state slope and intercept: a and b for the working cell and a' and b' for the reference cell. We do not make any attempt to calculate or calibrate the temporal response of these cells to a change in input Joule heat or thermal conditions. Instead, in the differential mode, we assume that the only

differences between the responses of the working and reference cells are those due to the difference in the steady-state calibration coefficients (a and a', b and b') and the possible existence of extraneous heat, Q_u, in the working cell. That is,

Working cell: $a\Delta T + b = IV + Q_u$

Reference cell: $a'\Delta T' + b' = IV'$

$$Q_u = a\Delta T + b - (a'\Delta T' + b')\ V/V' \qquad (3\text{-}4)$$

Equation (3-4) reflects the extraneous heat if all influences on the two cells are the same except for the quantified and calibrated differences between the primed and unprimed variables. This procedure yields a positive excess if the extraneous heat occurs in the working (solid Pd) cell, a "negative excess" if this heat occurs in the reference (Pd coating) cell, and zero if there are no extraneous, uncorrelated influences.

Results. Table 3-2 displays a chronology of observations. Except for the times noted in Table 3-2, the differential calorimeter operated with Q_u close to zero, with a statistical fluctuation of ± 200 mW. We observed anomalous enthalpic effects from the experimental cells and possibly also from the reference cell. The enthalpic events referred to occured when the output power, observed as heat, was in excess of the input power.

The events described in the Table as ∂V refer to occasions when the cell voltage underwent spontaneous changes at constant current, temperature, and pressure. These events occurred without accompanying bursts of power in excess of that provided by the input electrical power, and they were observed for the experimental cell only.

TABLE 3-2
CHRONOLOGY OF ANOMALOUS EVENTS IN THE DIFFERENTIAL CALORIMETER

Date	Time	Event	H(kJ)
5/15	2300	$\partial H\ XS_{Cu}$	<3
5/17	1800	$\partial H\ XS_{Cu}$	~10
5/18	0530	∂V_{Pd}	0
5/18	2100	$\partial H\ XS_{Pd}$	5
5/19	0800	$\partial H\ XS_{Pd}$	32
5/20	0100	∂V_{Pd}	0
5/21	2200	∂V_{Pd}	0
5/22	1900	∂V_{Pd}	0
5/24	1800	$\partial H\ XS_{Pd}$	<3
5/26	1700	∂V_{Pd}	0
5/31	1300	$\partial H\ XS_{Pd}$	26
6/01	$0700_{(2)}$	$\partial H\ XS_{Pd}$	6

where H = enthalpy, V = voltage, XS = excess.

Figures 3-5 and 3-6 show data for Q_u calculated using Eq. 3-4. Also displayed is the excess energy for the two periods of essentially 12 hours each, although the features in Figure 3-6 presumably are continuations of the event in Figure 3-5 (note that the vertical scales of the two figures differ). The event in Figure 3-5 appears to have been initiated by a transient decrease in the cell temperature; both occurred in the interval between 16 and 17 hours in that figure. During this time a slowly increasing current ramp was begun, although it was initiated some 20 minutes after the leading edge of the apparent positive power excess.

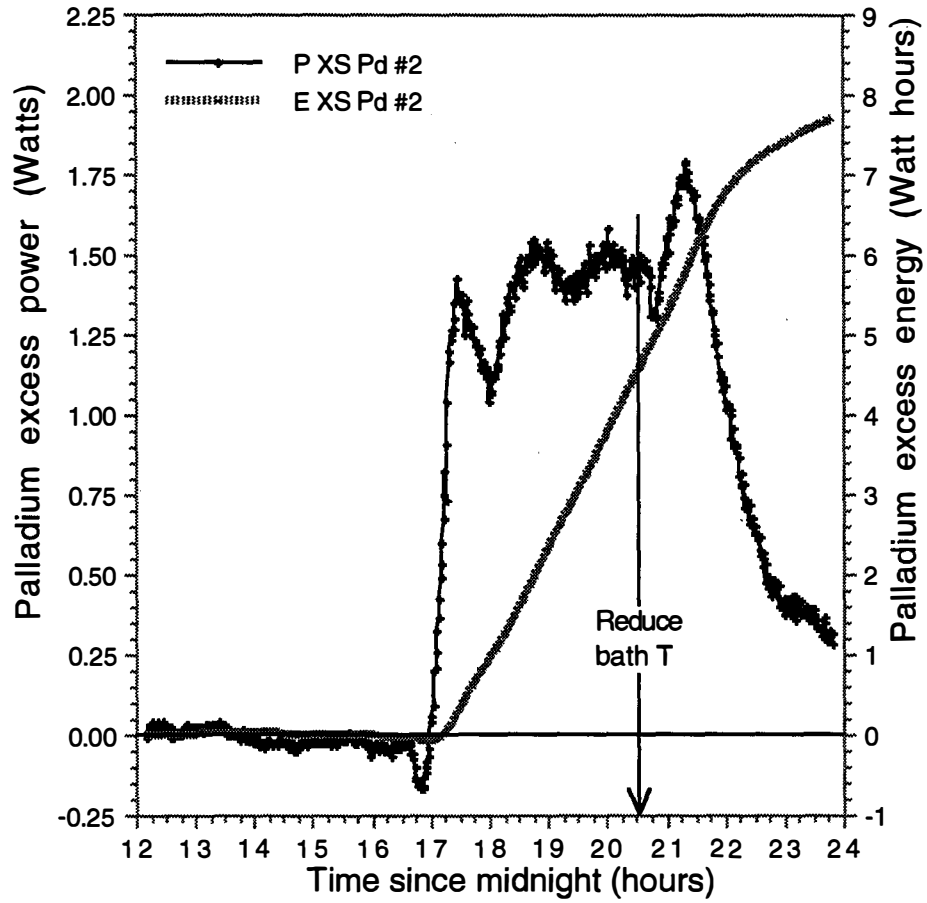

Figure 3-5 Differential calorimeter excess power and energy: May 31, 1989.

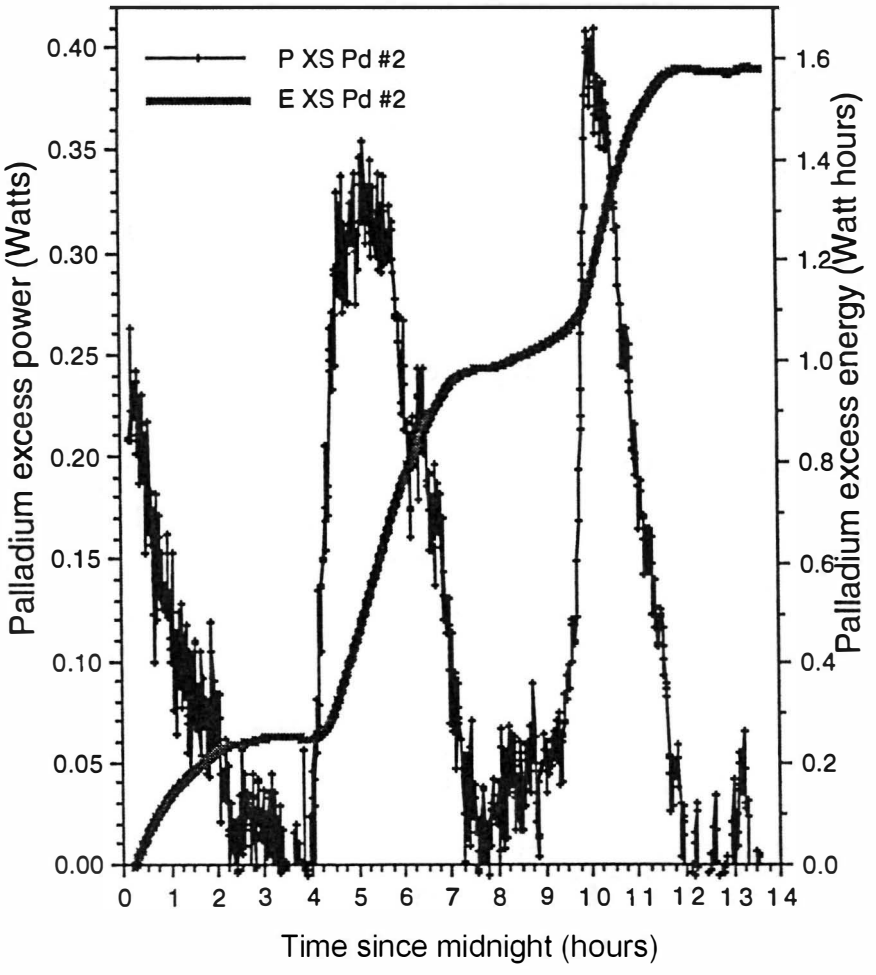

Figure 3-6 Differential calorimeter excess power and energy; June 1, 1989.

3.2.3 *Flow Calorimetry*

Concept. A second series of experiments was performed in a flow calorimeter operated isothermally. Figure 3-7 depicts the calorimeter schematically. In the experiment described here, only one calorimeter cell was used. During operation, the electrochemical cell was contained inside the calorimeter Dewar flask and the heat transfer fluid (silicone oil) was pumped through it. Temperature control was maintained by mounting the calorimeter in a well regulated bath (±0.01°C) and by equilibrating the temperature of the oil with that of the bath before it was pumped into the Dewar flask. The flow rate was maintained constant to within ±1% by means of an FMI metering pump; this was monitored continuously with a rotameter-type flow meter and periodically by weighing timed samples removed from the flow. Two RTD temperature sensors were placed in the inlet to and the outlet from the calorimeter; turbulence promoters were employed to ensure that the fluid was well mixed before it passed over the outlet sensors.

The electrochemical cell was a nickel pressure vessel whose interior and all other fittings were coated with Pt (5 μm). Provision was made for four-terminal resistance measurements and a reference electrode. A helical electrical heater was mounted in grooves on the outside of the pressure vessel.

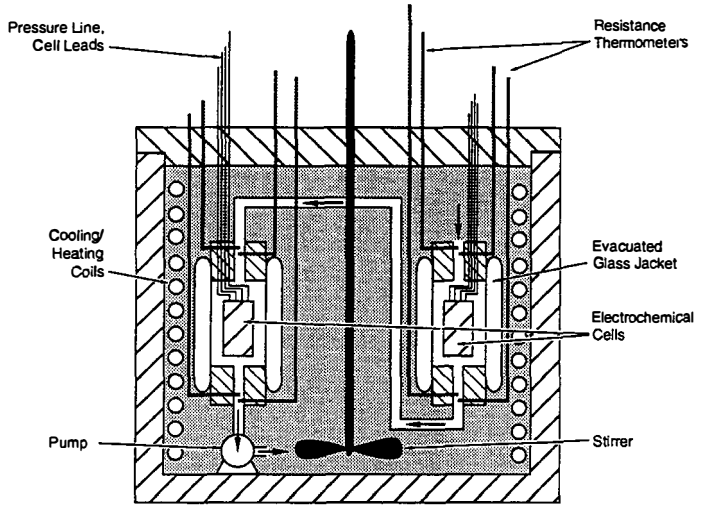

Figure 3-7 Schematic Diagram of Differential Calorimeter.

Calorimetry. To assist in rapid transfer of heat to the heat transfer fluid, a "finned jacket" was placed around the outside of the vessel. In operation, the total input

power to the calorimeter was maintained at a preset constant value by using the data acquisition computer to calculate the input electrochemical power and adjust the heater power. In this way, at constant mass flow of calorimetric fluid, the presence of excess power could be inferred from an increase in the temperature difference measured between the inflow and outflow. In the absence of excess power, any second-order effects of heat loss should remain constant since the temperature profile inside the Dewar flask is essentially constant.

The calorimeter was calibrated by several methods: by adjusting the heater power and the electrochemical power in a stepwise manner allowing the system to come to a steady state, and by dynamic methods where a sinusoidal or sawtooth waveform was applied to the heater.

The thermal output of the calorimeter is observed to have the following dependence on input power:

$$P_{heater} + P_{electrochem} = (C_p\ dm/dt + k')\ \Delta T \qquad (3\text{-}5)$$

where C_p is the heat capacity of the calorimetric fluid, dm/dt is the rate of mass flow through the calorimeter, and k' is a small loss term due primarily to heat loss through the electrical and pressure interconnects that penetrate the top of the calorimeter vessel.

The values of the constants C_p and k' were determined by a series of calibrations, where the input heater power was varied at constant flow rate and the flow rate was varied at constant input power. The value of C_p obtained was in precise accord with that obtained by independent heat capacity measurements and with the value supplied by the manufacturer. At the flow rates normally employed in the calorimeter (2-3 g/s), k' represents less than 5% loss due to conduction.

Experimental. LiOD of 0.1 M concentration was prepared by reacting pure Li metal with D_2O under nitrogen in a glove box.

The Pd electrode was prepared by etching in aqua regia, annealing the sample in a vacuum for 4 hours at 800°C, and then cooling under D_2. Upon cooling to room temperature, the electrode was placed in the electrochemical cell.

Parameters monitored were the cell current and voltage, reference voltage, Pd resistance, two inlet and two outlet temperatures, two cell temperatures, cell pressure, and calorimetric fluid flow rate. Electrochemical impedance measurements were made at regular intervals to monitor the kinetic processes at the Pd/LiOD interface.

The cell was operated with 60 atm of D_2 pressure and with varying cathodic current densities up to 600 mA cm^{-2}. Experiments were performed at 25°C and 4°C.

Table 3-3 displays a chronology of excess heat observations, where ΔT increased spontaneously in the apparent absence of any spurious effects. Figure 3-8 shows the raw data for Event #2, calculated from the difference between the calorimeter output power, determined from Eq. (3-5), and the known input power, $P_{electrochem} + P_{heater}$. This figure provides a good indication of the level of baseline variation of the "excess" power; for some period prior to and subsequent to the positive excursion shown in Figure 3-8, the "excess" power registers zero, with a random variation of roughly 0.2 W. The structured variation of the "excess" power apart from the burst is due to the enthalpy of partial recombination of D_2 and O_2. At high current densities, the anodic reaction is not completely depolarized by the D_2 pressure, and electrolysis occurs. The products of this reaction (and all the associated enthalpic effects) are contained within the calorimeter. Recombination occurs on the inner exposed surfaces of the Pt-coated pressure vessel, and its progress can be monitored by the pressure. We observed pressure oscillations with a period of approximately 30 minutes, consistent with small positive and negative fluctuations of the "excess" heat. No significant change was observed in the cell pressure associated with the heat burst shown in Figure 3-8, and the recombination fluctuations occurred throughout this positive heat excursion.

TABLE 3-3
CELL P2 EXCESS ENTHALPY

Date	Time	Duration (h)	H(kJ)
10/11	21:40	Cell Start-up	
11/1	22:00	13	49
11/3	10:00	11	49
11/5	23:00	24	154
12/10	12:00	46	46
		TOTAL	298

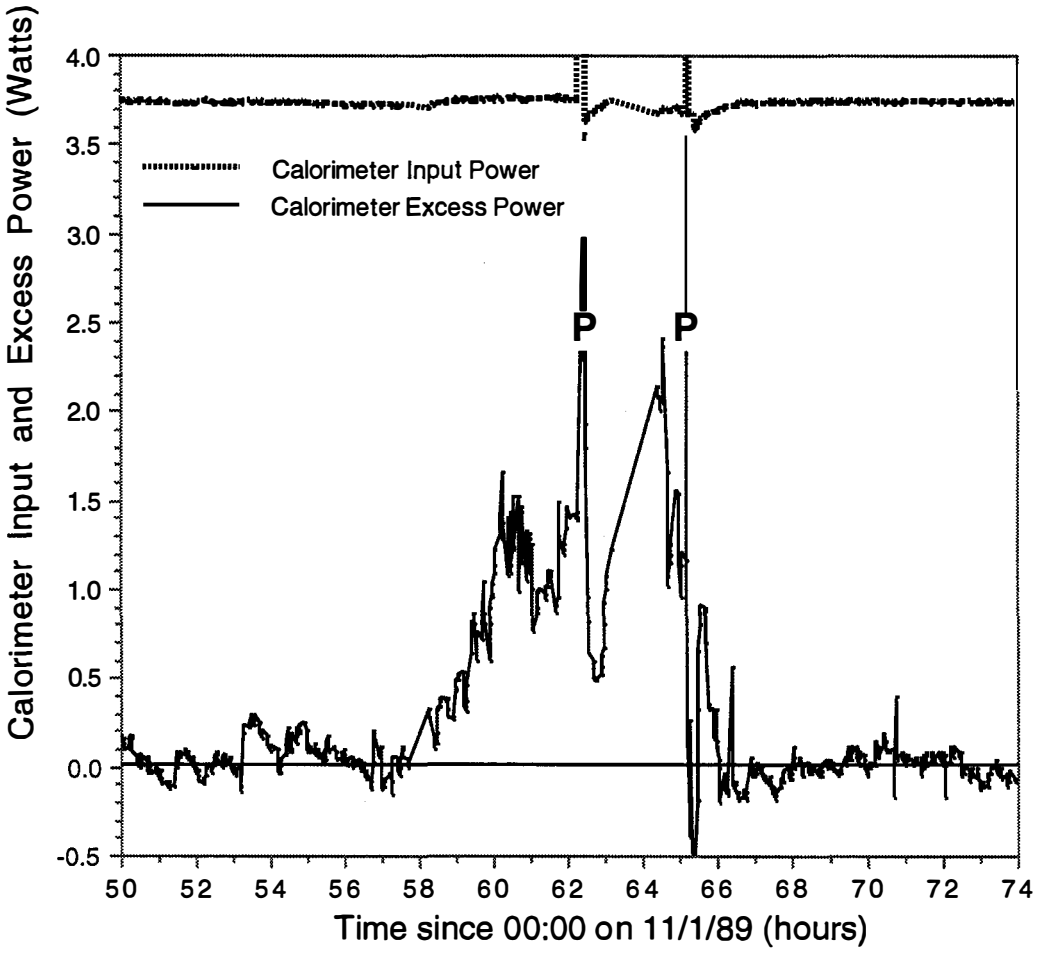

Figure 3-8 Flow calorimeter excess power and energy: November 1, 1989.

Also shown in Figure 3-8 is the electrochemical input power. At this time the heater was employed for power calibration only at the times marked "P". The average of the positive excursion is approximately 1.25 W, nearly 33% of the total input power to the calorimeter at that time. The excess energy was calculated from the area of the envelope of the event in Figure 3-8 to be 49 kJ, excluding the effects of the heater calibration pulse, which are incompletely removed from the steady-state calculation. At no time were negative excursions of similar form or comparable magnitude observed in the data record. The energy total of the four events of apparent excess heat in this experiment was 298 kJ. This energy represents 7.45 MJ/mol for an electrode that comprised 0.04 mol of Pd.

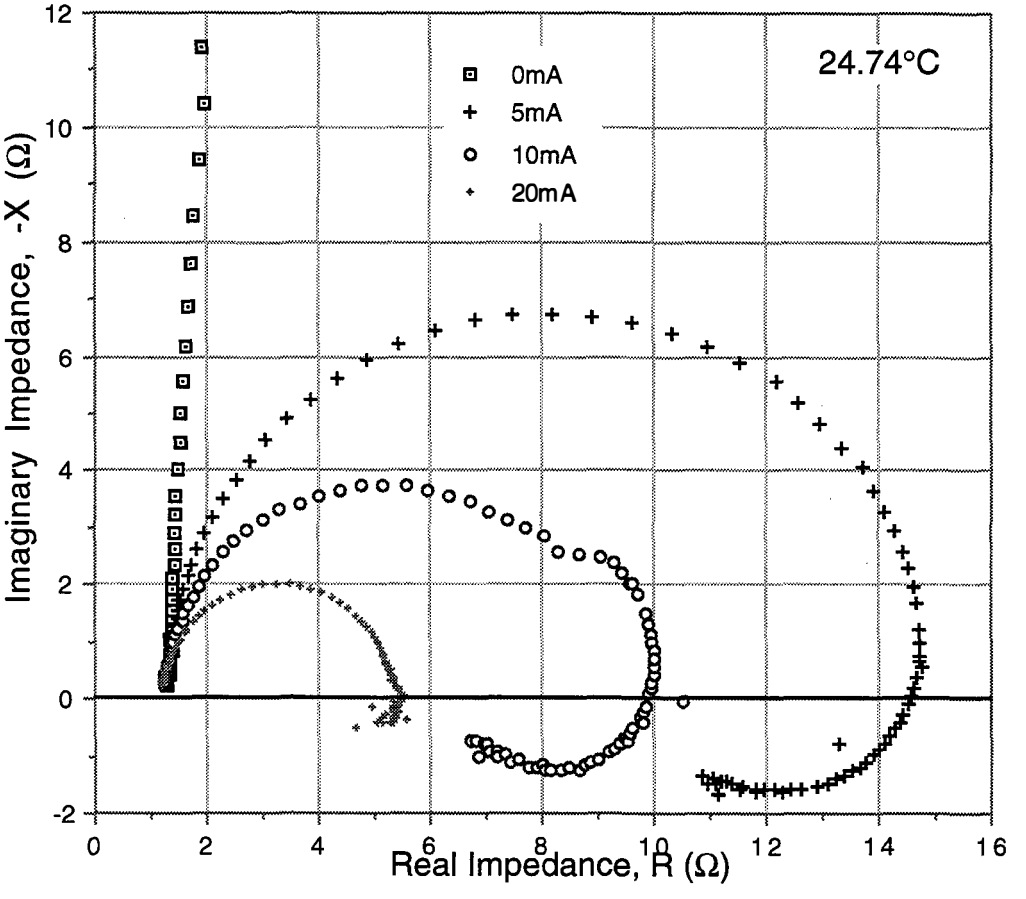

Figure 3-9 Pressurized Cell P2; complex plane impedance plot as a function of applied cathodic bias.

Impedance Measurement. At low loading levels, the electrochemical impedance of the Pd/LiOD interface exhibits a single semicircle in the complex plane, which suggests that the response is due to the double layer capacitance and charge transfer resistance. At high rates of loading (high surface loading) or high equilibrium loading levels (high bulk loading), the interfacial impedance response exhibits a more complex behavior.

Figure 3-9 shows the impedance response of the electrode in the pressurized isothermal flow calorimeter at 25°C as a function of applied cathodic current (for an electrode with area of 4 cm^2). From the measured resistance ratio and the extrapolation of known data suggested by Figure 3-1, the electrode in this experiment had a bulk D/Pd loading of approximately 1.

Post-Test Analysis. One week after the electrode was removed from the pressurized isothermal flow calorimeter, it was placed between two layers of Polaroid ASA 3000 film for 12 days. Details of the resulting films are shown in Figure 3-10. Clear evidence of some type of ionizing radiation is observed. The points of light with diffuse halo exposure suggest that some of the radiation may be coming from point sources within the metal and being scattered by the lattice structure.

The surface and near surface of the sample were subjected to surface analysis by laser ionization (SALI) and compared to an identically treated blank electrode. No changes in isotopic composition were observed, and no unexpected elements were observed that might be consistent with fission products.

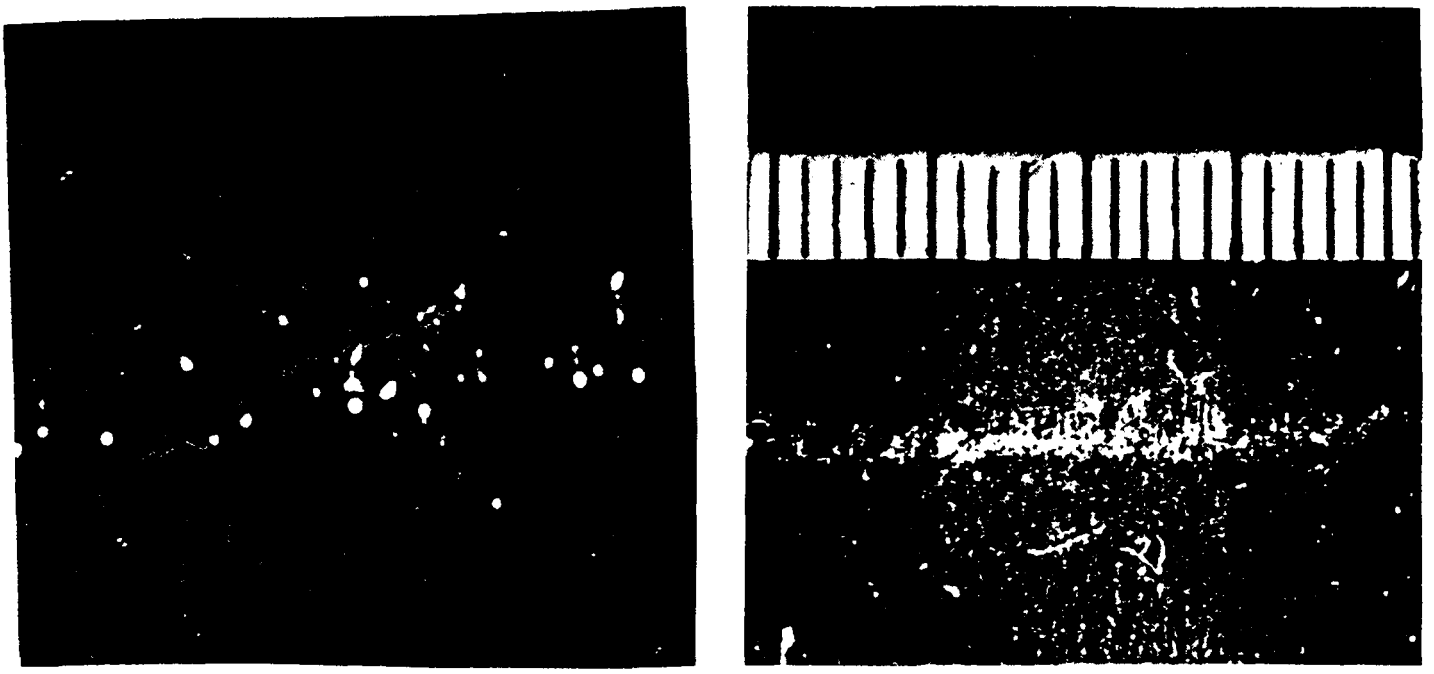

Figure 3-10 Autoradiograph of flow calorimeter, pressurized cell P2 electrode, after 12-day exposure; shown at 4x and 50x magnification (markings in centimeters).

Approximately 10% (2.5 g) of the total mass of the electrode, comprising one sample from the surface and one from the bulk, were analyzed by Rockwell International for ^{3}He and ^{4}He by mass spectrometry of a molten sample. This technique is capable of detecting ~4×10^{10} atoms per gram of Pd; no He was observed at that detection level.

Mass spectrometry was used to analyze the residual D_2 gas in the pressure vessel for ^{3}H, ^{3}He, and ^{4}He. At a detection level of 1 ppm, none of these isotopes were found.

The electrolyte was sampled for tritium before emplacement in the cell and after removal; no increase in tritium was observed above the background level (1.3×10^{11} atoms).

3.2.4 *Discussion*

Experiments were performed in two electrochemical cells comprising a Pt anode, LiOD electrolyte, Pd cathode, and D_2 gas. Both experiments appeared to give bursts of heat output in excess of the known sources of Joule input heat. In one experiment, differential calorimetry was employed; in a subsequent experiment, a more sophisticated isothermal flow calorimeter was used. The results nevertheless

were qualitatively similar: considerable periods in which the calorimeters were poised in thermal balance, with occasional positive excursions of output power that lasted hours or tens of hours and had magnitudes of several tens of kilojoules.

It is difficult to discuss the initiation of these events, given the apparent stochastic nature of the excess heat bursts. Nevertheless, we have observed no heat excess from electrodes that were loaded to D/Pd $\lesssim$ 1 (based on an extrapolation of known resistance ratio data). It may be that such loading is necessary. However, it is clearly *not* sufficient to produce the anomalous heat effects. In both cases, the Pd had achieved its minimum resistance (from which we infer maximum loading) condition several weeks prior to the observation of anomalous heat.

The interfacial impedance data may give a clue to other conditions that are necessary for anomalous heat effects to be observed. The impedance feature evidenced at low frequencies and appearing in the fourth quadrant of Figure 3-9 is not present at all times, even for a highly loaded electrode. In a subsequent paper, we will demonstrate that the impedance spectra can be accounted for quantitatively by the double layer capacitance in combination with the charge transfer resistance for D adsorption coupled with recombination and absorption at a fractional monolayer coverage of D. The fourth-quadrant feature derives from the coupling of the potential dependent adsorption coverage and the concentration dependent absorption flux. In qualitative terms, this "inductive" feature appears only when there is a significant absorption flux; it can be used as an indicator that the electrode surface is in a state such that the electrode is capable of further absorbing D.

Extended cathodization provides an opportunity for electroreducible minority components to deposit on the cathode surface. While we did not observe macroscopic fouling of the electrodes in this study, one might expect that the presence of a film of cathodically deposited contaminant species on the surface would block D absorption. In our experience, however, the presence of certain deliberately added impurities appears to create the inductive term *and* facilitate loading, whereas anodic stripping of the Pd appears to eliminate the fourth-quadrant term. It is therefore likely that the inductive effect is a feature of a specifically modified Pd surface, one that is of unknown origin but may be beneficial to loading.

The presence or absence of the inductive term, the existence of which effectively reduces the DC interfacial resistance, can be used also to account for the anomalous changes observed in the cathodic overvoltage of highly loaded electrodes. For both calorimeter cells, we have observed cases where the voltage measured between the surface of the cathode and an adjacent Pt pseudo-reference electrode has spontaneously and over a period of several hours increased at constant current or decreased at constant current—and in one case, the overvoltage was observed to decrease with increasing current.

It is possible that both high loading and high interfacial flux are necessary for the anomalous effects to be manifest. In our experience, certain conditions facilitate high loading: high temperature gas loading prior to cathodization, electrode activation in strong acid, low temperature electrochemistry, high current densities, and high pressures of D_2. In a number of instances, the occurrence of "excess heat bursts" appears to correlate with a change in condition that might well stimulate high D fluxes at the interface of a highly loaded electrode: transient or stepped increases *or decreases* in the cathodic current and decreases in the temperature. The event shown in Figure 3-5 occurred 20-30 minutes after a transient decrease in the cell temperature. A decrease in the temperature might be expected to result in an increased absorption flux, since the solubility and thus the equilibrium loading level of D in Pd is increased. Additionally, lower temperature is likely to result in an increased electrochemical impedance for the recombination step; at constant current, this change may result in a higher adsorption coverage and a larger dynamic overvoltage and facilitate the adsorbed to absorbed reaction step.

The last excess heat event observed in the isothermal flow calorimeter (Event #4 in Table 3-3) was associated with a decrease in cell current and persisted for some hours following the reversal of cell potential for anodic deloading. If a flux of D is necessary, then the direction may not be important. If both high flux and high loadings are necessary, then it is difficult to maintain high loading at a high steady-state outward D flux, while it is difficult to achieve a high steady-state inward flux at a high loading level. It might be possible to resolve this apparent impasse by periodically reversing the direction of the flux.

In both experiments, the excess energy in any burst represents at most 1% of the total energy input to the calorimeter before the excess heat event. The precision with

which we establish our calorimetric baseline is not sufficient to eliminate the possibility that energy is being stored in the system during the long periods of time that the calorimeters are in apparent thermal balance, and is released in bursts. While the thermodynamic properties of the D/Pd system are not known for mole fractions of D near 1, we nevertheless consider it unlikely that the excess energies represented by the events chronicled in Tables 3-2 and 3-3 can be accounted for by chemical processes. In particular, it is unlikely that spontaneous transformation to a more stable (and hitherto unobserved) phase is occurring. If this were so, we would expect to see some evidence in the mechanical character and some evidence in the resistance. No such evidence is observed.

We do not claim to have examined all possible sources of systematic error in our calorimetry. However, highly instrumented and monitored experiments, using calorimeters of considerably different design and principle, have resulted in qualitatively and quantitatively similar results, i.e., apparent excess heat bursts outside the standard deviation of the random errors by factors up to 50.

It has been suggested[1] that excess heat is produced in the D/Pd system by nuclear processes. Our evidence from the isothermal flow calorimeter cell which produced 300 kJ of excess heat is that sources of ionizing radiation are contained within the Pd cathode but are not present in a blank electrode prepared identically from the same stock. Experience from autoradiographs of other electrodes heavily electrolyzed in LiOD and LiOH suggests strongly that the exposure evidenced in Figure 3-10 is not due to contact printing or to chemical exposure by reducing species such as lithium or hydrogen. Autoradiography while sensitive is not specific, and we were unable to identify the species that produced the film exposure, or any other species that might be a product of nuclear reaction. We were unable to identify any isotopic changes or the presence of ^{3}He or ^{4}He in the metal, the presence of ^{3}H in the electrolyte, or the presence of ^{3}H, ^{3}He or ^{4}He in the gas. Within the respective detection limits of the various techniques employed, it is not clear that we would expect to see the ~1-5 x 10^{17} atoms of product that would be associated with 300 kJ of heat from a nuclear process.

3.3 Experiments P12 Through P16

The research reported here was carried out during the period from August 1990 to February 1991. As mentioned in earlier sections, the experimental approach differs significantly from that originally described by Fleischmann et. al[1] and from those used in most subsequent calorimetric studies (for reviews of previous work, see Refs. 5 and 6).

3.3.1 *Experimental Methods*

Electrochemical Cell Design. All the experiments reported here were carried out in thermodynamically closed electrochemical cells that operated at approximately atmospheric pressure. The closed system, Figure 3-11 consisted essentially of two components, a PTFE vessel that housed the electrochemical components, and a sealed aluminum vessel that in turn contained the PTFE vessel. A large area catalyst was provided in the head space of the PTFE cell to recombine evolved oxygen and deuterium (or hydrogen) so that, after the cathode had loaded, there were no net thermal effects due to electrolysis. All experiments were performed using 0.3-cm-diameter x 5-cm-long Engelhard palladium cathodes of 99.9% purity. Anodes were coaxial helices of Engelhard CP Platinum STD Grade platinum thermocouple wire formed from 100 cm of 0.5-mm-diameter wire wound on a form consisting of six silica rods. In all cases the electrolyte was 1.0 M lithium hydroxide or deuteroxide formed by the reaction of 99.8% purity (natural isotopic ratio) Aesar lithium with light or heavy water. In addition, the presence of approximately 200 ppm of dissolved aluminum (or silicon) in the electrolyte was found to facilitate the reproducible attainment and maintenance of high loadings. A Tecrad model DMO-350 micro-ohmmeter was employed to measure *in situ* the axial electrical resistance of the palladium cathodes.[7] The associated palladium loading was thus determined from the known resistance/loading variations in the H/Pd and D/Pd systems.

The data shown in Figure 3-12 are compiled from the results of several resistance/loading studies, in particular those reported in Refs. 3 and 8-11

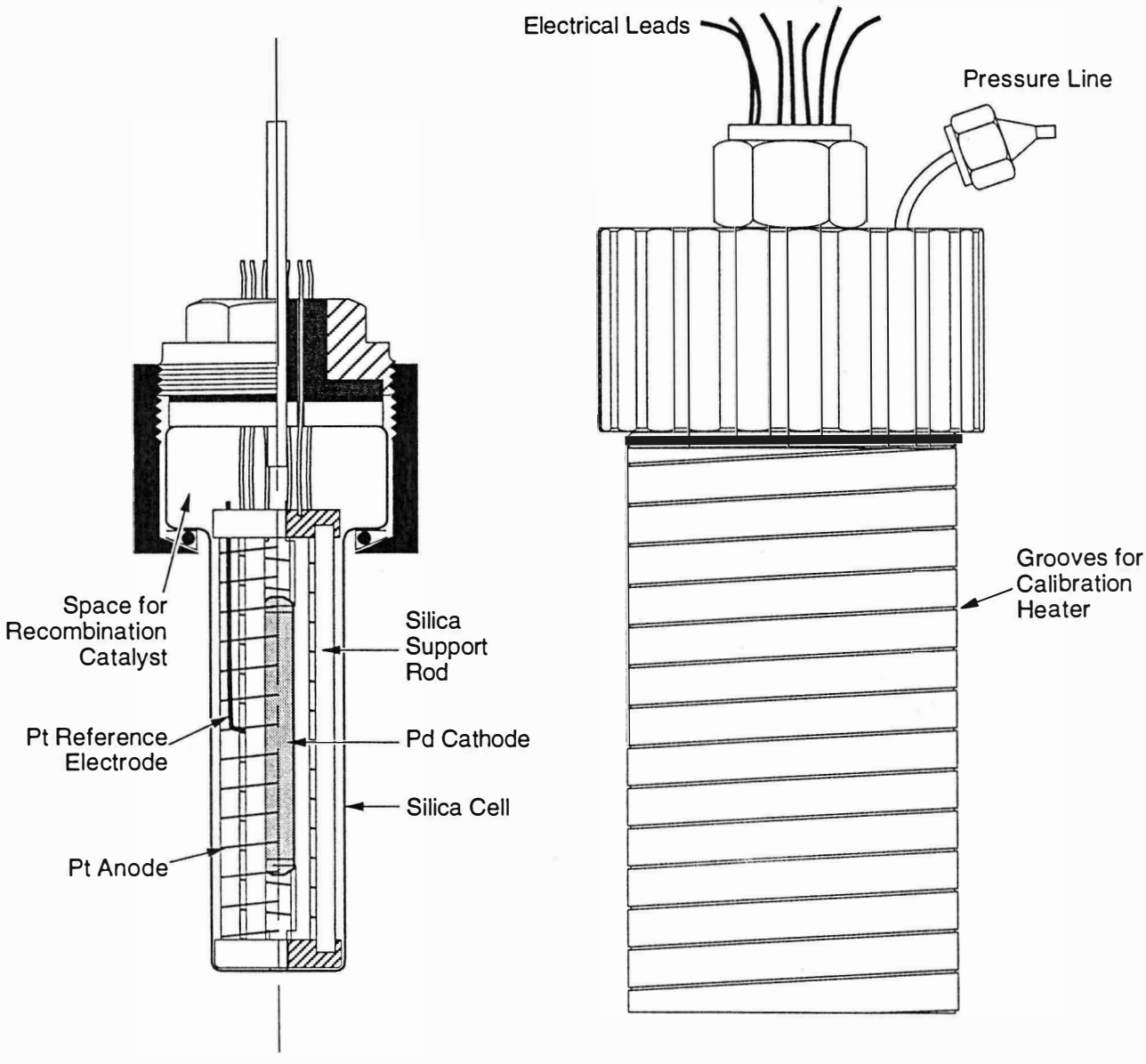

Figure 3-11
Electrochemical Cell and Aluminum Vessel Design.

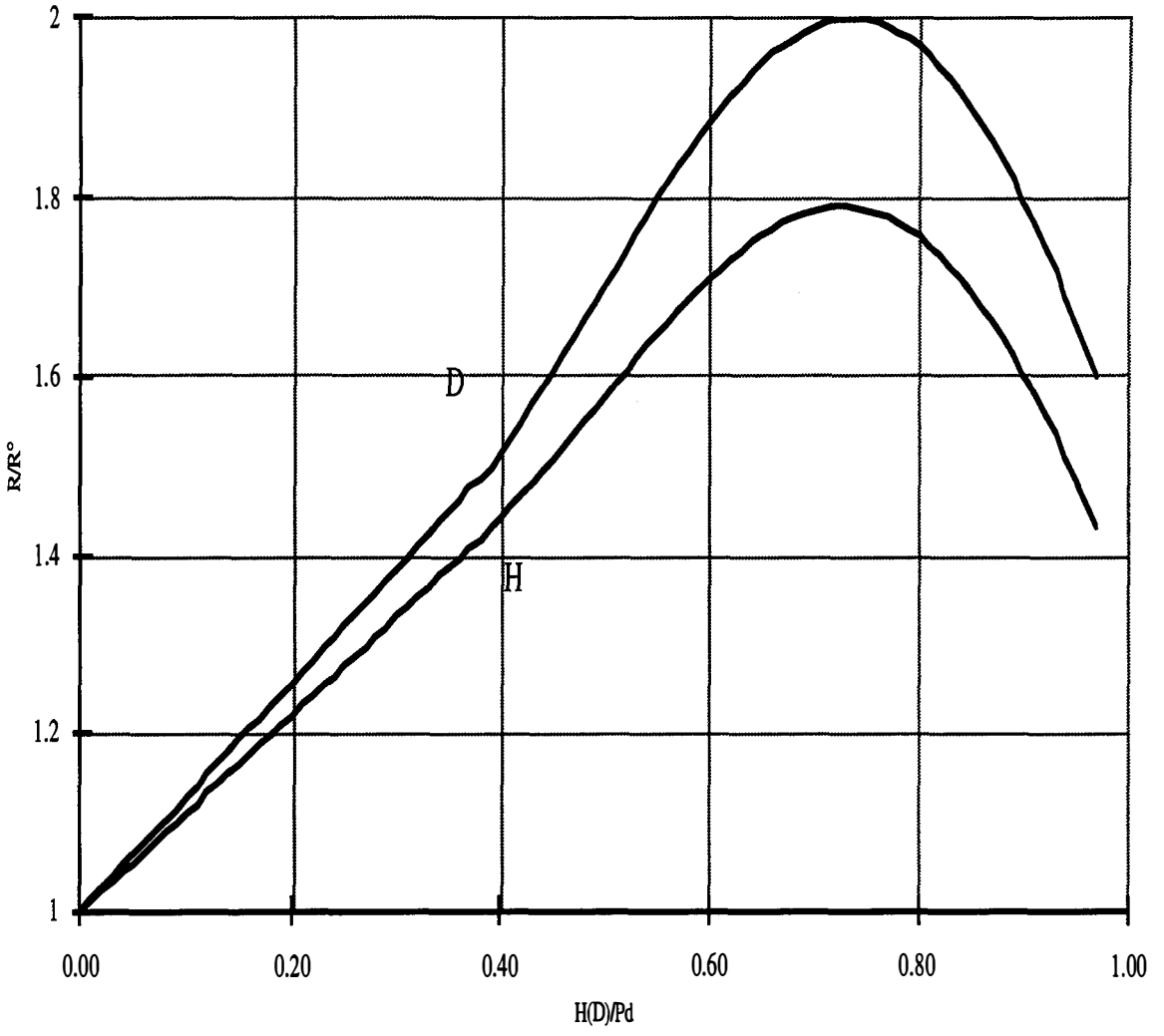

Figure 3-12
Resistance ratio/loading variations in the H/Pd and D/Pd systems at room temperature

To perform an experiment, cathodes first were machined to the correct diameter and furnished with grooves to receive the four 0.5-mm platinum wire contacts for current supply and axial resistance measurement. The electrodes then were degreased and cleaned. After being annealed for 2 hours at 850°C *in vacuo* and allowed to cool in deoxygenated, high purity argon, the four wires for cathode current and voltage contact were mechanically wrapped and spot-welded into place. Two surface pretreatments were employed to facilitate loading; either (1) rinsing in "heavy" or "light" aqua regia (for heavy or light water experiments, respectively), or (2) surface modification by helium implantation to a depth of approximately 3 microns. Following pretreatment, the cathodes were carefully mounted inside the pre-prepared anode cage, with contaminant contact avoided. The assembled structure was placed inside the PTFE vessel, freshly prepared electrolyte was added, and the aluminum vessel was then sealed. The aluminum vessel was initially pressurized with the appropriate amount of deuterium (or hydrogen) gas (calculated assuming a final loading of unity) to recombine the excess oxygen evolved during the initial charging of the cathode.

Calorimeter Design. The sealed aluminum vessel was fitted externally with a helically wound compensation (and calibration) heater and sheathed with axially oriented heat exchanging fins. This unit was immersed directly in the heat transfer fluid of a flow calorimeter (see Figure 3-13).

The body of the calorimeter consisted of an evacuated, silvered glass Dewar, the ends of which were closed with tightly fitting end-pieces made of a PMMA acrylic plastic. Rubber gaskets were used to achieve a water-tight seal. The calorimeter was itself immersed in a well-regulated (±3 mK) bath of the same fluid maintained at approximately 30°C. For most of the experiments reported here, the calorimetric fluid was silicone oil, chosen for its low heat capacity, low corrosivity, and good electrical insulation properties.[12]

The heat transfer fluid was pumped from the bath and past the cell inside the calorimeter volume by Fluid Metering, Inc. (Oyster Bay, NY), mode QV-OSSY constant displacement pumps. The mass flow rate was determined by pumping the flow to an auto-siphon device placed on a Setra model 5000L digital balance. Precautions were taken to ensure that fluid was not lost following its transit through the cell and before flow rate determination. In the calorimeter design

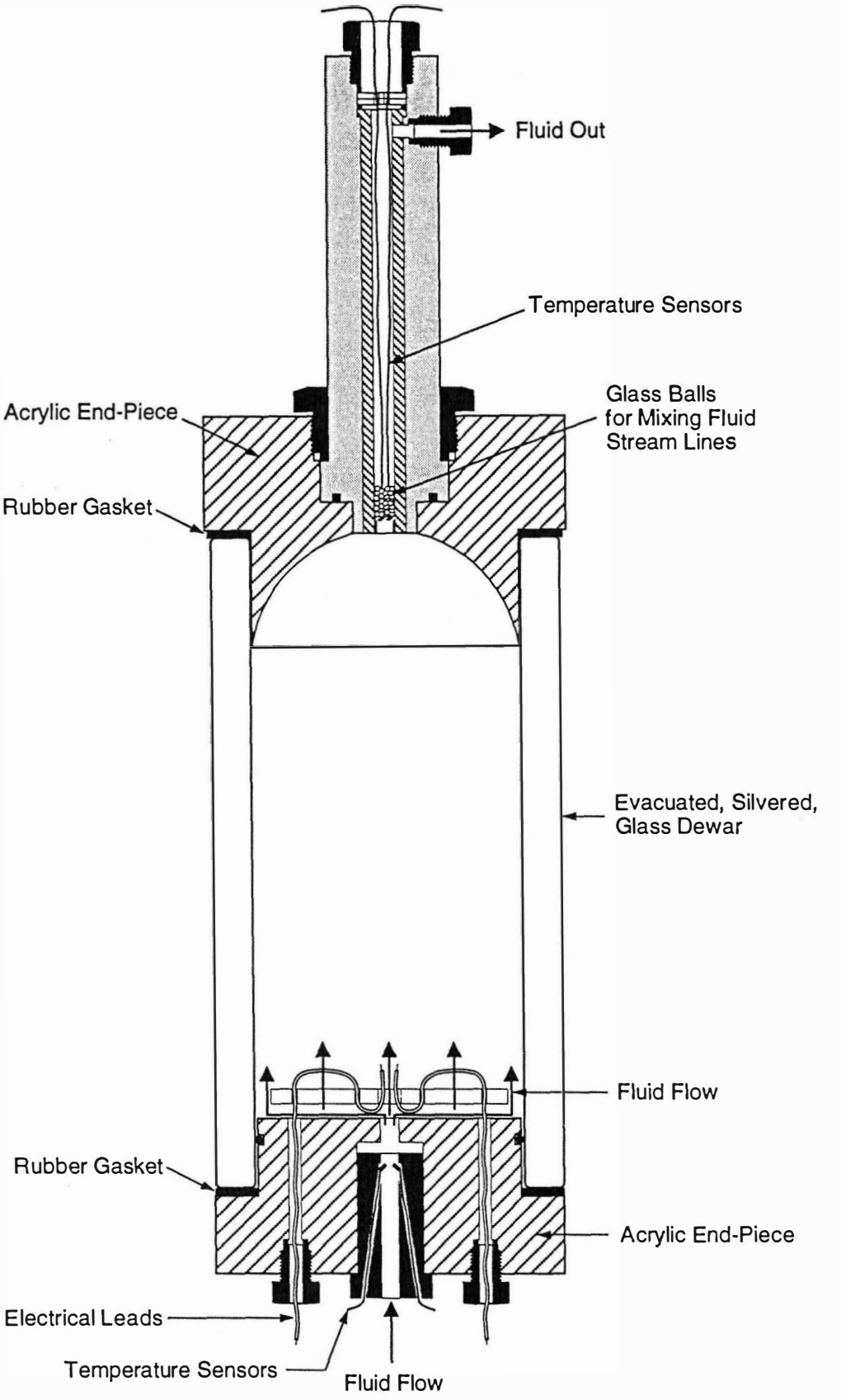

Figure 3-13 Flow Calorimeter Design

described here, the incoming fluid was at the same temperature as the bath, and the predominant heat transport was upward. All electrical leads were taken through the bottom insulating boundary across which the temperature gradient (and therefore conductive loss) was at a minimum. A pressure pipe (not shown in Figure 3-13) extended from the cell, through the top acrylic end-piece, to a pressure transducer above the bath. The pressure pipe also contained a PTFE catheter that was used to insert chemical species into operating cells. Since the pressure pipe emerged through the top insulating boundary, it was expected to contribute to conductive heat loss from the calorimeter, discussed further below.

The inlet and outlet heat transfer fluid temperatures were measured with platinum resistance temperature devices (RTDs). Two RTDs were used to sense each temperature; the temperature difference was then calculated from the two independent pairs. The required resistance measurements were made in a four-terminal mode, where all the RTDs were multiplexed sequentially to a single multimeter calibrated against National Institute of Standards and Technology (NIST) traceable standards.

Calorimetric measurements were carried out isothermally, under constant input power conditions, whenever possible. The power input to the calorimeter by the electrochemical current was considered to be the product of that current and the voltage *at the isothermal boundary*. Under experimental conditions, this input power changed owing to voltage or resistance variations in the cell or at times when the current was ramped. This change had two undesirable consequences: First, a change in input power changed the cell temperature so that the electrochemical conditions were no longer under control, and second, a change in temperature moved the calorimeter from its steady state as the calorimeter contents took up or released heat. To minimize these effects, the compensation heater was used to correct for changes in electrochemical power so that the sum of the heater and electrochemical power inputs to the calorimeter was held constant. Computer-controlled power supplies were used for both the electrochemical power and the compensation heater element; both were operated in galvanostatic mode to avoid possible unmeasured rms heat input. The heater also was used for periodic calorimeter calibration.

The cell and heater currents were each measured as the voltage dropped across a calibrated, series resistor. Voltages were measured using a Keithley 195A 5.5-digit digital multimeter with 0.01% DC volt accuracy and 0.015% resistance accuracy. Resolution was 1 ppm (Ω) and 10 ppm (DCV). Each 5.5-digit measurement was averaged 32 times before being recorded. Resistance standards were calibrated periodically against NIST traceable standards, using NIST traceable calibration instruments yielding an accuracy of ~0.1%.

Apple Macintosh computers (equipped with a IO-tech IEEE-488 interface, Keithley 706 scanner, Keithley P95A DMM, Tecrad DMO-350 micro-ohmmeter, Setra 5000L balance, and Black Box COS/4 serial port multiplexer) were used to record the parameters of the experiment. The Macintosh interface controlled a Kepco BOP 20-20M power supply to apply cell current and a Kepco BOP 50-2M power supply to control compensation heater power. The power supplies were commanded to their set current by using internal IEEE-488 interfaces.

Excess Power Determination. The steady-state equation for the power output from the calorimeter is

$$P_{output} = \left(C_p \frac{\delta m}{\delta t} + k'\right) (T_{out} - T_{in}) \qquad (3\text{-}6)$$

where C_p is the average value of the heat capacity of the calorimetric fluid in its transit through the calorimeter (1.646 J K^{-1} g^{-1} for silicone oil, 4.188 J K^{-1} g^{-1} for air-saturated water), $\delta m / \delta t$ is the fluid mass flow rate, k' is an effective conductive loss constant, T_{in} is the inlet (from bath) temperature, and T_{out} is the mean temperature of the emerging fluid.

Similarly, for the power input to the calorimeter,

$$P_{input} = |I_c V_c| + |I_h V_h| \qquad (3\text{-}7)$$

where I is the current and V is the voltage measured at the calorimeter boundary, and the subscripts c and h refer to the electrochemical cell and the compensation heater, respectively. In a closed system, the difference between the output and input powers may be described as an "excess power." In the absence of extensive, time-

dependent changes in temperature, pressure, or overall composition within the system, the excess power is expected to be zero (in the absence of anomalous power-producing or consuming processes).

For the cell and heater currents,

$$I_c = \frac{V_{cr}}{R_c} \;\; ; \;\; I_h = \frac{V_{hr}}{R_h} \tag{3-8}$$

where V_r is the measured voltage drop across a calibrated resistance (the subscripts c and h again refer to the electrochemical cell and compensation heater, respectively). The primary temperature measurements were made with RTDs, so that

$$T = T^\circ + \frac{(R - R^\circ)}{\alpha R^\circ} \tag{3-9}$$

where T° is the temperature at which the device resistance is R°, and a is the (known) temperature coefficient of resistance of platinum. Hence, we can write

$$P_{excess} = P_{output} - P_{input}$$

$$= \left\{C_p \frac{\delta m}{\delta t} + k'\right\} \left\{\frac{R_{out}}{R^\circ_{out}} - \frac{R_{in}}{R^\circ_{in}}\right\} \frac{1}{\alpha} - \frac{V_h V_{hr}}{R_h} - \frac{V_c V_{cr}}{R_c} \tag{3-10}$$

The terms in this equation can be divided into three classes: (i) measured variables (δm, δt, R_{out}, R_{in}, V_h, V_{hr}, V_c, and V_{cr}); (ii) predetermined constants (C_p, α, R°_{out}, R°_{in}, R_h, and R_c); and (iii) the conductive loss constant (k').

The use of a conductive loss constant, k', requires further discussion. Conductive heat transport occurs because the electrochemical cell, its contents, and the contents of the insulating, isothermal boundary of the calorimeter vessel are at a different temperature than their surroundings. An added complexity is heat transported through the pressure pipe that emerges through the top insulating boundary. Thus, depending on the ambient and cell temperatures, heat may be conducted into or out of the calorimeter. In view of the potential importance of conductive loss, the constant k' has been the subject of extensive analysis (not reported here) which indicates that, although several heat sources exist within the aluminum vessel, the

value of k' is negligibly influenced by the spatial distribution of these sources or the anticipated variations in the bath and air temperatures. Thus k' was treated as a constant, its value determined during the calibration procedure, as described below. For the calorimetric fluid flow rates used (approximately 1 g s^{-1}), conductive power loss represented typically 3-5% of the total input power.

Calibration and General Operating Procedures. Calibration required to determine R° values for the RTDs and the conductive loss constant k' was performed at the outset of the calorimetric experiment. The values of R° were determined *in situ*, under flow conditions at known bath temperature and zero or low input power. The total input power was then stepped to successively higher values by using the heater (in the presence of low electrochemical power), allowing times of at least 20 calorimeter time constants (approximately 6 hours) to reach a steady state. The quantities δm, δt, R_{out}, R_{in}, V_h, V_{hr}, V_c, and V_{cr} were measured on-line and the steady-state values were used with Eq. (3-10), assuming $P_{excess} = 0$, to determine k'. It should be noted that this method of calibration determines k' in terms of the other externally calibrated constants: C_p, R°_{out}, R°_{in}, a, R_h, R_c and the voltage calibration of the multimeter. In this way the cumulative inaccuracy of the determination of k' was greatly reduced.

To confirm that the value of k' determined during calibration was time-invariant, a second procedure was undertaken occasionally during routine operation of the calorimeter. It entailed varying the total input power (by stepping the heater power at constant electrochemical cell current) and observing the resulting excess power response (at times when the excess power was zero). For a properly calibrated calorimeter, the excess power should, of course, not change as the result of such a power step. This procedure, together with the use of redundant temperature sensors, served to check continually the results of the initial calibration procedure. It also enabled the validity of Eq. 3-10 to be verified at very high total input powers, a procedure that was found to be more time-efficient when carried out in this manner than when undertaken at the outset of the experiment.

In general, two different experiments were performed simultaneously in the same bath; the electrochemical cells were connected electrically in series, but the calorimetric systems were hydraulically in parallel. Separate pumps were provided for each calorimeter, and the flows from the two cells were multiplexed to a single

mass balance. All measurements were multiplexed to a single multimeter that was periodically interchanged with another precalibrated meter. In this way, one series cell effectively acted as a standard for the other: if P_{excess} was observed not to be zero in one cell while it was zero in another, this difference was unlikely to be an artifact due to the current source or voltmeter miscalibration. Further, the current-measuring resistors were interchanged, replaced, and removed and recalibrated during periods of excess power production, a procedure reducing the likelihood that errors were associated with the measurement of current.

Typically, constant current or slowly ramped current conditions were employed. As stated above, the calorimeter was run under conditions of constant power. Thus, during a current ramp, the heater power was reduced slowly while the electrochemical power was ramped up, thereby maintaining approximately constant total power. Under current control, the cell voltage frequently was observed to fluctuate significantly, particularly at high current densities where the presence of large deuterium (or hydrogen) and oxygen bubbles disrupted the electrolyte continuity. Because the cell current is provided from a source that is sensibly immune to noise and level fluctuations, the current operates on the cell voltage (or resistance) as a scalar. Hence, as long as the voltage noise or resistance fluctuations are random, no unmeasured rms heating can result under constant current control, provided that the average voltage is measured accurately.

Fixed Errors, Uncertainty Propagation, and Transient Effects. Although it is impossible to eliminate all the fixed (or bias) errors in a given experiment, it is possible to reduce the magnitude of such errors and, more importantly, their time dependence, by suitable system design and data procedures, as described extensively above. Clearly, problems will occur if new fixed errors arise during the course of an experiment, or if those fixed errors present during the initial calibration procedure are able to vary at a later time.

For a closed electrochemical cell, the expected value of the excess power is zero in the absence of anomalous processes and large variations in the cell temperature, pressure, and/or internal composition. Clearly, assessment of the significance of a measured deviation in the excess power from its "expected" value require an estimate of the uncertainty in the excess power measurement. Since the magnitude of the excess power at a given time cannot (presently) be predicted, excess power

determinations are considered to be examples of single-sample measurement.[13] Equation 3-11 relates the uncertainty in the excess power to the uncertainties in the variables that enter into Eq. 3-10:

$$\delta P_{excess} = \sqrt{\sum \left| \frac{\partial P_{excess}}{\partial X} \right|^2 \delta X^2} \qquad (3\text{-}11)$$

where the quantities X and their uncertainties are as follows: C_p (0.002 J K^{-1} g^{-1}), $\delta m/\delta t$ (0.0001 g s^{-1}), R (0.002 Ω), α (0.00002 K^{-1}), input heater power (0.2% of power), and input electrochemical power (0.2% of power). Uncertainties are ascribed to C_p and α, since the (small) temperature dependencies of these quantities are not explicitly included in Eq. 3-10. The uncertainties in the input powers were determined from the scatter in the measured power data during periods of nominally constant input power. The uncertainty in the RTD resistance was determined from the difference between the temperature readings for two sensors in the same constant-temperature bath. Since mass flow measurements are an average taken over a relatively extended period, the quoted uncertainty is an estimate. Where determined empirically, the quoted uncertainties are at the 95% confidence level (or higher); it is assumed that this confidence level applies to the derived value of δP_{excess}.

When the calorimeter or its contents depart from a steady state, a transient departure from power balance will occur. Such departures result principally from changes in the enthalpy of the cell contents, via fluctuations in temperature, pressure, and composition. With the assumption that the observed pressure fluctuations (which are typically less than 1 psi) during an experiment are due to nonconstant recombiner operation, a correction to the derived value of the excess power can be calculated. It is typically a few milliwatts. We are presently unable to make a corresponding temperature-related correction; however, the effect of temperature is presumably included in the short-term "scatter" in the measured excess power data, and thus its magnitude may be estimated. Further, it is important to note that, although they affect the measured value of the excess power, such transient effects will not affect the excess energy over a period for which the initial and final states of the cell contents are identical.

In addition, apparent departures from the steady-state behavior described by Eq. 3-6 will result, since the input variables (inlet temperature, electrical power, and flow rate) are measured essentially instantaneously whereas the output variable (outlet temperature) can respond only with the time constants of the (conductive) transfer of heat from the cell to the calorimetric fluid and the calorimeter was observed to exhibit (convective) transfer of the heated fluid to the outlet temperature sensor. In the range of mass flow rates employed in the experiments described here, the calorimeter was observed to exhibit a single (exponential) time constant of approximately 15 minutes, dominated by the convective terms. A correction has been applied to the excess power data reported here according to this time constant.

3.3.2 *Results*

The results presented here are from a series of five experiments performed in sequence; these experiments are designated P12 through P16. Experiment P12, a heavy water experiment that was the prototype for the sequence of experiments described here, was performed alone in the calorimeter bath. P13 was prepared as a light water blank for P12 and replaced P12 in the calorimeter; P13 was run, initially alone, using the same electronics as had been used for P12. P14, a heavy water replica of P12, was run electrically in series with P13 and was multiplexed to the same electronics. Experiments P15 and P16 were electrically in series and, were started simultaneously, following the termination of P13 and P14. P15 and P16 both were heavy water cells. The cathodes in experiments P12, P14, and P16 were helium-implanted as part of the electrode surface pretreatment.

In the space available, it is not possible to present the data for the complete duration of any one of the experiments reported. Therefore, what we present here are primarily results of excess power determinations. A single episode of excess power is presented for each of the cells P12 through P15; these are intended to exemplify particular features of the apparent excess power production.

Each of the cells P12 through P16 exhibited occasions when, for nominally identical current ramps, similar average cathode loadings were obtained but with no manifestation of excess power, within the sensitivity of the calorimeter. For the full duration of Experiment P13, the calorimeter was observed in the steady state to be within approximately 50 mW of zero excess power production.

Figure 3-14 shows the time evolution of the current density, together with the calculated excess power and its associated uncertainty, for P12 for the time period 1222-1558 hours (the associated reference voltage and cathode resistance ratio data are given in Ref. 12). At the beginning of this period, the calorimeter was operated at a constant input power of 10 W. During this time, the current was held constant at 0.1 A (approximately 20 mA cm^{-2}) and 2.0 A (400 mA cm^{-2}) and ramped and stepped between these limits. At the initial current density, the resistance ratio attained a value of about 1.75, which decreased slightly with time (the decrease corresponding to increasing loading) while the calorimeter maintained a power balance. As the current was increased, the resistance ratio fell to about 1.67 at approximately 100 mA cm^{-2}, an indication that the electrode was loading further. The increase in current density and absorption of deuterium were accompanied in this case by the production of excess power. The excess power responded apparently monotonically to the current density above a certain threshold value. At each instance of a step in the current density, the excess power responded, apparently with the time constant of the calorimeter. That is, the phenomenon that gave rise to this effect itself had a time constant of a few tens of minutes or less.

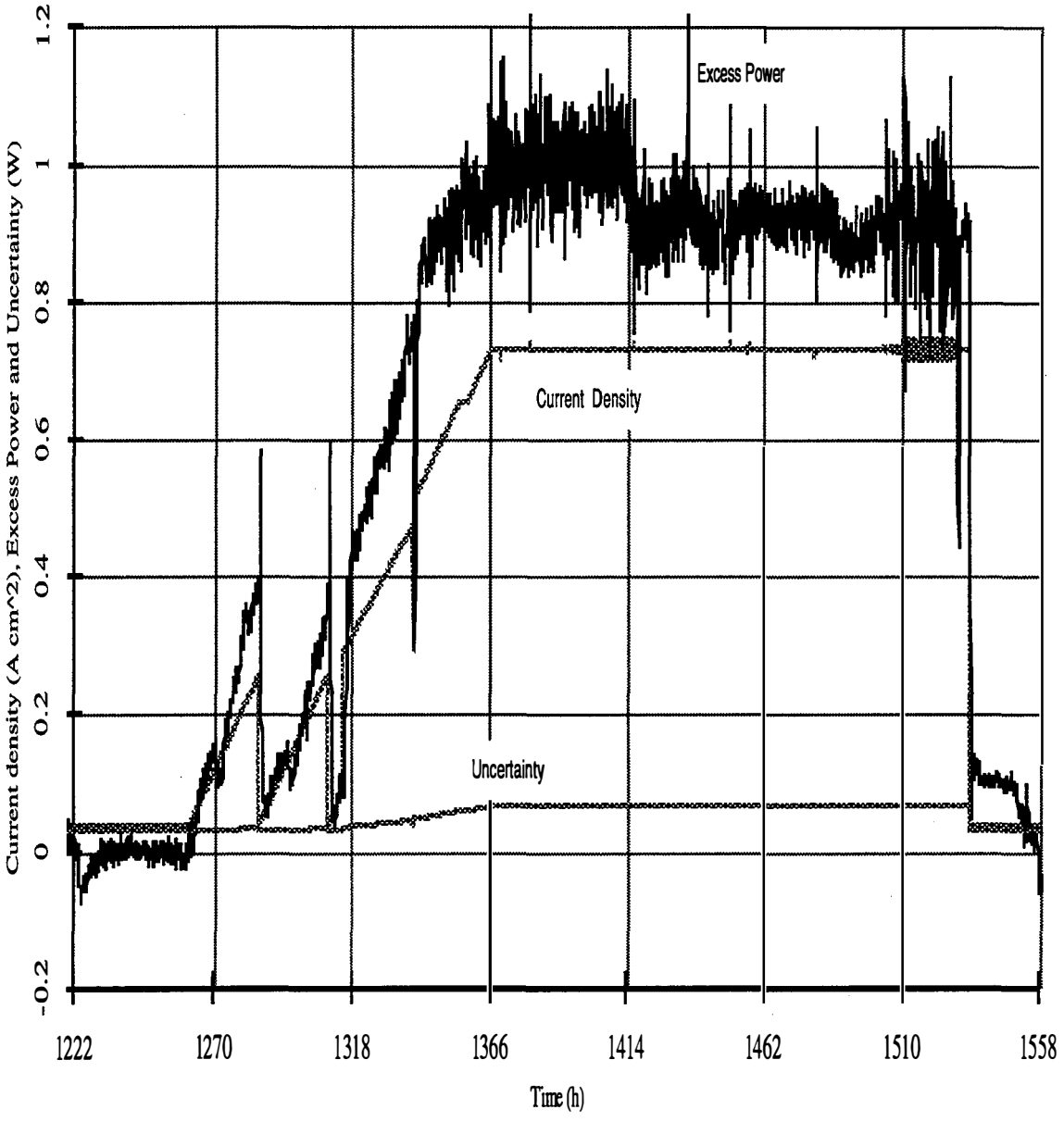

Figure 3-14
Variation of excess power (W), current density (A cm^{-2}), and calculated measurement uncertainty (W) with time since start of experiment for P12

It should be noted, however, that the resistance ratio did not decrease monotonically with increasing current density, a maximum in loading apparently being achieved in this experiment at current densities as low as about 200 mA cm^{-2}. At higher current densities, the loading appeared to decrease somewhat, while the excess power increased.

During the sustained hold at high current density from approximately 1366 to 1534 hours, the cell voltage slowly increased, presumably because of loss of conductive species from the liquid phase in the cell. Toward the end of the current plateau, the input electrochemical power exceeded 10 W, so the system departed further from its steady state and the quality of data was reduced. At approximately 1534 hours, the current was reduced to 0.1 A. At this point, it was clear from the resistance ratio that the electrode had de-loaded. In subsequent experiments it was impossible to reload the electrode with deuterium or to obtain excess power.

Following termination of P12, P13 was placed in the calorimeter; the same hardware, electronics, and flow system were used. An attempt was made to achieve conditions nearly identical to those of P12, the only exceptions being that the electrolyte was prepared from light water and the cathode was not implanted with helium. This experiment was operated for a total of 815 hours and exercised over the same range of current densities and loadings as P12, during which time no excess power was observed, to within approximately 50 mW.

P13 was operated alone in the calorimetric bath for about 290 hours, at which time P14 was added, connected electrically in series and hydraulically in parallel with P13. The current was ramped through the two cells in series twice, with no observation of excess power in P13 or P14 despite the fact that both cells had apparently achieved loadings greater than 0.95. Figure 3-15 shows the results of the third occasion on which P13 and P14 were jointly subjected to current ramps. The excess power recorded for P13 was essentially flat and zero, while that for P14 departed significantly from zero at current densities above approximately 200 mA cm^{-2} and apparently increased with increased current density. In this comparative experiment, the current came from the same device, and the electrical and calorimetric parameters were measured with the same devices multiplexed between the two experiments, so it is extremely unlikely that the difference in results can be accounted for in terms of an instrumental artifact.

Experiments P13 and P14 were replaced with P15 and P16, both heavy water cells, nominally identical, and varying only in the electrode surface pretreatment. In part because of the difference in electrode surface pretreatment the effect of the ramped current density on the loading of the two cathodes differed. Figures 3-16 and 3-17 show a current ramp profile and the resulting cathode resistance changes during a particular time interval in this comparative experiment (which lasted a total of 1104 hours). The calorimetric fluid flow rates are also shown in Figure 3-16. The dashed line in Figure 3-17 interpolates a region where data were not recorded for P16. It is clear that both electrodes absorbed deuterium in response to the current ramp. For P16, the resistance ratio decreased from about 1.77 (D/Pd ≈ 0.91) at a current density of approximately 33 mA cm^{-2} to a minimum of about 1.6 (corresponding to a maximum loading of approximately 0.97) at a current density of approximately 500 mA cm^{-2}. For P15, the resistance ratio was always lower, corresponding to higher

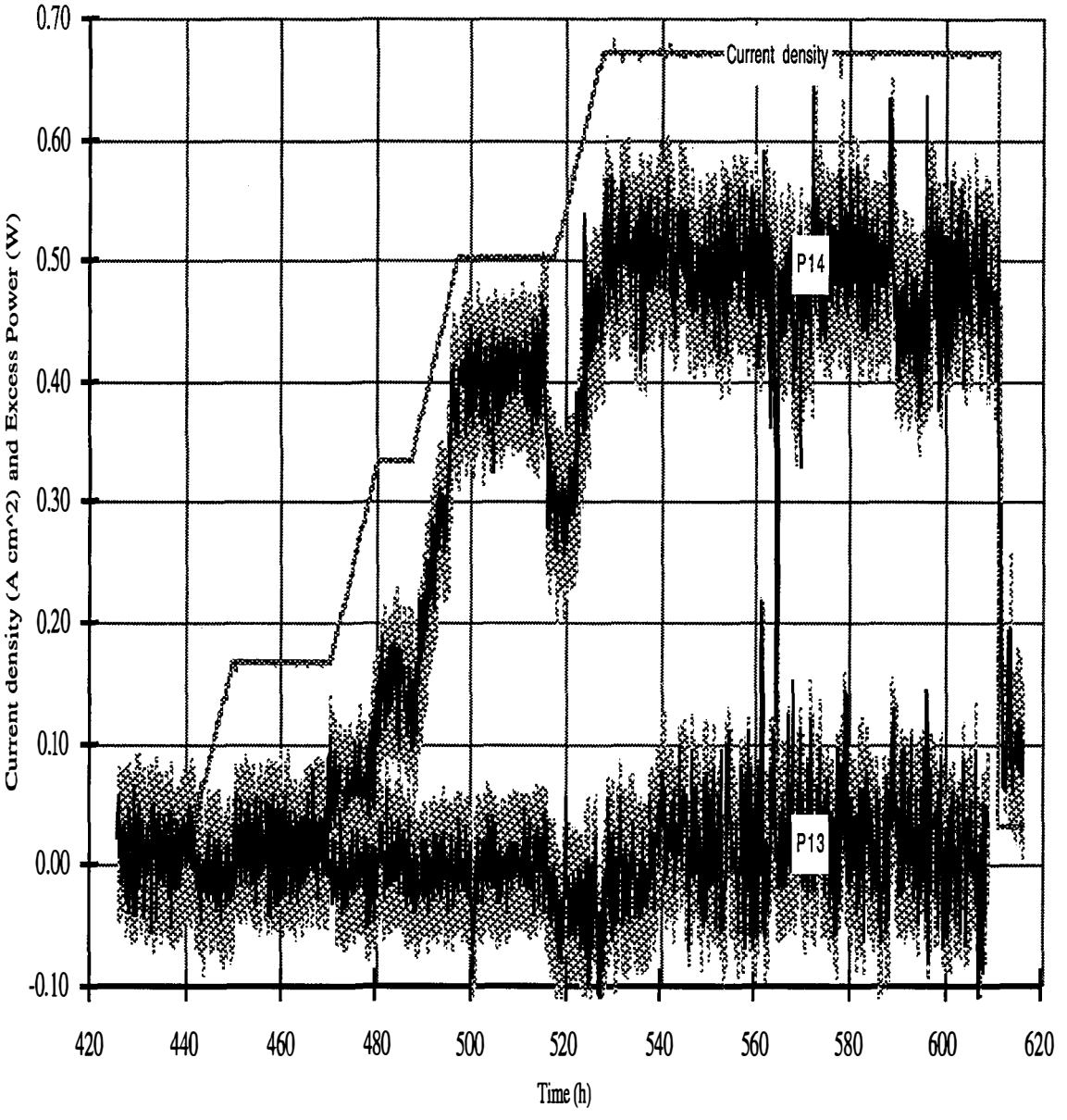

Figure 3-15
Variation of current density (A cm^{-2}) for P13 and P14, excess power (W) for P14, and excess power (W) for P13 with time (since start of P13). For each excess power curve (heavy line), the associated uncertainty span (hatched line) is superimposed

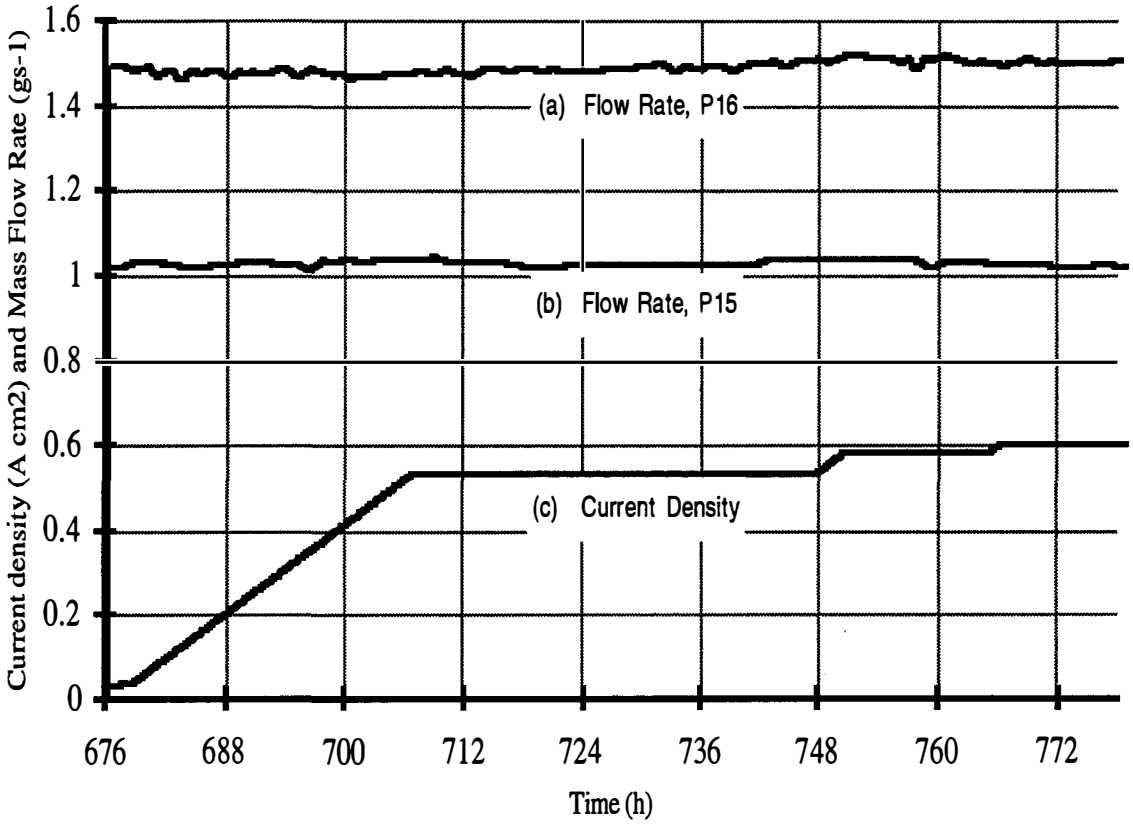

Figure 3-16
Variation of (a) calorimetric fluid flow rate (g s^{-1}) for P16, (b) calorimetric fluid flow rate (g s^{-1}) for P15, and (c) current density (A cm^{-2}) for P15 and P16 with time (since start of experiment)

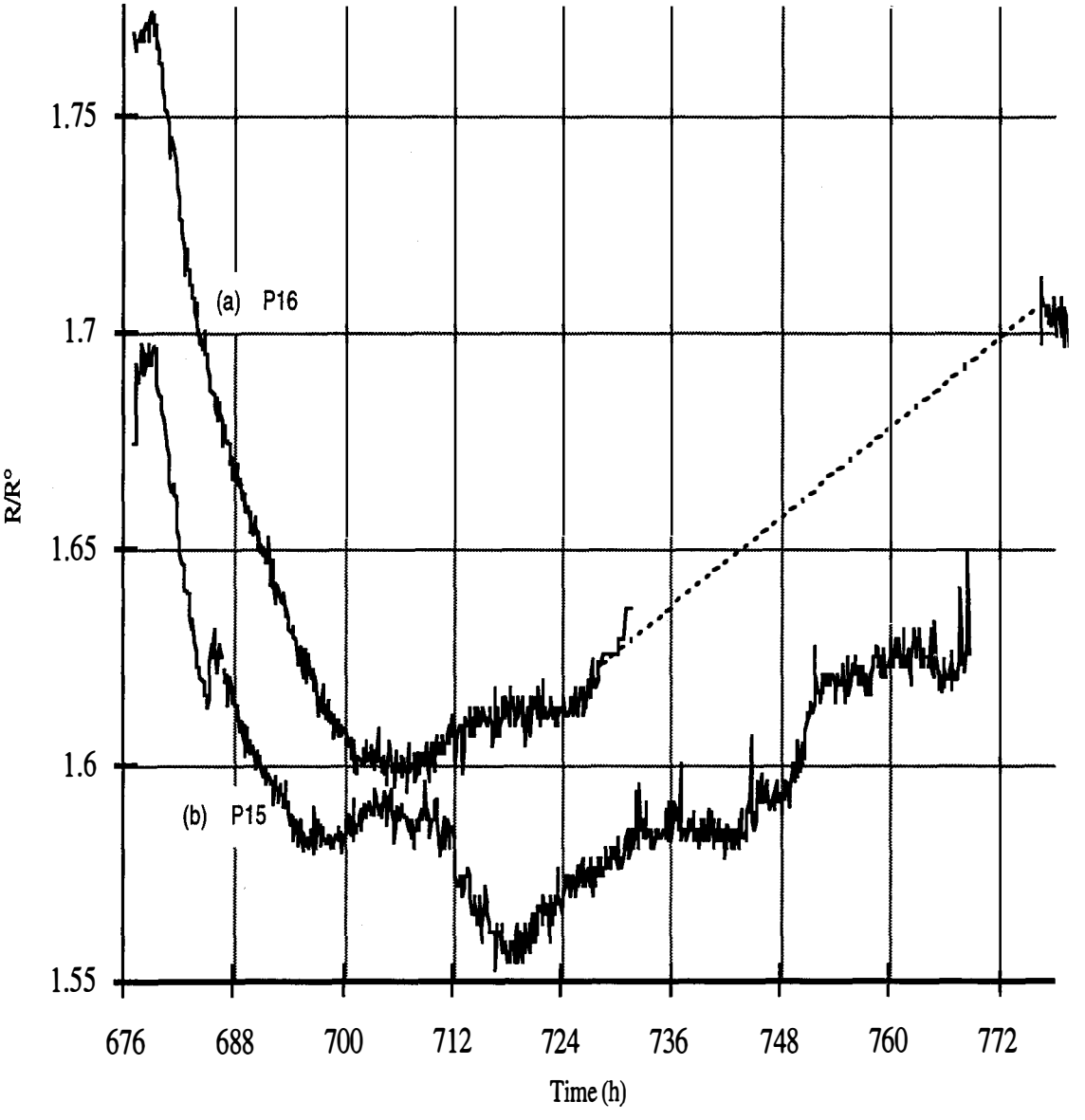

Figure 3-17
Resistance ratio variations for (a) P16 and (b) P15 with time (since start of experiment)

loadings, and decreased from about 1.69 (D/Pd ≈ 0.94) to a minimum of approximately 1.56 (D/Pd ≈ 0.99).

For P15, the mass flow rate, the inlet temperature, and the total input power all were sensibly constant during the time interval shown; thus, in the absence of excess power, the outlet temperatures should have remained constant. Figure 3-18 shows the measured temperature profiles for both the RTDs in the outlet plenum of the P15 calorimeter. For this experiment, two thermistors also were present in the outlet flow stream. All four sensors record essentially the same temperature response, and these responses were not constant but varied by as much as 0.6°C (with a measurement accuracy of a millidegree for the RTDs, less for the thermistors), indicating the presence of excess power. Figure 3-19 shows the excess power normalized with respect to the measured electrochemical input power and the (controlled) total input power. A very irregular profile of excess power is seen, with a threshold at approximately 200 mA cm^{-2}. The high-frequency fluctuations in the period between 0.1 and 1 hour are probably due to non-constant recombination catalyst operation. Also superimposed on the ramped response to current are apparently spontaneous fluctuations with substantially greater amplitude and period (some 3 to 6 hours) that are not correlated with variations in pressure or any other of the measured parameters of the system. It is important to note that during this time interval, and subjected to the same current, P16 did not exhibit the excess power production detected (with the same monitoring instruments) for P15. However, P16 did exhibit excess power on other occasions, which are not described here.

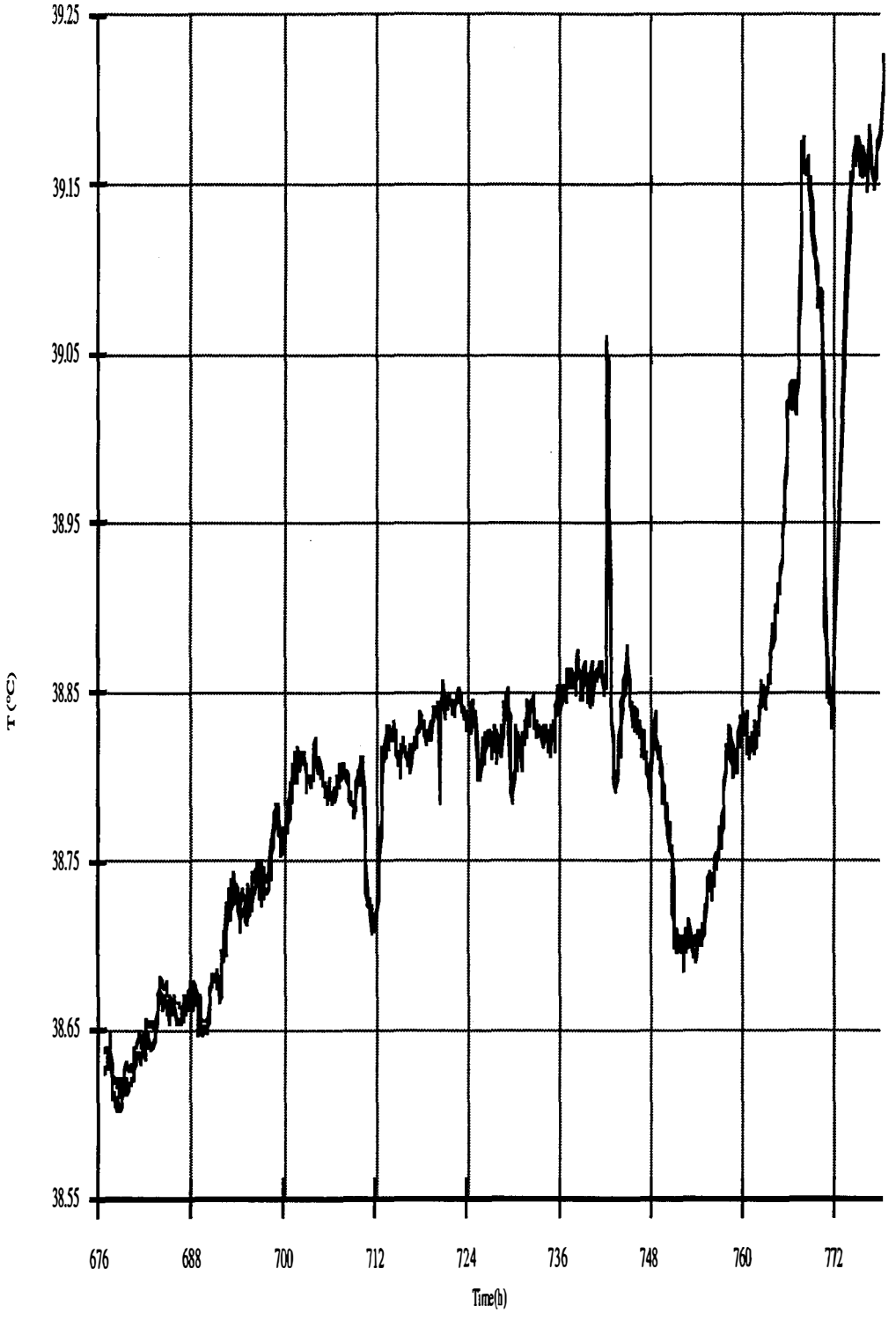

Figure 3-18
Variation of outlet temperatures with time (since start of experiment) for P15

Figure 3-19
Variation of excess power for P15 with time (since start of experiment), expressed (a) as a fraction of the electrochemical power, and (b) as a fraction of the total input power

3.3.3 *Discussion and Conclusions*

Here we have described a calorimetric tool and its use in observing the characteristics of (presently) unexplained power generation processes in the D/Pd system. Representative examples of results have been given from which a number of observations and conclusions may be drawn. Before describing these conclusions, however, it is useful to discuss what constitutes, in the context of the work carried out here, a "control" experiment, i.e., an experiment for which the outcome may be predicted in advance. First, since the origin of the excess power production process cannot be elucidated (be it a real physical phenomenon or the result of a measurement artifact) as a consequence of the results presented here, a light water experiment does not constitute a control. The fact that no excess power was observed in the light water experiment performed here constitutes a result equally as important as the observation of finite excess power production in the heavy water experiments. In this work, the role of a control experiment is to demonstrate that, during the course of an experiment (and under certain reproducible conditions, the converse of which are described in detail below), a calorimeter will detect accurately the absence of excess power production, thereby reducing (but not eliminating) the probability that the observation of finite excess power production is due to a time-dependent variation in the calorimeter function. *All* the experiments reported here contain such "control" periods; in fact, in all cases they exceed in duration the periods of excess power production.

For the thermodynamically closed and intentionally isothermal systems described here, excess power was observed to be as much as 28% above the electrochemical input power or 24% above the total input power. When excess power was present, it was more typically in the range 5-10%.

Excess power generation was observed when a minimum of three criteria were met: an average deuterium loading in the vicinity of unity; the maintenance of high loading for considerable periods relative to the time scale of the diffusional processes involving deuterium within the metal (several hundreds of hours for 3-mm-diameter cathodes); and the application of a current density in excess of a certain critical value. It should not be supposed that these criteria are completely independent. Thus, the threshold current density appeared to decrease with time, up to the point that high values of loading could no longer be attained or maintained because of interfacial or external effects.

With appropriate control of the interfacial conditions, it has been possible to load both hydrogen and deuterium into palladium to atomic ratios of approximately unity. Electrode surface pretreatment apparently plays a significant role in the ability to attain and maintain high loading under electrochemical conditions. Although helium implantation provides a suitable means of surface activation to facilitate loading, the presence of helium is not obviously implicated in the generation of excess power.

Except for times when a calorimeter was caused to depart significantly from its steady-state condition (for example, immediately following a change in total input power or during periodic fluctuations introduced by non-constant recombination catalyst operation), significant amounts of negative excess power were never observed. As demonstrated in the P13/P14 and P15/P16 series experiments, excess power was observed asynchronously in series cells. That is, cells subjected to the same current from the same source and monitored in a multiplexed manner with the same electronics were observed to yield excess power in one cell but not in the other. It is very difficult to attribute such an observation to an instrumental artifact.

Subject to satisfying the three criteria listed above, a level of experimental repeatability has been demonstrated, both within and between individual cells. All the heavy water experiments that met the three criteria produced excess power (although data for P16 are not shown here). It is worth noting, however, that excess power in these four experiments was *not* produced in exactly the same amounts, or at exactly the same times, in response to the same stimuli. However, we could not reproduce exactly the electrochemical conditions of cathodic overvoltage, loading, or the interfacial impedance. Clearly there are issues of interfacial contamination that still await resolution, in experiments with sustained high current electrolysis.

3.4 Experiment CI

From calorimetric results obtained to date,[14-16] it appears that one criterion (among others) for the observation of anomalous power generation is the attainment of average deuterium loadings of approximately 0.9 or greater. In view of the importance attached to the loading-related aspects of excess power production, considerable effort has been expended thus far on characterization of the kinetic features of the loading process and ways to achieve, maintain, and measure *in situ*

high deuterium loadings. Some aspects of these studies have been reported previously[7]; additional aspects are discussed further below.

Here the results of calorimetric measurements on an electrochemical cell of novel design are reported. These results enable apparent correlations to be established between the excess power generation, the electrochemical current, and the average deuterium loading. These correlations are discussed in terms of the phenomenological model for excess power generation introduced previously.[15,16]

Approximately 70 hours after the excess power event described here, an accident occurred that caused termination of the experiment. The cause of this accident is discussed in a paper published elsewhere.

3.4.1 *Experimental Methods*

Maintenance of High Deuterium Loading. The ability to maintain a high steady-state loading is determined essentially by the extent to which the rates of the reactions that lead to the loss of deuterium from the cathode can be suppressed. One important factor is the imposition of a uniform current density distribution over as much of the cathode surface as practical. This is partly achievable with suitable cell design, in particular, appropriate relative cathode/anode deposition. In addition, production of cracks on the cathode surface (either directly or via the expansion of internal voids) inevitably leads to a disruption of the local current density and loss of deuterium. Thus, processes likely to result in cracking (for example, repeated cycling through the α- β-phase transition in the case of palladium) should be avoided.

Classically, a number of so-called recombination poisons (typically, sulfur-containing compounds, e.g., thiourea) have been employed to retard the rate of gaseous hydrogen evolution from the cathode surface and thereby enhance the net loading rate. However, such electrolyte additives have little effect on the maintenance of high loadings because of their volatility or electrochemical decomposition over long tperiods. As a possible solution to this problem, we have observed that the addition of small amounts (typically 200 ppm) of non-classical additives such as aluminum or silicon (in metallic and oxide form, respectively) to the electrolyte results in the ability to maintain high loadings for longer periods without impeding the initial attainment of high loadings. In this context, it should

be mentioned that, in cells utilizing glass components, silicon-containing species will accumulate in basic electrolytes over extended periods.

Electrochemical Cell Design. The cell design shown in Figure 3-20 was employed in this study. The cell body was made of stainless steel for convenience in manufacture and to ensure good thermal contact between the cell and the heat transfer fluid. A PTFE liner was employed to prevent the highly corrosive electrolyte, 1 M LIOD + 200 ppm Al, from making contact with the metal cell body.

Two concentric-cylinder palladium sheet anodes were used. These were 25 μm thick, approximately 5 cm high, and 2 and 4 cm in. diameter, respectively. A 1-mm-diameter vacuum-annealed palladium wire cathode approximately 45 cm long (with 36 cm submerged in the electrolyte) was secured by four PTFE pegs from below and mounted between the concentric anodes in the manner shown in Figure 3-20. The anodes were mounted between two parallel PTFE plates that were themselves held in position by a PTFE pillar placed inside the inner anode and a series of PTFE posts placed outside the outer anode.

Recombination of the evolved deuterium and oxygen was achieved using porous, platinum-coated alumina spheres held within a wide-mesh platinum cage. The cage was suspended below a PTFE plate at the top of the cell. The collapse of deuterium and oxygen bubbles above the electrolyte surface projects liquid a considerable vertical distance during the operation of the cell at high current. In the absence of suitable precautions, the head space of the cell would fill with LiOD-saturated mist, which might affect the recombiner function. To prevent this problem, a PTFE cone was mounted between the electrodes and the recombiner. The center of the cone was removed and a static mixer inserted to remove LiOD-containing droplets from the gas stream reaching the recombiner. Small holes were drilled in the periphery of the cone so that recombined D_2O could drip back into the electrolyte.

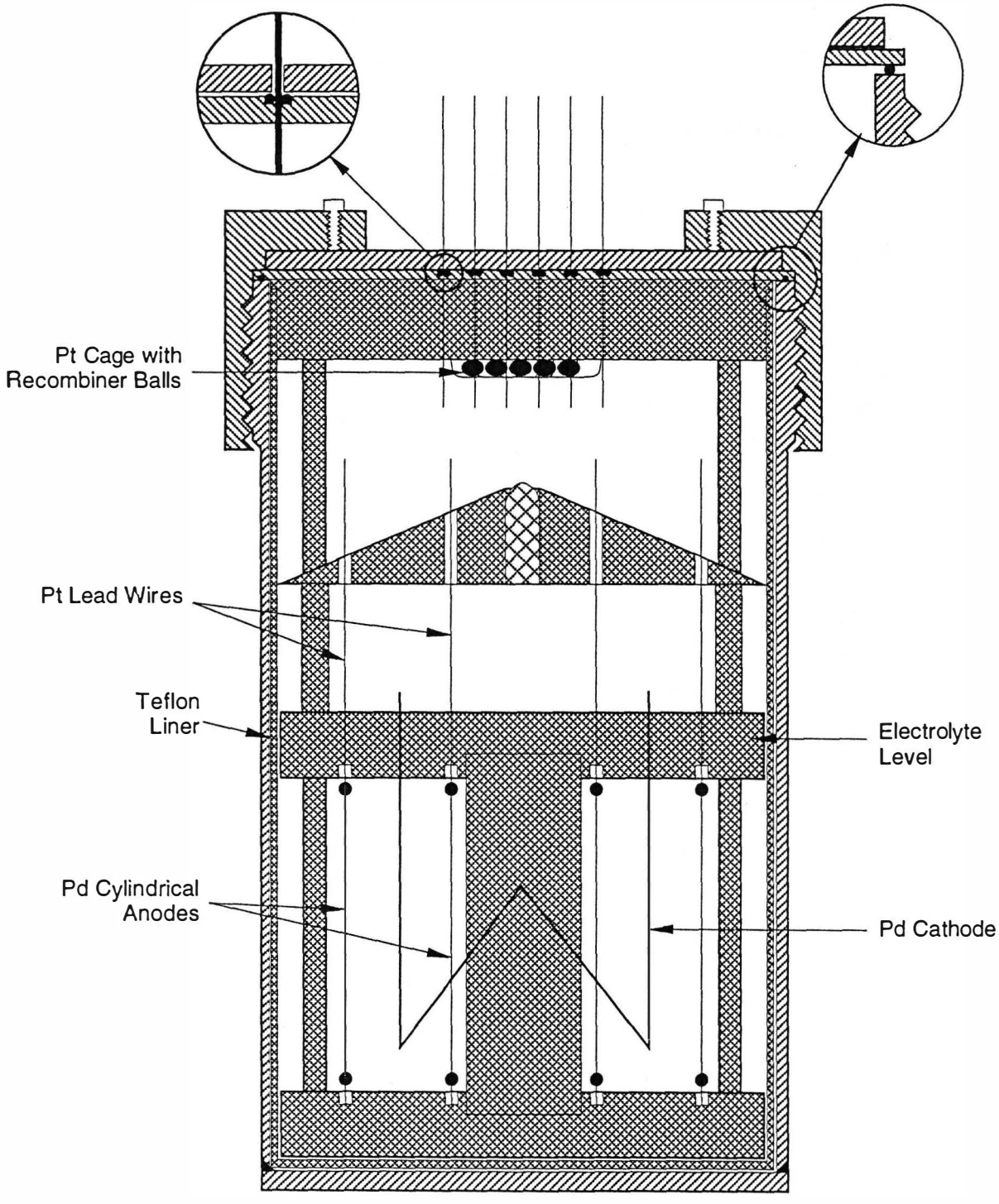

Figure 3-20 Electrochemical Cell Design

A pressure pipe connected the inside of the cell to a pressure transducer mounted above the calorimeter. The cell body was sheathed with a brass cylinder containing a resistive heater. To ensure good thermal contact with the calorimetric fluid, cooling fins were brazed to the outside of the brass cylinder.

Once the apparatus was assembled, approximately 200 cm^3 of electrolyte was added to the cell, enough to reach a level just below the bottom of the PTFE cone. The residual head space within the cell was approximately 100 cm^3.

Before the cell was sealed initially, it was filled with deuterium gas at approximately 1 atm pressure.

Calorimetry. The electrochemical cell described above was contained within a mass flow calorimeter (Figure 3-21), the design and operation of which have been described previously.[15,16] Briefly, the calorimeter consisted of an approximately adiabatic enclosure—comprised largely of a silvered, evacuated Dewar—that contained the electrochemical cell and through which the calorimetric fluid (water) was pumped. The calorimeter was situated in a constant temperature bath maintained at 30 ± 0.003°C, which also served as the source of the calorimetric fluid. An auto-siphon device mounted on an electronic balance was used to determine the mass flow rate of the calorimetric fluid after the fluid passed through the calorimeter. The internal heater, described above, permitted operation at constant total input power so as to keep the mean electrochemical cell temperature approximately constant. The output from the calorimeter was determined essentially by the mass flow rate, the change in the temperature of the calorimetric

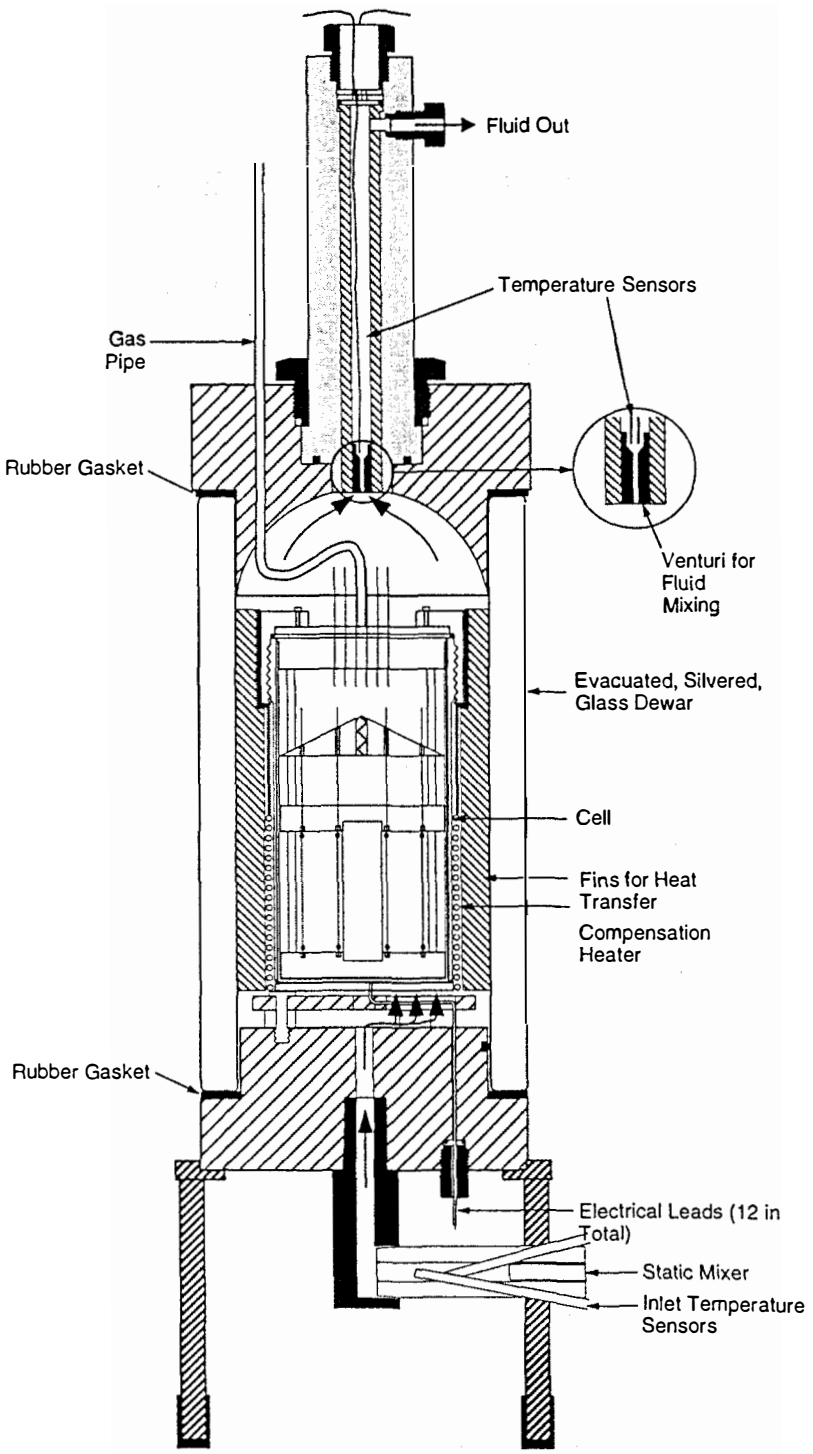

Figure 3-21 Calorimeter Containing Electrochemical Cell

fluid on its transit through the calorimeter, and a power loss term, discussed further below. Experimental control and data acquisition were achieved with a Macintosh microcomputer.

Data Analysis. The difference between the output power and the power input to the calorimeter (both electrochemical and heater) may be referred to as an "excess power," P_{xs}. For the calorimetric system employed here, this quantity is given by

$$P_{xs} = (C_p \frac{dm}{dt} + k') (T_{out} - T_{in}) - P_{el} - P_h \quad (3\text{-}12)$$

where C_p is the heat capacity of water, $\delta m/\delta t$ the mass flow rate, T_{out} the outlet temperature of the calorimetric fluid, T_{in} the corresponding inlet temperature, P_{el} the input electrochemical power, and P_h the input heater power. The power loss term k' is retained to account for the fact that the adiabatic calorimeter boundary is inevitably imperfect and some conductive heat loss is expected. The methods employed for determining k' at the outset of an experiment and for confirming its constancy during the course of an experiment, the exact means employed for measuring the other quantities in the above equation, and the steps taken to reduce systematic errors in their respective measurements have been described.[15,16] The measurement uncertainty in the excess power, treated as an example of a single-sample measurement,[13] was calculated as described previously[16] and is quoted (approximately) at the 95% confidence level ($\pm 2\ \sigma$).

3.4.2 *Results*

Figures 3-22 through 3-24 show electrochemical and calorimetric data for the experiment described here during the period from 300 to 780 hours. Before 300 hours, either statistically significant quantities of excess power were not produced or complete calorimetric data were not obtained (owing to a bath malfunction). For the calorimeter employed in this experiment, k' was 0.46 ± 0.05 W K^{-1}. Figure 3-22 shows the variation of input electrochemical and heater powers and the resulting total input power. Figure 3-23 describes the measured cell voltage and the electrochemical current during the period from 300 to 780 hours. Note that a cell current of, for example, 5 A is equivalent to a current density of 0.44 A cm^{-2}. The calculated excess power with its associated measurement uncertainty and the average cathode loading are shown in Figure 3-24. Figures 3-25 and 3-26 depict the

variation of excess power with electrochemical current and average cathode loading, respectively.

3.4.3 *Discussion*

During the period of interest, excess power up to approximately 1.2 W was produced. Although the excess power in this particular experiment was significant with respect to the measurement uncertainty, it was relatively small, particularly in comparison to the total input power. The excess energy produced *during the period of interest* was 1.2 ± 0.3 MJ, or approximately 4.3 MJ per cubic centimeter of palladium cathode. During this period, the total input electrochemical energy was 36.3 ± 0.07 MJ and the heater energy was 12.6 ± 0.03 MJ.

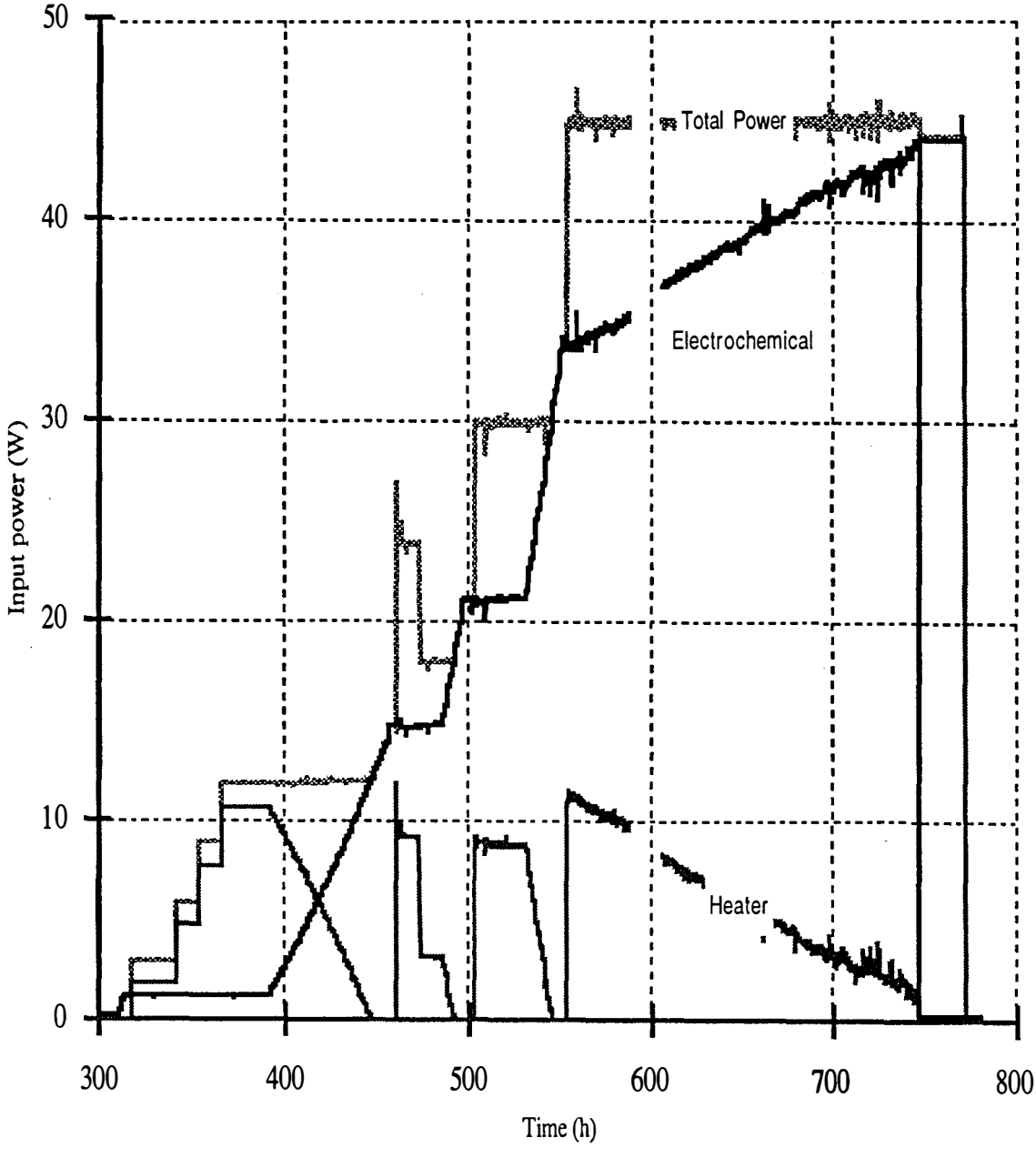

Figure 3-22
Variation of Input Power with Time

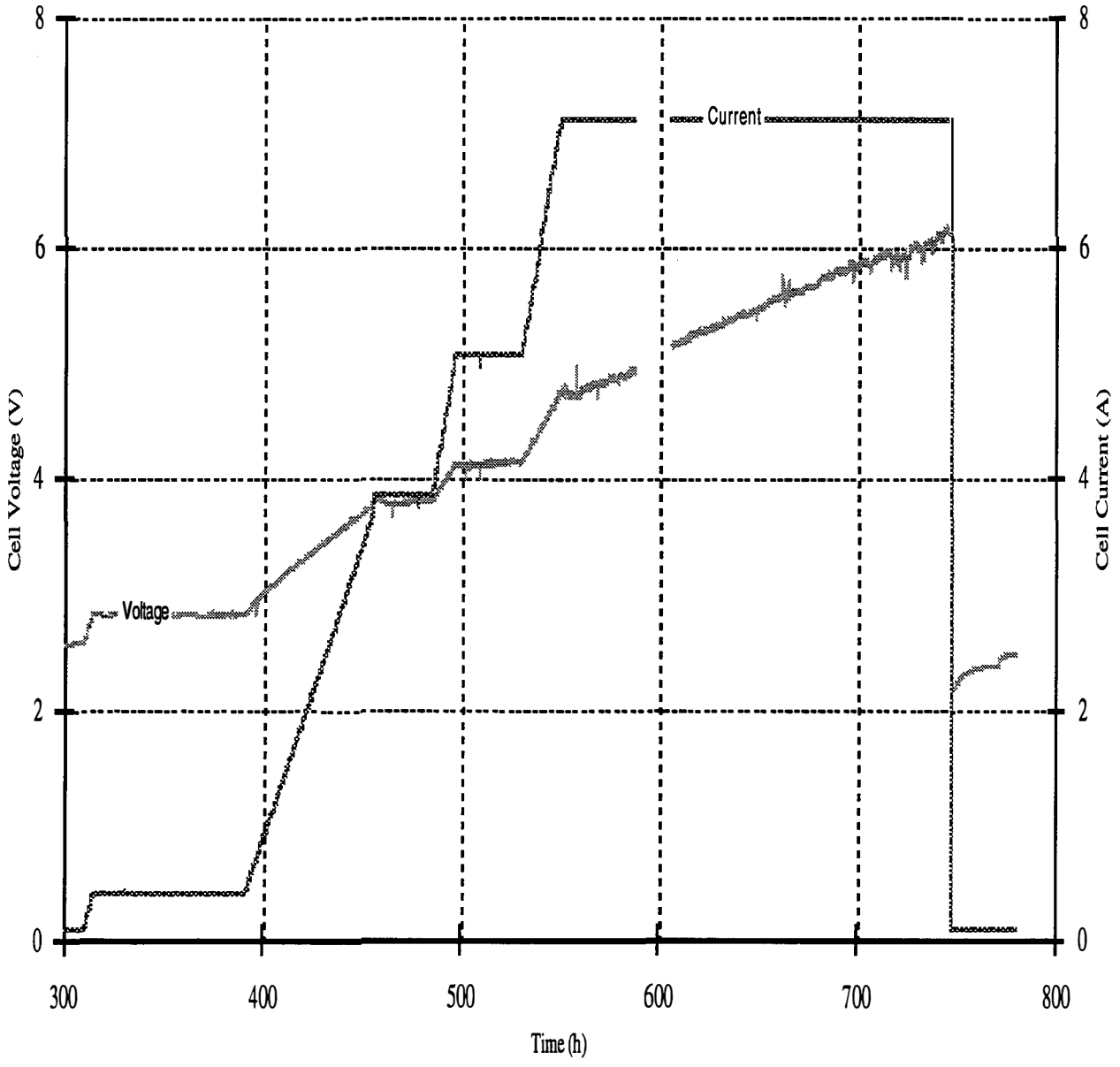

Figure 3-23
Variation of Cell Voltage and Current with Time

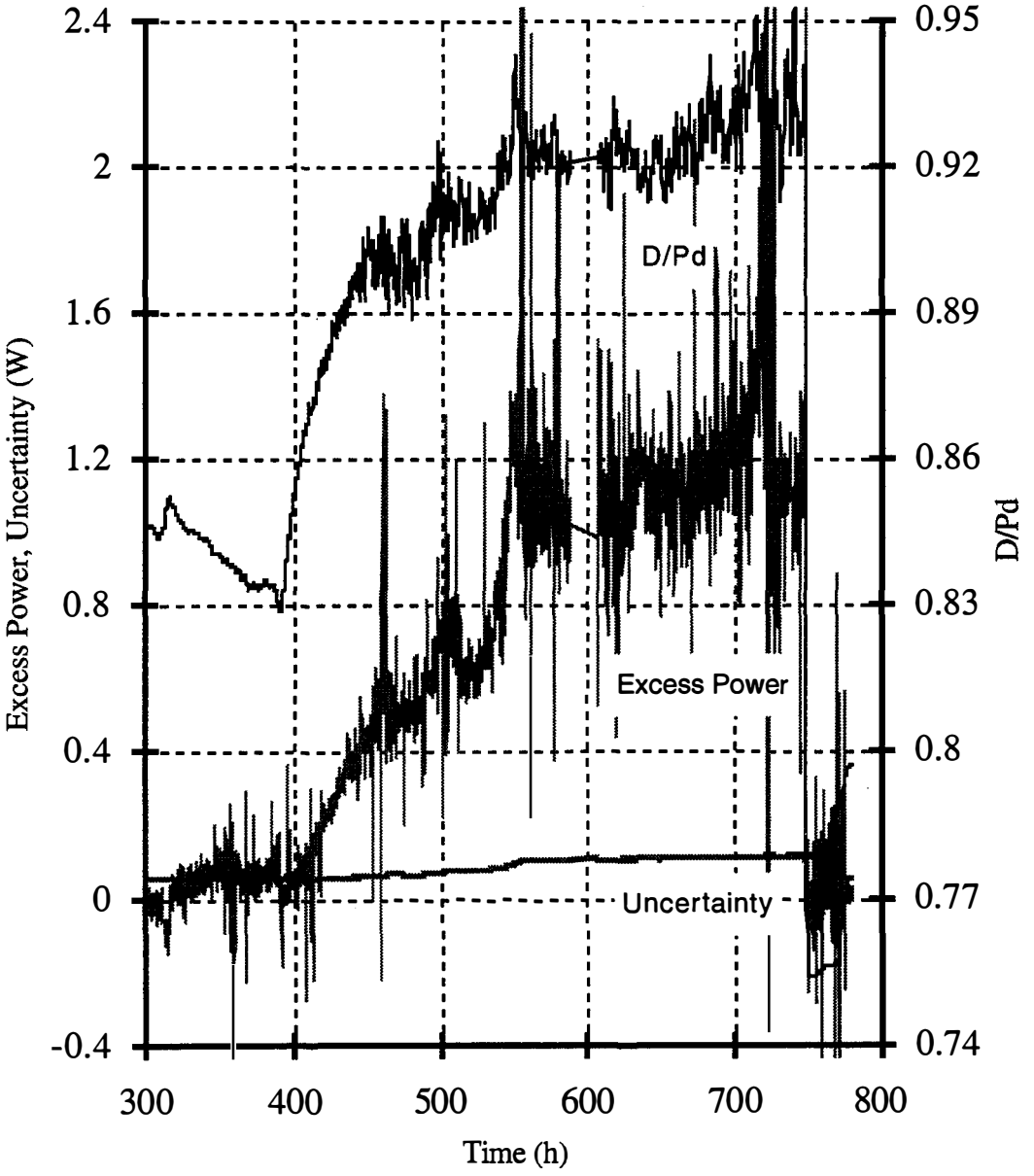

Figure 3-24
Variation of Excess Power, Uncertainty, and Loading

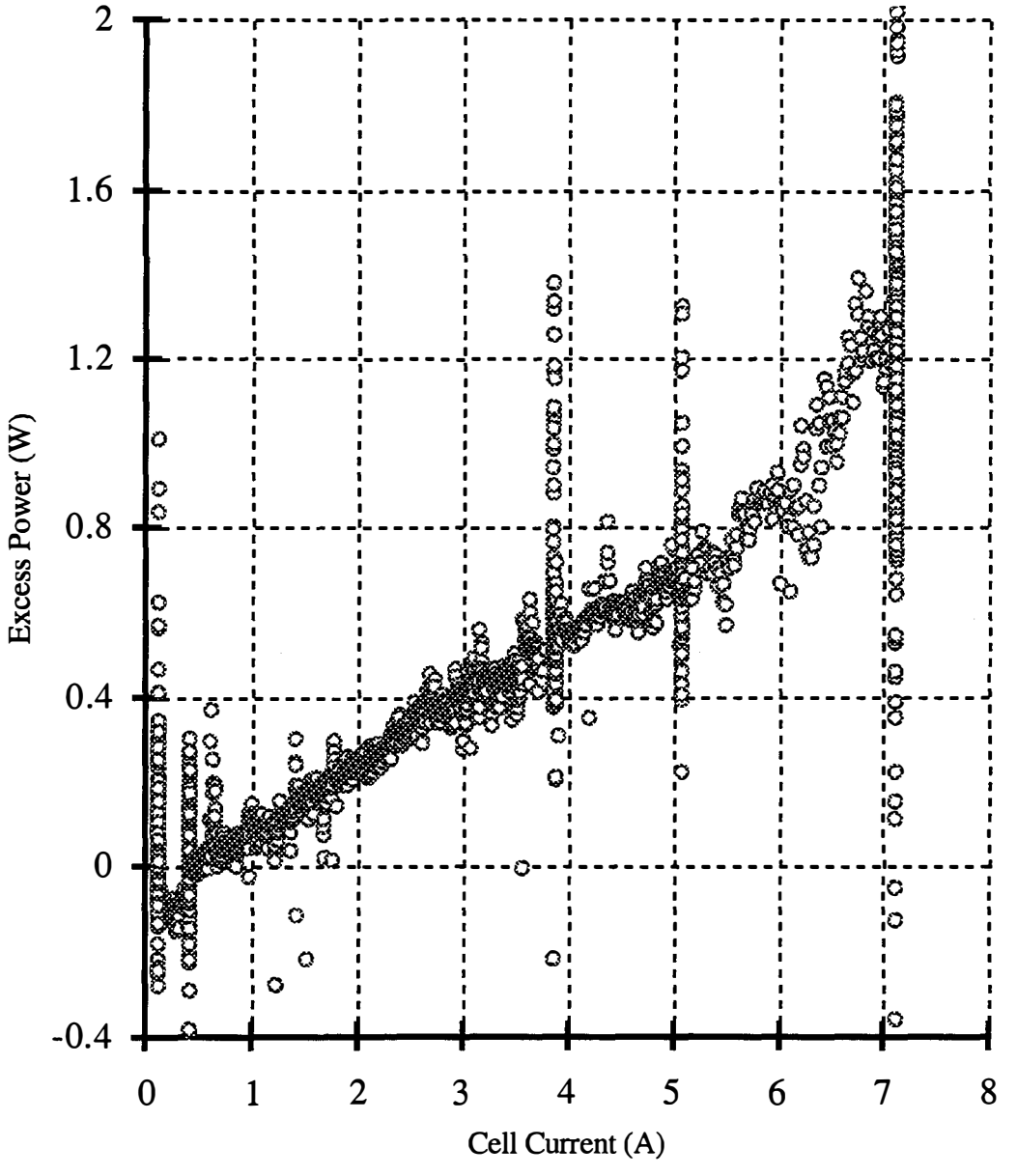

Figure 3-25
Variation of Excess Power with Cell Current

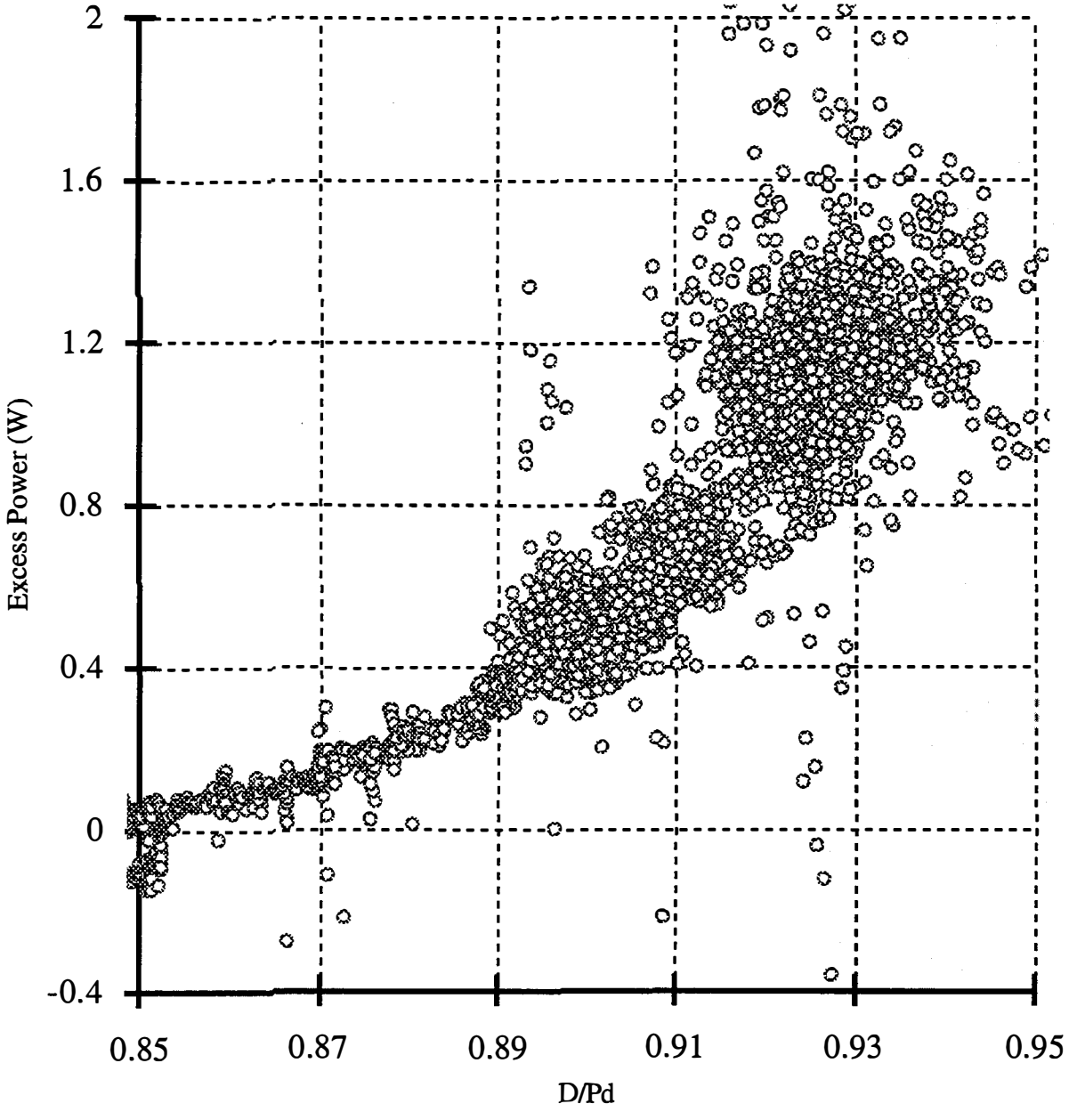

Figure 3-26
Variation of Excess Power with Loading

As in previous experiments,[15,16] the excess power production observed here appears to conform to a certain phenomenology, which is discussed below. In addition, for the experimental configuration utilized here, the excess power varies systematically with current and in a second-order manner (approximately) with average loading, above a loading threshold.

Fleischmann et al.,[17] in a different calorimetric system, reported a higher-than-first-order dependence for the variation of excess power with electrochemical current. An important distinction between this previous study and SRI's results is that in the former case the calorimetric system was not operated at constant total input power with an efficient heat removal mechanism, a setup that ensures an approximately constant mean cell temperature. Instead, the system was operated at constant electrochemical current in a heat-retaining calorimeter design, a setup that forces the mean cell temperature to increase with increasing current. Clearly, further work is required to elucidate the nature of this apparent temperature dependence of the excess power.

The approximately quadratic dependence of excess power on average cathode loading reported here serves to reinforce the remarks made above concerning the need for care in cell design and operation if high loadings are to be realized. At present, since the origin of the excess power production phenomenon in electrochemical systems utilizing deuterated palladium cathodes is unknown, the significance, if any, of the data in Figure 3-26 remains unclear, although the data are intriguing.

3.5 Phenomenological Model

On the basis of our calorimetric studies to date, we can construct a phenomenological model for excess power production from deuterium-based electrochemical systems employing palladium cathodes. For an (initially) unalloyed cathode, the following three factors (at least) are associated with the observation of excess power production: (1) The average cathode loading should exceed (approximately) 0.9; (2) the required initiation time (typically several hundred hours) is long compared with the time required for initial deuterium loading; and (3) changes in the excess power level are usually associated with departures from the electrochemical steady state, which are caused primarily by varying the current. Although the mechanistic significance, if any, and interdependence of these factors

are presently unknown, the following supplementary, necessarily somewhat speculative, suggestions are offered:

First, current density inhomogeneities on the cathode surface make it likely that regions exist within the cathode where the loading exceeds the average value, perhaps significantly. Thus, in a cathode with a high average loading, it may be possible for the local loading in certain regions to approach unity. In this connection, the development of new methods to increase and maintain loading may be important. In addition, techniques for accurate characterization of loading inhomogeneities may prove useful.

In the studies carried out here, the cathode dimensions were such that deuterium loading was achieved on a time scale of hours, certainly much sooner than the several hundred hours required for the production of excess power. This observation raises the interesting possibility that one or more species besides deuterium must be present in the cathode if excess power is to be observed, and that these additional species are not present initially and are thus required to diffuse into the cathode, presumably from the electrolyte. Analyses of used cathodes have revealed the presence of several light elements in the near-surface region (to a depth of several micrometers), particularly lithium. Clearly, calorimetric experiments involving the use of selectively pre-alloyed cathodes are of interest.

For a cathode initially in the steady state (with respect to loading), a departure from this state will lead to modification of the deuterium fluxes within the electrode. Since it has been observed that excess power levels generally increase with increasing current density, the possible role of the interplay between the ionic and electronic fluxes within the metal merits consideration, particularly with respect to its influence on the (local) loading.

To understand the origin and/or mechanism of the excess power phenomenon, it is clearly essential to identify either the fuel(s) or the product(s)—preferably both—of the energy-producing process, with the assumption for the moment, that it is artifactual in nature. This task is easier if the excess power (and hence the integrated excess energy) levels are caused to increase intensively. We are presently investigating using the phenomenological model described here to achieve intensive scale-up of the excess power effect.

3.6 REFERENCES

1. M. Fleischmann, S. Pons and M. Hawkins. "Electrochemically induced nuclear fusion of deuterium." J. Electroanal. Chem., **261** 301 (1989), and errata **263**, 87 (1989).

2. D. D. Macdonald, M.C.H. McKubre, A. C. Scott, and P. R. Wentrcek. "Continuous in-situ method for the measurement of dissolved hydrogen in high-temperature aqueous systems." I&EC Fundamentals **20**, 290 (1981).

3. B. Baranowski and R. Wisniewski, Phys. Stat. Sol., **35** 539 (1969).

4. J. C. Barton, F. A. Lewis, and I. Woodward. Trans. Faraday Soc., **59** 1201 (1963).

5. M. Srinivasan. Current Sci. **60**, 417 (1991).

6. E. Storms. Fusion Technol., **20**, 433 (1991).

7. M.C.H. McKubre, S. Crouch-Baker, A. M. Riley, R. C. Rocha-Filho, M. Schreiber, S. I. Smedley, F. L. Tanzella. In *Proceedings of the Symposium on Hydrogen Storage Materials, Batteries, and Electrochemistry*, Eds. D. A. Corrigan and S. Srinivasan. The Electrochemical Society, Inc., p. 269. 1992.

8. A. W. Szafranski and B. Baranowski. Phys. Stat. Sol. (a), **9**, 435 (1972).

9. B. Baranowski, S. M. Filipek, M. Szustakowski, J. Farny, and W. Woryna. J. Less-Common Metals **158**, 347 (1990).

10. G. Bambakidis, R. J. Smith, and D. A. Otterson. Phys. Rev., **177**, 1044 (1969).

11. R. J. Smith and D. A. Otterson. J. Phys. Chem. Solids, **31**, 187 (1970).

12. A preliminary account of the work reported here contains a misstatement concerning the identity of the calorimetric fluid (M.C.H. McKubre et. al., in *The Science of Cold Fusion: Proceedings of the 2nd Annual Conference on Cold Fusion"*, Conference Proceedings Vol. 33, Eds. T. Bressani, E. Del Giudice, and G. Preparata. Bologna, Italy: The Italian Physical Society, 1992, p. 419.

13. S. J. Kline and F. A. McClintock. Mech. Eng. (Jan. 1953); R. J. Moffat. J. Fluids Eng., **104**, 253 (1982).

14. M.C.H. McKubre, R. C. Rocha-Filho, S. I. Smedley, F. L. Tanzella, J. Chao, B. Chexal, T. O. Passell, and J. Santucci. In *Proceedings of the First Annual Conference on Cold Fusion.* Salt Lake City, UT: National Cold Fusion Institute, 1990, p. 20.

15. M.C.H. McKubre, R. C. Rocha-Filho, S. I. Smedley, F. L. Tanzella, S. Crouch-Baker, T. O. Passell, and J. Santucci. In *The Science of Cold Fusion* , Conference Proceedings Vol. 33, Eds. T. Bressani, E. Del Giudice and G. Preparata. Bologna, Italy: Italian Physical Society, 1992, p. 419.

16. M.C.H. McKubre, S. Crouch-Baker, R. C. Rocha-Filho, S. I. Smedley, F. L. Tanzella, T. O. Passell, and J. Santucci. Accepted for publication in J. Electroanal. Chem. 386, pp. 55–66 (1994).

17. M. Fleischmann, S. Pons, M. W. Anderson, L. J. Li, and M. Hawkins. J. Electroanal. Chem. **287**, 293 (1990).

3A

EXPERIMENT P19: A COMPREHENSIVE DATA COMPILATION

3A.1 Experimental Setup

3A.1.1 *Electrode*

An electrode was constructed with 3 cm x 3 mm diameter Engelhard palladium rod and machined from wire stock to receive the four wire contacts for resistance ratio measurement and current contact. The electrode was degreased and then furnished with spot welded contacts for the four-terminal measurements using Pt wire. The assembly was annealed in vacuum at a temperature of 850°C. The cooled assembly was rinsed in heavy aqua regia (3:1 DCl:DNO_3).

3A.1.2 *Electrolyte*

1.0 M LiOD electrolyte containing 200 ppm B was prepared in an N_2 glove bag by adding Li metal and $B(OH)_3$ to D_2O.

3A.1.3 *Cell*

The experiment was prepared in the "P12" PTFE lined aluminum pressure cell.

3A.1.4 *Calorimeter*

The calorimeter was as described in Section 3.2 of this report.

Two RTD temperature sensors were used at both the inlet and outlet of the calorimeter; two thermistors were also employed at the outlet.

3A.2 Data Collection

The data record has been divided (arbitrarily) into six windows, each covering several hundred hours of cell operation. These windows cover the following basic phases of cell operation.

3A.2.1 *Data Windows*

Period 1. Time 0-204 hours; initial load at 0.1 A and first ramp to 1.6 A.

Period 2. Time 194-350 hours; current steps and ramps at 12 W total power; first anodic strip.

Period 3. Time 348-660 hours; current ramp 0.1 A $\rightarrow$ 2.1 A, step to $\rightarrow$ 0.1 A and total power steps.

Period 4. Time 656-848 hours; second current reversal and current ramps 0.1 A $\rightarrow$ 1.6 A $\rightarrow$ 0.1 A.

Period 5. Time 840-1128 hours; third current reversal, current ramp 0.1 A $\rightarrow$ 1.85 A.

Period 6. Time 1080-1266 hours; current 1.7 A and 2.2 A; development of contact faults and experiment termination.

3A.2.2 *Parameters*

At the end of this section, plots are presented of the raw and primary derived data for each of the periods indicated. These figures are grouped by period, and their numbers reflect the period and the parameter set. The following parameters are plotted:

Set a: Input Powers. The input powers included total, heater, and electrochemical, where, in the calorimetrically closed cell,

$$P_{electrochem} = I_{electrochem} * V_{electrochem}$$

$$P_{heater} = I_{heater} * V_{heater}$$

$$P_{total} = P_{electrochem} + P_{heater}$$

In each case, the currents were measured as the voltage dropped across a calibrated shunt resistance, and the voltages were measured directly with sense wires to the calorimeter boundary.

Set b: Cell Current and Pd Resistance Ratio. Cell current was measured across a calibrated shunt resistance. Two values of resistance ratio are plotted, denoted "raw" and "temperature corrected."

$$R/R°_{raw} = R_{measured}/R_{initial}$$

$$R/R°_{corrected} = R/R°_{raw}\,(1 + \alpha\Delta T)^{-1}$$

where α is the temperature coefficient of resistance of Pd, and ΔT is the difference between the cathode temperature and the initial measurement temperature, calculated approximately from the formula

$$\Delta T \approx T_{cell\ wall} + \gamma\, IV - T_{initial}$$

$$T_{cell\ wall} \approx (T_{out} - T_{in})/2$$

and the coefficient $\gamma \approx 1$ reflects the extent to which the cathode is heated above the temperature of the cell wall by the input of electrochemical power to the cell.

Set c: Cell Pressure. The cell pressure (in psi) was measured as a voltage from a load cell pressure transducer.

Set d: Mass Flow Rate. The mass flow rate of the calorimeter fluid (water) was determined as

$$\text{Mass Flow Rate} = (M_{t_2} - M_{t_1})/(t_2 - t_1)$$

where M is mass and t_1 and t_2 are the times of successive measurement cycles.

Set e: RTD Temperatures. The two inlet temperatures, two outlet temperatures, and room temperature were measured as the resistance of a (nominal) 100-Ω platinum resistance temperature sensor. Reported temperatures are derived from the measured resistance using the formula

$$T = T° + R/R° - 1)/\alpha$$

where R° is the resistance at device temperature T° (taken as 0°C) and $\alpha = 0.00385$ is the temperature coefficient of platinum resistance.

Set f: Outlet Temperature. Two RTDs and two thermistors were employed to sense the temperature of the fluid emerging from the calorimeter. In the limited interval of outlet temperature variation, the thermistor resistance responded approximately linearly, so that

$$T = T° - (R° - R)/\beta$$

where β is the thermistor temperature coefficient of resistance.

Set g: Cell Current and Excess Power. Excess power is defined as

$$P_{xs} = P_{out} - P_{in}$$

where $P_{in} = P_{total}$

and $$P_{out} = (C_p \frac{dm}{dt} + k') (T_{out} - T_{in})$$

where C_p is the heat capacity of the flowing calorimeter fluid (air saturated water), dm/dt is its flow rate, and k' is the rate at which heat is lost conductively from the calorimeter envelope (determined by heater calibration).

3A.2.3 *Constants*

The following constants were employed in the analysis:

Site	Temp. Sensor	R° at (0°C)	α	β
Room	0	100.00	0.00385	
Inlet	1	99.471	0.00385	
Inlet	2	99.443	0.00385	
Outlet	3	99.312	0.00385	
Outlet	4	98.947	0.00385	
Outlet	5	24390		920
Outlet	6	23420		930

Heat capacity of air saturated water C_p = 4.184 J g^{-1} K^{-1}
Conductive loss constant k' = 0.380 W K^{-1}
Cathode area = 2.827 cm^2

3A.3 Analysis

3A.3.1 *Period 1*

An initial period of 160 hours at low current density (~30 mA cm^{-2}) was employed for D loading following an initial pre-load in D_2 gas at standard temperature and pressure (STP). During this time a ~12 W heater step was used to determine k'. A stable mass flow rate of 1.08 ± 0.01 g s^{-1}, and an initial pressure of 29.5 ± 0.5 psi were established. A substantial variation in room temperature, with primarily diurnal components, was observed. Nevertheless, the bath in which the calorimeter and electrochemical cell were submerged maintained a constant value of 29.96 ± 0.007°C, with no indication of diurnal variation, as measured by the temperature recorded at the two inlet sensors.

The first current ramp at a rate of 50 mA/hour, commenced at t = 162 hours, resulted in further loading of the cathode, as indicated by the appreciable decrease in R/R° and cell pressure for the first 6 hours following the start of the current ramp. These observations together are consistent with an initial increase in D loading of ~5% to a maximum value of ~0.93. It is important to recognize that, because boron is present in the electrolyte, the extent to which B absorbs into the Pd cathode presents an ambiguity in the interpretation of the resistance ratio in terms of D loading alone. We interpret the rise in resistance ratio with current following t = 168 hours (Figures 3A-1b and 3A-2b) as resulting, at least in part, from the

incorporation of B into the PdD_x lattice, presumably in substitution for D. This process is considerably slower than the resistance changes induced by absorption of D, possibly because of the reduced mobility of B.

Figure 3A-1g shows the excess power (or power balance) calculated from the temperatures measured at the two independent pairs of RTD sensors, 4-1 and 3-2. The values plotted are the result of an instantaneous subtraction of the raw input power from the raw output power data, with no correction for changes in the state of the calorimeter contents (temperature, pressure, moles of reactant species, etc.) or departures from the steady state. Mismeasured numbers have not been removed, nor are the data smoothed; the resulting plot is therefore noisy. For the first 180 hours the calorimeter maintains a thermal balance within ±50 mW. This level of scatter is typical of our calorimetric results at times of no anomaly, for total input powers ≤ 20 W. The data scatter of ± 50 mW/12 W total is also comparable with the absolute accuracy of the calorimetric determination being ~0.4%. Following the termination of the first ramp at t = 180 hours, there is a very small indication of excess power building up to ~150 ± 50 mW. This power excess reduces to zero when the current is stepped down from 1.1 A to 0.1 A at t = 206 hours (see Figure 3A-2g). It should be noted that, while this excess power observation clearly correlates with electrochemical current, it represents at most a 3σ observation, and, in total, less than 10 kJ of excess energy. This excess power thus is statistically insignificant and is comparable in energy only to that of chemical processes possible within the cell.

3A.3.2 *Period 2*

During this period the input power was maintained at a nominal value of 12 W total. For ~6 hours following the current step-down at t = 206 hours, and for the first ~12 hours of the second current ramp (started at t = 210 hours), the calorimeter maintained a calorimetric balance within the accuracy and precision of the determination.

Figure 3A-2f shows the outlet temperatures measured by the four sensors. Although no systematic difference is observed in the four temperatures measured, the individual measurements each reflect some scatter, such that the average variation of each sensor from the mean value sensed by the four output sensors is ~ 2 mK (-2 mK for sensors 3 and 4, 3 mK for sensor 5, and 1 mK for sensor 6).

In addition to instantaneous scatter (reflecting electrical noise and small temporal or spatial variations), the mean output temperature varies with time. To the extent that these variations are not reflected in (small and measured) variations in input temperature, input power, and mass flow rate, the output temperature variations must be interpreted as indicating the presence of unaccounted for power sources or sinks within the calorimeter.

Figure 3A-2g plots the excess power (or power balance) computed in this case from one RTD sensor pair (3-2) compared with that for a thermistor minus RTD pair 6-1. This is done simply to demonstrate that outlet temperature sensors operating on two different principles (metallic and semiconducting resistance) measure the same temperature variations.

Figure 3A-2g shows a small power excess, initiating at a current of ~1 A (~350 mA cm^{-2}), then increasing somewhat with increasing current to a maximum value of ~250 mW at 1.6 A (~ 530 mA cm^{-2}). This excess power spontaneously decreases at constant current, going to zero, and re-establishing the calorimetric balance only when the current density is dropped below its initiating threshold at t = 328 hours.

In this instance the observed excess power persists for more than 100 hours, with an effect as large as 6 times the calorimeter accuracy (6 σ). The effect is observed simultaneously and (within measurement uncertainty) identically on each of the outlet temperature sensors. However, this excess power event is small, accounting for only 50 kJ of excess energy.

At t = 330 hours and with a current of 100 mA (~30 mA cm^{-2}), the current was reversed for one hour to anodically strip the cathode surface. This procedure resulted in partial de-loading of the cathode, as indicated by the pressure and resistance ratio measurements. Close inspection of the R/R° data reveals a complex profile having two maxima on the de-load and two more on the re-load after restoration of the cathodic current.

This occasion represents the first observation (to our knowledge) of multi-peaked resistance-versus-loading behavior for the Pd/D/B system. However, this phenomenon was observed on several further occasions in experiment P19 and in subsequent experiments with electrolytic boron additions. The cause of this

complex behavior is not fully understood; it will be discussed in the conclusions to this section.

3A.3.3 *Period 3*

An attempt was made to replicate the current and excess power observations in Period 2 by starting a current ramp at t = 380 hours. The appearance of excess power in Period 3 was functionally identical to that of Period 2. Figure 3A-3f in this case again displays the raw power excess for the two independent pairs of RTD sensors, 4-1 and 3-2. It should be noted that in the period t = 444 to 460 hours, the thermistors (Figure 3A-3e) both registered a higher temperature than the RTDs. This phenomenon was observed on several occasions and will be commented on below.

A period of pump failures and poor pump performance render the data from t = 550 to 614 hours calorimetrically meaningless. During this time the current was held at 0.1 A.

A good calorimetric baseline was established in the period t = 614 to 639 hours, following restoration of a constant mass flow. At t = 640 hours the total power was stepped to 7.5 W and at t = 646 hours to 14.8 W, while the current was kept constant at 0.1 A. The calorimeter responds to the first of the heater power steps with ~100 mW of excess power (Figure 3A-3f), this response suggesting either the existence of a temperature dependent heat source or miscalibration of the conductive loss term k'. The lack of further calorimeter response to the second heater step, in which the total input power is more than doubled, suggests strongly that the value of k' is well calibrated and unchanged. It is likely, therefore, that a heat source has appeared within the calorimeter; unlike the case with previous observations, this heat source has appeared at constant current, perhaps initiated by the temperature rise in the cell accompanying the first heater power step to 7.5 W total.

3A.3.4 *Period 4*

Unaware of the possible existence of excess power within the calorimeter, the operators prepared to anodically strip the cathode surface at a low current density by first reducing the current to 30 mA (~10 mA cm^{-2}) and then reversing the current. This sequence led to extraordinary observations of resistance and thermal anomalies, shown respectively in Figures 3A-4b and 3A-4f.

Approximately 3.5 hours before the current was stepped down from 100 to 30 mA cathodic, the excess power was observed (Figure 3A-4f) to increase, apparently spontaneously, from the (small) value of ~100 mW established after the first heater step to a value of ~500 mW. This value was maintained when the current (density) was stepped down from 100 mA (~33 mA cm^{-2}) to 30 mA (~10 mA cm^{-2}) but slowly reduced toward zero power excess during the 6.7-hour strip at -30 mA (-10 mA cm^{-2}). When the current polarity subsequently was reversed to restore cathodic polarization, the excess power increased over a period of ~ 6 hours, returning to the value of ~500 mW achieved prior to stripping.

When the current was subsequently stepped back to 100 mA (~33 mA cm^{-2}) cathodic, the excess power increased to a maximum of ~900 mW in the period t = 688 to 712 hours. It is important to recognize that the electrochemical power in the period just discussed is very small, and small variations in electrochemical input appear to induce substantial change in the excess power. One should also note that the total power to the cell was nevertheless large compared to the measured power excess, since ~98% of the power was provided by the complementary heater.

The contemporaneous resistance anomaly referred to above is shown in Figure 3A-4b, where it is indicated by an arrow. It is similar to the phenomenon observed in Period 2 but appears here with greater intensity and resolution. During stripping at 10 mA cm^{-2} anodic, the palladium resistance exhibits two maxima, the second and larger of which displays a resistance ratio of >3.6. During subsequent loading at 10 mA cathodic, a complementary pair of resistance maxima are observed, resistance ratio of the first being >4.2 and that of the second approximately 2.1. The expected resistance ratio maximum for the Pd/D system in the absence of B is slightly less than 2. Thus, the magnitude of all the resistance peaks, as well as the existence of two pairs, is unexpected and not fully explained at present (see Conclusions section below).

Two heater steps, 1 W at t = 694 hours and 7 W at 713 hours, were employed in an attempt to recalibrate the calorimeter in the presence of the anomalous power source. Performing such a calibration requires that the effect of temperature changes induced by heater power steps on the unknown power source be negligible. For the two calibration steps performed, this assumption appears to be valid, and the calorimeter was found to be operating in its nominal condition; that is, the

constants necessary to determine the input and output power had their expected values both initially and later.

In an attempt to increase the magnitude of the excess power, the current was ramped at 50 mA/hour from 0.1 A to 0.6 A and then from 0.6 A to 1.1 A. During this period, the excess power displayed some variation about a mean value of ~850 mW but was essentially uninfluenced by the current, despite an essentially complete substitution of electrochemical input power for heater. This latter finding suggests that mismeasurement of the heater input power is not a significant contributing source in the excess power determination).

During the ramps from 0.1 A to 1.1 A, the power excess was not appreciably influenced by the current density, even though the loading responded positively to the current (Figure 3A-4b, expanded). The current ramps finished at t = 764 hours, at which time the excess power was ~0.9 W (with a total power input of 7 W). Approximately 3 hours later, while the system was maintained at constant current and input power, the excess power decreased, apparently spontaneously, and approximately exponentially, to a new value of ~ 0.3 W excess. From the measured resistance ratio (Figure 3A-4b expanded), the decrease in excess power occurred at a time when the electrode was either de-loading D or absorbing B (i.e., increasing $R/R°$).

At t = 761 hours, the total power input was reduced by 1.5 W to ~5.5W by switching the heater off. This appears to have precipitated a small decrease in the measured excess power, from ~0.3W to ~0.2 W. This negative correlation of excess power with heater power (or cell temperature) was unlike the insensitivity displayed in the two previous heater power steps. The heater was kept off for the remainder of the experiment.

At t = 786 hours, the current was further ramped to 1.6 A. This ramp served to restore the Pd resistance to its previous (high loading) value (Figure 3A-4b, expanded). The excess power (Figure 3A-4f) displayed a transient decrease during this ramp. Because the calorimeter was no longer operating in its constant power mode (heater off), the decrease in P_{xs} in the raw data is due to the departure of the calorimeter from its steady-state condition during the ramp. At the end of the ramp, the excess power had re-established the value of ~0.3 W attained before the 1.5-W

heater step. It is not clear whether this increase was due to the increased current, loading, or temperature or to some other effect.

At the end of Period 4, the current was ramped at -50 mW/hour from 1.6 A to 0.1 A, where the initial effect had been observed. During this ramp the excess power measured for the two RTD pairs decreased to a value between 0.1 W and 0.2 W. The records for these two sensor pairs do diverge, however, which suggests a misfunction or mismeasurement of one sensor; this effect had not previously been observed.

3A.3.5 *Period 5*

The current was maintained at low values for ~140 hours to re-establish the calorimetric baseline. During this time, the cathode was stripped briefly and again demonstrated two complementary pairs of resistance maxima.

Inspection of the excess power for the RTD (Figure 3A-5g) and thermistor/RTD (Figure 3A-5h) sensor pairs reveals that sensor 4 (RTD) was indicating a higher temperature than the other three outlet sensors for the period t = 820 to 980 hours. We conclude, therefore, that the correct excess power for the interval from t = 840 to 1000 hours was ~0.1 W. In the context of temperature sensor variations, it is interesting that, following an inadvertent interruption to the bath heater control, the RTDs (Figure 3A-5g) restored themselves to their initial temperature values far more quickly than the thermistors (Figure A-5h). This pattern is reproduced during a second, longer, bath control interruption at t = 1032 hours.

At t = 975 hours, the current was ramped up to 1.86 A (~620 mA cm^{-2}). At a current of ~1 A (~330 mA cm^{-2}), the excess power increased to a maximum of ~500 mW.

3A.3.6 *Period 6*

The current was maintained at 1.86 A and then stepped to 2.15 A at t = 1,242 hours and maintained there until the experiment was terminated because of a cathode contact fault at t = 1,288 hours (54 days). During this time the excess power fluctuated from a minimum value of ~0.1 W to a maximum of ~0.6 W (reflecting ~5% in excess of the measured power input), with an oscillatory period of ~4 days. The total energy for the excess power observed in Periods 5 and 6 (from t = 840 to 1,288 hours) was 0.417 MJ.

3A.4 Discussion

We have chosen to present a detailed analysis of Experiment P19, particularly the raw data, for a number of reasons. This was the first experiment performed with boron added to the electrolyte and therefore may be of interest historically. Although the data were rendered somewhat ambiguous by the absorption of B and its effect on the resistance, this electrode apparently attained rather high D loadings.

In some ways this experiment was typical of those performed before and since, but in two important ways it was anomalous:

- The combination of D and B desorption and absorption resulted in a resistance profile anomalous in both the multiplicity of peaks and their magnitudes.
- Excess power was observed five times in the 54-day experiment; the first observation, although very small, was atypically early: at 180 hours (7.5 days). Four of these observations of excess power were typical of those made in other experiments and are reported elsewhere in this report; that is, after an initiation period, excess power was observed only when the cathode had achieved a high D loading and the current was above a critical cathode current density. However, one of the excess power observations initiated, apparently spontaneously, with the cathode at low current density (Figure 3A-4h). This phenomenon had never been observed previously. Further, this anomalous power excess did not appear to be strongly or positively correlated with current density, and it persisted from some time, during a brief portion of which the surface of the cathode (at least) was substantially deloaded. The excess power observed in this burst was large (up to 1 W excess), while the input electrochemical power was small because of the low current. Thus, this event represents a very large (>500%) power gain when only the electrochemical input is considered.

Excess power was observed for more than half the duration of the experiment. This was the first experiment in which two thermistors were used (as well as two RTDs) at the calorimeter outlet.

Table 3A-1 presents a summary of the excess power observations (see end of section). Several features of this experiment are noteworthy and merit further discussion. They are considered below.

3A.4.1 *Energy*

The total energy input to the cell during the 1288 hours of operation (heater plus electrochemistry) was 41.95 MJ, the electrochemical energy input was 24.72 MJ, and the integrated excess power was 0.79 MJ. The energy excess therefore represents 1.9% of the known total energy input, or 3.2% of the known electrochemical input. Under the conditions of the experiment, the calorimeter has a measurement uncertainty of ~0.4%; the observation of excess energy therefore represents five times the uncertainty ("5σ") of the total input, and eight times the uncertainty of the electrochemical energy measurement.

The total inventory of Pd in the cathode was 0.024 mols. The excess energy summed over all five observations therefore represents 33 MJ/mol Pd, or 343 eV/atom Pd.

This observed energy excess is large in absolute terms, and extremely large when normalized to the known chemical components of the cathode (Pd and D). However, the need to account accurately for all input power in the 1288-hour duration of the experiment, which incorporates a substantial initiation time where no effect was observed and a very significant amount (>40%) of heater power employed to maintain near-steady-state operation, reduces the observed excess energy in relative terms. The total observed energy excess nevertheless is statistically significant, and its source must be accounted for. First we will attempt a chemical explanation.

The chemical state of the calorimeter (cell) contents is monitored by several means: the pressure and head space temperature measurements indicate the number of moles of gas in the head space; palladium resistance measurements indicate the integrity of the cathode as reflected in metal loss or gain or substantive chemical change, as well as the D/Pd (and indirectly the B/Pd) loading; and electrolyte

resistance measurements obtained from the cell current/voltage relationship reflect the D_2O level and Li content. These various measurements do not indicate the occurrence of substantial chemical reaction at the times when excess power was being generated. Likewise, post-test observation and analysis did not indicate any change in system chemistry beyond the (quantified) loading/de-loading of D in the Pd lattice as well as low levels of B and Li incorporation in the lattice.

If, nevertheless, we presume that chemical changes take place which are not reflected in the pressure and resistance measurements, we can set a rough upper limit on the energy that can be generated by a change in chemical state of the cell contents.

The inventory of chemicals in Experiment P19 was as follows:

		Species	Mols
Solid phase*	cathode	Pd	0.024
		D	0.023
	anode	Pt**	0.016
Solid + liquid phase		B	0.0004
Liquid phase		Li	0.02
Gas phase		D_2	0.002
		O_2	0.001
		D_2O	0.024

*Other solid parts are Al_2O_3, SiO_2, and PTFE, which are considered in this analysis to be nonreactive.

**As much as 0.1 mols of Pt is included in the cell as structural and electrically conductive members. This Pt does not contact the electrolyte and is considered in this analysis to be nonreactive.

One can imagine various reactions by which these chemical species may interact to release or store energy. Below we enumerate various reactions and their associated (approximate) enthalpies of reaction:

[1] $PdD_x \Leftrightarrow Pd + D_2$ ~1 kJ mol^{-1}

[2] $D_2 + 1/2\, O_2 \Leftrightarrow D_2O$ ~290 kJ mol^{-1}

[3] $2\,Li + 1/2\,O_2 + D_2O \Leftrightarrow 2\,LiOD$ ~683 kJ mol^{-1}

[4] $2B + 3/2\,O_2 \Leftrightarrow B_2O_3$ ~127 kJ mol^{-1}

Some comment is necessary for the above reactions. Reaction [1] is exothermic for x greater than 0.7 and endothermic below this value. Reaction [2] measures the extent to which recombination occurs; in a closed system, the rate of this reaction is measured by the rate of pressure change and is one of the corrections normally made(departure from initial state) in our data analysis; if the system is not closed (leaking), the correction is always endothermic at constant pressure. Reaction [3] is extremely unlikely, since LiOD (solid) is unstable in the D_2O environment. Further, the extent to which Li is consumed would be reflected in the (calculated) electrolyte resistance. Nevertheless, Reaction [3] is in chemical terms a very highly energetic reaction and therefore is incorporated in the analysis to ensure that a conservative upper bound is achieved for the chemical energy potential of the cell. Reaction [4] was selected for reasons similar to those for [3] and is similarly implausible. Note. that we have specifically excluded the burning of the noble metals Pt and Pd. Platinum oxide is known to form only at very insignificant levels even as an anode. Palladium oxide, while thermodynamically slightly less stable, cannot, in any case, form at the cathode.

Let us consider that all four reactions proceed to the right, simultaneously (with release of enthalpy).

Reaction	Moles of Reactant	Specific Enthalpy (kJ/mol)	Total Heat (kJ)
[1]	0.024*	10	0.024
[2]	0.002	290	0.58
[3]	0.02	683/2	6.83
[4]	0.0004	127/2	0.025
		Total	7.459

*Only about one-third of this is available spontaneously unless the cathode is heated or the pressure reduced.

It is clear that only about 7.5 kJ is available if all of the reactable chemicals react to the most energetic products, even given an unlimited supply of oxygen (e.g., via a leak). Contrast this number with the excess energy values in Table 3A-1. If we postulate that whatever chemical reactions proceed to release heat during the observed "bursts" are reversed (without measured endotherm or other physical effect) in the low-current periods between current ramps, then we must treat each of the events in Table 3A-1 singly. Thus ~75% of the energy observed in Event 1 can be accounted for by the (essentially complete) chemical reaction of the cell contents, whereas ~10% of Events 2 and 3 can be accounted by chemistry. For Events 4 and 5, only 2% or 3% of the observed energy can come from a known chemical source, and a total of less than 1% between events (allowing no "recharge"). In conclusion, we can state that most of the excess energy observed in this experiment cannot have arisen from chemical sources. Furthermore, even the "chemical energy" prediction described above is, in practice, extremely unlikely and certainly overestimates the amount of chemical energy that is realistically available.

3A.4.2 *Nuclear Products*

While it is clear that extraordinary (hitherto unexpected and unobserved) chemical effects would be required to produce the energies in Table 3A-1, these values are—at least energetically—well within the compass of known nuclear processes which are on the order of 10^6 times more energetic than chemical processes per participant nucleus (or atom). We wish to make clear, at the outset of this discussion, that no nuclear products or consumption of nuclear reactant was detected in Experiment

P19. The discussion which follows is superficial and general but is intended to highlight constraints that this failure to detect reactant loss and products imposes on any nuclear process in the Pd lattice.

From the total production of 0.8 ± 0.2 MJ of energy, we can calculate approximately the expected number of nuclei consumed and produced. Taking an approximate value of 10 MeV per nucleus, we calculate ~5 x 10^{17} nuclei lost and produced.

Experiment P19 contained ~24 mM of Pd, or 1.4 x 10^{22} atoms of Pd. At a loading $x \approx 1$, the cathode also contained ~10^{22} atoms of D (as well as ~10^{20} atoms of Li and B). If the reactant (or one of the reactants) was D, there is no possibility of detecting its depletion, and this difficulty is exacerbated by the very large inventory of D in the liquid and gaseous phases.

The presence of the adjacent liquid and gas volumes must be taken into account when considering the product sensitivity and distribution. Products that remain in the cathode offer different possibilities and problems for detection than those which escape to the electrolyte (and thence, ultimately, to the gas). In particular, integrating methods that involve dissolution or volatilization of the cathode provide a relatively sensitive (ppm or better) method of determining an average value; these methods are destructive however. Surface analytical methods involving mass spectrometric determination of material sputtered from spots offer relatively low elemental or isotopic accuracy (~1%) but offer the advantage—and problem—of providing information that is highly localized in area and depth.

In the present case, we need to detect ~5 x 10^{17} product nuclei in ~1.4 x 10^{22} atoms, provided that these nuclei remain behind in the Pd (the total number of atoms in the cell is >10^{25} atoms). That is, we need to be able to detect compositional or isotopic changes on the order of 0.003% or 34 ppm, of products contained within the cathode. The sensitivity and accuracy required from most chemical species are not readily available. This difficulty is exacerbated by high background levels and the possibility of contamination.

If the postulated nuclear reaction is accompanied by penetrating radiation or energetic charged particles, then the search for a nuclear process is greatly simplified,

as it also is if one or more products is radioactive. Our experiments have been routinely monitored for neutrons and gamma radiation, and all electrolyte samples have been subjected to post-test analysis for tritium. In no instance have radiation levels of radioactive products been detected above background.

We can conclude from the foregoing discussion that in each instance of excess heat in Table 3A-1, the observed energy exceeds the sum of the enthalpies of known chemical reactions—on average by a factor of ~20, and in total by a factor of more than 100. Energetic radiation and radioactive products have not been detected however. Thus, if a nuclear process gives rise to the heat, the process does not involve easily detected penetrating radiation or energetic charged particles and does not result in qualitatively commensurate radioactive product species.

3A.4.3 *Power*

Measurement of total integrated excess energy is important in deciding whether one is observing an energy production rather than an energy storage process. However, the existence question, i.e., whether there indeed exists a phenomenon to observe and explain, is more easily and accurately answered by analyzing the instantaneous calorimetric power balance. Therefore, the experiment discussed here was designed to make accurate and stable measurements of the input and output power so that the difference (denoted here as "excess power") can be explained.

One of the more startling observations of excess power is that represented by Event 4 in Table 3A-1. This event is discussed in greater detail here so we can draw conclusions. Figures 3A-6a through 3A-6c highlight the time interval between 650 and 806 hours. Figure 3A-6a shows the cell current, voltage, and reference voltage, together with the excess power averaged from the four pairs of temperature sensors (4-1, 3-2, 6-1 and 5-2), fully corrected for departures from the calorimetric and chemical steady state. Particular attention is drawn to the apparently spontaneous (i.e., not initiated by cell current, reference voltage, or cell power) increase (at 690 hours) and decrease (at 748 hours) in the observed power excess. Note also that the P_{xs} increase at 690 hours occurred while the calorimeter was in constant power control at ~14 W, with the heater contributing ~13.7 W, but the P_{xs} decrease at 748 hours occurred while the heater was off. Most importantly, the excess power in Figure 3A-6a shows little correlation, or even anti-correlation, with the electrochemical current.

Figure 3A-6b shows the excess power for each of the four sensor pairs separately; this power is expressed as a percentage of the total input power. The measurement uncertainty in this interval is between 0.4% and 0.6% of P_{total}, and except for the interval from 738 hours to 748 hours, where the thermistors (sensors 5 and 6) register a somewhat higher (~0.05°C) temperature, the excess power values calculated from all sensor pairs lie together within the measurement accuracy. During the interval shown in Figure 3A-6, the maximum excess power observed on all four pairs was ~11%, corresponding to 18-28 times the measurement uncertainty.

The data in Figure 3A-6b are presented normalized to the total measured input power, as one would do in examining a statistically weak signal or in examining an artifact. In examining the hypothesis that the excess power is a property of the D/Pd system and is achieved, for example, by electrochemical compression of deuterium in the palladium lattice, it is more appropriate to normalize the measured P_{xs} by the electrochemical power input only. This is equivalent to assuming that the power excess is not a property of the electrical heater.

Figure 3A-6c presents the measured power excess, averaged from the response of the four sensor pairs and corrected for departures from the chemical and calorimetric steady state. In this case the response has been normalized to the measured electrochemical power input, which is simply the product of the average cell current, I, delivered from a constant current supply, and the average cell voltage, V_{cell}, measured at the calorimetric boundary.

As can be seen by comparing Figures 3A-6a and 3A-6c, for periods when the cell current and voltage were low and P_{xs} was still large, the power multiplier P_{xs}/I^*V_{cell} was relatively large. The uncertainty presented in Figure 3A-6c is based on the total measured input (and not just the uncertainty associated with the electrochemical power input). Therefore, the uncertainty also reflects a large and variable percentage of I^*V_{cell}. Nevertheless, the excess power average over the four sensor pairs clearly represents a statistically large effect, exceeding 20 times the measurement uncertainty for significant intervals. Further, the measured power excess represents more than 500% of I^*V_{cell} for more than one day, and more than 200% of I^*V_{cell} for another three days. The effect is thus neither small nor fleeting.

It remains, however, difficult to produce the circumstances under which the effect is obtained.

Another way of accessing and addressing the significance of the observed excess power is to examine the integrated energy with its associated uncertainty. The thin lines in Figure 3A-6d plot the energy from t = 650 hours onward for each pair of temperature sensors, with each pair of sensors considered separately. Also shown, by broader lines, is the mean value of the excess energies recorded by the RTD pairs (sensor pairs 4-1 and 3-2), both plus and minus the experimental uncertainty. Thus the broad lines place an upper and lower bound on the excess energy. Each of the four measured values lies within these bounds; the thermistors, however, register a slightly higher energy (17 kJ) than the RTDs because of the positive excursion of the sensors between 738 and 748 hours.

Table 3A-2 summarizes the energies recorded between 650 and 806 hours.

Table 3A-2

Energy Input and Output Between 650 and 806 Hours

		Mean	Uncertainty
Input (MJ)	Total	3.31	±0.05
	I^*V_{cell}	0.84	±0.05
	Heater	2.47	±0.05
Output - Input (MJ)	RTDs	0.224	±0.048
	Thermistors	0.241	±0.048
	Average	0.233	±0.048

With the RTD values taken as being more reliable, the excess energy represents 6.77 ± 1.45% of the total power input in the interval shown, or 26.7 ± 5.7% of the electrochemical power input.

3A.5 Conclusions

In an experiment lasting a total of 1288 hours, excess power was observed on five occasions. The excess energy in each of these events was statistically significant.

Further, the energy excess in each event (and accumulated over the experiment's duration) exceeded the sum of known and plausible chemical reactions—for the last two events, by very large factors.

In seeking a nuclear explanation, perhaps with Pd, D, Li, or B as participants, one would expect to see on the order of 5×10^{17} product nuclei. Such products were not detected. For most chemical species, detectors with the required sensitivity and accuracy are not readily available. This difficulty is exacerbated by high background levels and the possibility of contamination and of heterogeneous distribution.

We can conclude that if a nuclear process gives rise to the heat, it does so largely by the production of stable nuclei which so far have not been detected but have not yet been seriously sought.

In general, the events of excess power generation occur when three criteria are met:

1. The D/Pd atomic ratio exceeds a critical value, which was found to be ~0.85 in other experiments using a 3-mm and smaller dimension orthogonal to the current flow.

2. The atomic ratio is maintained for a critical time, called the initiation time, which shows some variation but is typically 200-600 hours.

3. The current density is raised above a threshold value, typically 200-400 mA cm^{-2}.

In four of the five excess power events discussed in this section and summarized in Table 3A-1 these criteria are well obeyed. Event 1 initiated at 178 hours at a current density of 212 mA cm^{-2}. This initiation time was unusually short but the excess power was very small, which suggests that the initiation process, whatever it may be, may not have been complete by 178 hours. Events 2, 3, and 5 initiated at 354, 389, and 399 mA, respectively, and showed excess power characteristics typical of those observed in other experiments. Event 4, however, was distinctly atypical. Instead of initiation during a current ramp, Event 4 initiated, apparently spontaneously, at a steady current of 35 mA cm^{-2}. The excess power was maintained when the current was reduced and then reversed for a short time. During a current ramp, the excess

power showed little correlation, or even showed anti-correlation, with the electrochemical current.

Because the excess power in Event 4 appeared at low current densities, it represents a very large effect when expressed as a percentage of I^*V_{cell}, representing more than >500% for one day and >200% for another three days.

In conclusion, the excess power and energy observed in Experiment P19 represent statistically large effects that cannot be accounted for by known chemical reactions.

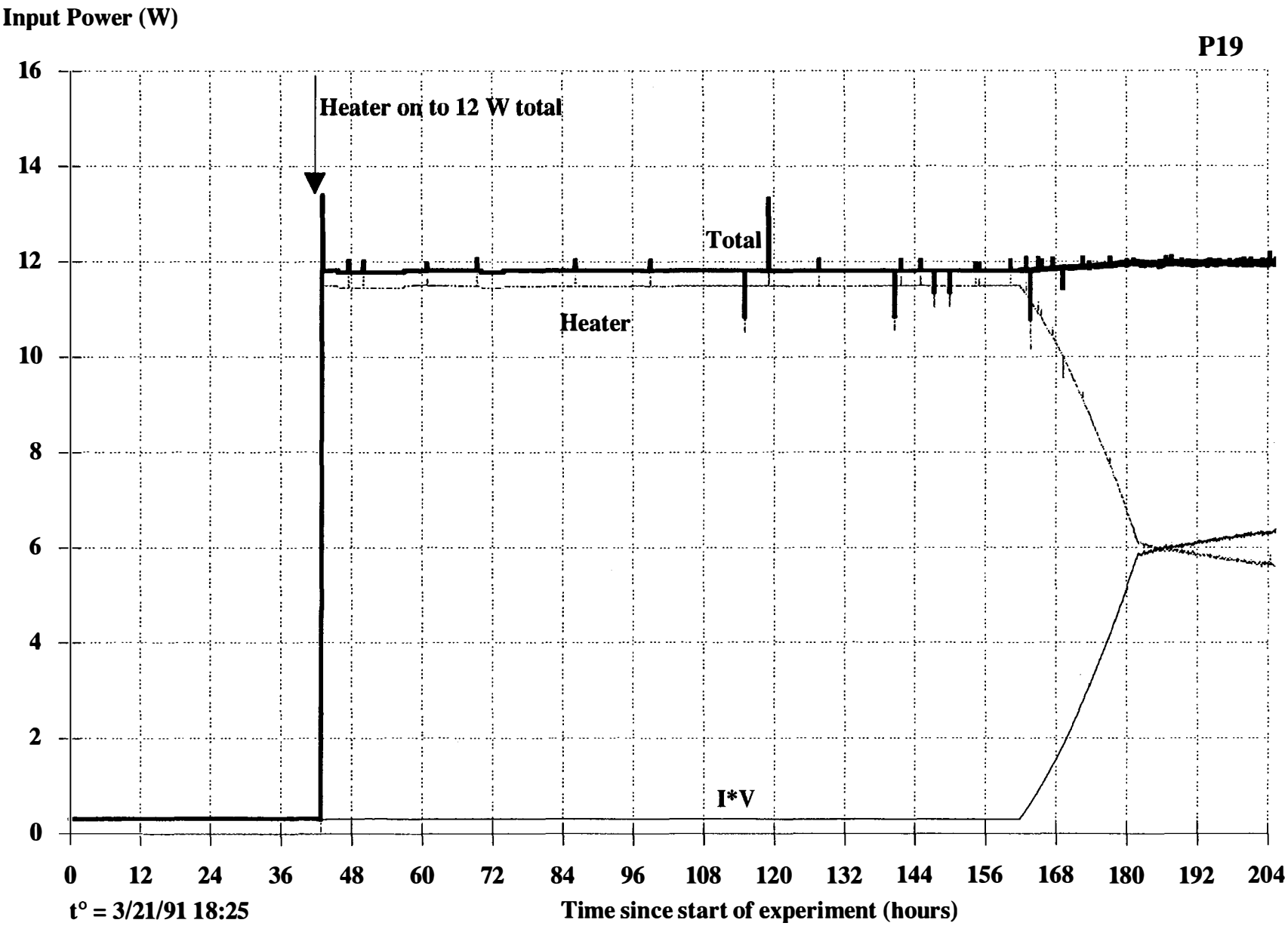
Input Power (W)
P19
16
14
12
10
8
6
4
2
0
Heater on to 12 W total
Total
Heater
I*V
0
12
24
36
48
60
72
84
96
108
120
132
144
156
168
180
192
204
t° = 3/21/91 18:25
Time since start of experiment (hours)

Figure A-1a

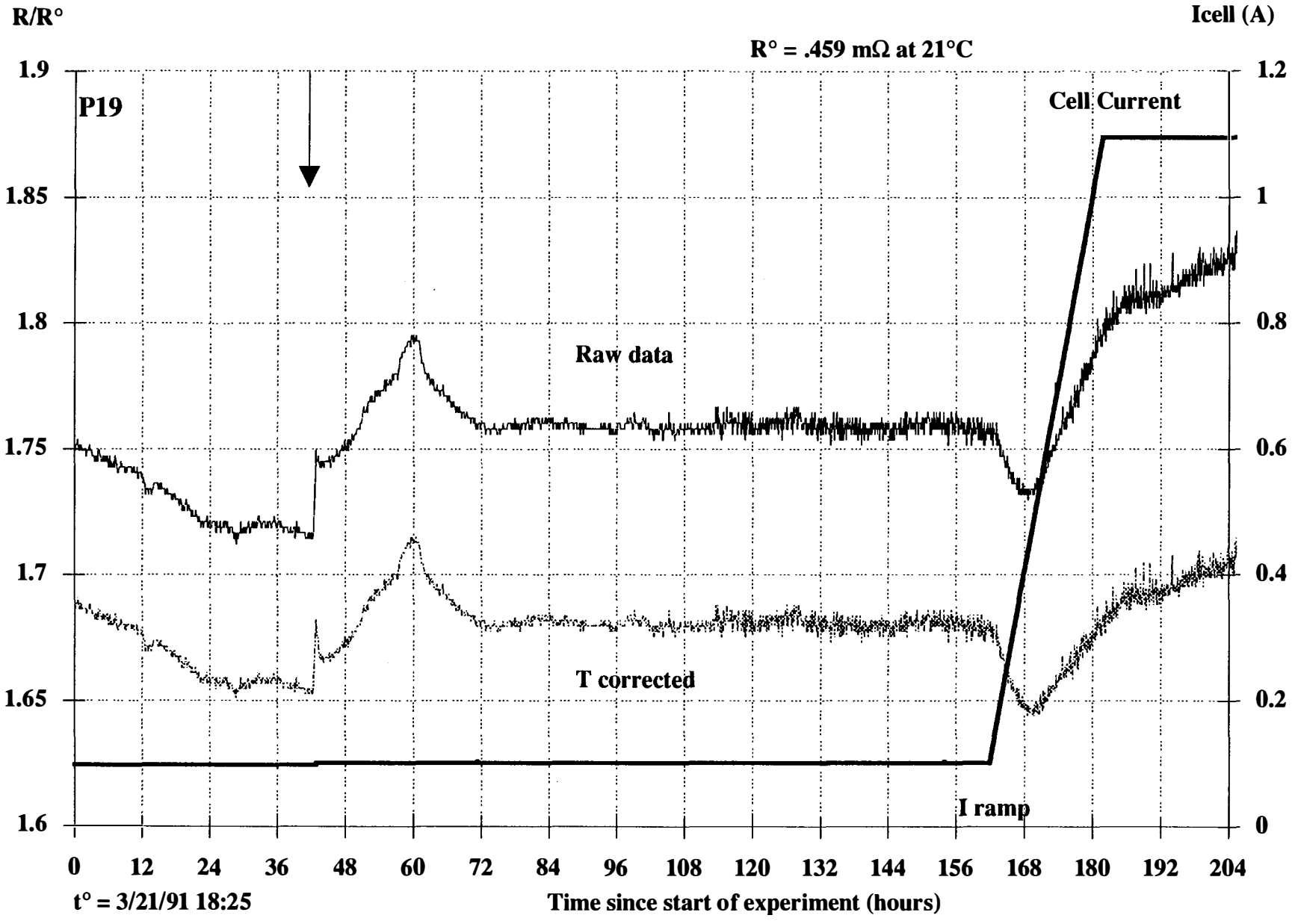
R/R°
Icell (A)
R° = .459 mΩ at 21°C
P19
Cell Current
Raw data
T corrected
I ramp
1.9
1.85
1.8
1.75
1.7
1.65
1.6
1.2
1
0.8
0.6
0.4
0.2
0
0 12 24 36 48 60 72 84 96 108 120 132 144 156 168 180 192 204
t° = 3/21/91 18:25
Time since start of experiment (hours)

Figure A-1b

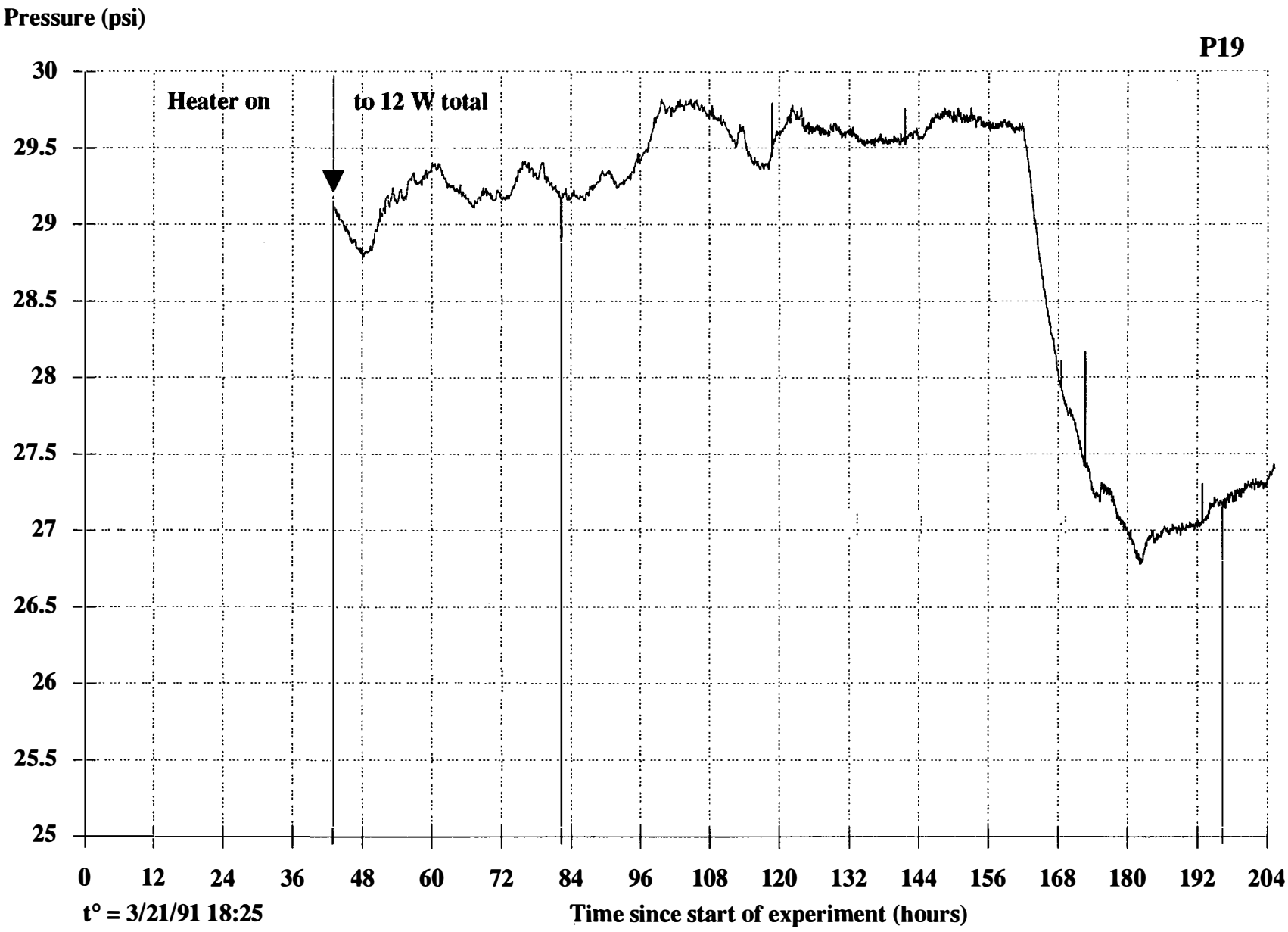
Pressure (psi)
P19
Heater on
to 12 W total
30
29.5
29
28.5
28
27.5
27
26.5
26
25.5
25
0
12
24
36
48
60
72
84
96
108
120
132
144
156
168
180
192
204
t° = 3/21/91 18:25
Time since start of experiment (hours)

Figure A-1c

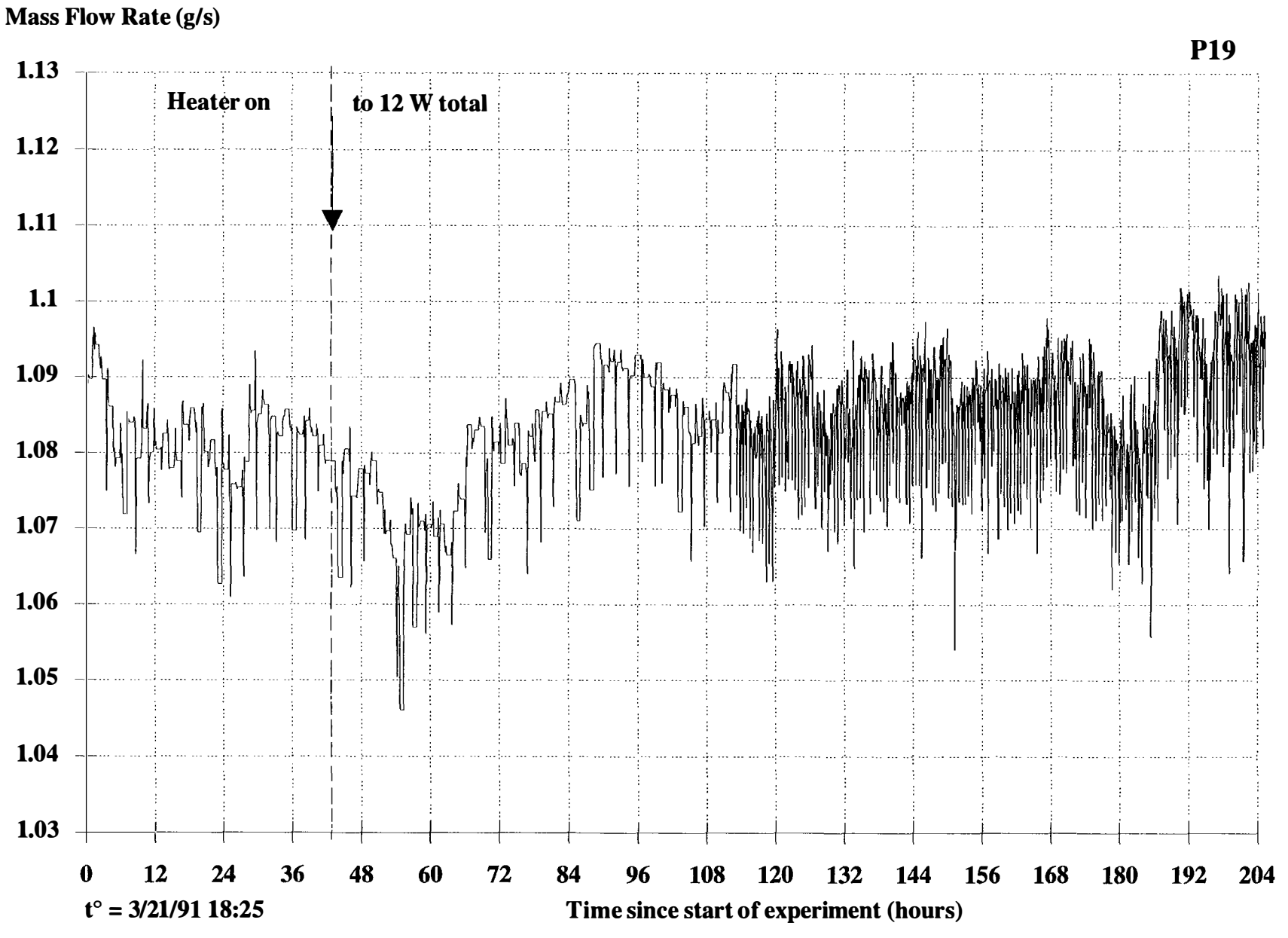
Mass Flow Rate (g/s)
P19
Heater on
to 12 W total
1.13
1.12
1.11
1.1
1.09
1.08
1.07
1.06
1.05
1.04
1.03
0
12
24
36
48
60
72
84
96
108
120
132
144
156
168
180
192
204
t° = 3/21/91 18:25
Time since start of experiment (hours)

Figure A-1d

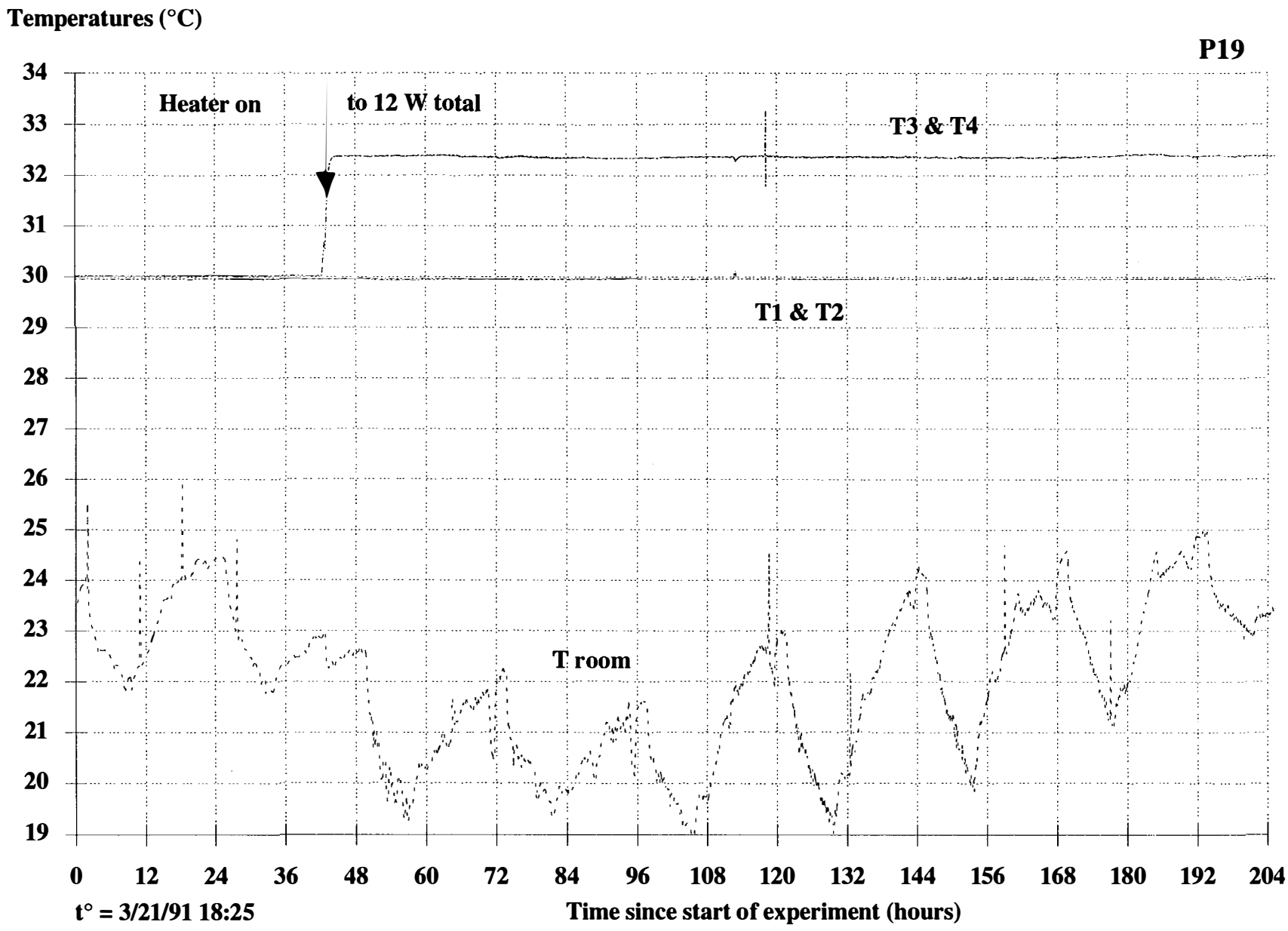
Temperatures (°C)
P19
Heater on
to 12 W total
T3 & T4
T1 & T2
T room
34
33
32
31
30
29
28
27
26
25
24
23
22
21
20
19
0
12
24
36
48
60
72
84
96
108
120
132
144
156
168
180
192
204
t° = 3/21/91 18:25
Time since start of experiment (hours)

Figure A-1e

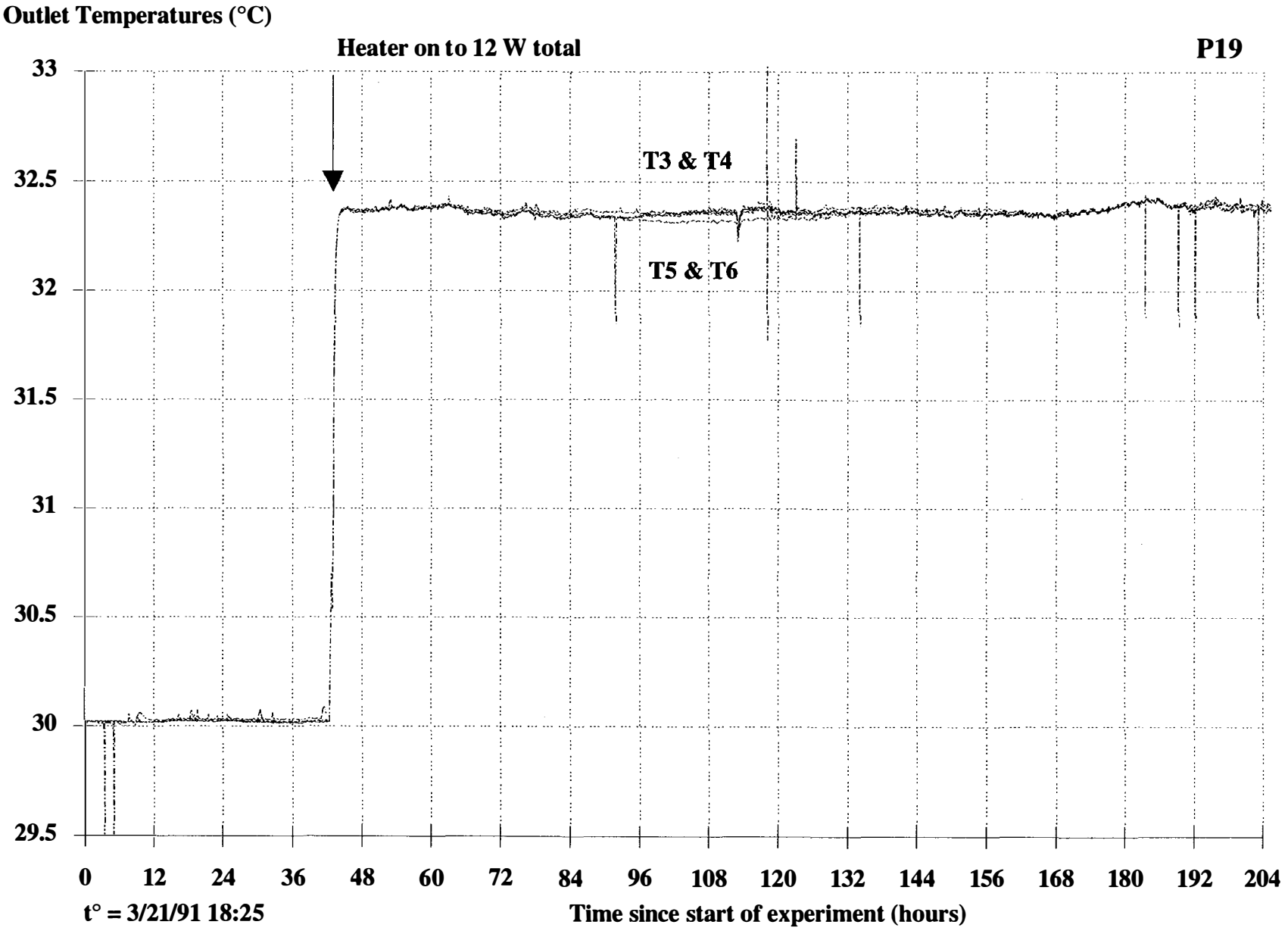
Outlet Temperatures (°C)
Heater on to 12 W total
P19
T3 & T4
T5 & T6
33
32.5
32
31.5
31
30.5
30
29.5
0
12
24
36
48
60
72
84
96
108
120
132
144
156
168
180
192
204
t° = 3/21/91 18:25
Time since start of experiment (hours)

Figure A-1f

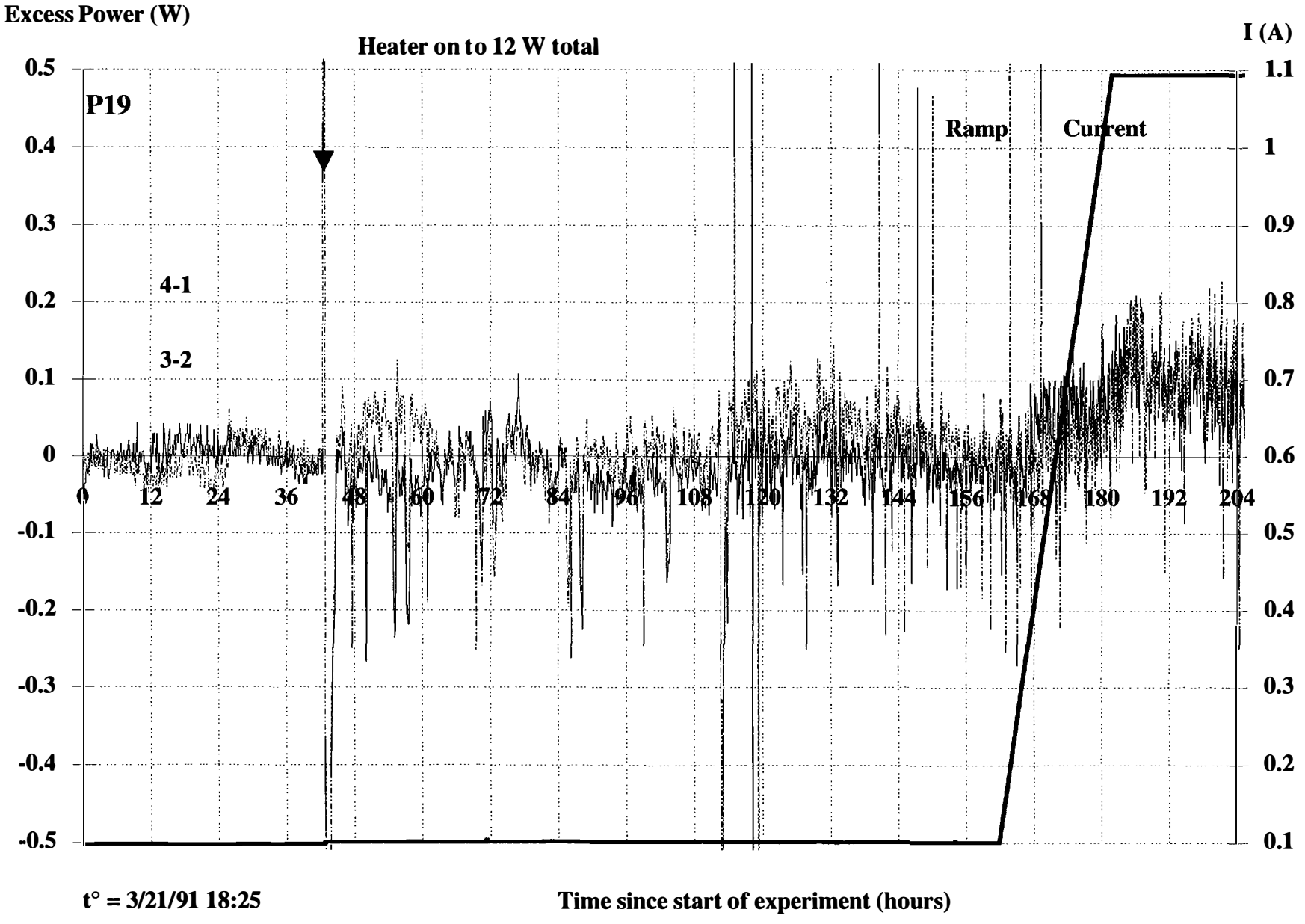
Excess Power (W)
Heater on to 12 W total
I (A)
P19
Ramp
Current
4-1
3-2
0.5
0.4
0.3
0.2
0.1
0
-0.1
-0.2
-0.3
-0.4
-0.5
1.1
1
0.9
0.8
0.7
0.6
0.5
0.4
0.3
0.2
0.1
0
12
24
36
48
60
72
84
96
108
120
132
144
156
168
180
192
204
t° = 3/21/91 18:25
Time since start of experiment (hours)

Figure A-1g

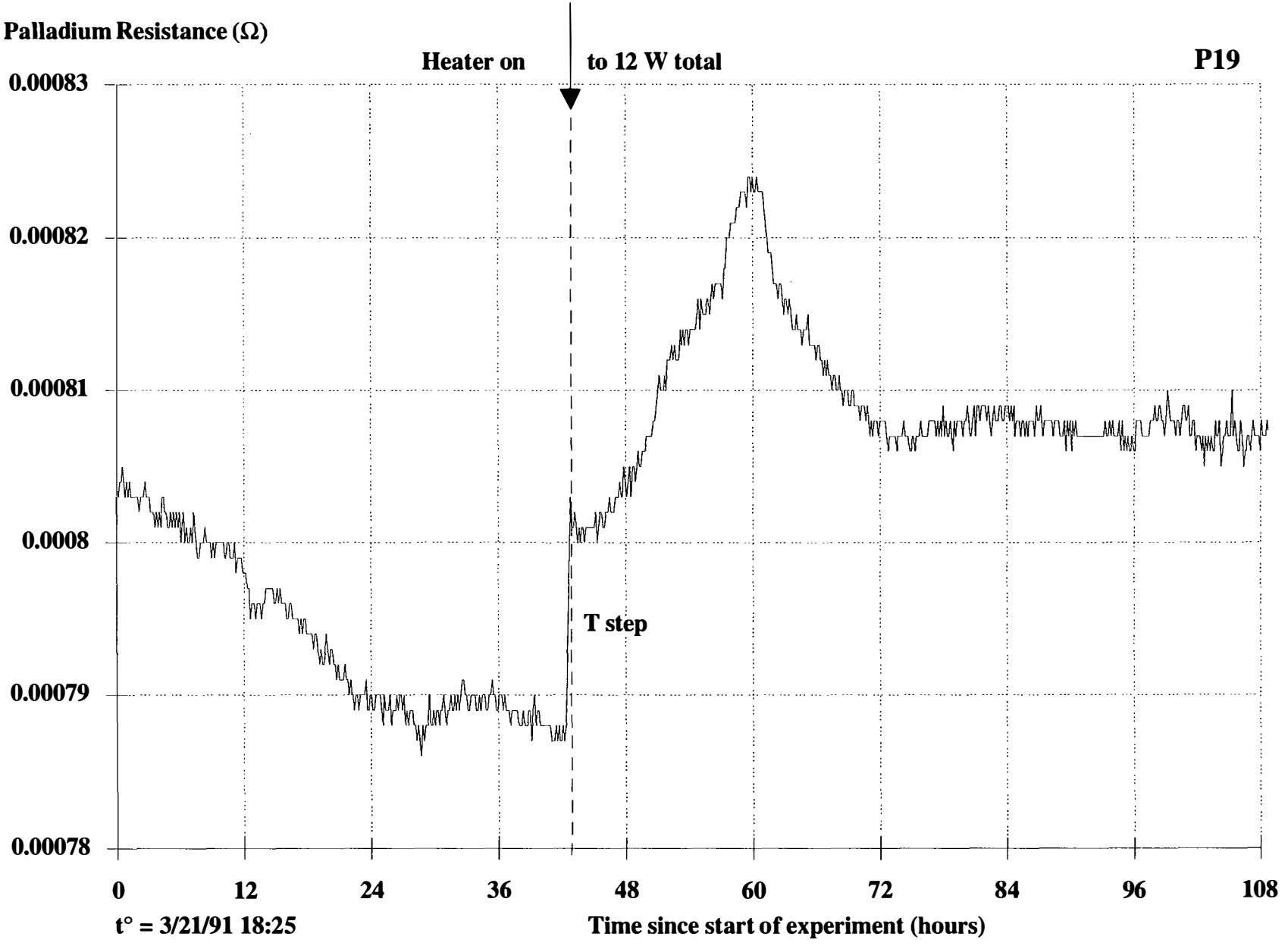
Palladium Resistance (Ω)
Heater on
to 12 W total
P19
0.00083
0.00082
0.00081
0.0008
0.00079
0.00078
T step
0
12
24
36
48
60
72
84
96
108
t° = 3/21/91 18:25
Time since start of experiment (hours)

Figure A-1h

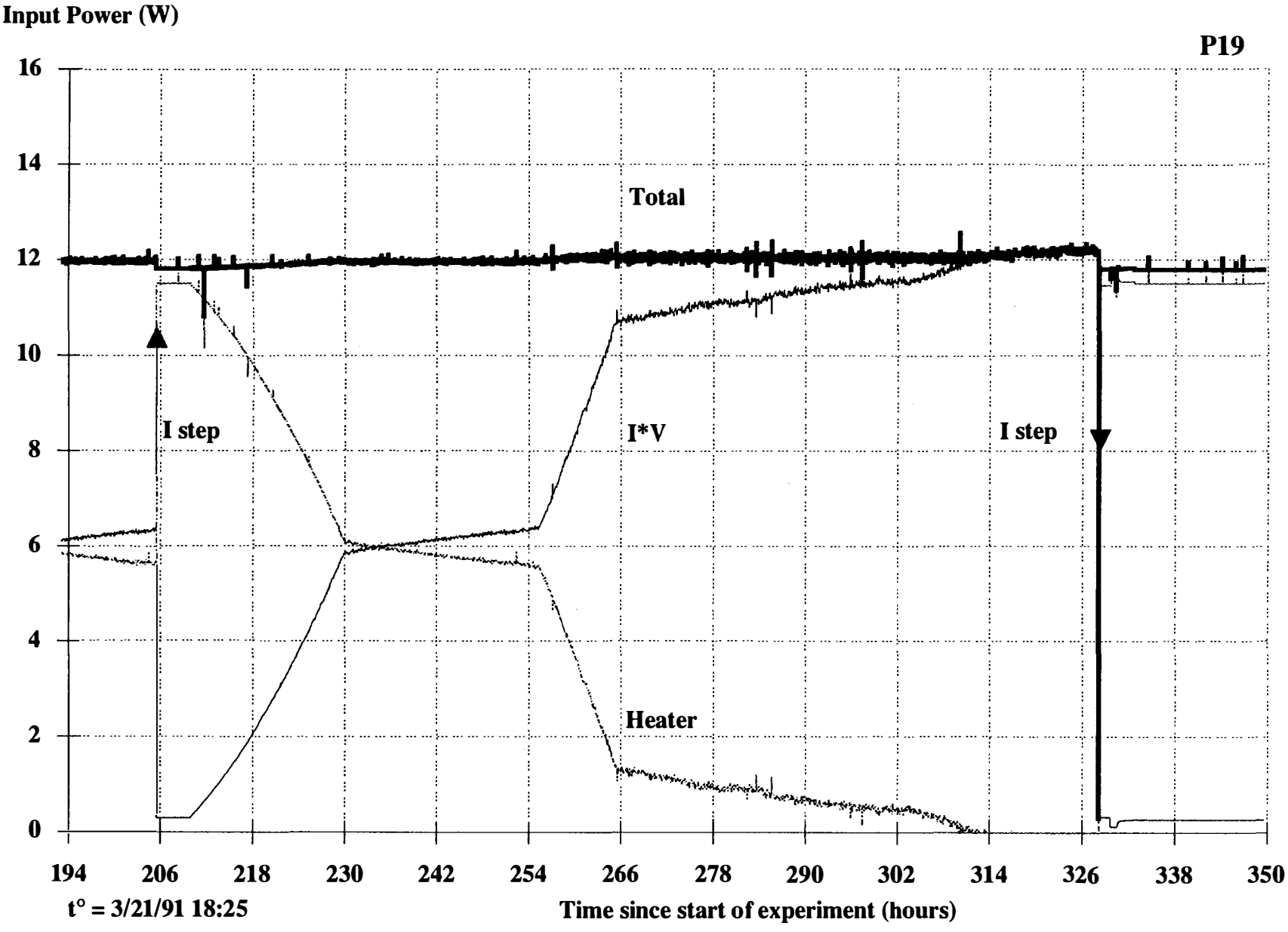
Input Power (W)
P19
16
14
12
10
8
6
4
2
0
Total
I step
I*V
I step
Heater
194
206
218
230
242
254
266
278
290
302
314
326
338
350
t° = 3/21/91 18:25
Time since start of experiment (hours)

Figure A-2a

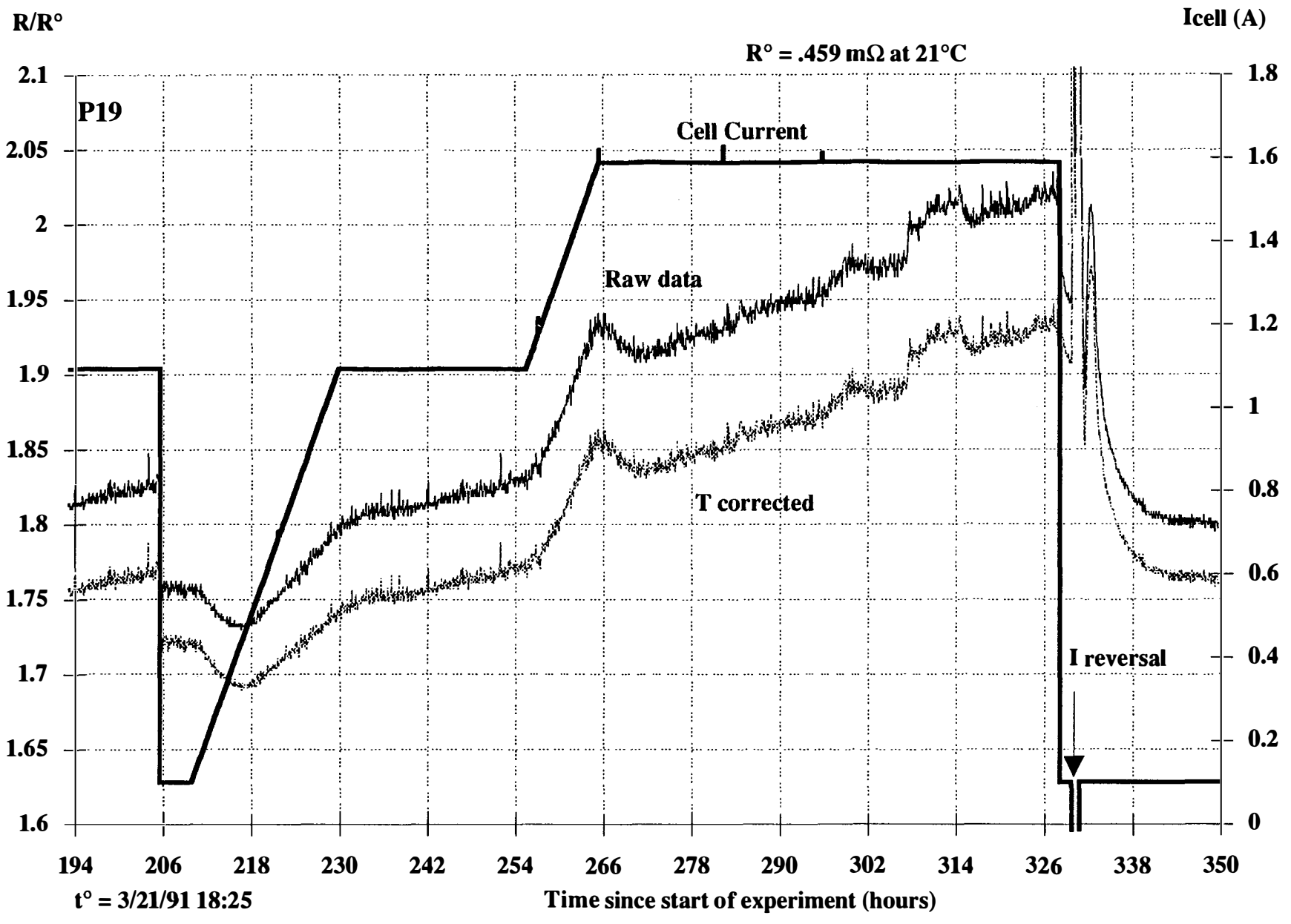
R/R°
Icell (A)
R° = .459 mΩ at 21°C
P19
Cell Current
Raw data
T corrected
I reversal
2.1
2.05
2
1.95
1.9
1.85
1.8
1.75
1.7
1.65
1.6
1.8
1.6
1.4
1.2
1
0.8
0.6
0.4
0.2
0
194
206
218
230
242
254
266
278
290
302
314
326
338
350
t° = 3/21/91 18:25
Time since start of experiment (hours)

Figure A-2b

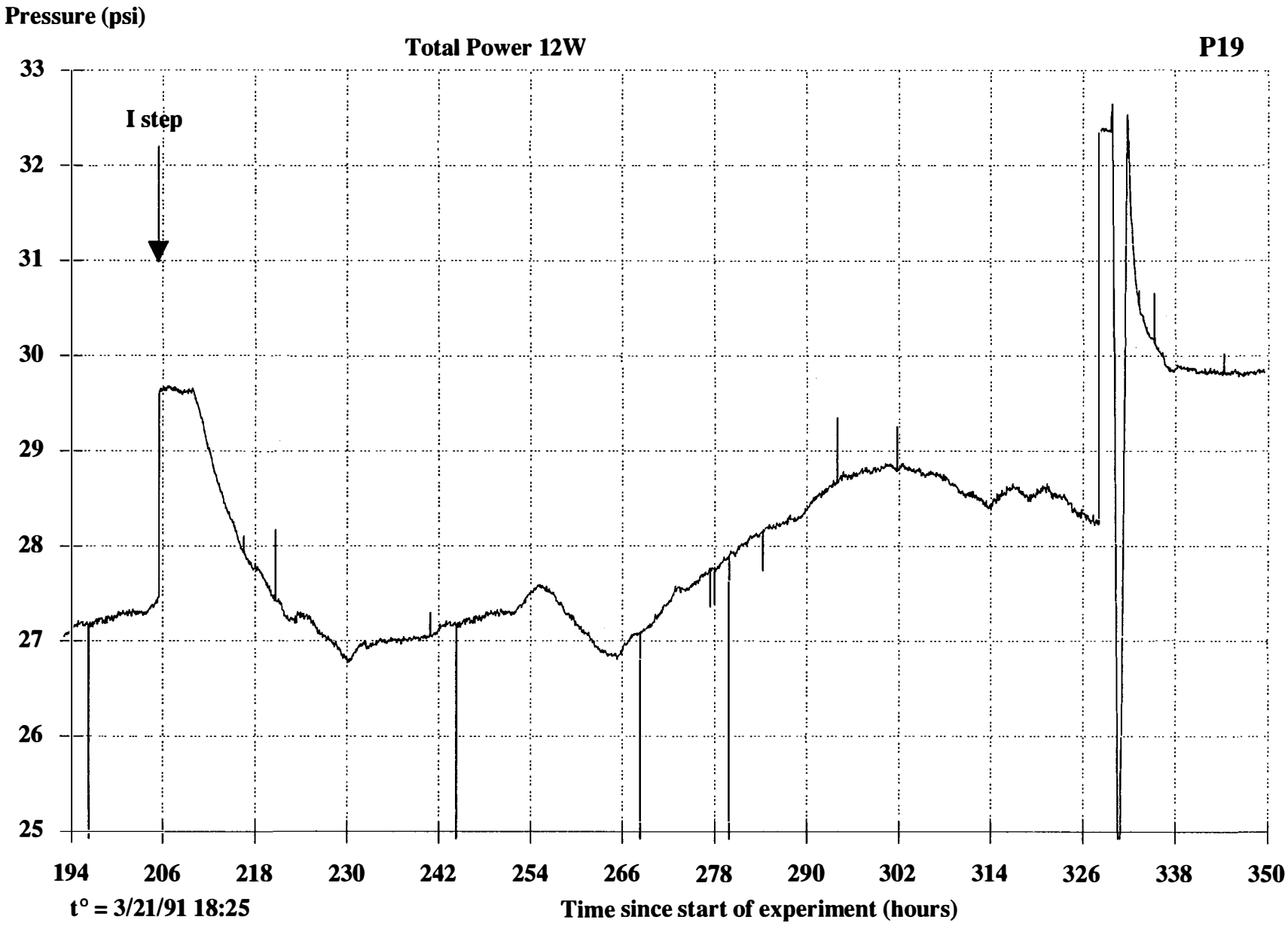
Pressure (psi)
Total Power 12W
P19
I step
33
32
31
30
29
28
27
26
25
194
206
218
230
242
254
266
278
290
302
314
326
338
350
t° = 3/21/91 18:25
Time since start of experiment (hours)

Figure A-2c

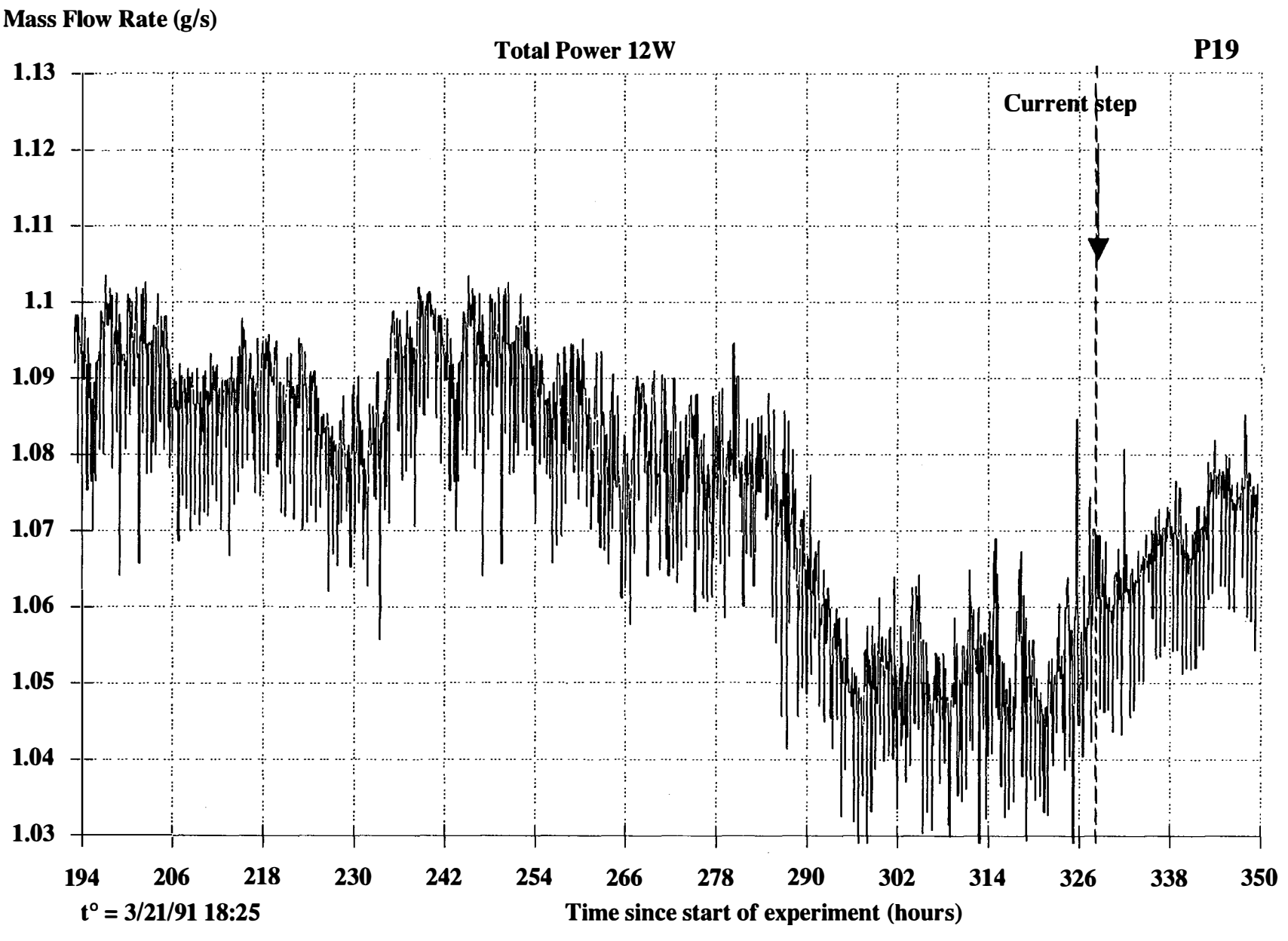
Mass Flow Rate (g/s)
Total Power 12W
P19
Current step
1.13
1.12
1.11
1.1
1.09
1.08
1.07
1.06
1.05
1.04
1.03
194
206
218
230
242
254
266
278
290
302
314
326
338
350
t° = 3/21/91 18:25
Time since start of experiment (hours)

Figure A-2d

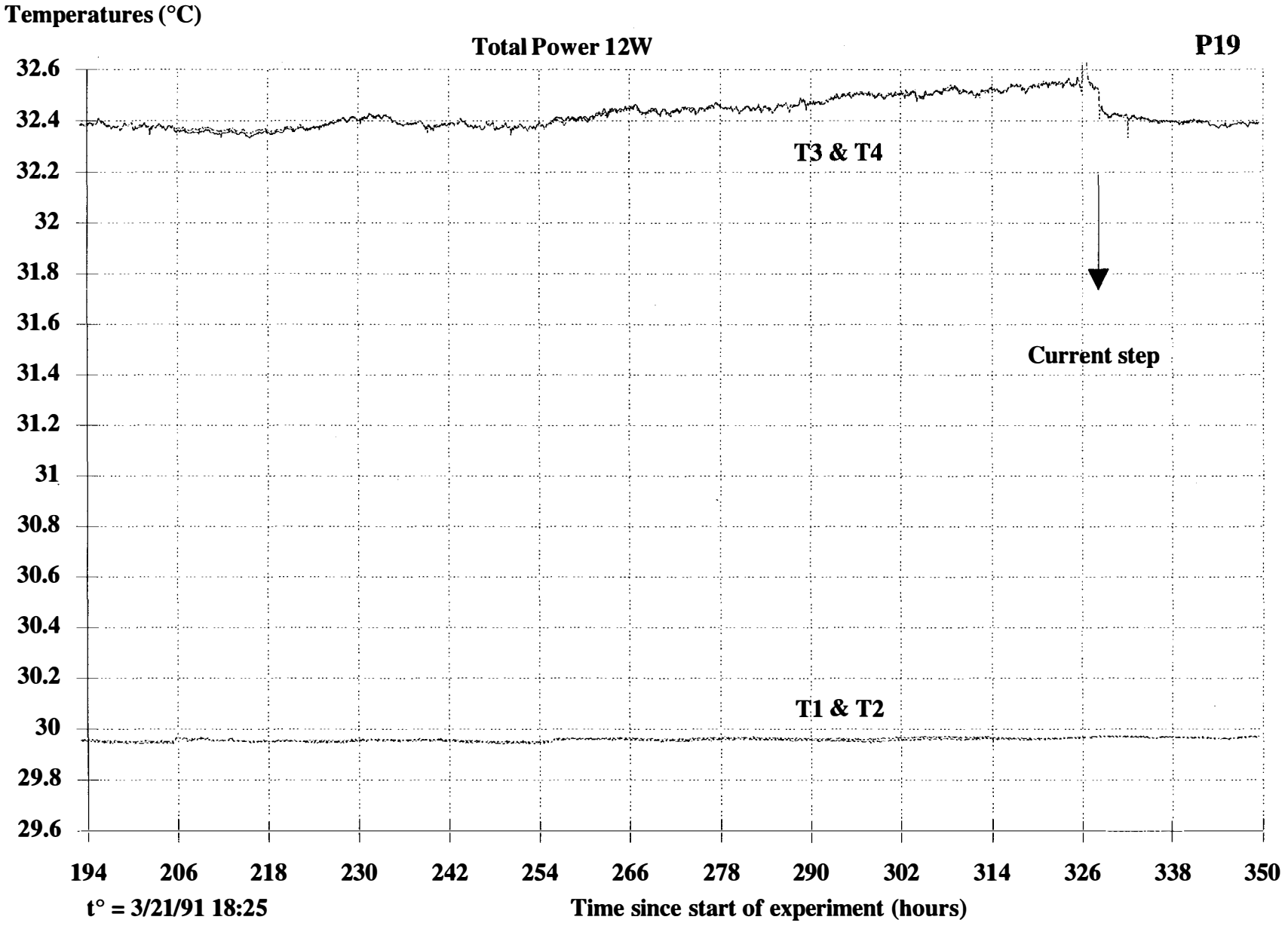
Temperatures (°C)
Total Power 12W
P19
32.6
32.4
32.2
32
31.8
31.6
31.4
31.2
31
30.8
30.6
30.4
30.2
30
29.8
29.6
T3 & T4
Current step
T1 & T2
194
206
218
230
242
254
266
278
290
302
314
326
338
350
t° = 3/21/91 18:25
Time since start of experiment (hours)

Figure A-2e

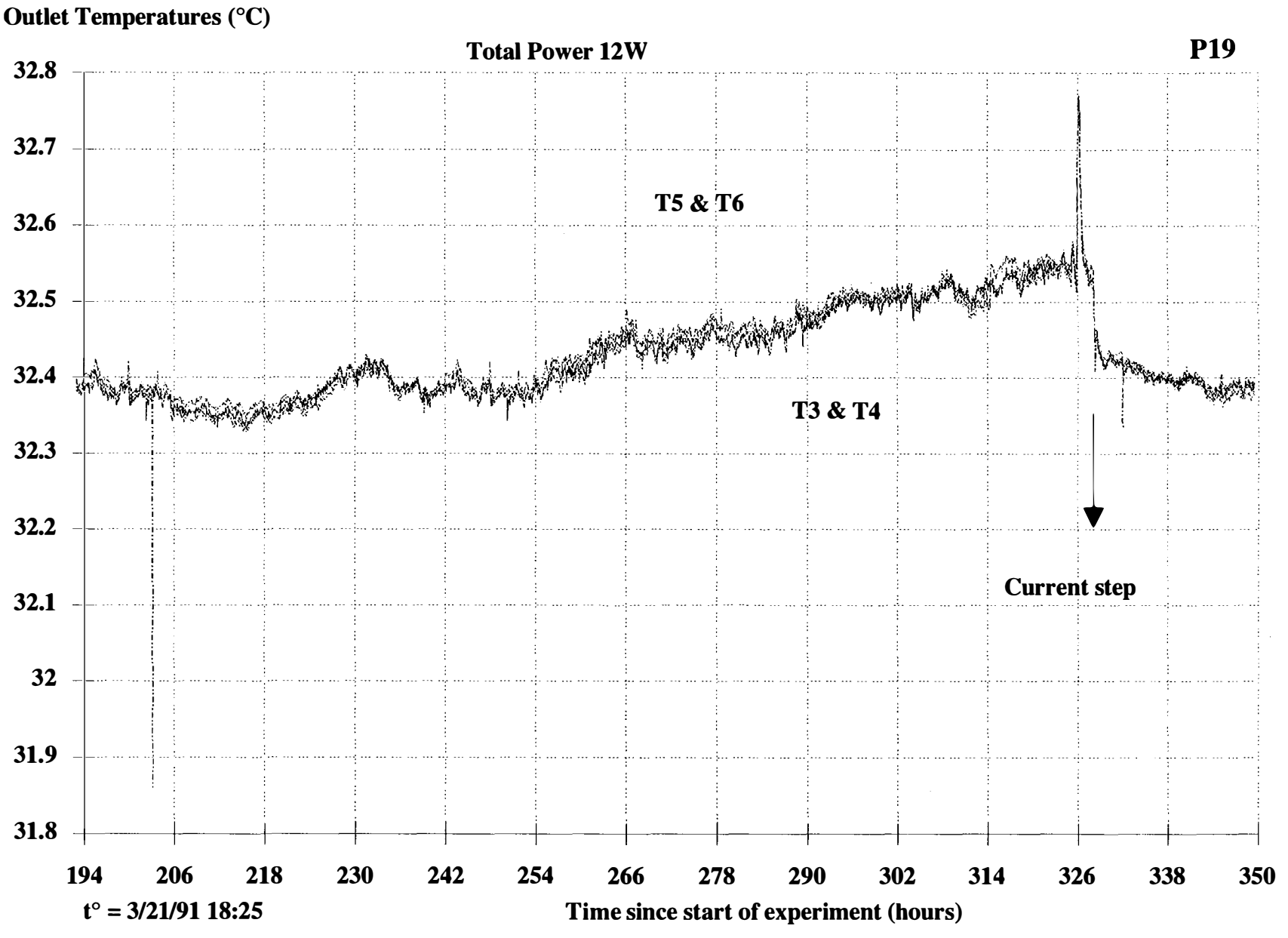
Outlet Temperatures (°C)
Total Power 12W
P19
32.8
32.7
32.6
32.5
32.4
32.3
32.2
32.1
32
31.9
31.8
T5 & T6
T3 & T4
Current step
194
206
218
230
242
254
266
278
290
302
314
326
338
350
t° = 3/21/91 18:25
Time since start of experiment (hours)

Figure A-2f

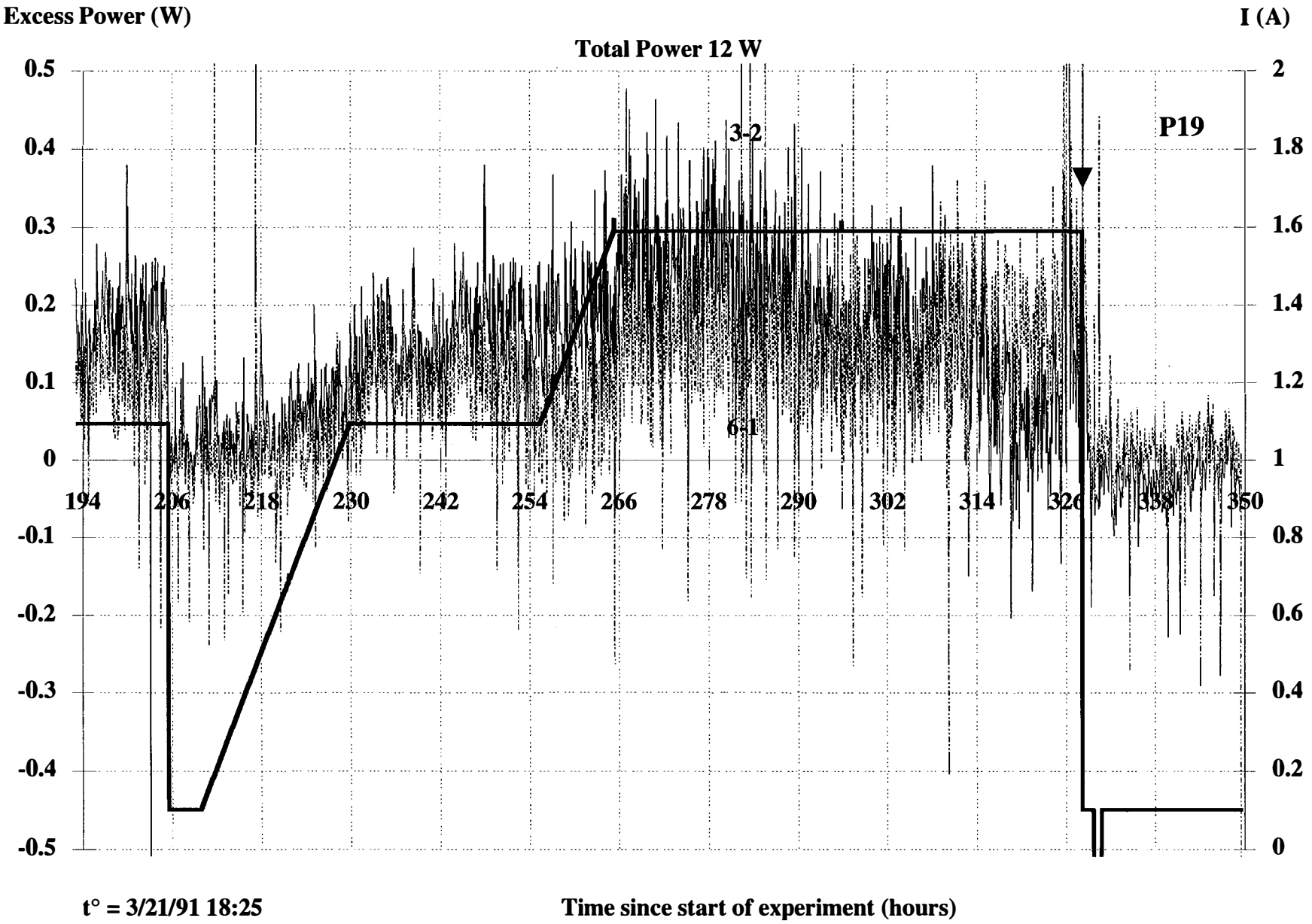
Excess Power (W)
I (A)
Total Power 12 W
0.5
0.4
0.3
0.2
0.1
0
-0.1
-0.2
-0.3
-0.4
-0.5
2
1.8
1.6
1.4
1.2
1
0.8
0.6
0.4
0.2
0
194
206
218
230
242
254
266
278
290
302
314
326
338
350
3-2
6-1
P19
t° = 3/21/91 18:25
Time since start of experiment (hours)

Figure A-2g

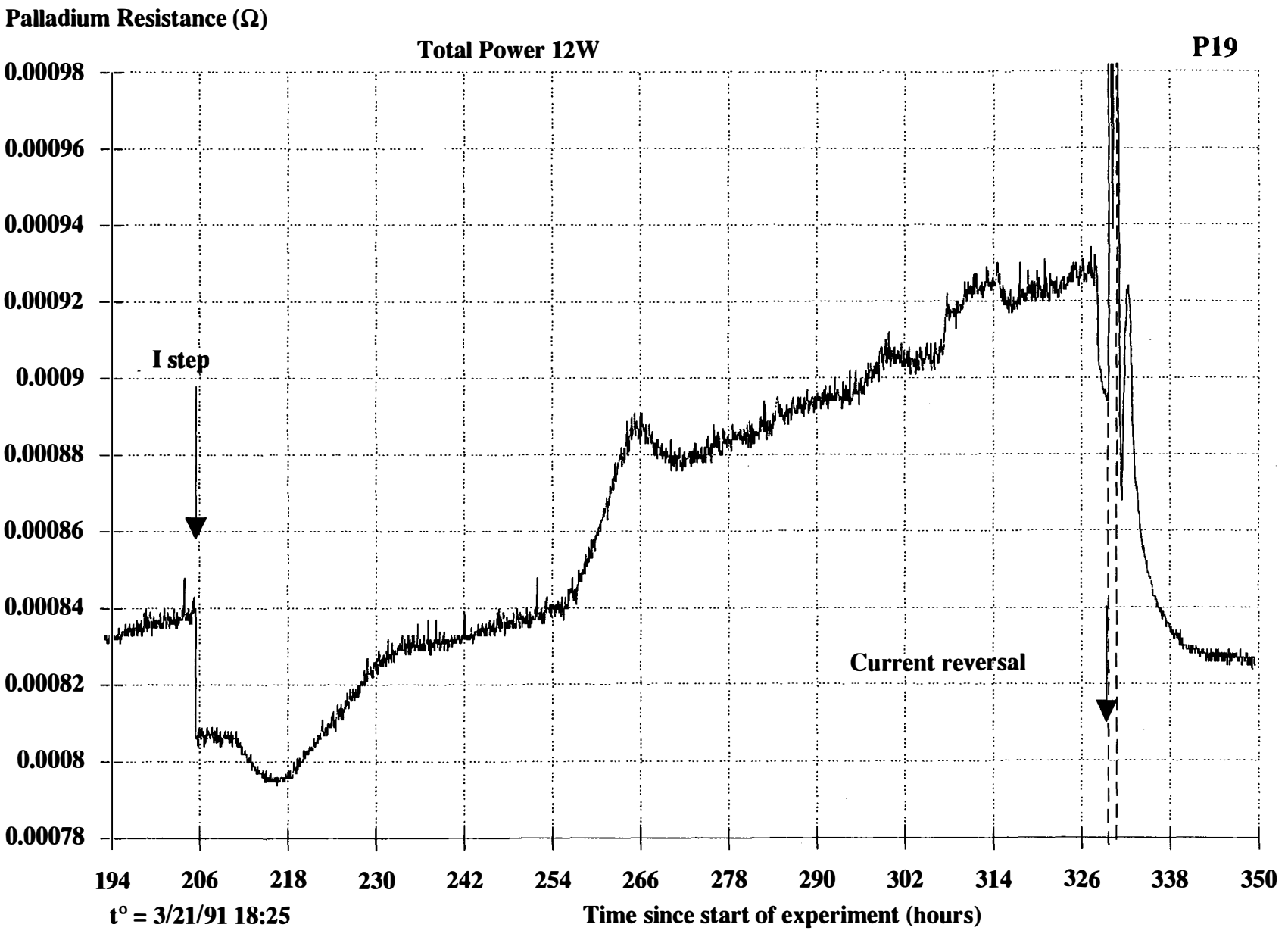
Palladium Resistance (Ω)
Total Power 12W
P19
0.00098
0.00096
0.00094
0.00092
0.0009
0.00088
0.00086
0.00084
0.00082
0.0008
0.00078
I step
Current reversal
194
206
218
230
242
254
266
278
290
302
314
326
338
350
t° = 3/21/91 18:25
Time since start of experiment (hours)

Figure A-2h

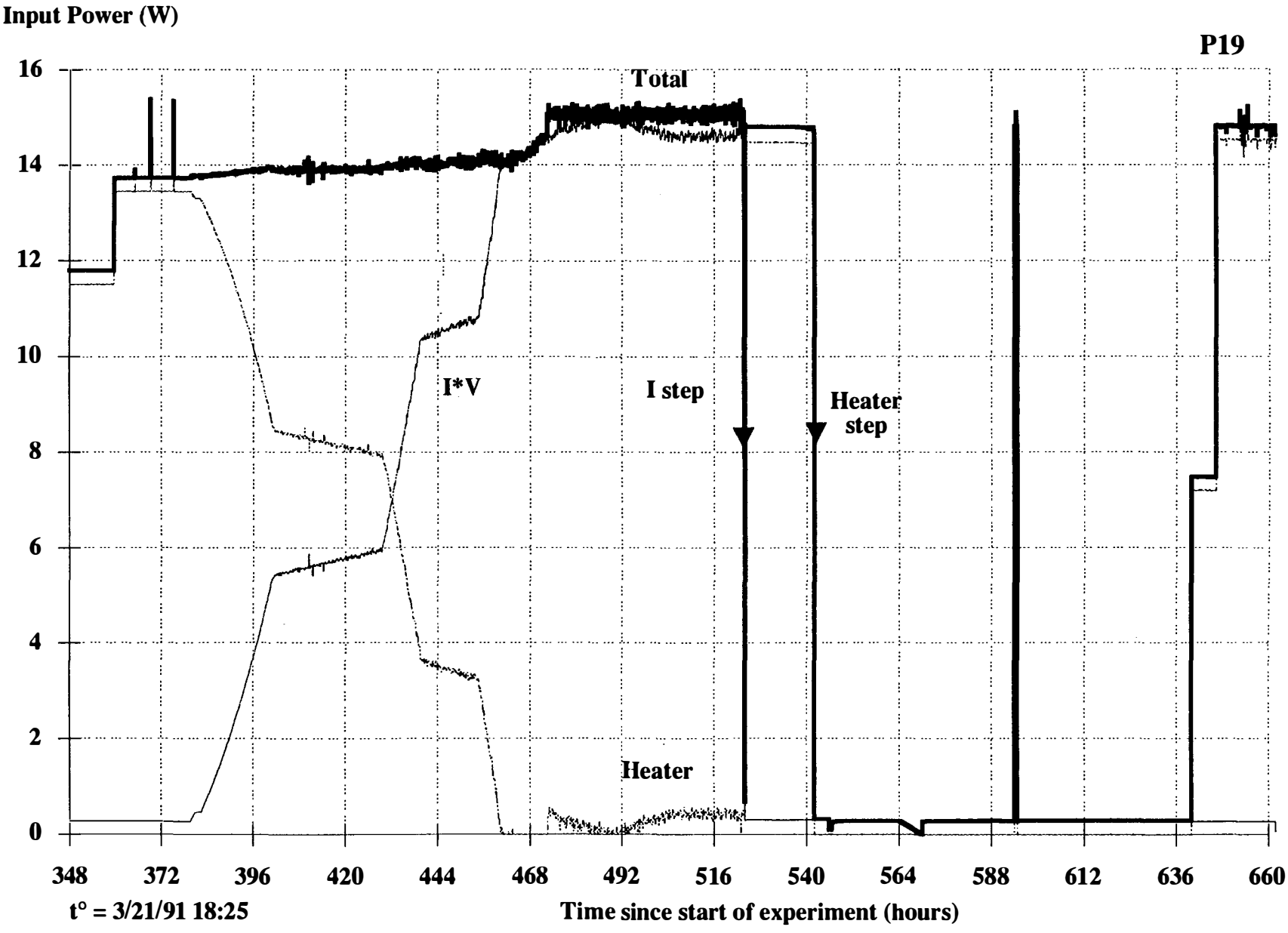
Input Power (W)
P19
16
14
12
10
8
6
4
2
0
Total
I*V
I step
Heater step
Heater
348
372
396
420
444
468
492
516
540
564
588
612
636
660
t° = 3/21/91 18:25
Time since start of experiment (hours)

Fig. A-3a

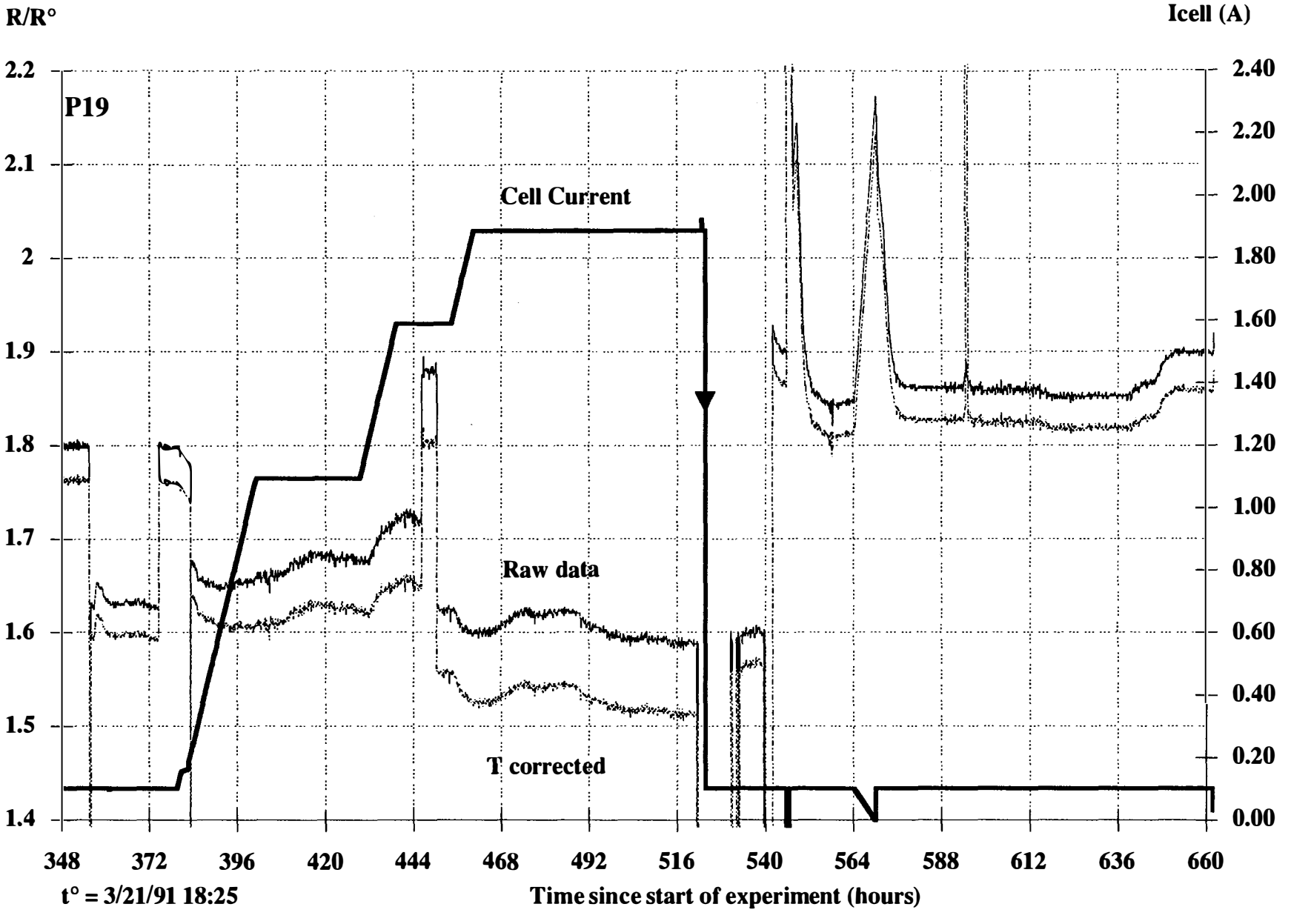
R/R°
Icell (A)
P19
Cell Current
Raw data
T corrected
2.2
2.1
2
1.9
1.8
1.7
1.6
1.5
1.4
2.40
2.20
2.00
1.80
1.60
1.40
1.20
1.00
0.80
0.60
0.40
0.20
0.00
348
372
396
420
444
468
492
516
540
564
588
612
636
660
t° = 3/21/91 18:25
Time since start of experiment (hours)

Figure A-3b

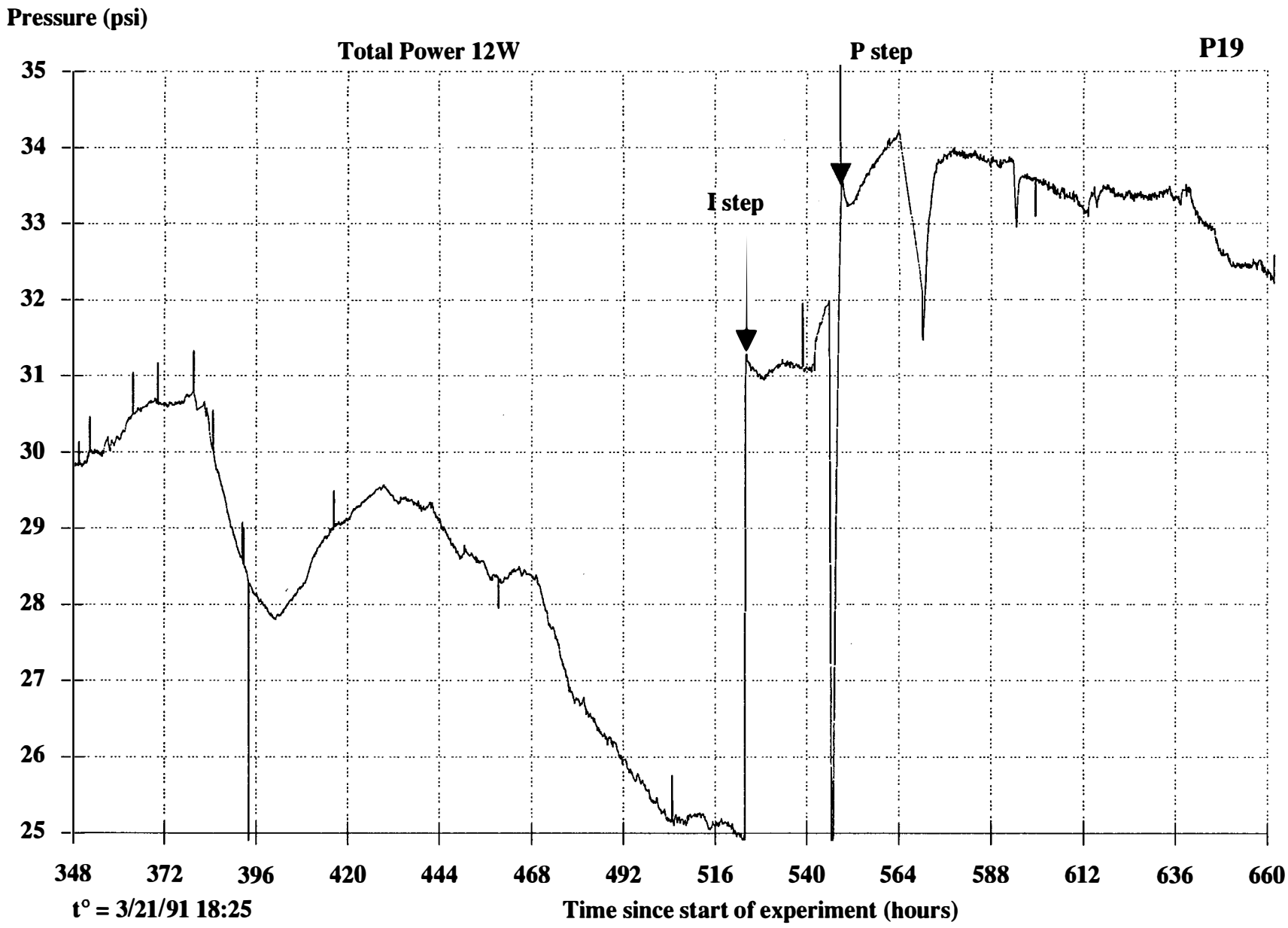
Pressure (psi)
Total Power 12W
P step
P19
I step
35
34
33
32
31
30
29
28
27
26
25
348
372
396
420
444
468
492
516
540
564
588
612
636
660
t° = 3/21/91 18:25
Time since start of experiment (hours)

Figure A-3c

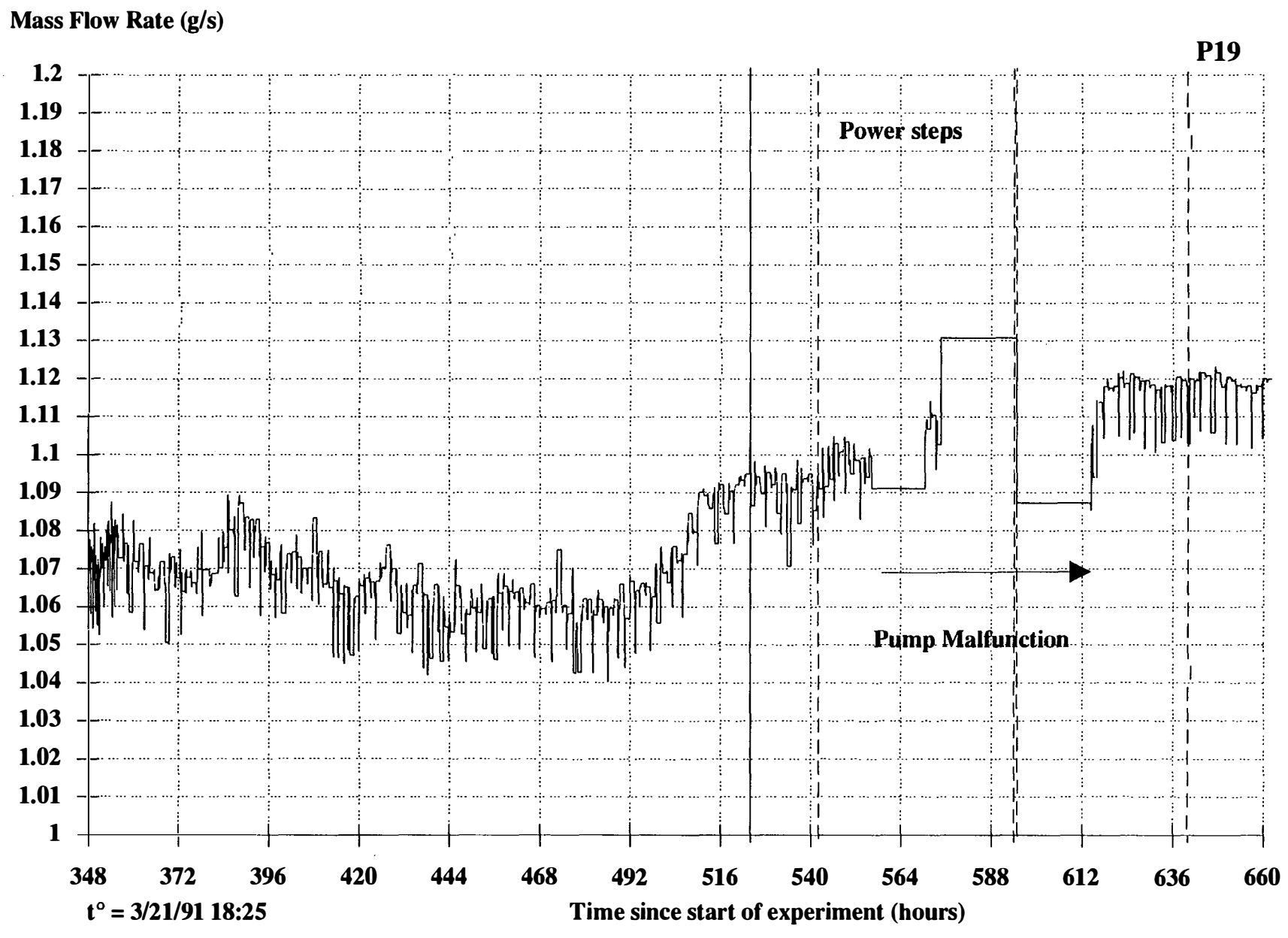
Mass Flow Rate (g/s)
P19
Power steps
Pump Malfunction
1.2
1.19
1.18
1.17
1.16
1.15
1.14
1.13
1.12
1.11
1.1
1.09
1.08
1.07
1.06
1.05
1.04
1.03
1.02
1.01
1
348
372
396
420
444
468
492
516
540
564
588
612
636
660
t° = 3/21/91 18:25
Time since start of experiment (hours)

Figure A-3d

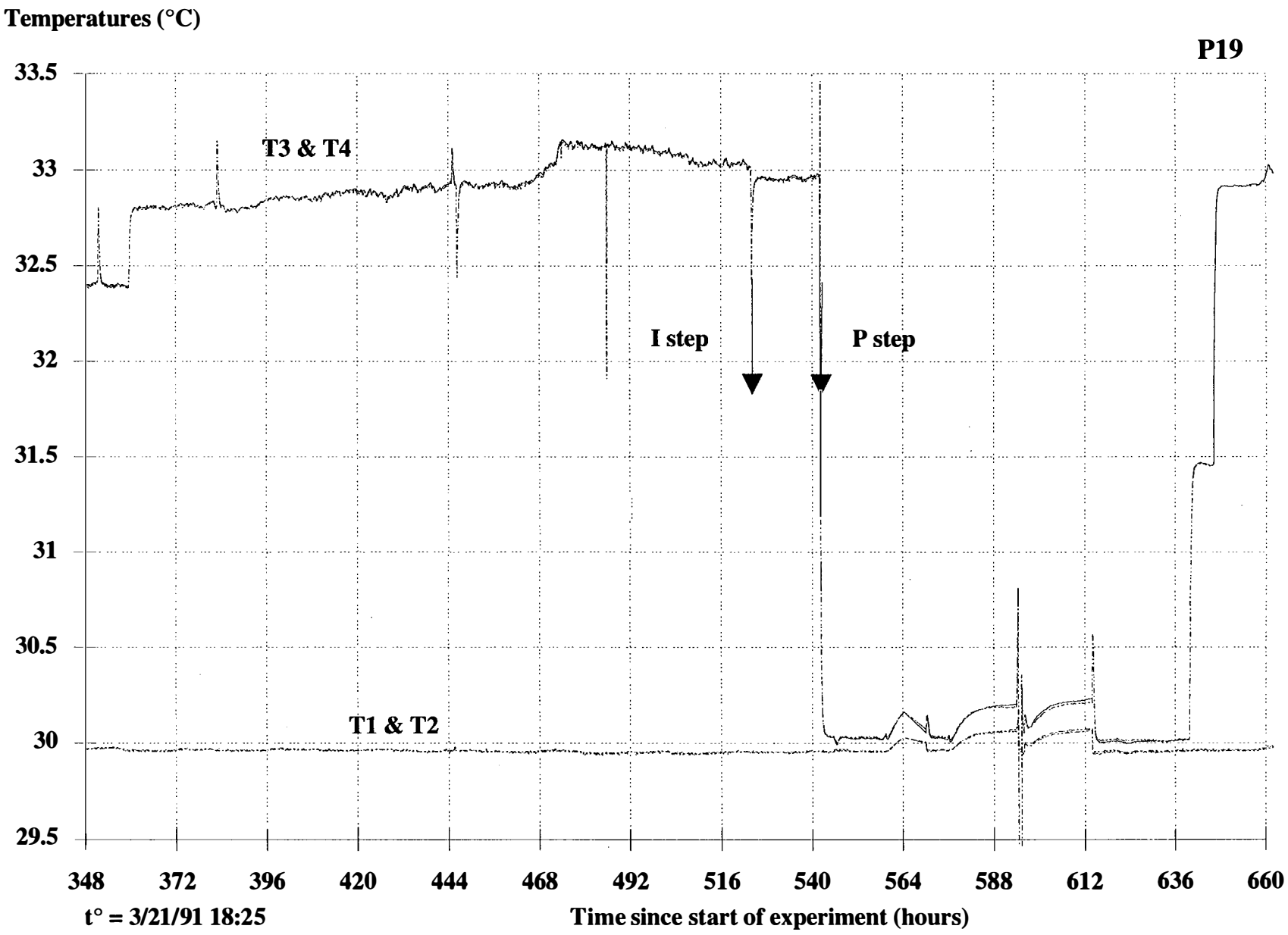
Temperatures (°C)
P19
33.5
33
32.5
32
31.5
31
30.5
30
29.5
T3 & T4
I step
P step
T1 & T2
348
372
396
420
444
468
492
516
540
564
588
612
636
660
t° = 3/21/91 18:25
Time since start of experiment (hours)

Figure A-3e

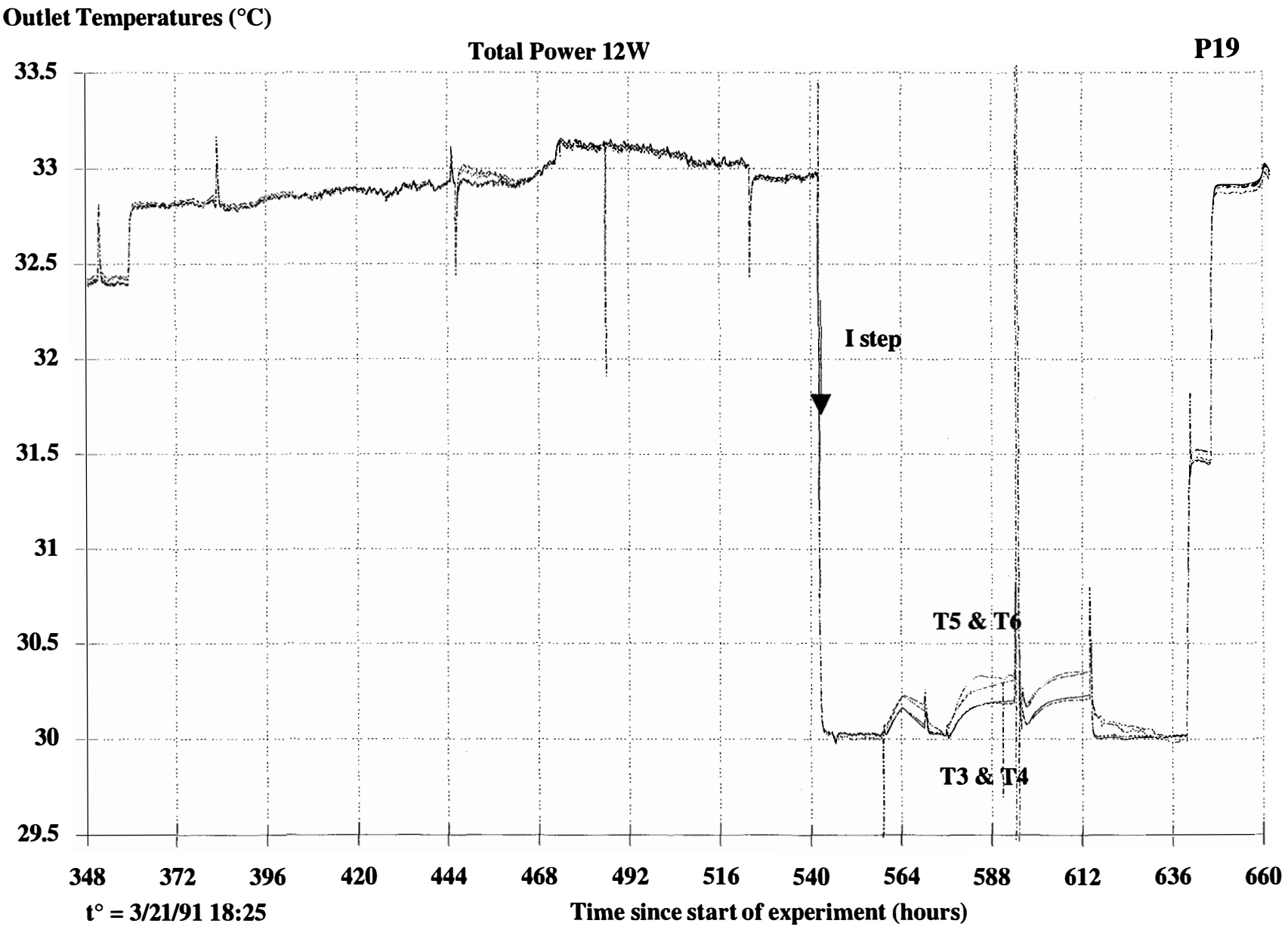
Outlet Temperatures (°C)
Total Power 12W
P19
33.5
33
32.5
32
31.5
31
30.5
30
29.5
I step
T5 & T6
T3 & T4
348
372
396
420
444
468
492
516
540
564
588
612
636
660
t° = 3/21/91 18:25
Time since start of experiment (hours)

Figure A-3f

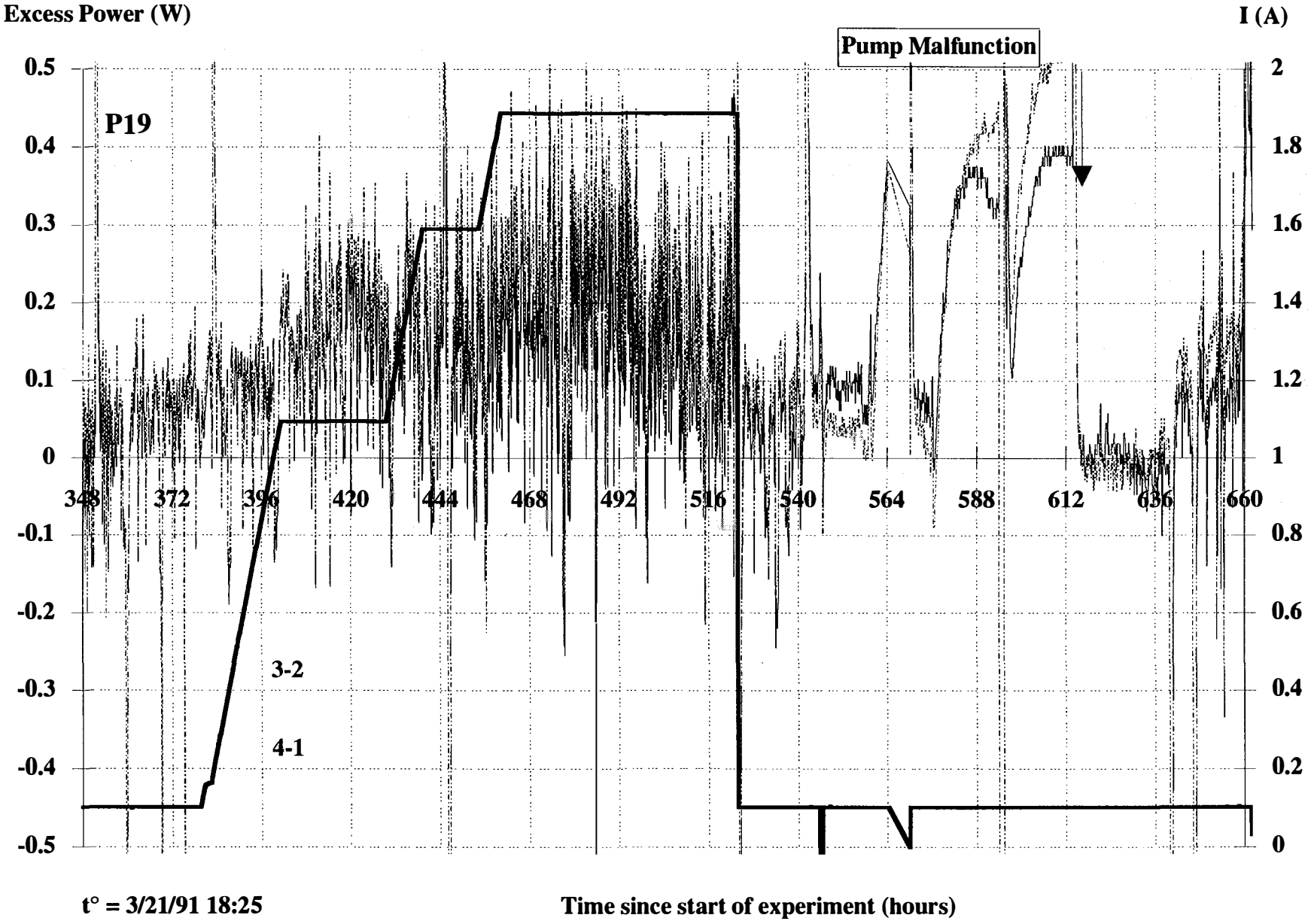
Excess Power (W)
I (A)
Pump Malfunction
P19
0.5
0.4
0.3
0.2
0.1
0
-0.1
-0.2
-0.3
-0.4
-0.5
2
1.8
1.6
1.4
1.2
1
0.8
0.6
0.4
0.2
0
348
372
396
420
444
468
492
516
540
564
588
612
636
660
3-2
4-1
t° = 3/21/91 18:25
Time since start of experiment (hours)

Figure A-3g

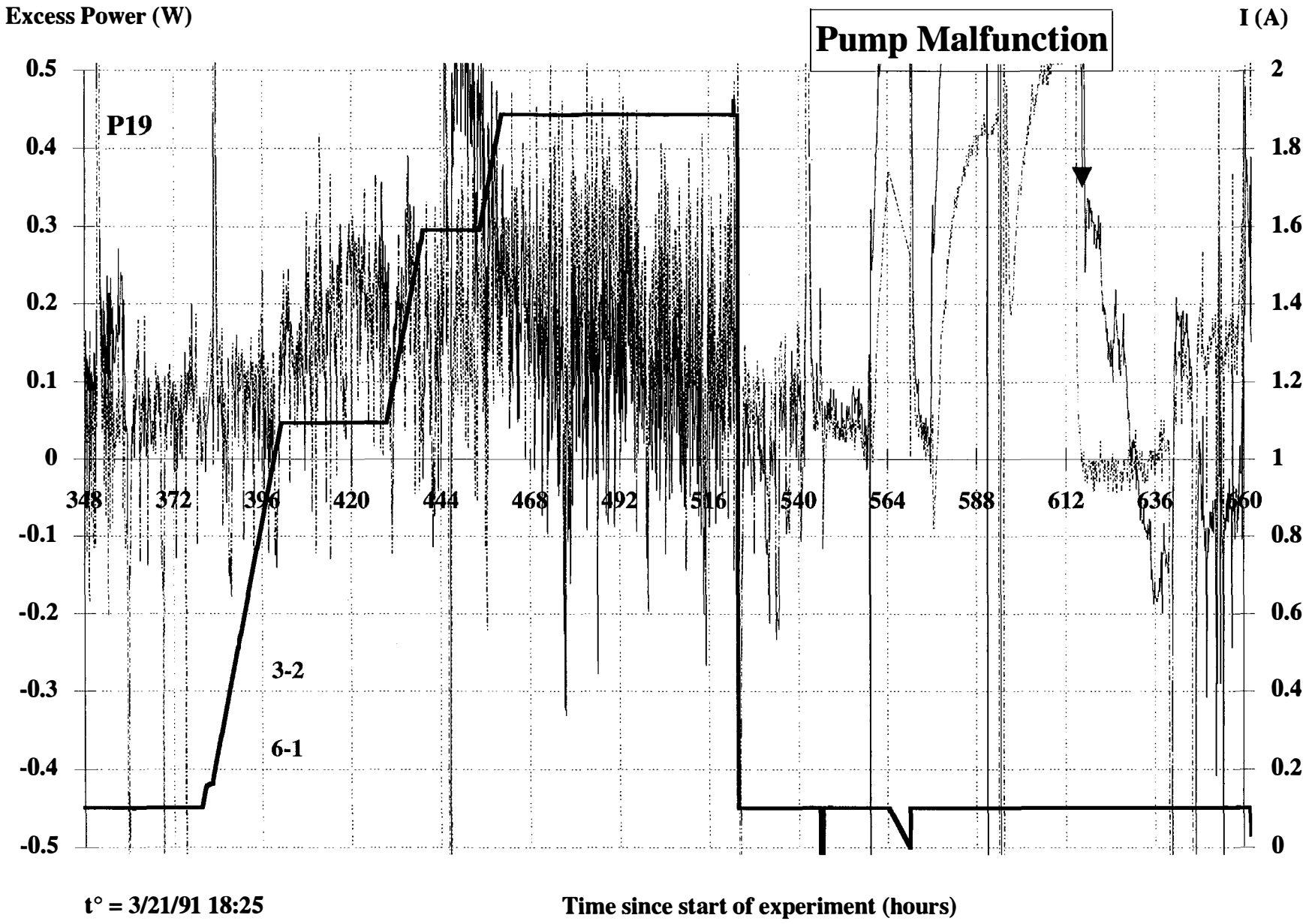
Excess Power (W)
I (A)
Pump Malfunction
P19
0.5
0.4
0.3
0.2
0.1
0
-0.1
-0.2
-0.3
-0.4
-0.5
2
1.8
1.6
1.4
1.2
1
0.8
0.6
0.4
0.2
0
348
372
396
420
444
468
492
516
540
564
588
612
636
660
3-2
6-1
t° = 3/21/91 18:25
Time since start of experiment (hours)

Figure A-3h

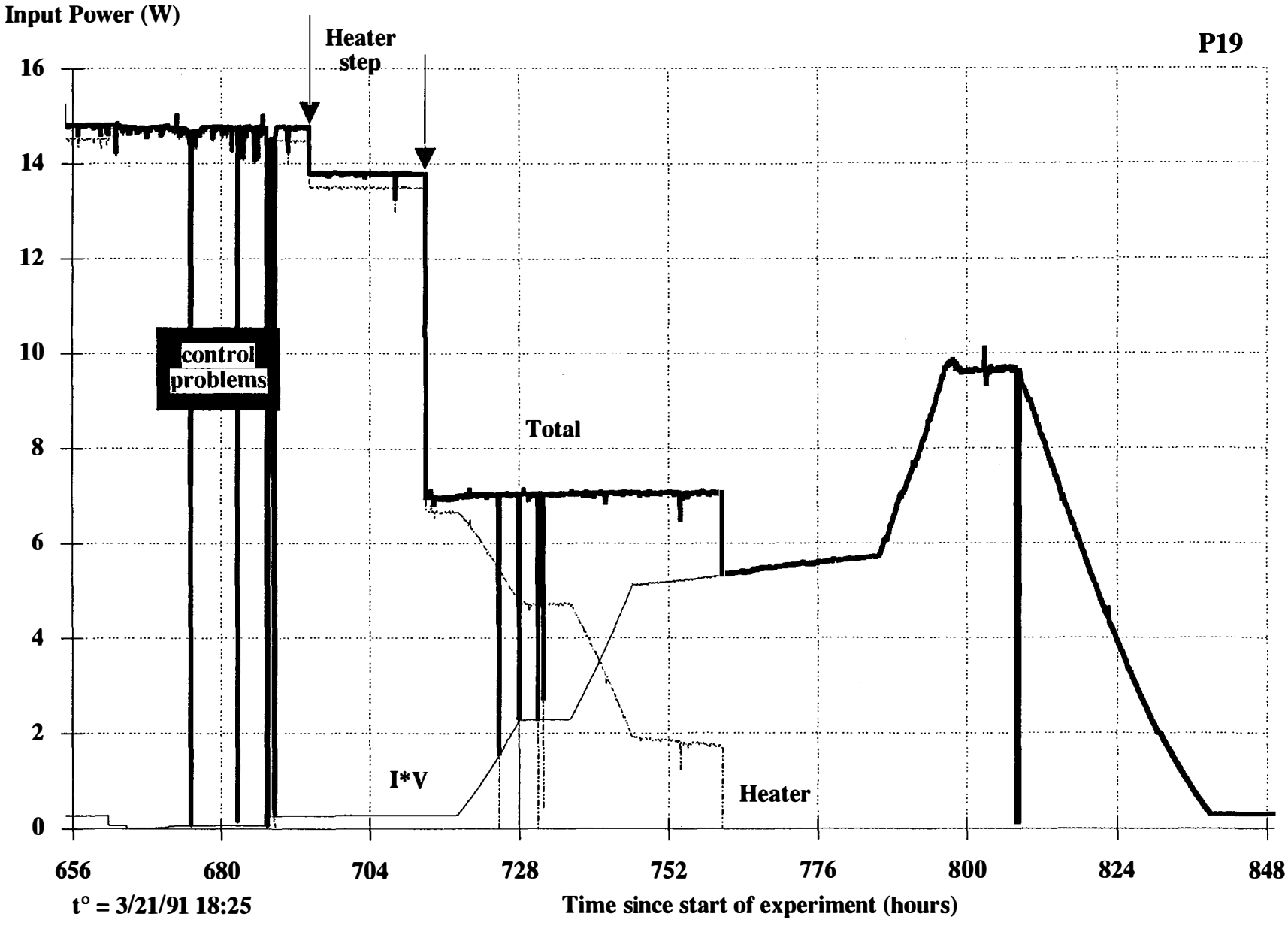
Input Power (W)
Heater step
P19
16
14
12
10
8
6
4
2
0
control problems
Total
I*V
Heater
656
680
704
728
752
776
800
824
848
t° = 3/21/91 18:25
Time since start of experiment (hours)

Fig. A-4a

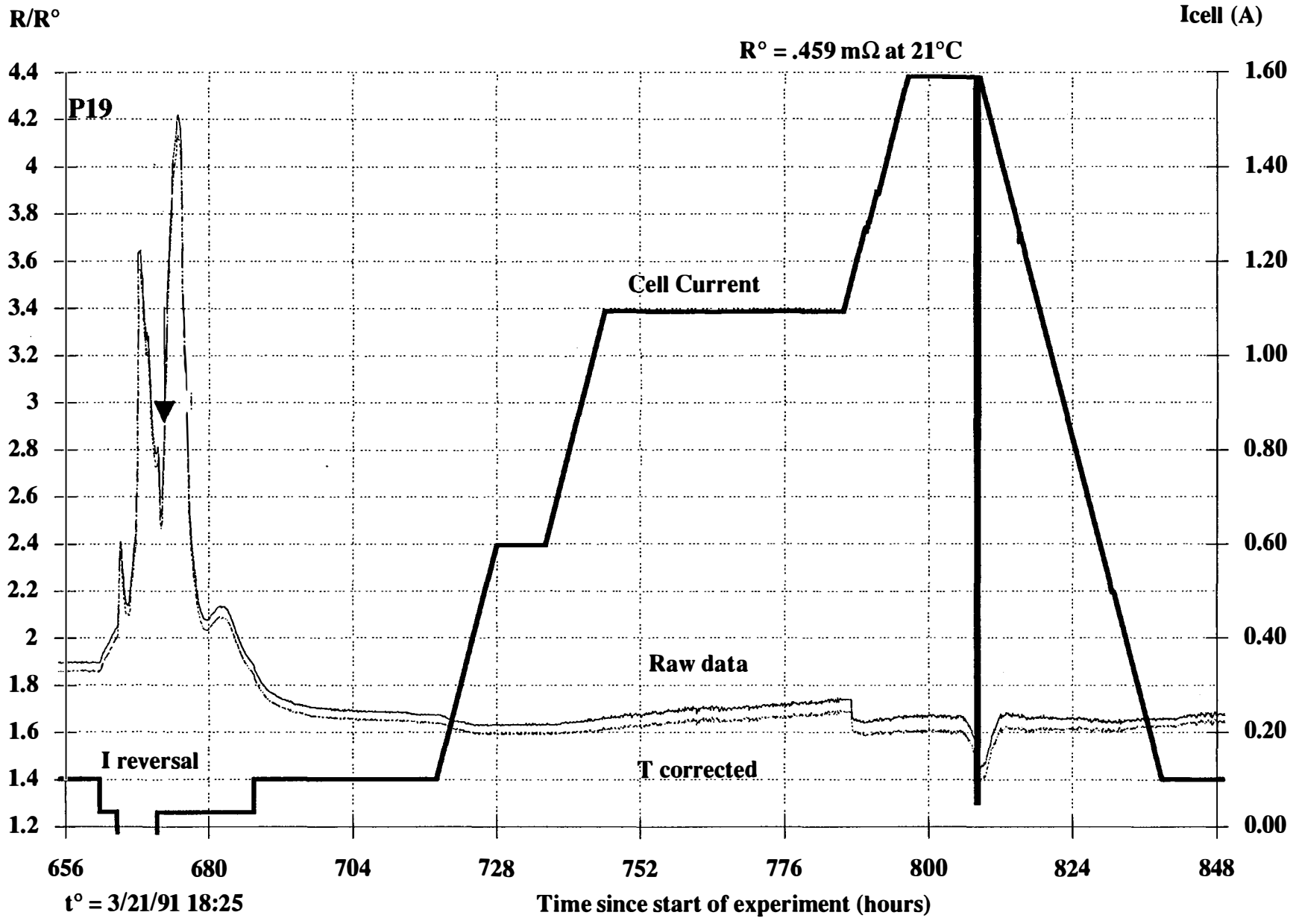
R/R°
Icell (A)
R° = .459 mΩ at 21°C
P19
Cell Current
Raw data
T corrected
I reversal
4.4
4.2
4
3.8
3.6
3.4
3.2
3
2.8
2.6
2.4
2.2
2
1.8
1.6
1.4
1.2
1.60
1.40
1.20
1.00
0.80
0.60
0.40
0.20
0.00
656
680
704
728
752
776
800
824
848
t° = 3/21/91 18:25
Time since start of experiment (hours)

Figure A-4b

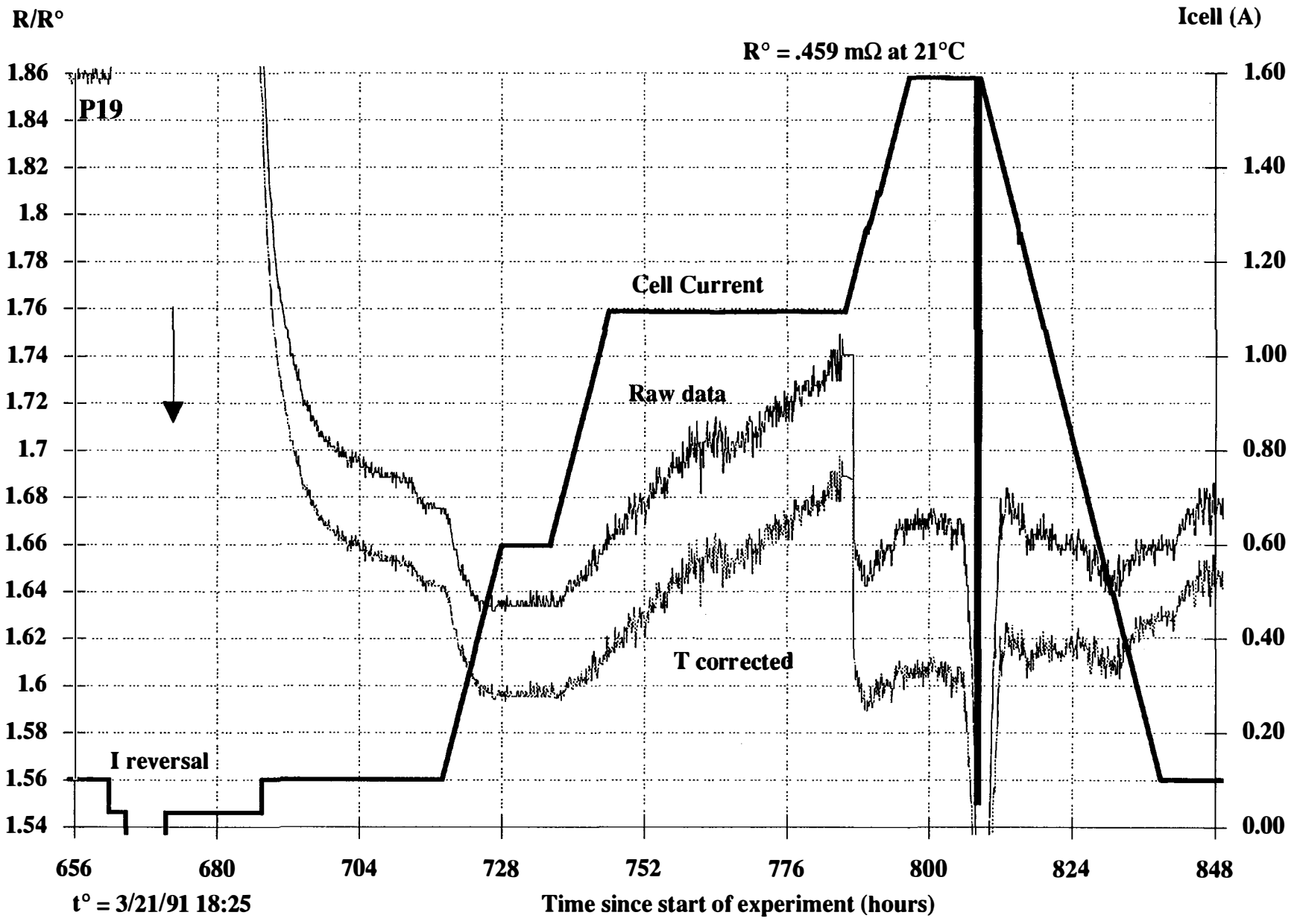

Figure A-4b expanded

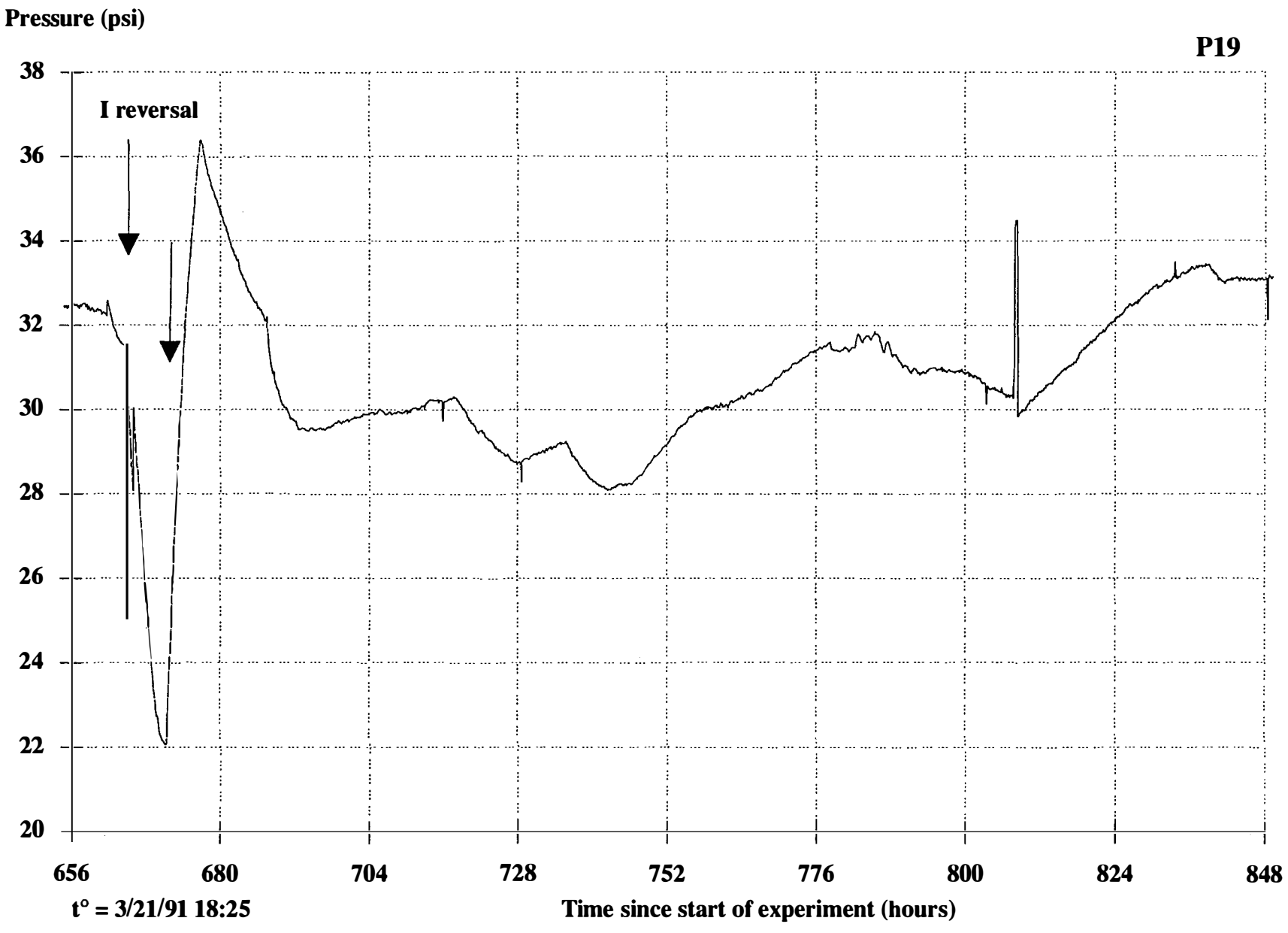
Pressure (psi)
P19
I reversal
38
36
34
32
30
28
26
24
22
20
656
680
704
728
752
776
800
824
848
t° = 3/21/91 18:25
Time since start of experiment (hours)

Figure A-4c

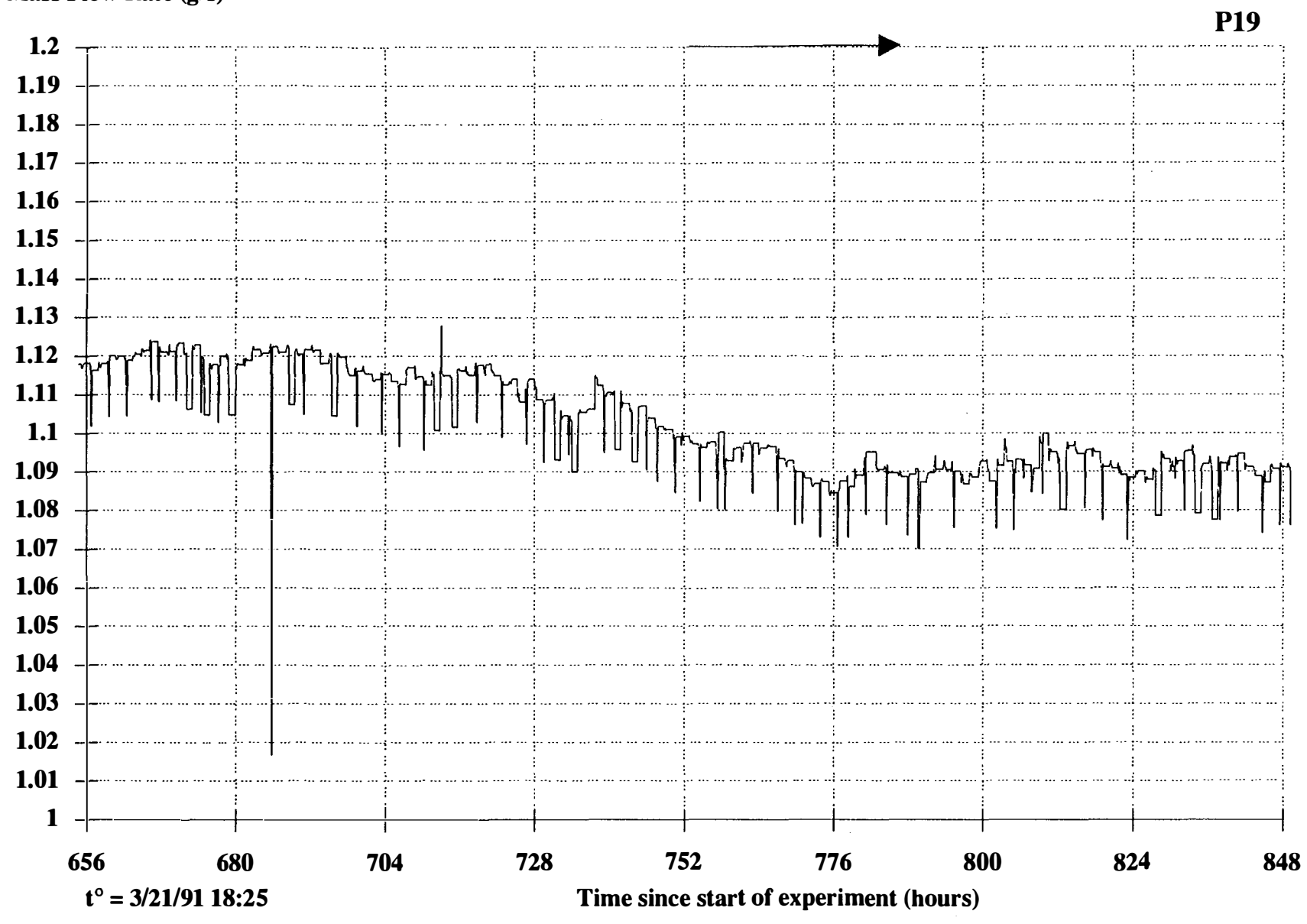
Mass Flow Rate (g/s)
P19
1.2
1.19
1.18
1.17
1.16
1.15
1.14
1.13
1.12
1.11
1.1
1.09
1.08
1.07
1.06
1.05
1.04
1.03
1.02
1.01
1
656
680
704
728
752
776
800
824
848
t° = 3/21/91 18:25
Time since start of experiment (hours)

Figure A-4d

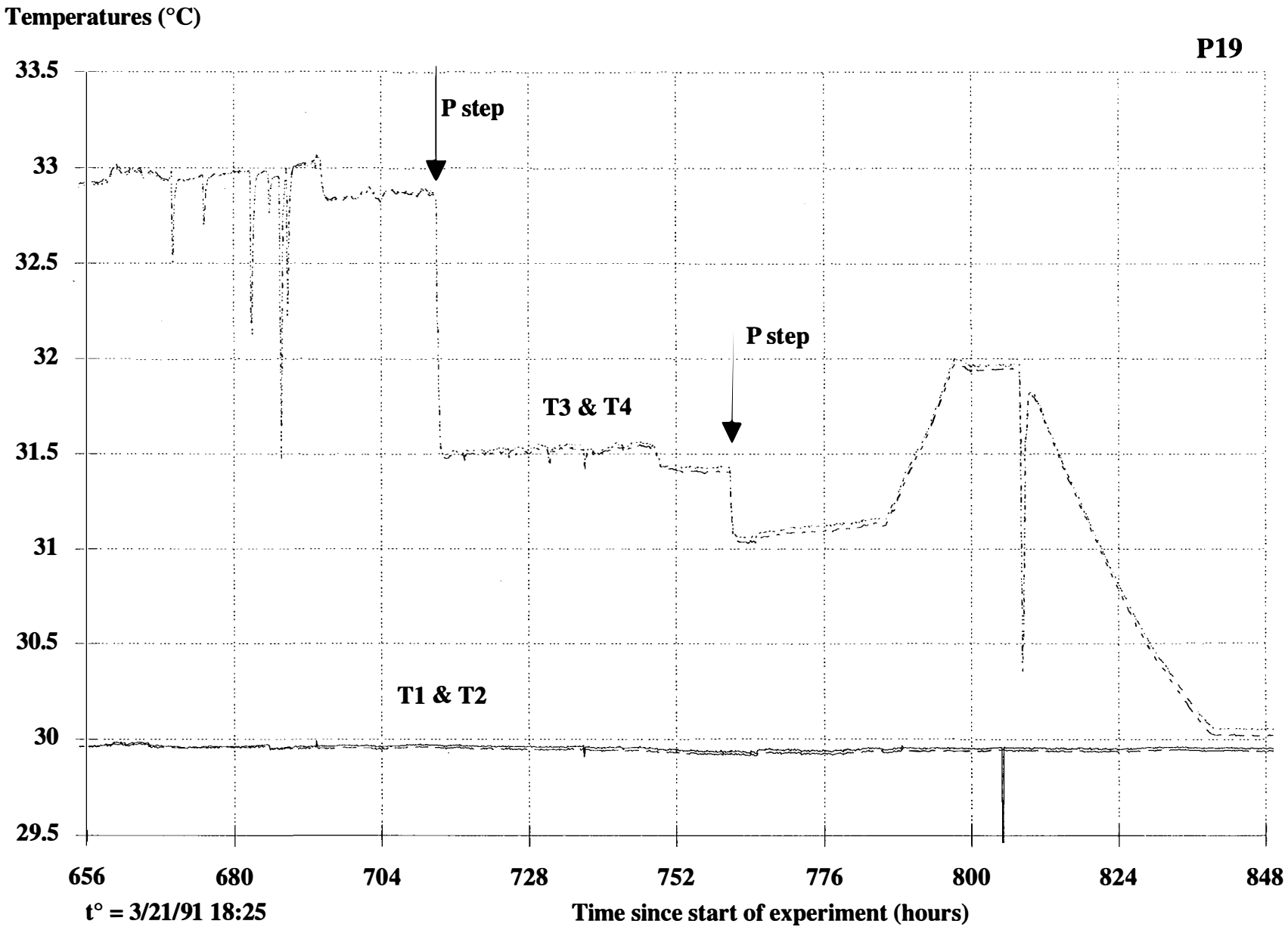
Temperatures (°C)
P19
33.5
33
32.5
32
31.5
31
30.5
30
29.5
P step
P step
T3 & T4
T1 & T2
656
680
704
728
752
776
800
824
848
t° = 3/21/91 18:25
Time since start of experiment (hours)

Figure A-4e

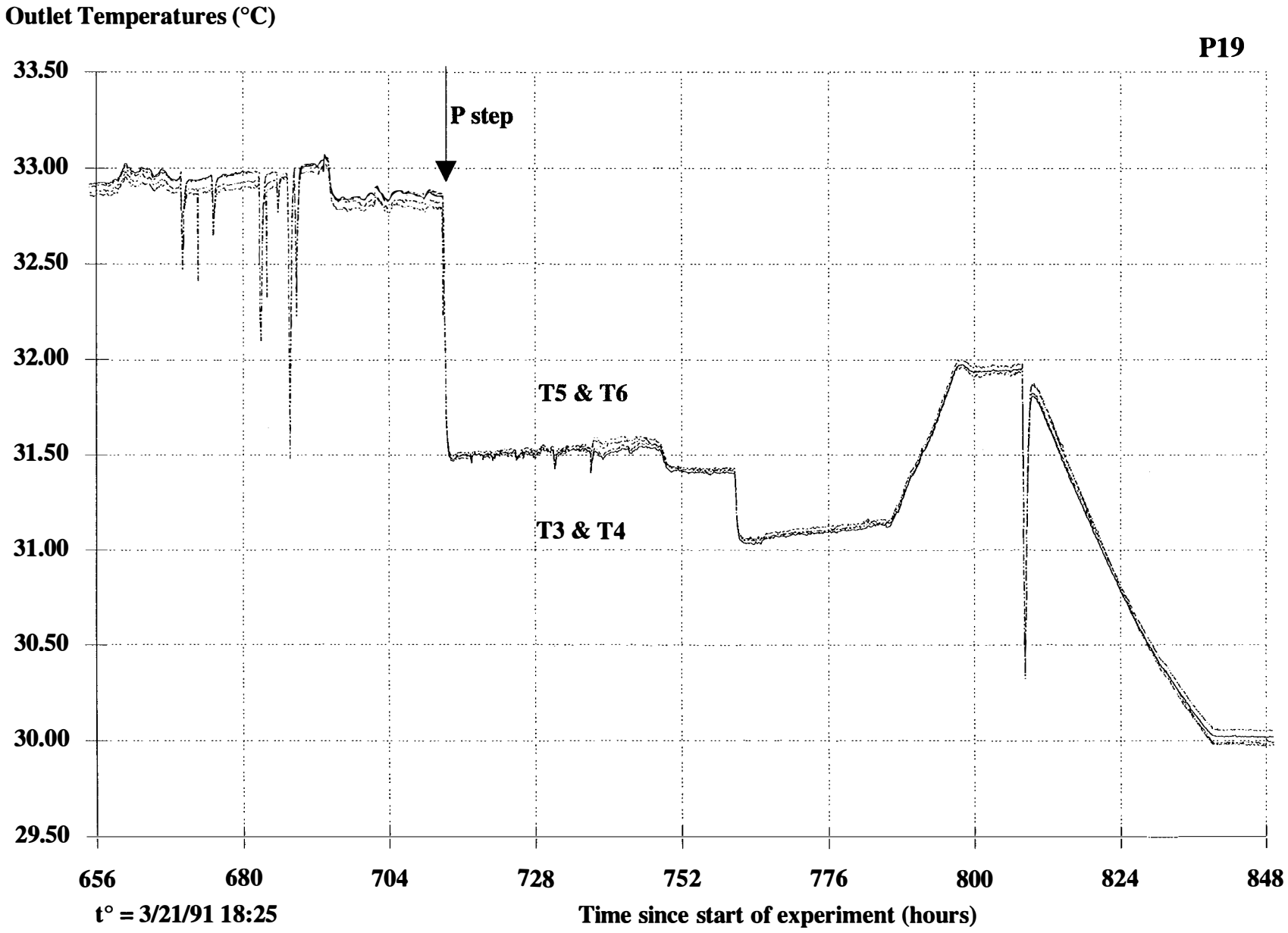
Outlet Temperatures (°C)
P19
33.50
33.00
32.50
32.00
31.50
31.00
30.50
30.00
29.50
P step
T5 & T6
T3 & T4
656
680
704
728
752
776
800
824
848
t° = 3/21/91 18:25
Time since start of experiment (hours)

Figure A-4f

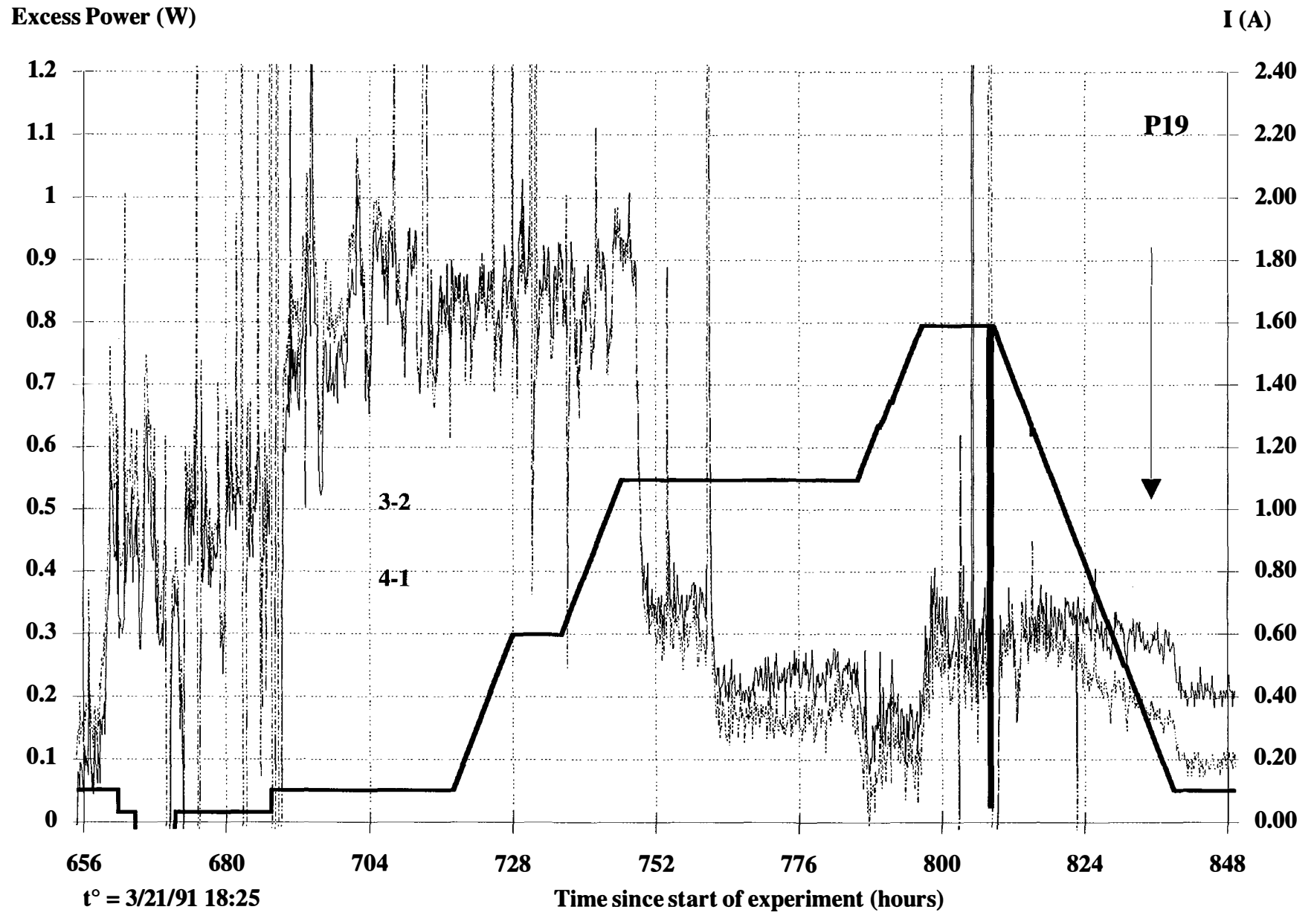
Excess Power (W)
I (A)
1.2
1.1
1
0.9
0.8
0.7
0.6
0.5
0.4
0.3
0.2
0.1
0
2.40
2.20
2.00
1.80
1.60
1.40
1.20
1.00
0.80
0.60
0.40
0.20
0.00
P19
3-2
4-1
656
680
704
728
752
776
800
824
848
t° = 3/21/91 18:25
Time since start of experiment (hours)

Figure A-4g

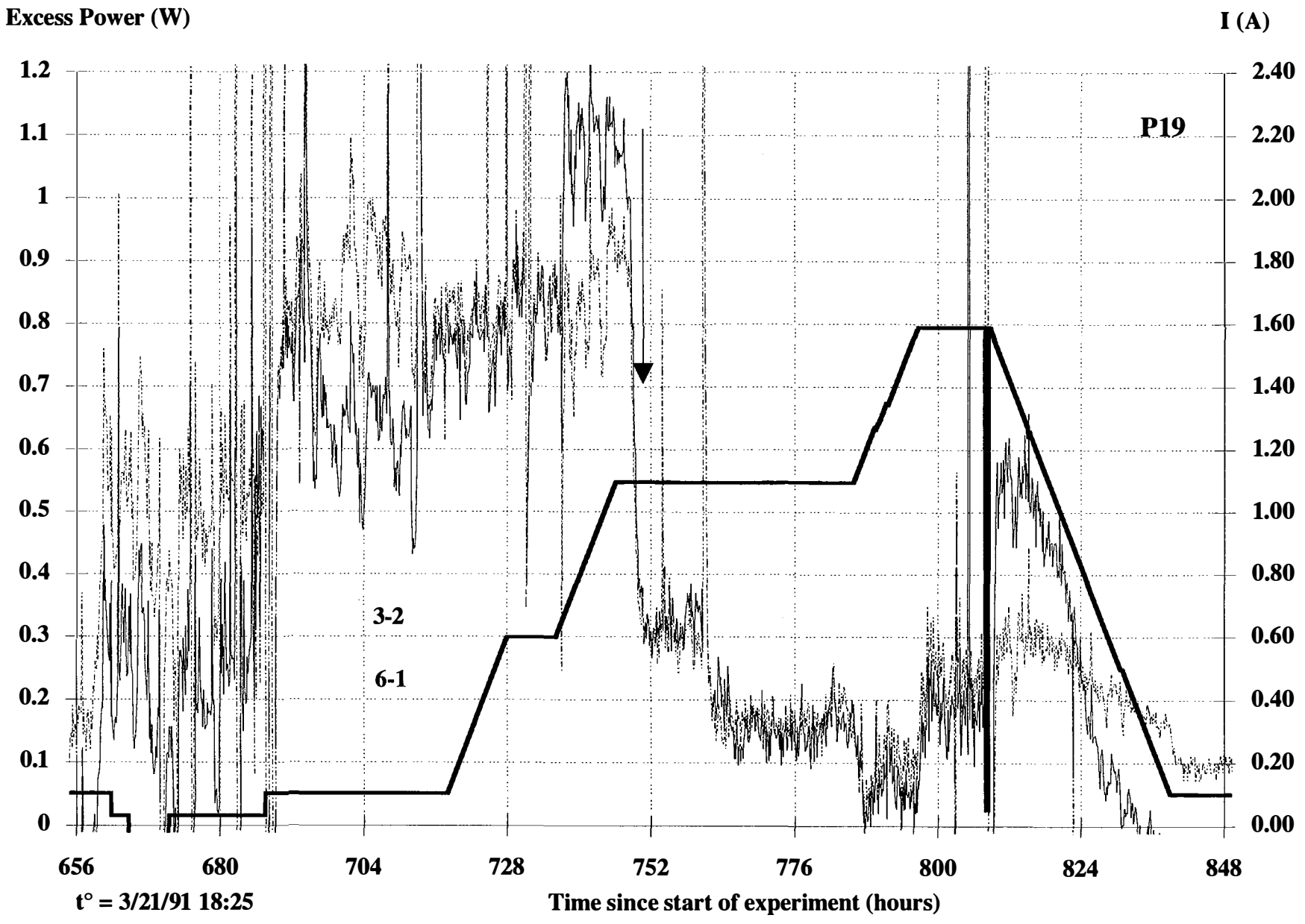
Excess Power (W)
I (A)
1.2
1.1
1
0.9
0.8
0.7
0.6
0.5
0.4
0.3
0.2
0.1
0
2.40
2.20
2.00
1.80
1.60
1.40
1.20
1.00
0.80
0.60
0.40
0.20
0.00
P19
3-2
6-1
656
680
704
728
752
776
800
824
848
t° = 3/21/91 18:25
Time since start of experiment (hours)

Figure A-4h

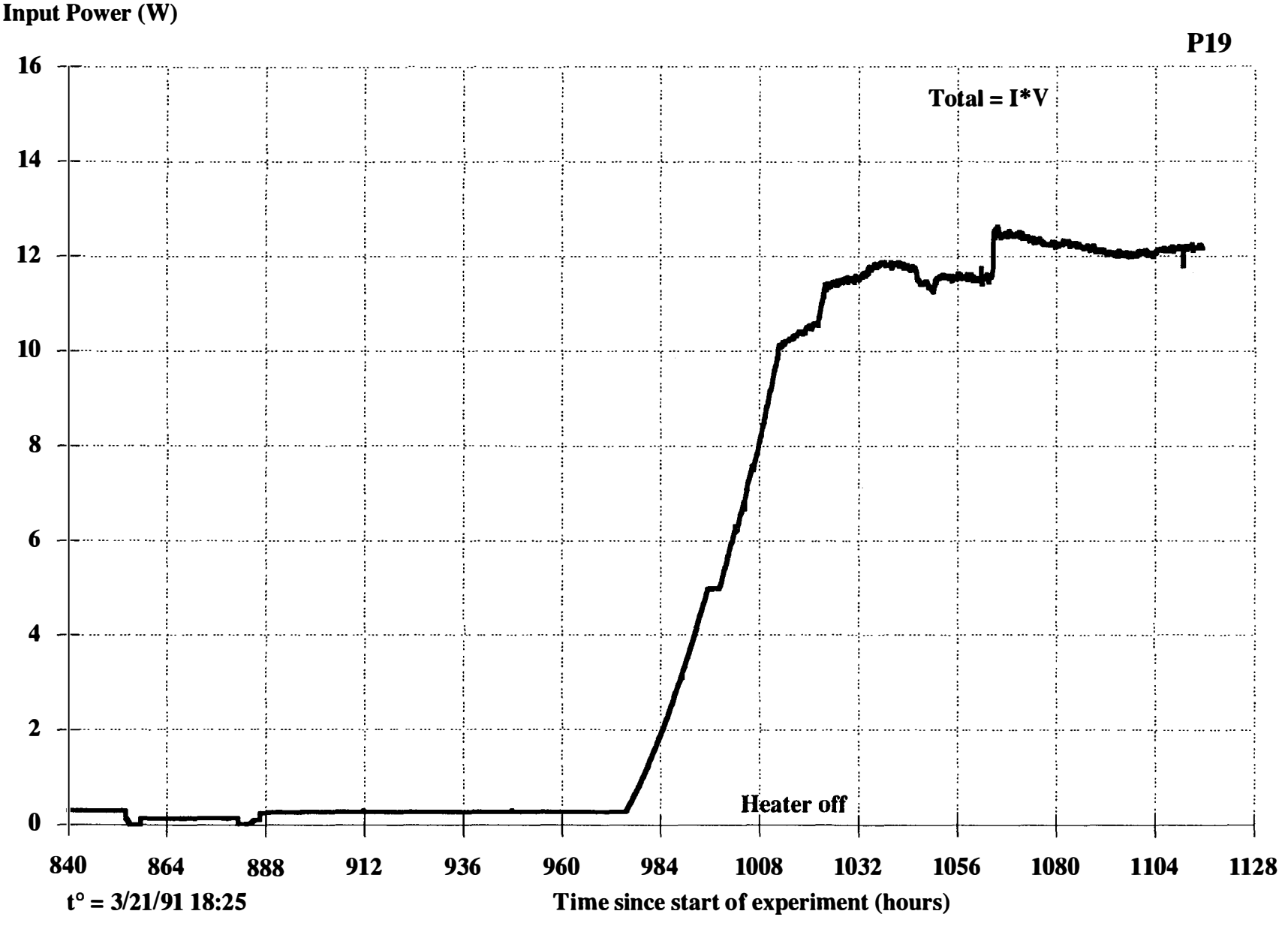
Input Power (W)
P19
Total = I*V
16
14
12
10
8
6
4
2
0
Heater off
840
864
888
912
936
960
984
1008
1032
1056
1080
1104
1128
t° = 3/21/91 18:25
Time since start of experiment (hours)

Figure A-5a

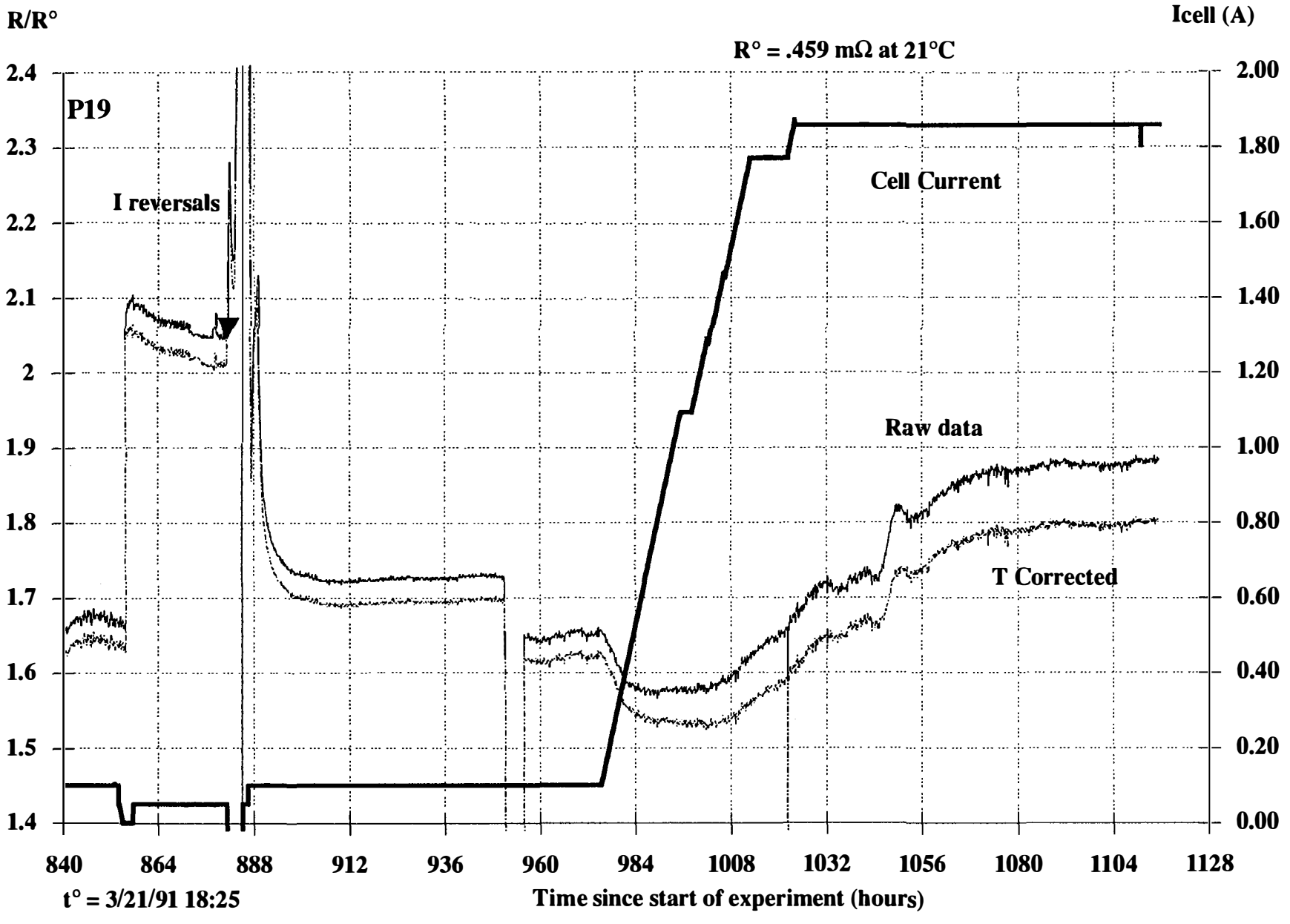
R/R°
Icell (A)
R° = .459 mΩ at 21°C
P19
I reversals
Cell Current
Raw data
T Corrected
2.4
2.3
2.2
2.1
2
1.9
1.8
1.7
1.6
1.5
1.4
2.00
1.80
1.60
1.40
1.20
1.00
0.80
0.60
0.40
0.20
0.00
840
864
888
912
936
960
984
1008
1032
1056
1080
1104
1128
t° = 3/21/91 18:25
Time since start of experiment (hours)

Figure A-5b

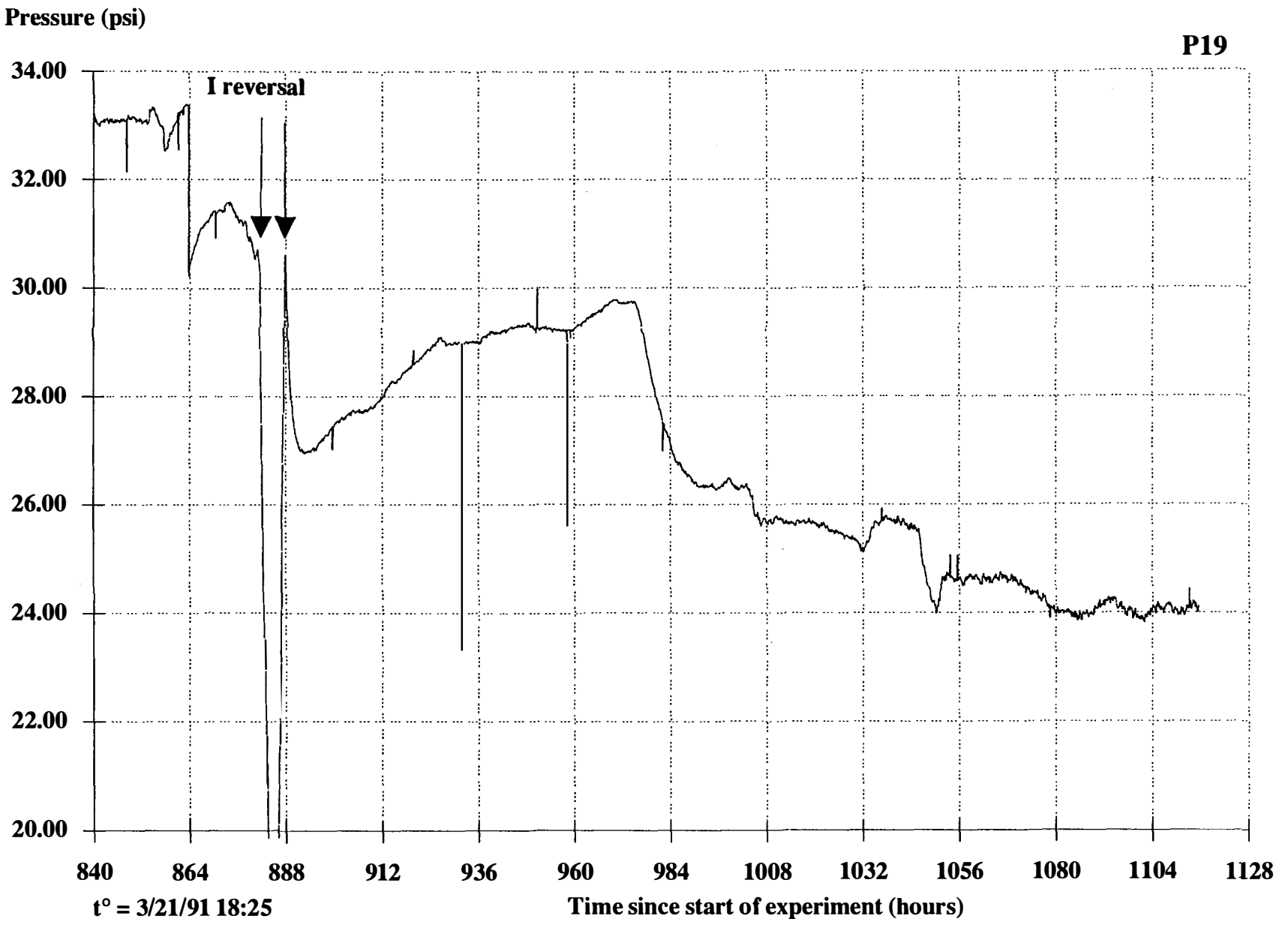
Pressure (psi)
P19
34.00
32.00
30.00
28.00
26.00
24.00
22.00
20.00
I reversal
840
864
888
912
936
960
984
1008
1032
1056
1080
1104
1128
t° = 3/21/91 18:25
Time since start of experiment (hours)

Figure A-5c

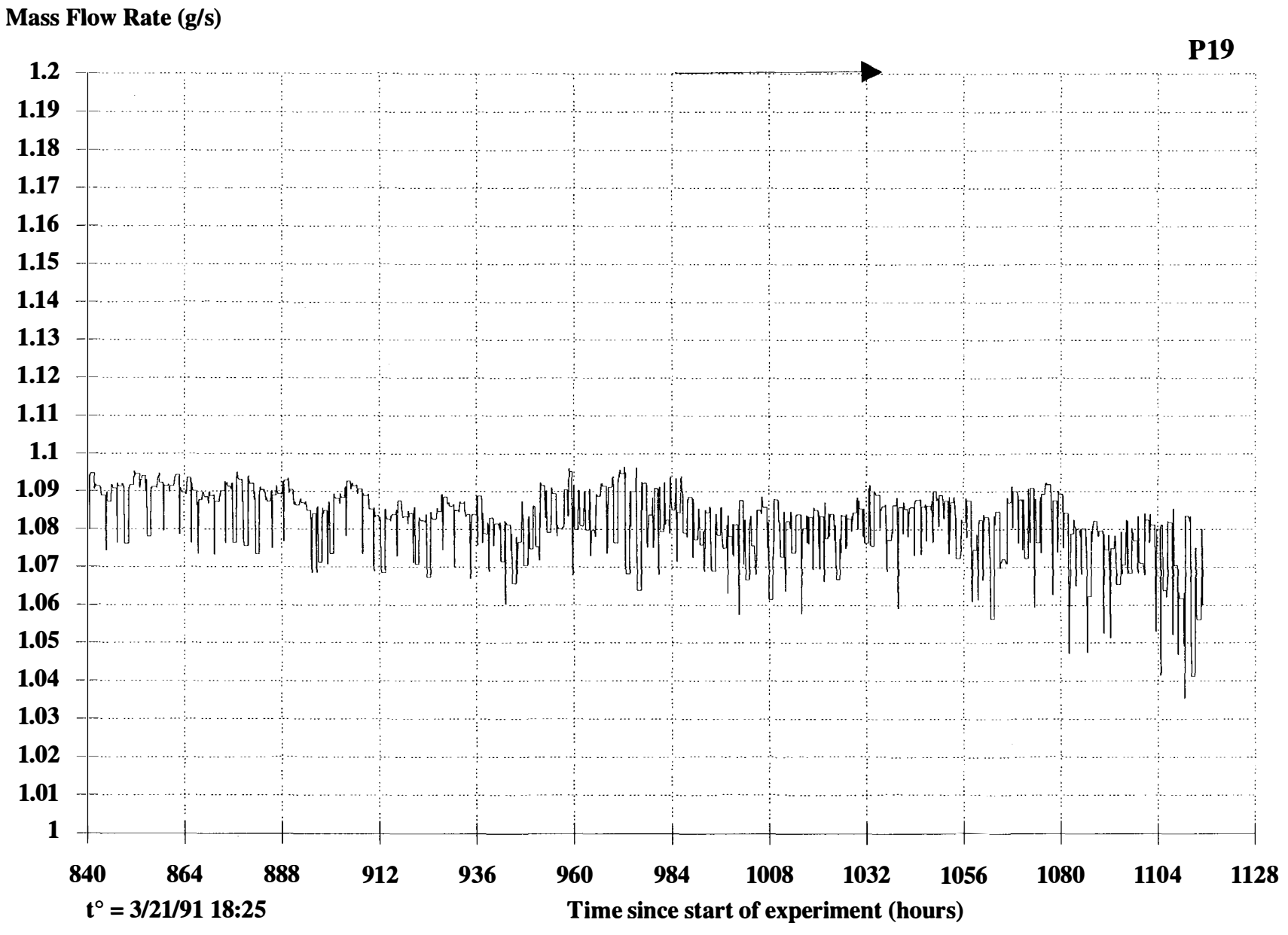
Mass Flow Rate (g/s)
P19
1.2
1.19
1.18
1.17
1.16
1.15
1.14
1.13
1.12
1.11
1.1
1.09
1.08
1.07
1.06
1.05
1.04
1.03
1.02
1.01
1
840
864
888
912
936
960
984
1008
1032
1056
1080
1104
1128
t° = 3/21/91 18:25
Time since start of experiment (hours)

Figure A-5d

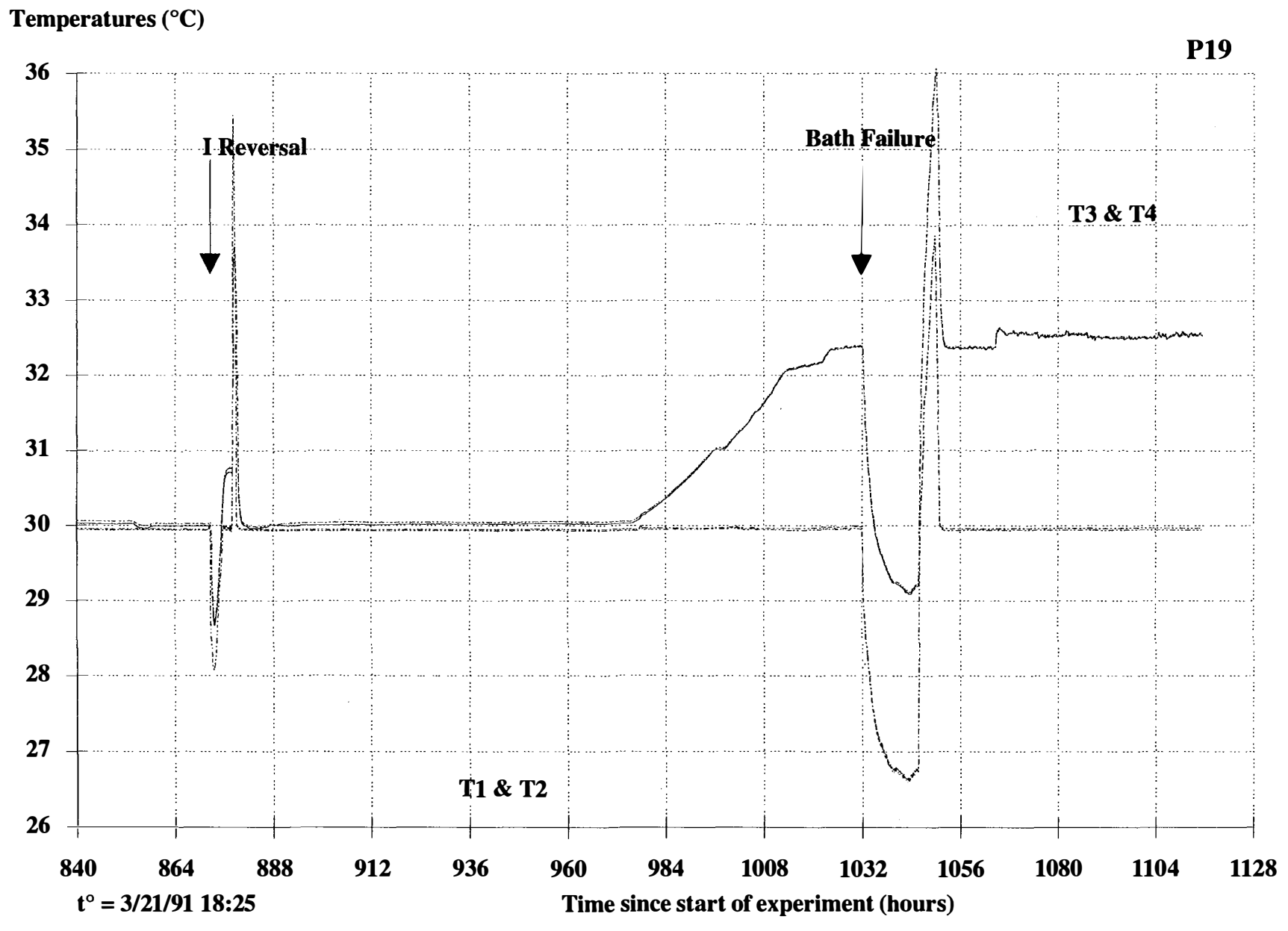
Temperatures (°C)
P19
36
35
34
33
32
31
30
29
28
27
26
I Reversal
Bath Failure
T3 & T4
T1 & T2
840
864
888
912
936
960
984
1008
1032
1056
1080
1104
1128
t° = 3/21/91 18:25
Time since start of experiment (hours)

Figure A-5e

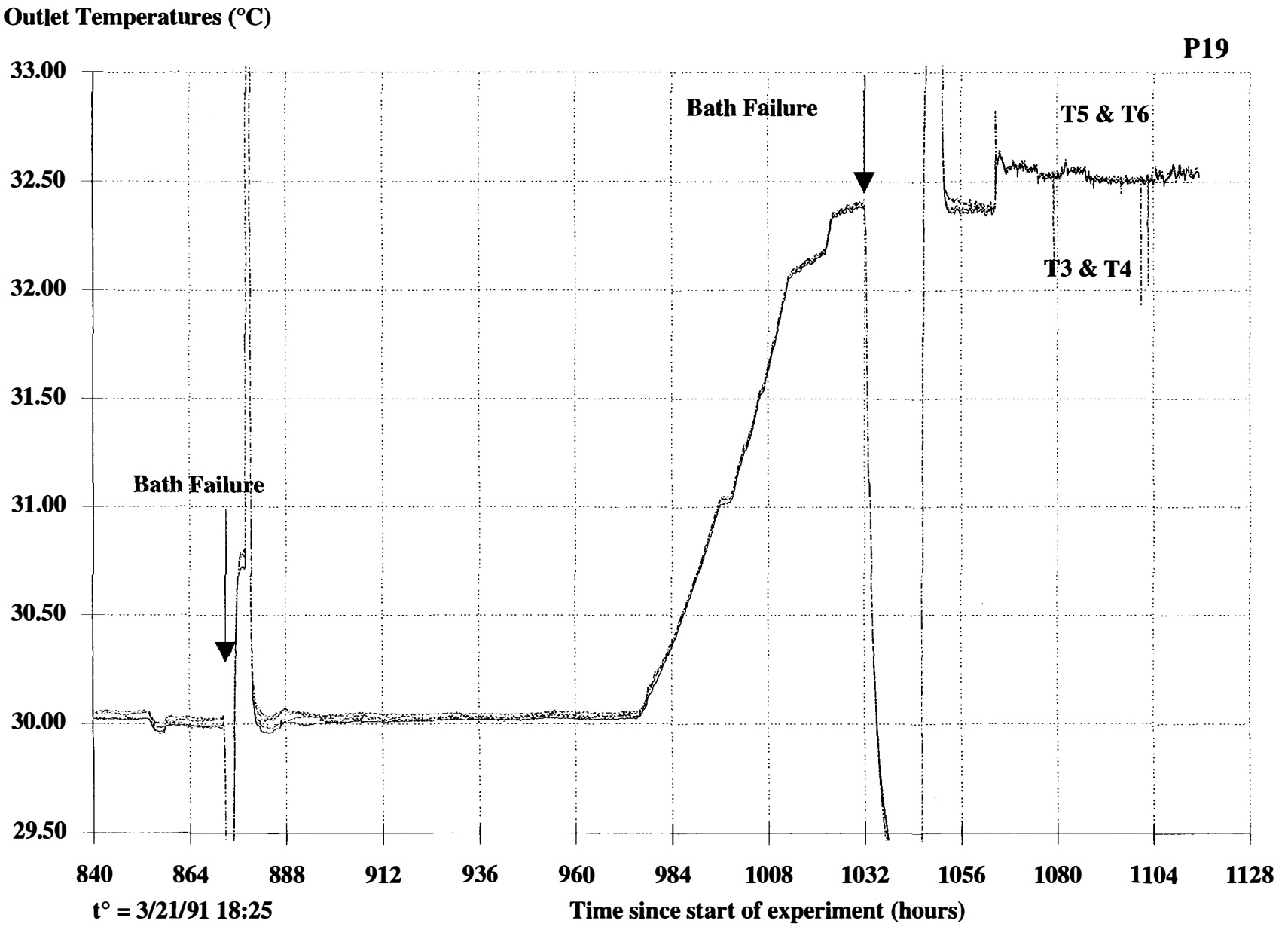
Outlet Temperatures (°C)
P19
33.00
32.50
32.00
31.50
31.00
30.50
30.00
29.50
Bath Failure
Bath Failure
T5 & T6
T3 & T4
840
864
888
912
936
960
984
1008
1032
1056
1080
1104
1128
t° = 3/21/91 18:25
Time since start of experiment (hours)

Figure A-5f

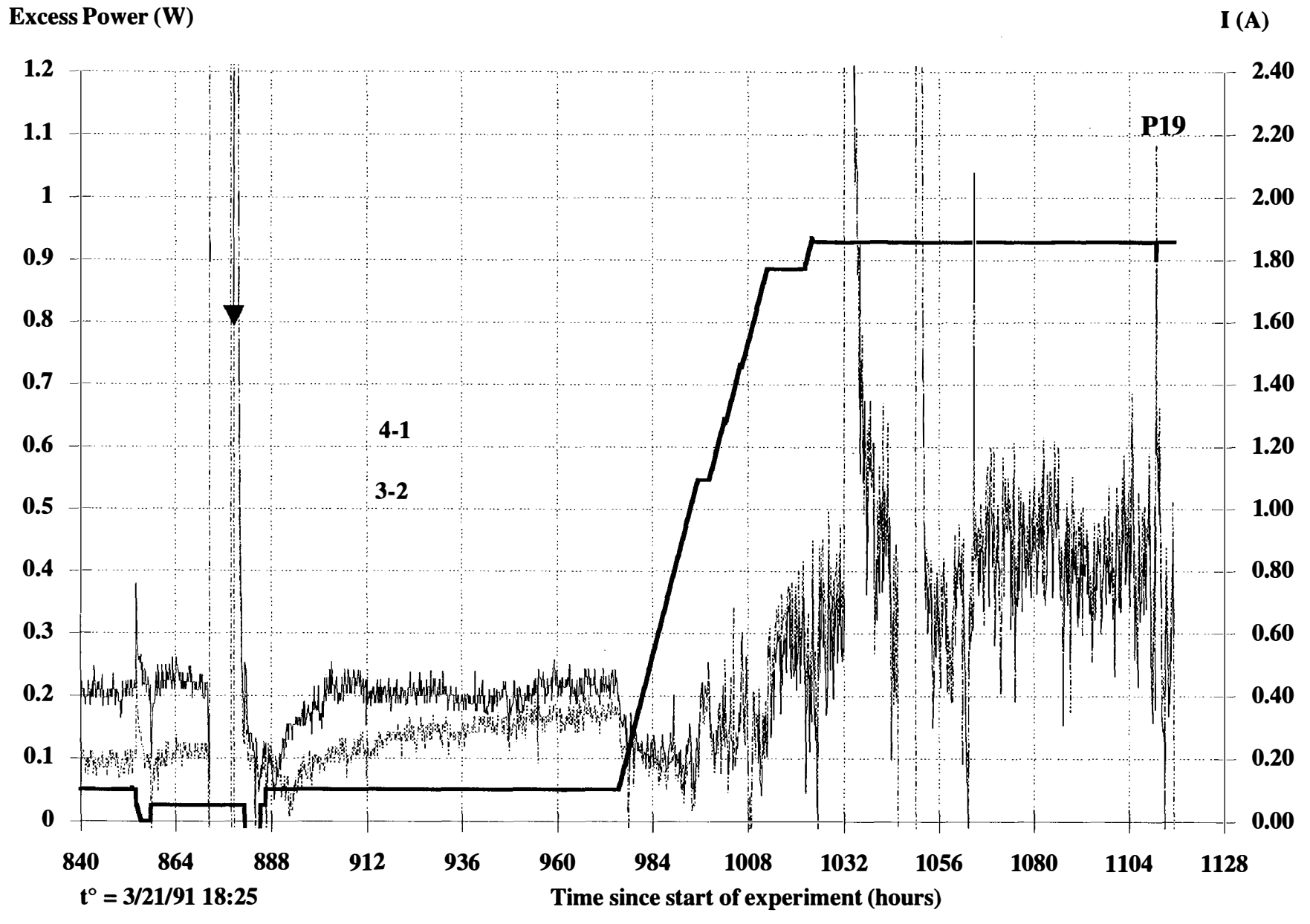
Excess Power (W)
I (A)
1.2
1.1
1
0.9
0.8
0.7
0.6
0.5
0.4
0.3
0.2
0.1
0
2.40
2.20
2.00
1.80
1.60
1.40
1.20
1.00
0.80
0.60
0.40
0.20
0.00
P19
4-1
3-2
840
864
888
912
936
960
984
1008
1032
1056
1080
1104
1128
t° = 3/21/91 18:25
Time since start of experiment (hours)

Figure A-5g

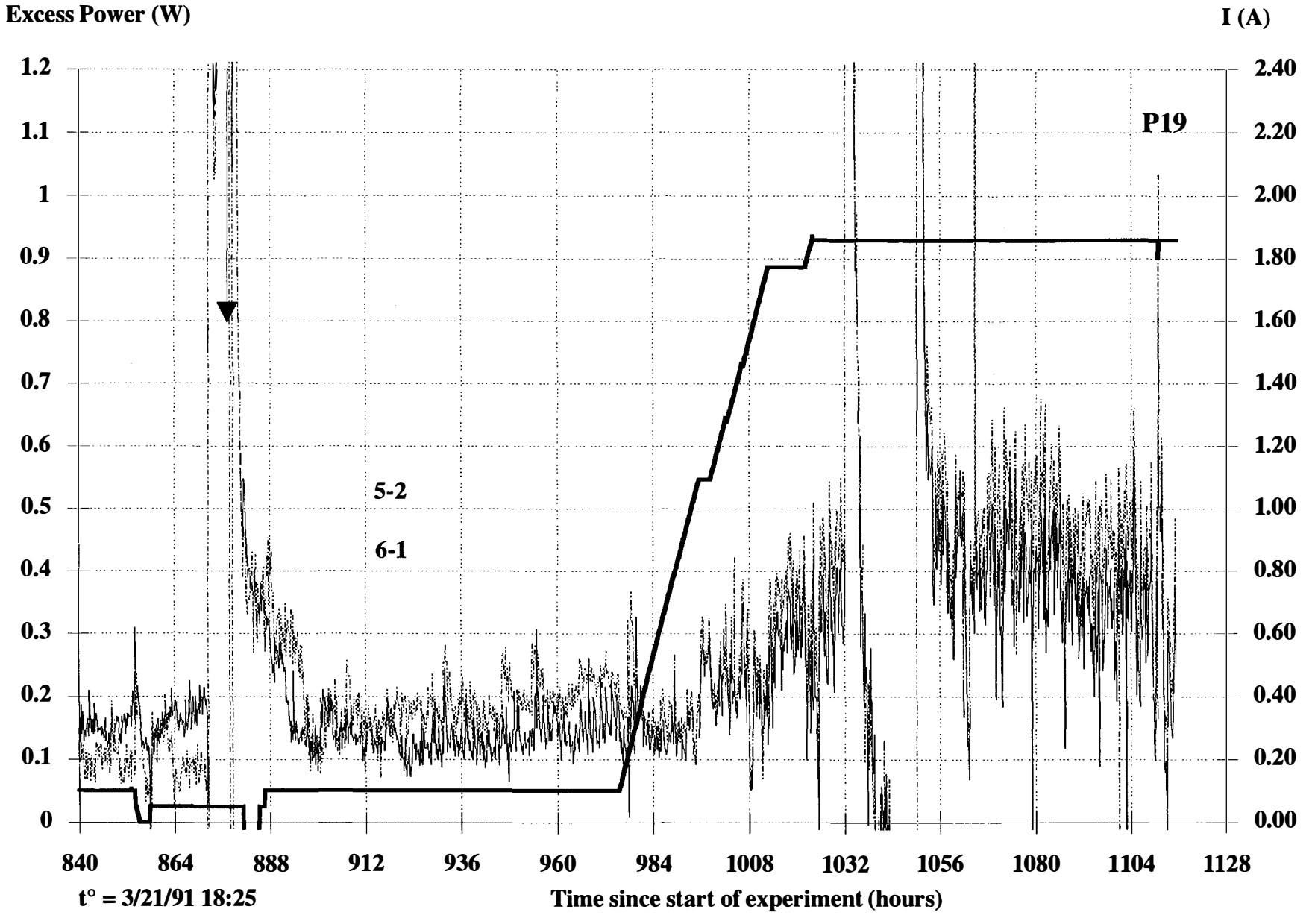
Excess Power (W)
I (A)
1.2
1.1
1
0.9
0.8
0.7
0.6
0.5
0.4
0.3
0.2
0.1
0
2.40
2.20
2.00
1.80
1.60
1.40
1.20
1.00
0.80
0.60
0.40
0.20
0.00
P19
5-2
6-1
840
864
888
912
936
960
984
1008
1032
1056
1080
1104
1128
t° = 3/21/91 18:25
Time since start of experiment (hours)

Figure A-5h

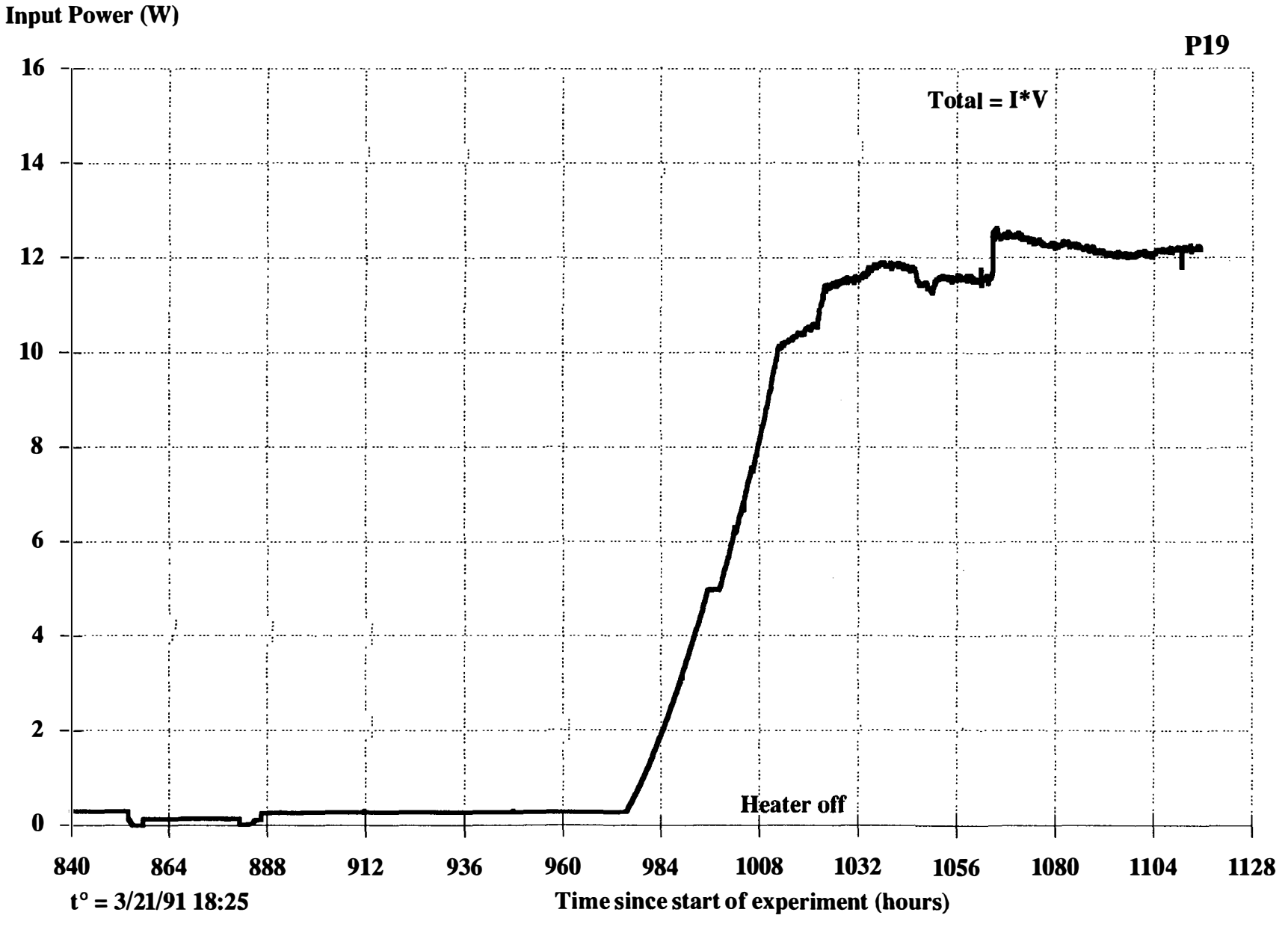
Input Power (W)
P19
Total = I*V
16
14
12
10
8
6
4
2
0
Heater off
840
864
888
912
936
960
984
1008
1032
1056
1080
1104
1128
t° = 3/21/91 18:25
Time since start of experiment (hours)

Figure A-6a

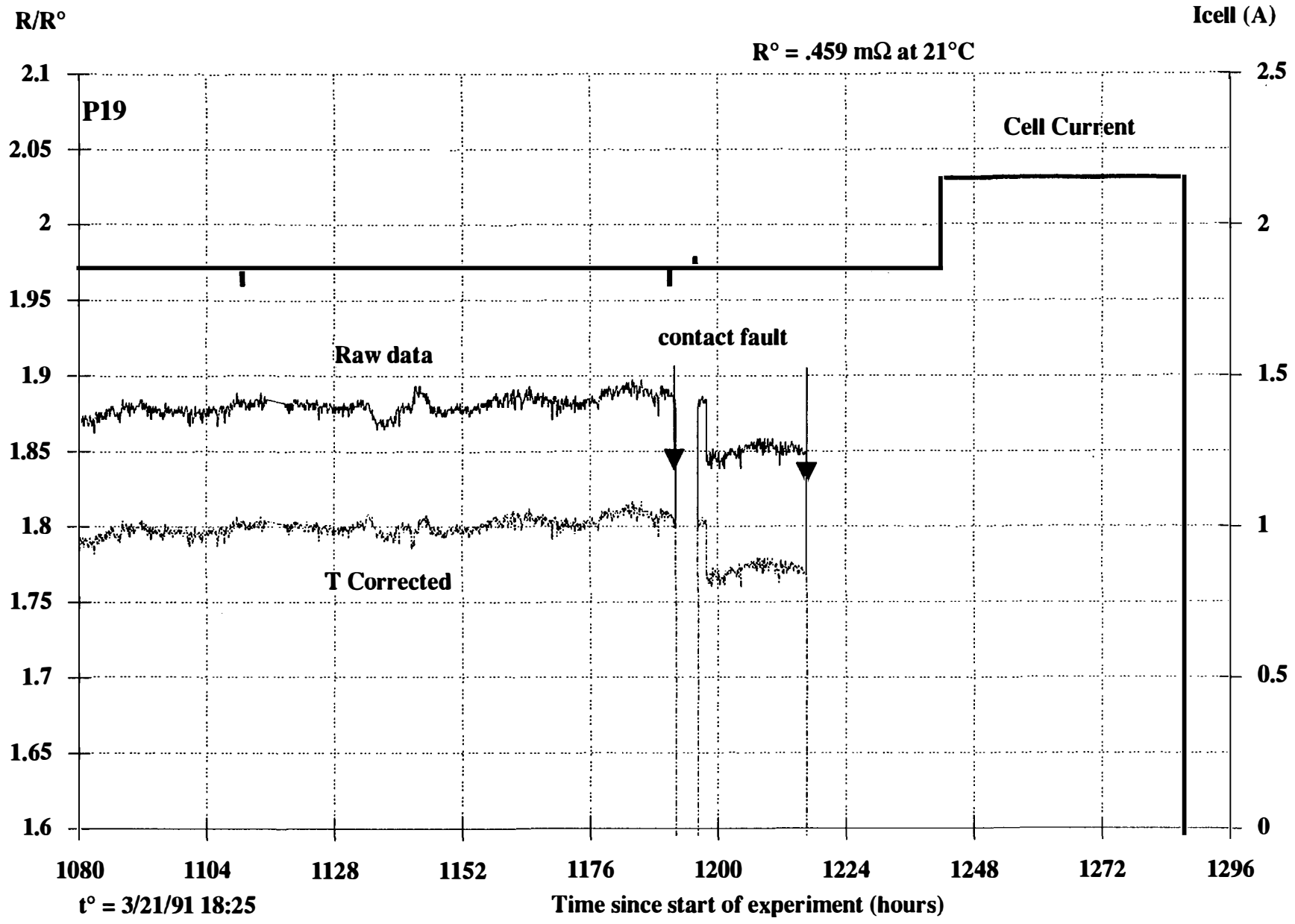
R/R°
Icell (A)
R° = .459 mΩ at 21°C
P19
Cell Current
Raw data
contact fault
T Corrected
2.1
2.05
2
1.95
1.9
1.85
1.8
1.75
1.7
1.65
1.6
2.5
2
1.5
1
0.5
0
1080
1104
1128
1152
1176
1200
1224
1248
1272
1296
t° = 3/21/91 18:25
Time since start of experiment (hours)

Figure A-6b

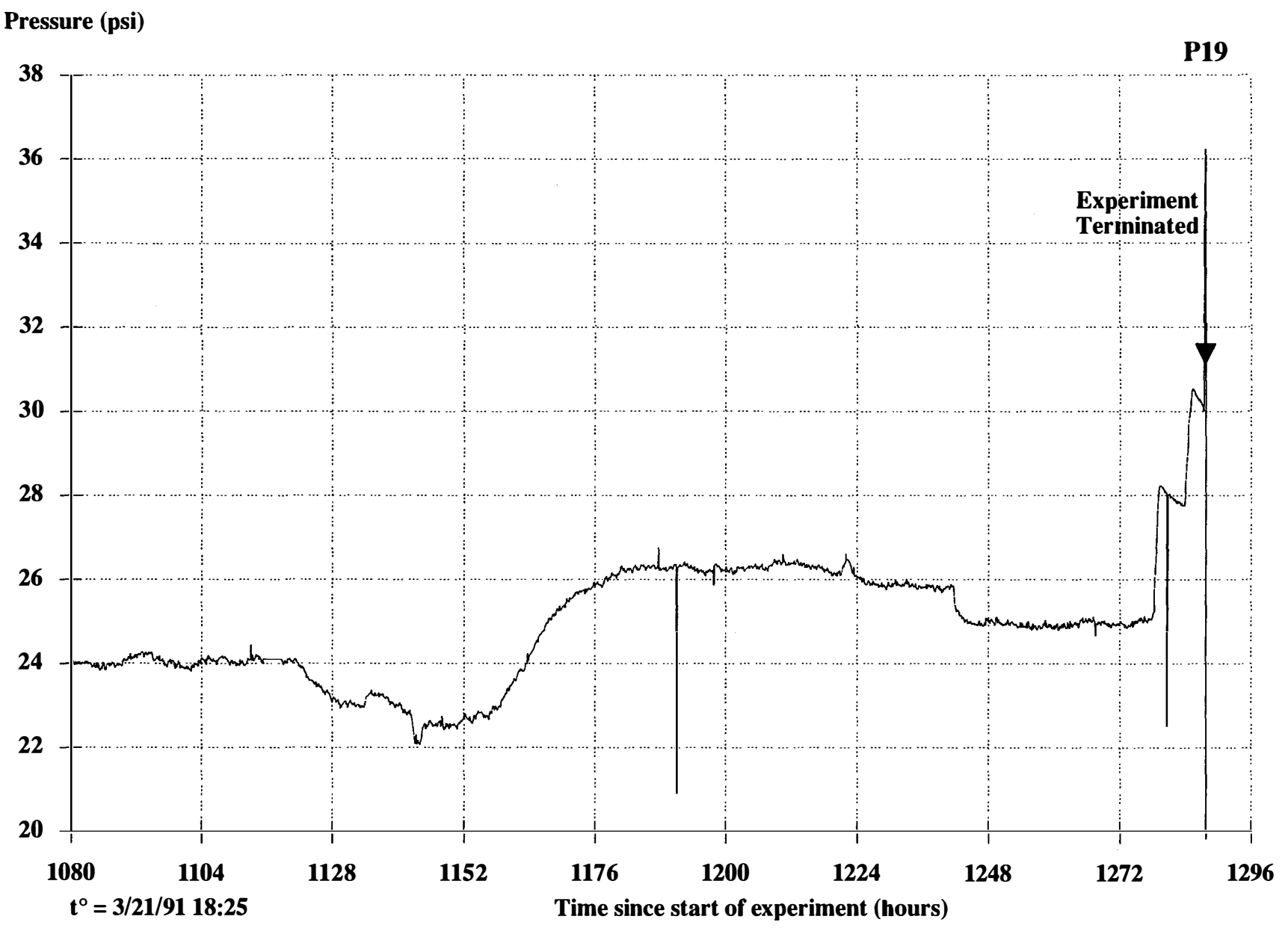
Pressure (psi)
P19
38
36
34
32
30
28
26
24
22
20
Experiment
Terminated
1080
1104
1128
1152
1176
1200
1224
1248
1272
1296
t° = 3/21/91 18:25
Time since start of experiment (hours)

Figure A-6c

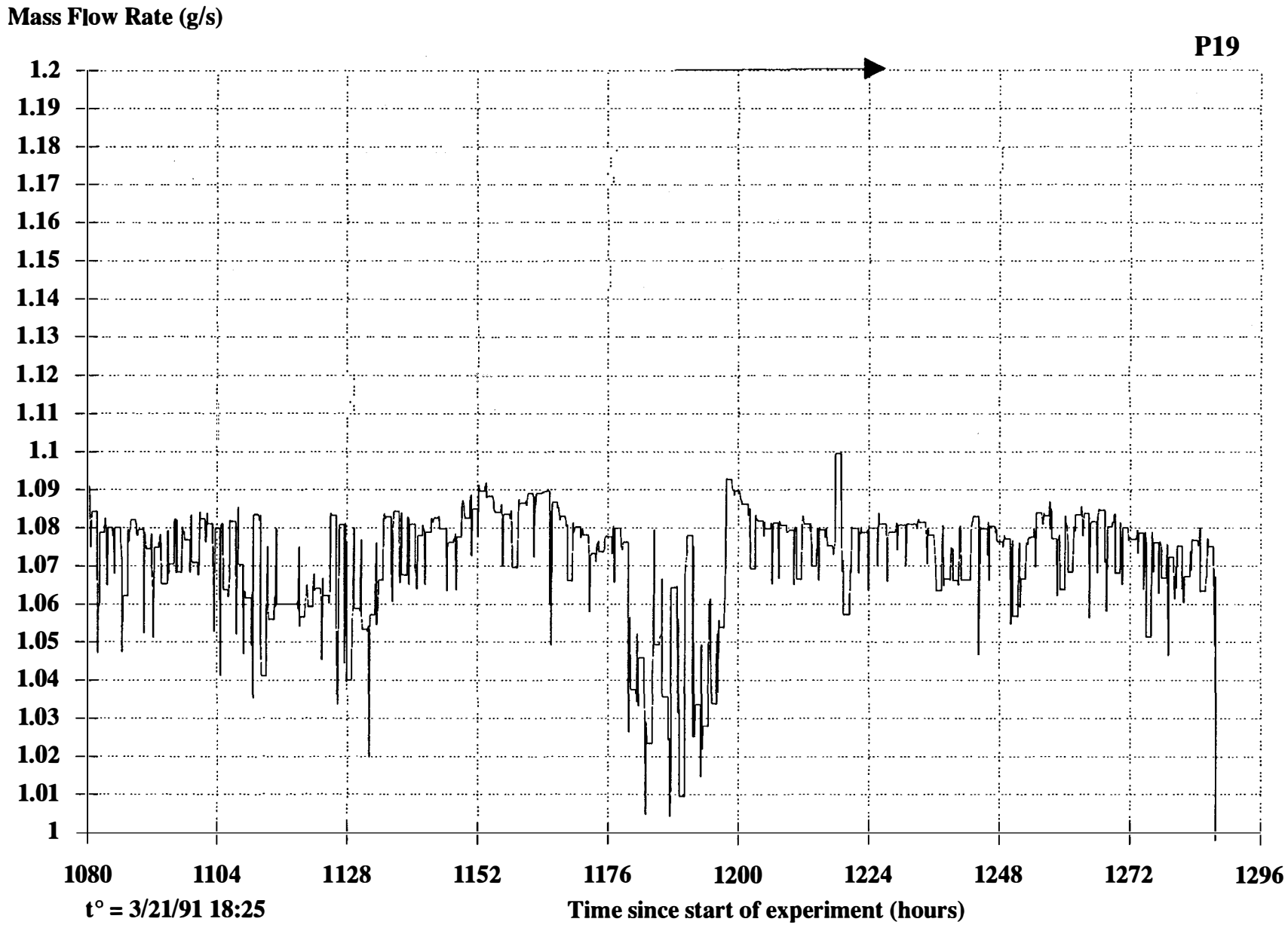
Mass Flow Rate (g/s)
P19
1.2
1.19
1.18
1.17
1.16
1.15
1.14
1.13
1.12
1.11
1.1
1.09
1.08
1.07
1.06
1.05
1.04
1.03
1.02
1.01
1
1080
1104
1128
1152
1176
1200
1224
1248
1272
1296
t° = 3/21/91 18:25
Time since start of experiment (hours)

Figure A-6d

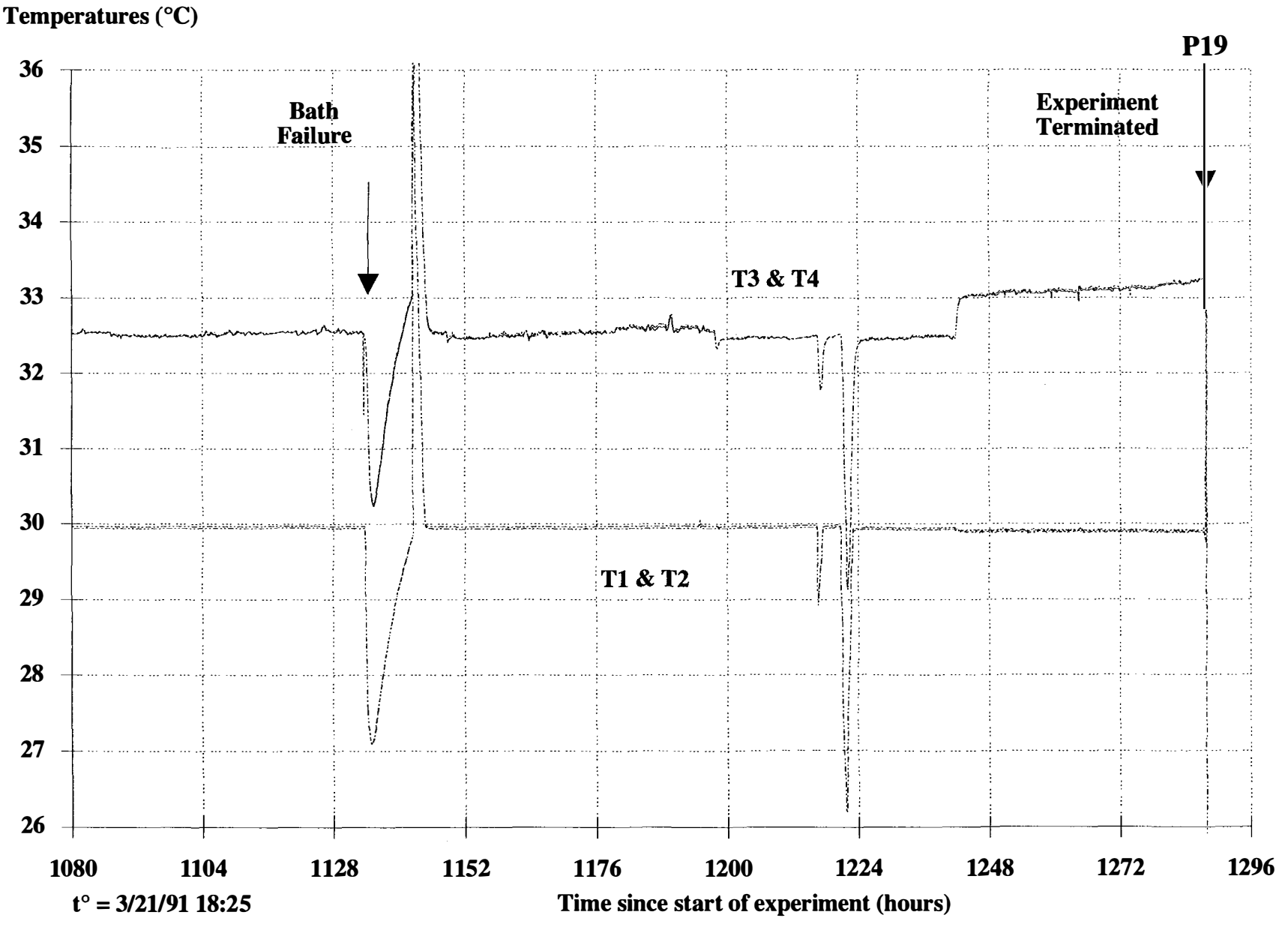
Temperatures (°C)
P19
Bath Failure
Experiment Terminated
T3 & T4
T1 & T2
36
35
34
33
32
31
30
29
28
27
26
1080
1104
1128
1152
1176
1200
1224
1248
1272
1296
t° = 3/21/91 18:25
Time since start of experiment (hours)

Figure A-6e

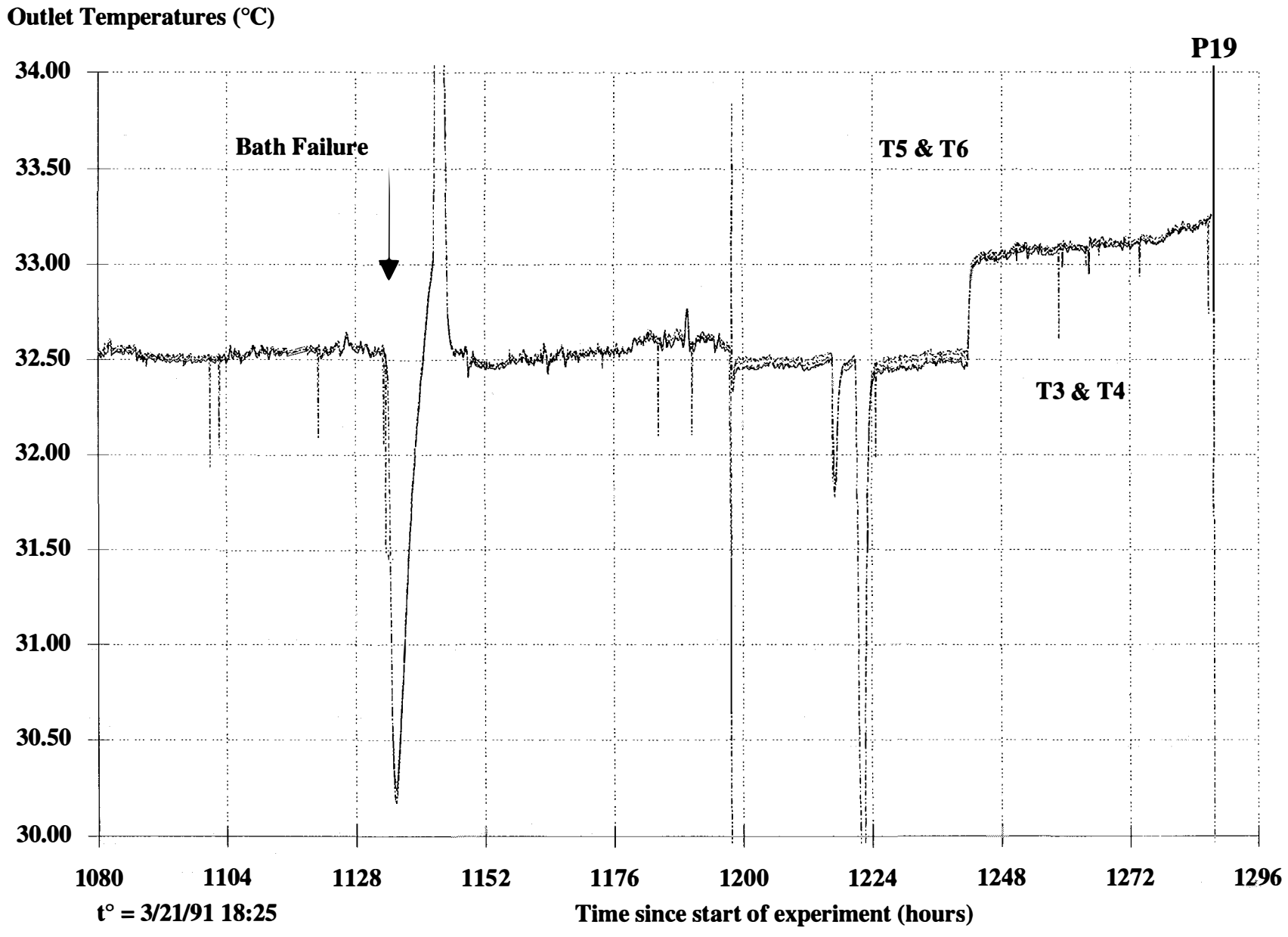
Outlet Temperatures (°C)
P19
34.00
33.50
33.00
32.50
32.00
31.50
31.00
30.50
30.00
Bath Failure
T5 & T6
T3 & T4
1080
1104
1128
1152
1176
1200
1224
1248
1272
1296
t° = 3/21/91 18:25
Time since start of experiment (hours)

Figure A-6f

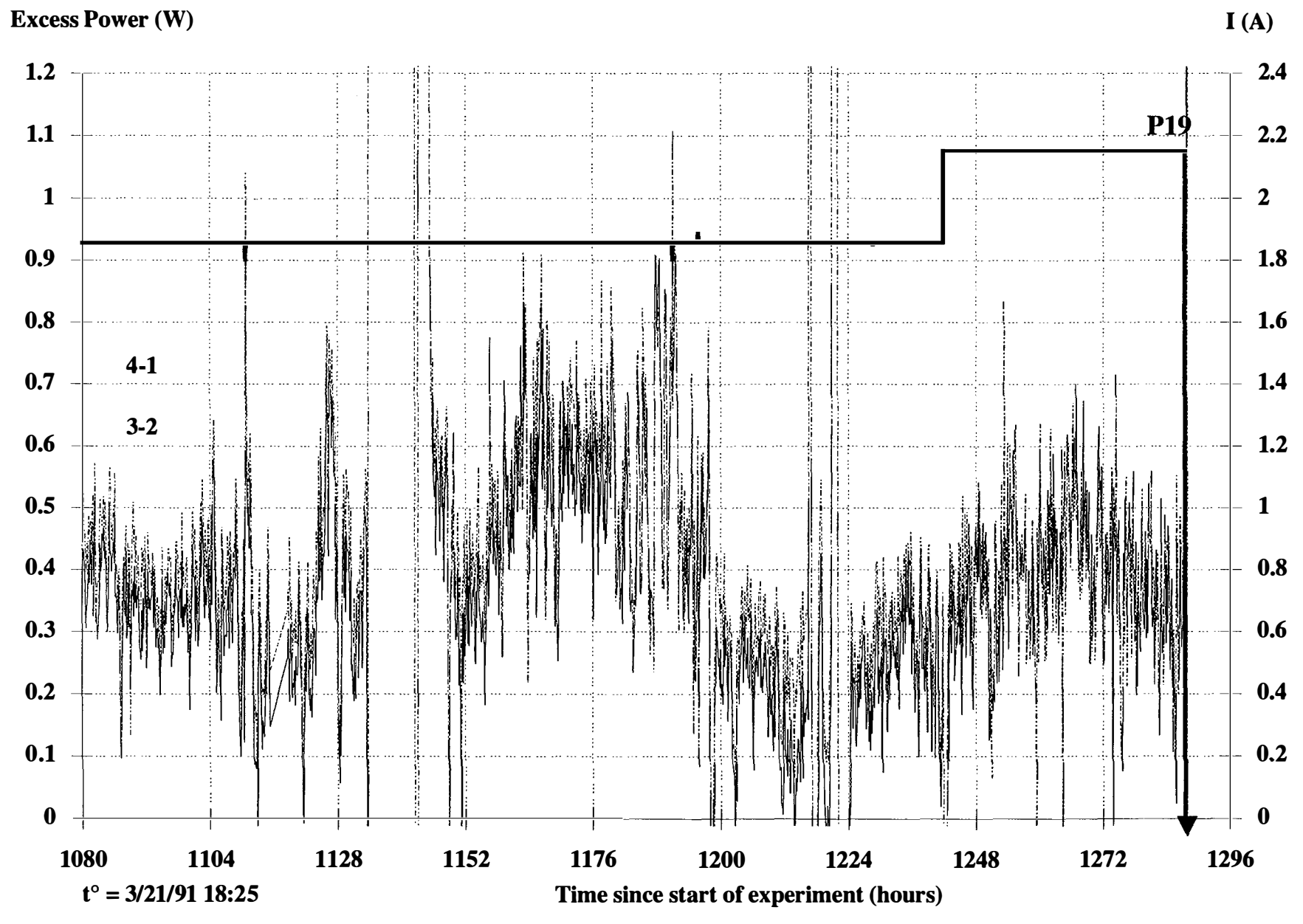
Excess Power (W)
I (A)
1.2
1.1
1
0.9
0.8
0.7
0.6
0.5
0.4
0.3
0.2
0.1
0
2.4
2.2
2
1.8
1.6
1.4
1.2
1
0.8
0.6
0.4
0.2
0
P19
4-1
3-2
1080
1104
1128
1152
1176
1200
1224
1248
1272
1296
t° = 3/21/91 18:25
Time since start of experiment (hours)

Figure A-6g

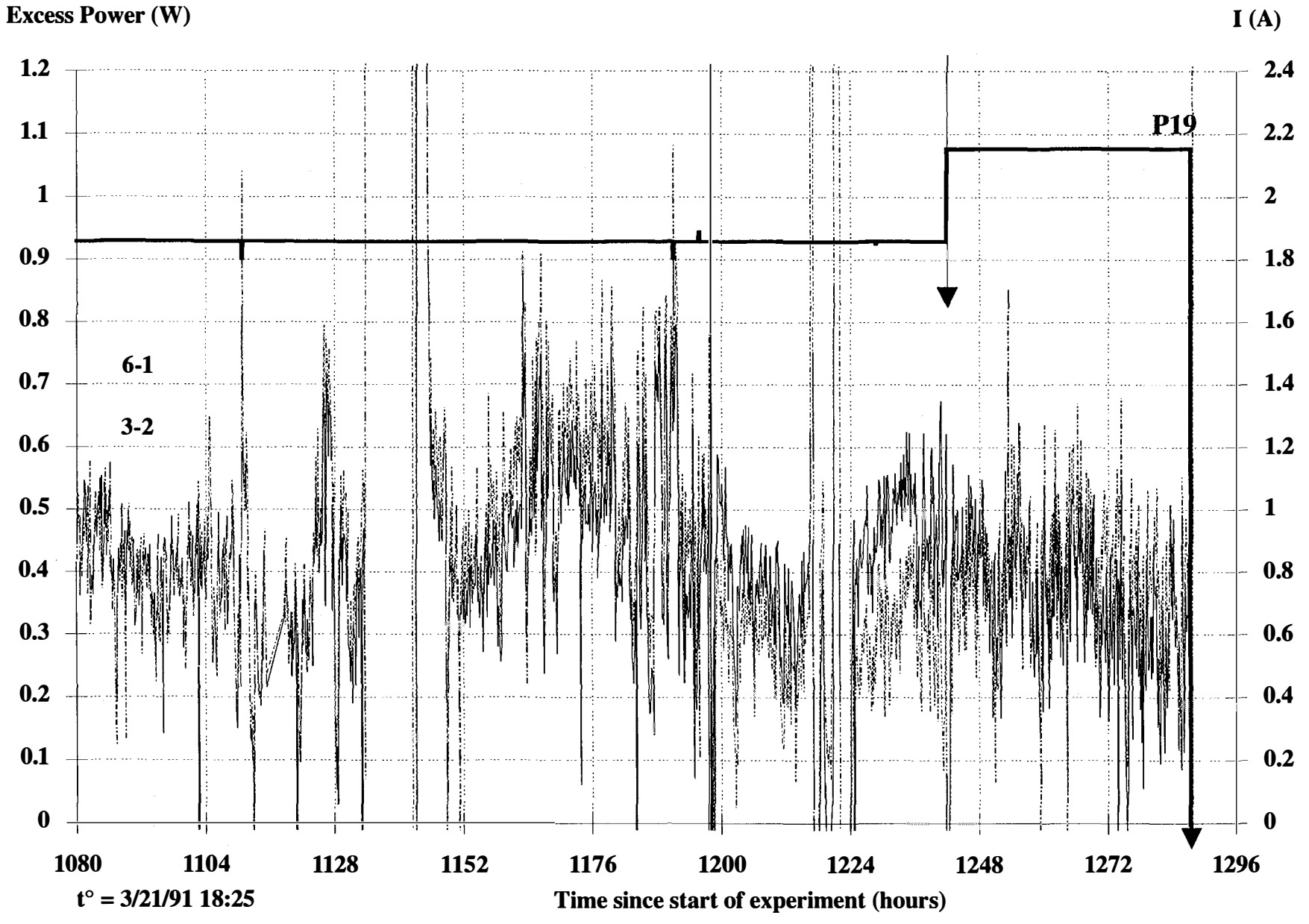
Excess Power (W)
I (A)
1.2
1.1
1
0.9
0.8
0.7
0.6
0.5
0.4
0.3
0.2
0.1
0
2.4
2.2
2
1.8
1.6
1.4
1.2
1
0.8
0.6
0.4
0.2
0
P19
6-1
3-2
1080
1104
1128
1152
1176
1200
1224
1248
1272
1296
t° = 3/21/91 18:25
Time since start of experiment (hours)

Figure A-6h

3B

EXPERIMENT P1b:

The differential calorimeter described in Section 3 employed as the reference a cell containing a copper cathode coated with ~3μm of palladium electroplate. On two occasions, this "reference" cell demonstrated a temperature rise in excess of that of the "working" cell (a 5 cm long x 0.7 cm diameter Pd rod). This experiment can be viewed as a test of the spatial distribution of the presumed heat source, since the coated specimen has the same area as the bulk Pd cathode but much less volume. It is also likely that the coated specimen would demonstrate a more rapid initiation of any phenomena facilitated by the electrochemically induced diffusion of species to or from the metal/electrolyte interface.

In this section we report the results of the one well-characterized observation of temperature excess for the Pd-coated "reference" cell. The experimental procedure is as described in Section 3 and Ref. 1. Briefly, the temperature difference measured between the center of the Pd-coated Cu rod cathode and the constant temperature bath surrounding the cell is compared to the temperature difference measured in a similar reference cell connected in series, the only difference being that the Pd-coated Cu cathode response is taken with reference to the bulk Pd cathode, the thermal response of which is presumed to reflect no anomalous heat source (within the period examined here).

3B.1 Calorimetry

If I is the current and V the cell voltage, then in the steady state the input power is the sum of the product I*V and any extraneous sources of heat, Q_u. If the calorimeter heat capacity and cooling constant are C_p and k, respectively, then for an elapsed time t,

$$I*V + Q_u/t = (C_p + k)\,\Delta T \qquad (3B\text{-}1)$$

where $\Delta T = T_{cell} - T_{bath}$.

This relationship can be further expressed as

$$I*V = C_p'\Delta T - Q_u/t \qquad (3B\text{-}2)$$

The calorimeter was calibrated by varying the input electrochemical power to the two cells in series. With $Q_u = 0$, we expect a linear relationship between the input Joule power to each cell, I*V, and the observed temperature difference between cell and bath:

$$I*V = a\Delta T + b \qquad (3B\text{-}3)$$

The reference and working cells were calibrated according to Eq. 3B-3, by using both stepped and ramped currents, to establish a steady-state slope and intercept: a and b for the working cell, and a' and b' for the reference cell. We do not make any attempt to calculate or calibrate the temporal response of these cells to a change in input Joule heat or thermal conditions. Instead, in the differential mode, we assume that the only differences between the responses of the working and reference cells are those due to the difference in the steady-state calibration coefficients (a and a', b and b') and the possible existence of extraneous heat, Q_u, in the working cell. That is,

Working cell: $a\Delta T + b = IV + Q_u/t$

Reference cell: $a'\Delta T' + b' = IV'$

$$Q_u/t = a\Delta T + b - (a'\Delta T' + b')\ V/V' \qquad (3B\text{-}4)$$

Eq. 3B-4 reflects the extraneous heat if all influences on the two cells are the same except for the quantified and calibrated differences between the primed and unprimed variables. This procedure yields a positive excess if the extraneous heat occurs in the working (in this case, the Pd-coated) cell, a "negative excess" if this heat occurs in the reference (in this case, the Pd-bulk) cell, and zero if there are no extraneous, uncorrelated influences or if these appear identically in both cells. Eq. 3B-4 also yields a positive excess if the reference cell undergoes an endothermic process. This latter effect can normally be distinguished from a real excess in the

working cell by looking at the ΔT versus input power response of each cell independently (i.e., in nondifferential mode).

3B.2 Results

Experiment P1 was started at 12:00 on 5/3/89. On 5/15/89 at 23:00, the Pd-coated cathode exhibited a small excursion of temperature, returning to the calorimetric baseline after ~5 hours. The apparent integrated excess was 2.5 ± 0.5 kJ. On 5/17/89 at 18:00, the Pd-coated cathode again exhibited a positive temperature excursion.

Figure 3B-1 presents the current applied to the two cells in series, the two cell voltages, and the excess power, Q_u/t, calculated from Eq. 3B-4. Note that when the current was stepped (from 0.637 to 0.85 to 0.99 A), the voltages measured in both cells first stepped and then relaxed. This phenomenon is a feature of the anode polarization and is thought to be due to the availability of (supersaturated) dissolved D_2 for the oxidation reaction. The extent of this relaxation is greater for the Pd-bulk cathode than for the Pd-coated cathode, in the interval shown. This was generally the case, and it may reflect more rapid achievement of the steady state by the Pd coating (because of its smaller capacity for deuterium absorption).

The data in Figure 3B-1 appear to show a slowly increasing power excess for the Pd-coated copper cathode, which steps to a higher value of excess at the point labeled "A" and then down at point "B."

The point labeled "A" does not appear to correlate with any change in the controlled or measured variables of either cell. Figure 3B-2 shows the temperature differences recorded between sensors placed in the center of each cathode and the common bath. (During the interval shown, the bath temperature was 8.84 ± 0.08°C) individual data points are shown for δT_{cu} (the temperature difference between the Pd-coated cathode and the bath sensors); these data were taken at 1-minute intervals.

The apparent increase in the power excess at point "A" is seen to be due to an (apparently spontaneous) increase in the Pd-coated cathode temperature, which occurs over a time scale of 5-10 minutes. Whether this time scale is reasonable for the temperature rise due to a putative 300 to 400-mW power source within the cathode (or cathode coating) is a complex function of the relative positions of this power source and the temperature sensor. Nevertheless, the thermal conductivity

and heat capacity of copper are such that a time constant of 5-10 minutes is not implausible.

The step-down in apparent power excess at point "B" appears to be correlated with a discontinuity observed in the Pd-bulk cathode cell voltage. Inspection of Eq. 3B-4 reveals the source of the effect of V' on Q_u/t. This effect arises because Eq. 3B-4 is strictly applicable only in the steady state, and nearly doubling the power in the reference cell moves that cell away from its steady state without a compensatory displacement of the working cell (the Pd-coated cathode). Nevertheless, the origin of the voltage step in V_{Pd}, and its calorimetric implications, require some explanation. The cause of the discontinuity in V' at point "B" is not known. The reference cell clearly experienced a rapid increase in cell resistance, due (presumably) to either the occurrence of a partial open circuit (e.g., the formation of a gas bubble in the cell), or the relief of a partial short circuit (e.g., an external or internal electrical or electrolyte bridge). Clearly this event affected not only the transient condition but also the steady state of the calorimeter, in that the apparent power excess values before and after point "B" are substantially different. Since this event occurred at 5:25 AM, when the laboratory was unoccupied, its occurrence was not initiated by the experimentalists.

When we examine the δT versus P_{in} response for the reference cell, in which the current steps (and the voltage step at "B") provide a dynamic calibration, it appears that the input power (i.e., I_{cell} and V_{cell}) and the temperature difference were being measured accurately, or at least consistently. This rules out the possibility that relief of a shunt external to the cell could have caused the discontinuity in the voltage.

Enough unanswered questions are associated with the observation discussed in this section that the existence of an excess power source in the Pd-coated cathode cannot be proposed with confidence. Nevertheless, the practical implications of heat production in a thin coating are great, so we will take the observation on face value and examine the implications further.

Figure 3B-3 shows a plot of the excess power displayed in Figure 3B-1, normalized to the measured power input to cell containing the Pd-coated cathode. Although the measurement uncertainty has not been well defined for this calorimeter, especially in view of possible artifacts or systematic errors discussed above, we nevertheless

can tentatively assign an uncertainty of ~5%. The excess power effect represented in Figure 3B-3 thus persisted for more than 18 hours and maintained a value of ~50% of P_{in} for 11 hours between points "A" and "B."

The integrated energy under the excess power curve of Figure 3B-1 achieved a maximum value of 21 ± 1 kJ. If the Pd coating (or the D contained within this Pd matrix) is associated with the source of this energy, then the rather small amount of net energy excess corresponds to a very large energy density. A 3-μm coating of Pd on an 11-cm^2 electrode has a volume of 0.003 cm^3, weights 0.036 g, and contains 3.7 x 10^{-4} mol of Pd (or D for D/Pd = 1). An energy excess of 21 kJ thus represents ~55 MJ mol^{-1}. The maximum excess power of ~0.44 W reflects ~130 W cm^{-3} of Pd. The excess energy and power densities are both impressive numbers but are within the bounds of values observed in later experiments where bulk Pd samples were examined with a more traditional calorimeter.

Resolution of whether thin Pd (or other metal) films can be made to display anomalous excess heat production is probably better achieved in a flat plate configuration with multiple temperature sensors employed to locate the source of any heat generation.

3B.3 References

1. D. D. Macdonald, M.C.H. McKubre, A. C. Scott, and P. R. Wentrcek. "Continuous in-situ method for the measurement of dissolved hydrogen in high-temperature aqueous systems." I&EC Fundamentals **20**, 290 (1981).

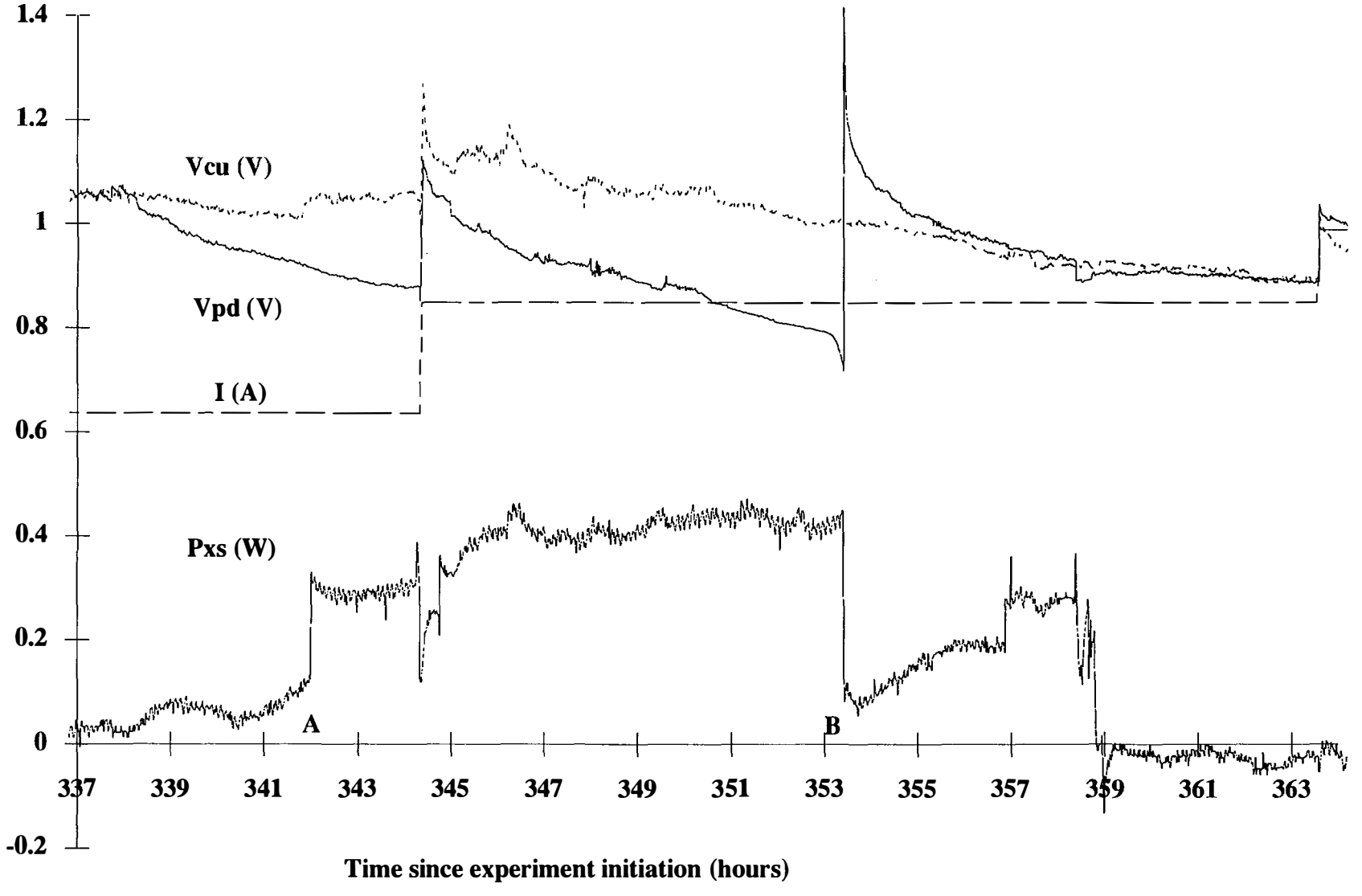
1.4
1.2
1
0.8
0.6
0.4
0.2
0
-0.2
Vcu (V)
Vpd (V)
I (A)
Pxs (W)
A
B
337
339
341
343
345
347
349
351
353
355
357
359
361
363
Time since experiment initiation (hours)

Figure B-1

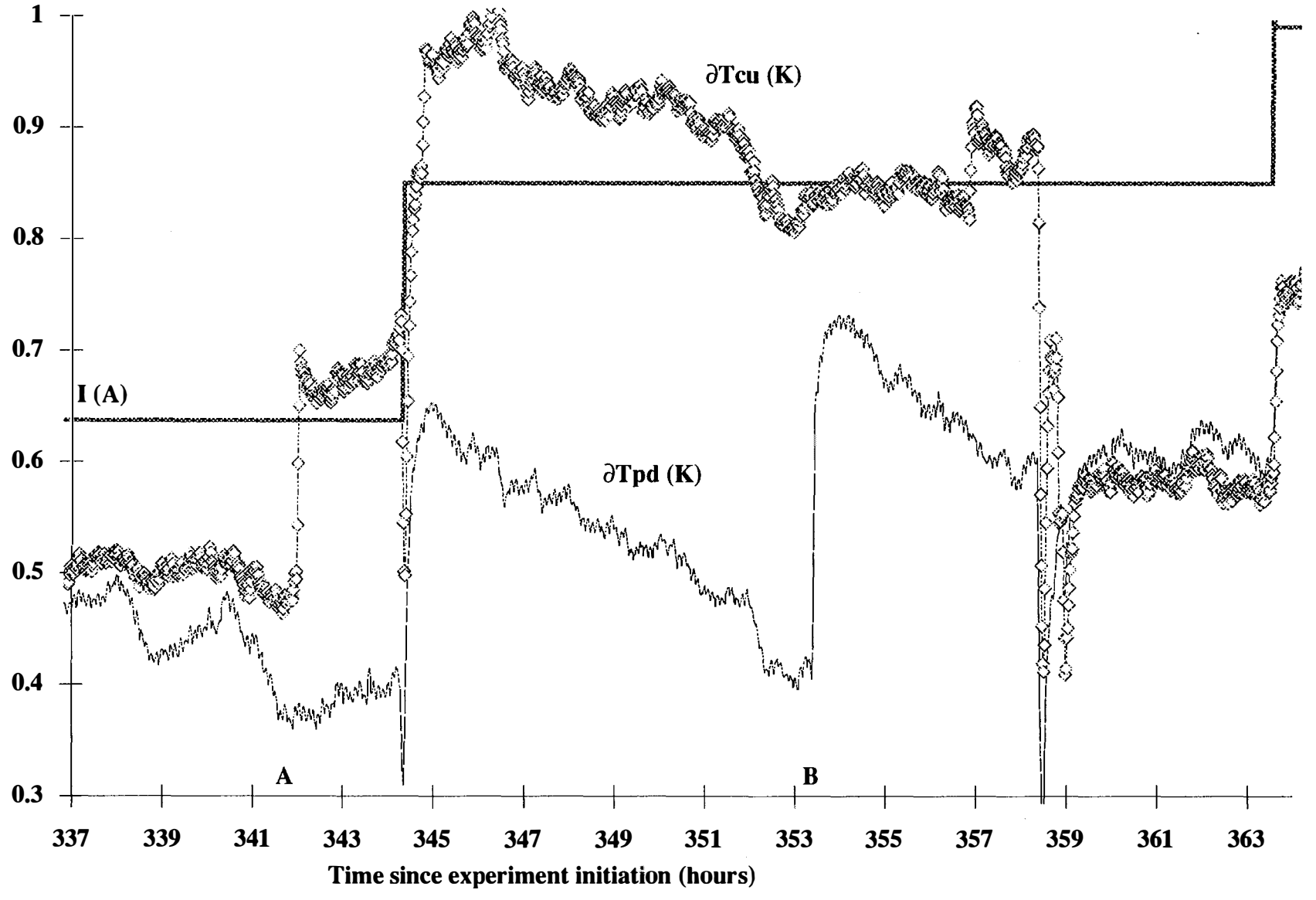
1
0.9
0.8
0.7
0.6
0.5
0.4
0.3
∂Tcu (K)
I (A)
∂Tpd (K)
A
B
337
339
341
343
345
347
349
351
353
355
357
359
361
363
Time since experiment initiation (hours)

Figure B-2

P1.F3 // 3/14/94 // 4:10 PM

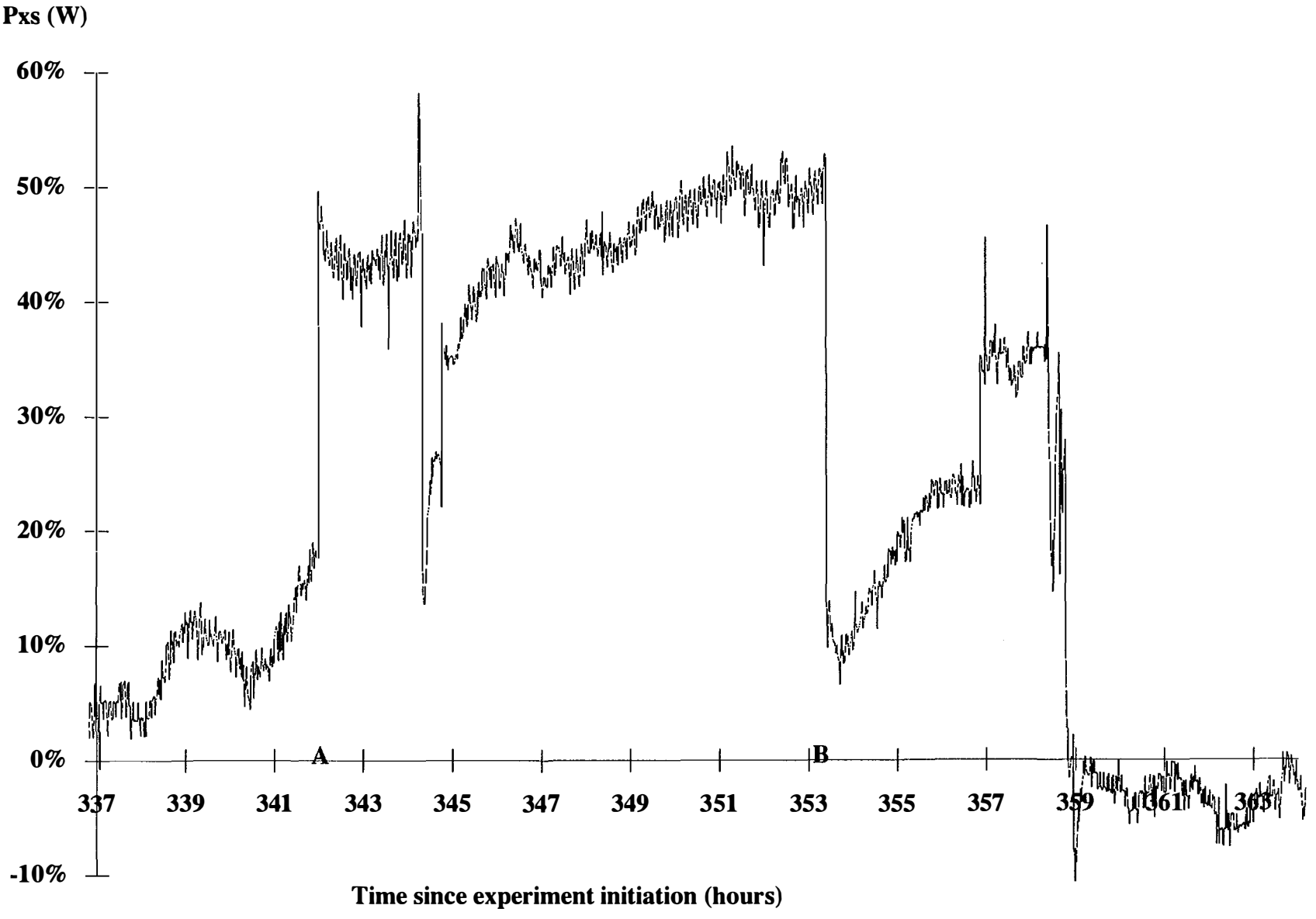

Figure B-3

4

RADIATION DETECTION ASPECTS OF ANOMALOUS EFFECTS IN DEUTERATED SYSTEMS

This topic is covered in Appendix A, "Radiation Detection Aspects of an Investigation of Anomalous Effects in Deuterated Systems."

5

SUMMARY AND DISCUSSION

This section summarizes and discusses some aspects of the experimental results presented in this report. Since there is not yet a detailed mechanistic understanding of the origin of the excess-power-producing phenomenon, the observation of which is the result of central importance reported here, any discussion is necessarily largely phenomenological. However, we present some implications of the phenomenological model developed here in connection with the search for a possible nuclear origin for the excess power production observed.

5.1 Experimental Observations

5.1.1 *Degree-of-Loading Experiments*

The central postulate guiding the experimental program was that anomalous effects previously unobserved or currently unexplained in the deuterium-palladium system occur at a very high D/Pd atomic ratio. Emphasis was placed on studying phenomena that provide a fundamental understanding of the mechanism by which D gains access to the Pd lattice and how very high atomic ratios (near, at, or perhaps beyond unity) can be achieved and maintained.

To characterize the electrochemical kinetic and thermodynamic processes that control the absorption of D into Pd, we measured the interfacial impedance and the Pd cathode voltage with respect to a reference electrode. Measurements of the Pd solid-phase resistivity were used to monitor on-line the degree of loading atomic ratios, specifically D/Pd, H/Pd, and H/D.

The overall conclusions of this study are that by careful control of the electrode pretreatment, the electrolyte composition, and the current density, we can load Pd to an atomic ratio D/Pd of approximately unity and sustain this loading for weeks.

5.1.2 *Calorimetric Experiments*

Calorimetric experiments were performed in palladium rods highly loaded with D and/or H and electrolyzed at substantial current densities (typically 300-600 mA

cm^{-2}, but up to 6400 mA cm^{-2}) for considerable periods (typically 1000-2000 hours). Our calorimeters were designed with the philosophy that in precise calorimetry and the search for unusual reaction products make it desirable to have a closed system and a knowledge at all times of the composition of the reacting system. All experiments were performed with closed and sealed electrochemical cells operating from 40 to 10,000 psi above atmospheric pressure. Axial resistance measurements were made to monitor the D/Pd or H/Pd ratio.

Approximately 30 experiments have been performed with flow calorimeters operating at constant power input. The calorimeters were designed and constructed with the following features:

- A conceptually simple system based on the first law of thermodynamics.
- Maintenance of complete control of operating parameters (including cell temperature).
- A large working range of power input and output (0.1-100 W).
- On-line monitoring of all important variables.
- Multiple redundancy of measurement of critical variables such as temperature.
- High accuracy (the greater of 50 mW or 0.5%) and precision (10 mW or 0.1%).
- Known sources of potential error to yield conservative estimates of output power.
- Steady-state operation, leading to simple analysis.

All experiments were performed with thermodynamically closed electrochemical cells. A large area catalyst was provided in the head space of the cells to recombine evolved O_2 and D_2 so that the net reaction in all cells after the Pd rod is loaded is $D_2O = D_2O$, for which the thermoneutral voltage is zero. Constant current or slowly

ramped conditions were used in all cases. Commonly, experiments were performed electrically in series to test the effects of different variables.

We have observed unexplained excess power in palladium cathodes when a minimum of three criteria were met:

(1) The average loading (D/Pd) approached or exceeded unity.

(2) This high loading was maintained for considerable periods (hundreds of hours for 3-mm-diameter cathodes).

(3) The interfacial current density exceeded a certain critical value.

For the thermodynamically closed and intentionally isothermal systems described here, output power was observed to be as much as 300% in excess of the electrochemical input power or 24% above the known total input power. When excess power was present, it was more typically in the range 5%-10%, in calorimeters that were accurate to better than approximately 0.5%. The largest observation of excess energy corresponded to 1.08 MJ, or 45.1 MJ/mol, or ~450 eV/atom normalized to the Pd lattice or to the deuterium in the palladium at a loading of ~1.

Some degree of experimental reproducibility between cells was also observed. Five experiments were performed in an attempt to replicate a prototype experiment, with only minor variations in electrode and electrolyte treatment. All the heavy water experiments produced excess heat and reproduced in general form the observation of excess heat in the prototype experiment. However, excess power in these four experiments was *not* produced in exactly the same amounts, or at exactly the same times, in response to the same stimuli. Except for times when the calorimeter was caused to depart significantly from its steady-state condition, "negative excess" was never observed.

Finally, we are unable to account for the observed excess heat by an artifact known to us and are forced to conclude that the source of the excess power is a property of the D/Pd system. Further, we cannot account for the measured excess power and energy by any chemical or mechanical process with which we are familiar.

5.2 Phenomenological Model for Excess Power Production

The association of apparent excess power with a set of necessary conditions for the D/Pd system implies a degree of reproducibility. These conditions are not easy to attain, a fact that may explain the irreproducibility of the phenomenon of excess heat. Examined separately, the three criteria may be taken as normal conditions of reacting systems (chemical or nuclear). The criterion of loading is of a thermodynamic driving force, a measure of the activity or chemical potential of a possible reactant species. The need to maintain loading for considerable periods before the onset of excess heat suggests a mass transport constraint, possibly involving nucleation and growth of an active region within the volume of the bulk Pd lattice.

The final requirement, a large interfacial current density, suggests a kinetic criterion. Cathodic current provides the means by which atomic hydrogen or deuterium is discharged onto the palladium electrode surface. The role of current density in producing calorimetric excess power in heavy water systems may be more complex than simply that of initiating adsorption. In our experiments, we observe that the excess heat, when present, increases roughly linearly with current density above some threshold value and achieves a maximum at an upper threshold of current density. Under different experimental conditions, others have observed a second-order or higher dependence of excess power on current density above an initiation threshold, but with no observed upper limit.

In energy-producing experiments, we observe that the loading initially increases monotonically with current density, but this increase is not sustained, and the apparent loading (determined from the resistance ratio) may decrease at moderate and high current densities while the excess power continues to increase. We also observe in repeated experiments that excess power can consistently be reduced to unmeasurably small values by reducing the current density below its lower threshold value. The decrease in excess power generally occurs faster than the time constants of diffusional loading.

These results suggest the potential for using current control as a very effective means of controlling a practical heat producing system. The current appears to act

by many complex mechanisms. Some suggested mechanisms follow:

- Controlling the loading through the electrochemical process of discharge, recombination, and adsorption.
- Providing kinetic impetus to possible interstitial nuclear processes by coupled motion of e^- and D^+ plasmas in the metal phase.
- Providing optical or acoustic phonon excitation to stimulate lattice neutron transfer reactions.
- Increasing the cathode temperature.

Current perturbation provides the most direct means of probing the electrochemical system and of controlling any practical device. For practical and fundamental reasons, it is critical that we gain a clear understanding of the methods by which it operates to induce excess power.

5.3 Influence of Temperature

The apparent discrepancy between our observation of a roughly linear dependence of excess power on current density and that of Fleischmann and Pons of a roughly second-order dependence may be resolved by understanding the influence of temperature. We have designed our experiments, as closely as possible, to decouple the influences of temperature and current density; calorimetric experiments are performed under constant input power conditions, approaching the steady state. Our calorimeters also have large heat conduction so that, even in the condition of substantial excess power, the cathode temperature is not raised appreciably. Under these conditions, we observe an approximately linear response of excess power with current density.

In the experiments of Pons and Fleischmann, the current density is raised without reducing the power in a compensatory heater, in a calorimeter with very low heat conduction. For this reason, the cell temperature rises markedly with increasing current density, and the temperature increase is exacerbated by the onset of any excess power production. Under these conditions, Fleischmann and Pons observed a second-order or higher power dependence of excess power on current density, with no observed maximum.

Taken together, these results suggest that the rate of excess enthalpy production increases at least transiently, with increasing temperature. Such a degree of autocatalysis would be useful in achieving large power gain; the apparent positive derivative with temperature suggests that it may be possible to produce heat efficiently at a usefully elevated temperature.

WARNING: This Document contains information classified under U.S. Export Control regulations as restricted from export outside the United States. You are under an obligation to ensure that you have a legal right to obtain access to this information and to ensure that you obtain an export license prior to any re-export of this information. Special restrictions apply to access by anyone that is not a United States citizen or a Permanent United States resident. For further information regarding your obligations, please see the information contained below in the section titled "Export Control Restrictions."

Export Control Restrictions

Access to and use of EPRI Intellectual Property is granted with the specific understanding and requirement that responsibility for ensuring full compliance with all applicable U.S. and foreign export laws and regulations is being undertaken by you and your company. This includes an obligation to ensure that any individual receiving access hereunder who is not a U.S. citizen or permanent U.S. resident is permitted access under applicable U.S. and foreign export laws and regulations. In the event you are uncertain whether you or your company may lawfully obtain access to this EPRI Intellectual Property, you acknowledge that it is your obligation to consult with your company's legal counsel to determine whether this access is lawful. Although EPRI may make available on a case by case basis an informal assessment of the applicable U.S. export classification for specific EPRI Intellectual Property, you and your company acknowledge that this assessment is solely for informational purposes and not for reliance purposes. You and your company acknowledge that it is still the obligation of you and your company to make your own assessment of the applicable U.S. export classification and ensure compliance accordingly. You and your company understand and acknowledge your obligations to make a prompt report to EPRI and the appropriate authorities regarding any access to or use of EPRI Intellectual Property hereunder that may be in violation of applicable U.S. or foreign export laws or regulations.

About EPRI

EPRI creates science and technology solutions for the global energy and energy services industry. U.S. electric utilities established the Electric Power Research Institute in 1973 as a nonprofit research consortium for the benefit of utility members, their customers, and society. Now known simply as EPRI, the company provides a wide range of innovative products and services to more than 1000 energy-related organizations in 40 countries. EPRI's multidisciplinary team of scientists and engineers draws on a worldwide network of technical and business expertise to help solve today's toughest energy and environmental problems.

EPRI. Electrify the World

TR-104195

EPRI • 3412 Hillview Avenue, Palo Alto, California 94304 • PO Box 10412, Palo Alto, California 94303 • USA
800.313.3774 • 650.855.2121 • askepri@epri.com • www.epri.com